รายงานวิจัยฉบับสมบูรณ์

โครงการ

“ความผันแปรของลมมรสุมฤดูร้อนในทวีปเอเชียสมัยโฮโลซีน:

การศึกษาเพื่อสังเคราะห์ข้อมูลที่บันทึกในหินงอกและวงปีไม้จากประเทศไทยและจีน”

(Asian summer monsoon variability during the Holocene:

a synthesis study on stalagmites and tree rings

from Thailand and China)

โดย

โชติกา เมืองสง และคณะ

ธันวาคม 2562

สัญญาเลขที่ **RDG5930014**

รายงานวิจัยฉบับสมบูรณ์

โครงการ

“ความผันแปรของลมมรสุมฤดูร้อนในทวีปเอเชียสมัยโฮโลซีน:
การศึกษาเพื่อสังเคราะห์ข้อมูลที่บันทึกในหินงอกและวงปีไม้จากประเทศไทยและจีน”

(Asian summer monsoon variability during the Holocene:
a synthesis study on stalagmites and tree rings
from Thailand and China)

	คณะผู้วิจัย	**สังกัด**
1.	ดร. โชติกา เมืองสง	มหาวิทยาลัยมหิดล
2.	รศ. ดร. นาฏสุดา ภูมิจำนงค์	มหาวิทยาลัยมหิดล
3.	ดร. สุภาภร บัวจันทร์	มหาวิทยาลัยมหิดล
4.	Prof. Dr. Binggui Cai	Fujian Normal University
5.	Prof. Dr. Guoliang Lei	Fujian Normal University
6.	Prof. Dr. Jiang Xiuyang	Fujian Normal University
7.	Dr. Xiuling Chen	Fujian Normal University
8.	นางสาวกิตตาภา มะลิมาตร	มหาวิทยาลัยมหิดล
9.	นางสาวทิพวรรณ ขันคูณ	มหาวิทยาลัยมหิดล
10.	นายนิกร แก้วโมรา	เขตรักษาพันธุ์สัตว์ป่าลุ่มน้ำปาย
11.	นายบำรุงรัตน์ พลอยดำ	เขตรักษาพันธุ์สัตว์ป่าเขาบรรทัด
12.	นายพัทยา เท็กกิ้ม	เขตรักษาพันธุ์สัตว์ป่าสันปันแดน
13.	นายศรัทธา กุนทอง	เขตรักษาพันธุ์สัตว์ป่าเชียงดาว
14.	นายวีระ กอแก้ว	อุทยานแห่งชาติแม่เมย
15.	นายสมศักดิ์ ฐิติชยาภรณ์	อุทยานแห่งชาติดอยผ้าห่มปก
16.	นายสมชาย นุชนานนท์เทพ	สำนักจัดการทรัพยากรป่าไม้ที่ 12 สาขากระบี่

สนับสนุนโดย

สำนักงานคณะกรรมการส่งเสริมวิทยาศาสตร์ วิจัย และนวัตกรรม (สกสว.)

(ความเห็นในรายงานนี้เป็นของผู้วิจัย สกสว. ไม่จำเป็นต้องเห็นด้วยเสมอไป)

EXECUTIVE SUMMARY

The Asian Summer Monsoon (ASM) is an important component of global monsoons and is one of the dominant summer rainfall regimes in the world. Changes in the ASM activity have strong implications for the economy and livelihood of more than two billion people, which are directly or indirectly affected by the timing and amount of precipitation during the ASM season. A better understanding of the nature of the ASM is necessary to improve our adaptability to extreme climate, especially under the background of ongoing global warming. History of the ASM during the Holocene (recent 11.6 ka) has long been one of key focuses of climatologist and global change research community. This epoch is the most important period for studying the relationship between humanity and Earth's system. Regional monsoons are driven by annual cycle of solar radiation and bonded by the global divergent circulation. They are closely correlated because of the large-scale Asian monsoon circulation. Synthetic study on the ASM variability based on proxies derived from high-resolution. Because of the limitation of long-term instrumental climate records, natural climate proxies have become vital dataset for exploring nature of Holocene. Until now, a large number of studies have been performed to reconstruct the ASM history during the Holocene. Among all of them, stalagmites and tree rings are the most important archives of the ASM. Stalagmite could provide well-dated and continuous climatic records over long time intervals, while tree-ring chronologies allow high-resolution (monthly to annual) calibration with climate and other factors. In addition, adequate understandings of the factors controlling speleothem and tree ring's properties have added the advantage over many other proxies.

The objectives of this project are; 1) To produce high-resolution composite records of Asian summer monsoon over the past few centuries based on stalagmites and tree rings collected from Northern, Northwestern, and Southern Thailand, and 2) To reconstruct and synthesize the large-scale and long-term dynamic changes of the Holocene Asian monsoon based on stalagmites from the two Asian monsoon regions (Yunnan and Fujian, China) and one transition region (Mae Hong Son, Thailand), 3)

To investigate both short-term and long-term driving mechanisms of the Asian monsoon circulation and its teleconnection to global climate change, and 4) To carry out a systematic cave and climate monitoring program in Thailand for better understanding of climate signal derived from stalagmites and tree rings.

Research methodologies can be divided into three parts as follows: 1) For analyses of stalagmites, stalagmite chronologies were developed based on either U-Th dating or lamina counting chronology. The measurements were performed on a magnetic sector inductively coupled plasma mass spectrometer. Growth rates were measured via Image-Pro Plus 5.1 software. Oxygen isotopic ($\delta^{18}O$) measurements were performed following the standard procedures on a MAT-253 mass spectrometer linked to a Gas Bench-II. 2) Cave and climate monitoring were carried on a monthly or seasonal timescales during both dry and wet seasons in order to understand the factors controlling stalagmite properties. Examples of selected parameters were stalagmite drip water properties (drip rate, Electrical Conductivity, pH, carbonate hardness, modern aragonite precipitates ($\delta^{18}O$, growth rate), and cave air conditions (relative humidity, temperature, and CO_2). 3) For tree rings, tree ring chronologies were performed using COFCHA program. Pure α-cellulose was extracted by a modified Jayme-Wise method. The cellulose $\delta^{18}O$ composition was determined with a continuous flow system by a pyrolysis-type elemental analyzer connected to a MAT-253 mass spectrometer via an open split interface.

Based on these results, observations and knowledge relating to climate changes during the Holocene epoch can be summarized as follows:

1) The early to mid-Holocene climate evolution in Thailand and China

1.1) In the early-Holocene, long-term pattern of summer monsoon in different regions are different. In Northern China, stalagmite isotope sequence showed the East Asian Summer Monsoon (EASM) was strong during the early-Holocene until 5.0 ka BP, followed by gradually declining trend. In Southeastern China, there also have a more moisture interval during mid-Holocene from approximately 6.5 ka BP to 4.5 ka BP. This wetter mid-Holocene was also observed in Northwestern Thailand. The accumulated density of stalagmites from Northwestern Thailand was low during the early Holocene, and then it increased to a peak from 11.0 ka BP until 8.0 ka BP. The second peak was found during time period between 6.0 and 3.0 ka BP. This

indicated that moisture situation during the mid-Holocene was higher compared to the early-Holocene. The moisture was increased since 8.0 ka BP, and its peak was observed during the interval between 6.0 and 3.0 ka BP. The Holocene moisture evolution pattern in Northwestern Thailand was similar with that of in Southeastern China, indicating a teleconnection between these two regions. The wetter mid-Holocene in these regions was different from those in the Indian Summer Monsoon (ISM) dominated region as observed by stalagmite records from Oman and Southwestern China. By comparing our results with insolation, we suggested that there were more regional precipitation in Northern China, Southeastern China, and Northwestern Thailand in the mid-Holocene when the ISM has shrunk since the early-Holocene. This indicated that hydrological changes in these three regions were not only influenced by orbital-driven insolation, but also by the sea-air interaction processes over the Western North Pacific Ocean.

1.2) Stalagmite isotopic records from Southern Thailand indicated higher rainfall in the early-Holocene, lower in the late-Holocene. Its long-term trend was similar to those in Oman and Southwestern China. Their Holocene change pattern were closely correlated with insolation in the Northern Hemisphere, supporting the hypothesis of insolation directly forcing mechanism via the Inter Tropical Convergence Zone (ITCZ) shifting northward at the early-Holocene and gradually moving southward then after.

1.3) For the millennium cold events in the Holocene, we investigated in-deep the cold events occurred at 2.8 ka BP, 5.5 ka BP and those occurred at the early-Holocene, depending on high-resolution stalagmite records from Northern China. We found that not all of cold events responding to solar activity. For the 2.8 ka event, the EASM indicated by Miaodong cave’s stalagmite record coincided with those of the total solar irradiance without any delay, indicating solar activity forcing via a fast dynamic mechanism, such as atmospheric remote-correlation. However, for the cold event 5.5 ka, our stalagmite records collected from Northeastern China exhibited two weak monsoon intervals, centering at 5.54 and 4.95 ka BP, respectively. There was no obvious corresponding relation between the EASM and solar activity indicators. We propose that the evidence of solar forcing on the EASM at 5.5 ka event was still limited. Inversely, the EASM indicated by our record do agree well with the

El Niño–Southern Oscillation (ENSO) event, indicating the ENSO forcing mechanism.

2) The late-Holocene climate evolution in Thailand

A 338-year oxygen isotope record from teak tree-ring cellulose revealed that over the entire period from AD 1678-2015, summer precipitation in Northwestern Thailand had decreased, and the reconstructed long-term average of May-October (rainy season) average precipitation was 253 mm. We found that during the 17^{th} and 18^{th} centuries, drought occurred during 8 years, respectively. In the 19^{th} century, there was drought during 19 years. In the 17^{th}, 18^{th}, and 19^{th} centuries, wet years occurred during 6, 10 and 1 years, respectively. The mechanism that may support drought in Southeast Asia is the southward shift in the ITCZ. In addition, these findings are consistent with other reconstructed mega drought events, especially those found in the 18^{th} century, such as the Strange Parallels drought (AD 1756-1768) and the East India drought (AD 1790-1796). Spatial correlations and spectral analyses revealed a strong impact of the ENSO on tree-ring $\delta^{18}O$. The ENSO influenced the tree-ring $\delta^{18}O$ more strongly in the AD 1870-1906, AD 1907-1943, and AD 1944-1980 periods than in the AD 1981-2015 period, which corresponded to periods of weaker and stronger ISM intensity.

Finally, proxy records of this study would probably be the most high-resolution and longest records for Thailand monsoon. High-quality and short term proxy records would have potentially significant implications to give a better understanding of teleconnections within the modern atmosphere as well as to quantify the climatological parameters in the long-term climate reconstruction. This study will most benefit to improve climate forecasts, especially in the monsoon transition area.

ABSTRACT

This study aims to 1) to produce high-resolution composite records of the Asian Summer Monsoon (ASM) over the past few centuries produce high-resolution composite records of Asian summer monsoon over the past few centuries based on stalagmites and tree rings collected from Northern, Northwestern, and Southern Thailand., (2) to reconstruct and synthesize the large-scale and long-term dynamic changes of the Holocene Asian monsoon based on stalagmites from the two Asian monsoon regions (Yunnan and Fujian, China) and one transition region (Mae Hong Son, Thailand), (3) to investigate both short-term and long-term driving mechanisms of the Asian monsoon circulation and its teleconnection to global climate change, and (4) to carry out a systematic cave and climate monitoring program in Thailand for better understanding of climate signal derived from stalagmites and tree rings.

These results demonstrated that (1) in the early and mid-Holocene, long-term patterns of the ASM in different regions were different. There was more regional precipitation in Northern China, Southeastern China, and Northwestern Thailand. This indicated that hydrological changes in these three regions were not only influenced by orbital-driven insolation, but also by the sea-air interaction processes over the Western North Pacific Ocean, (2) stalagmite records from Southern Thailand indicated higher rainfall in the early-Holocene, lower in the late-Holocene, supporting the hypothesis of insolation directly forcing mechanism via the Inter Tropical Convergence Zone (ITCZ) shifting northward at the early-Holocene and gradually moving southward then after, and (3) the late-Holocene climate evolution in Thailand derived from Thai teak (*Tectona grandis* Linn.) tree-ring cellulose oxygen isotopes ($\delta^{18}O$) indicated drought events, especially in 18^{th} century. The El Niño-Southern Oscillation (ENSO) influenced Thailand's climate more strongly in the AD 1870-1906, AD 1907-1943, and AD 1944-1980 periods than in the AD 1981-2015 period. Proxy records of this study would probably be the most high-resolution and longest records for Thailand monsoon. The output of this project could supply complementary high quality of the ASM records.

KEYWORDS: HOLOCENE / ASIAN SUMMER MONSOON / STALAGMIE / TEAK / TREE RING /GROWTH RATE / STABLE OXYGEN ISOTOPES

บทคัดย่อ

การศึกษาครั้งนี้มีวัตถุประสงค์เพื่อ (1) การประกอบรวมข้อมูลของลมมรสุมทวีปเอเชียที่มีความละเอียดสูงในช่วงระยะเวลาไม่กี่ร้อยปีที่ผ่านมาขึ้นจากวงปีไม้และหินงอกจากพื้นที่ภาคเหนือ ภาคตะวันตกเฉียงเหนือ และภาคใต้ประเทศไทย (2) การสร้างและสังเคราะห์พลวัฒน์การเปลี่ยนแปลงของลมมรสุมทวีปเอเชียระยะยาวในสมัยโฮโลซีนที่กินขอบเขตกว้างขวางด้วยข้อมูลจากหินงอกจากพื้นที่ตัวแทนของลมมรสุมระดับภูมิภาคจำนวนสองพื้นที่ (มณฑลยูนนานและมณฑลฝูเจี้ยน ประเทศจีน) และพื้นที่จุดเปลี่ยนผ่านรอยต่อของลมมรสุมจำนวนหนึ่งพื้นที่ (จังหวัดแม่ฮ่องสอน ประเทศไทย) (3) เพื่อศึกษากลไกขับเคลื่อนการไหลเวียนของลมมรสุมทวีปเอเชียทั้งระยะสั้นและระยะยาว รวมถึงศึกษาความสัมพันธ์กับการเปลี่ยนแปลงของภูมิอากาศระดับโลกในพื้นที่ห่างไกล และ (4) ศึกษากระบวนการเปลี่ยนแปลงของถ้ำและภูมิอากาศในปัจจุบัน ด้วยการติดตั้งระบบตรวจวัดเพื่อให้เกิดความเข้าใจสัญญาณภูมิอากาศที่ได้รับจากหินงอกและวงปีไม้ได้ดีขึ้น

ผลการศึกษาครั้งนี้แสดงให้เห็นว่า (1) ในยุคโฮโลซีนตอนต้นและตอนกลาง รูปแบบการเปลี่ยนแปลงของลมมรสุมทวีปเอเชียมีความแตกต่างกันไปในแต่ละพื้นที่ โดยฝนมีปริมาณมากในพื้นที่ภาคเหนือ ภาคตะวันออกเฉียงเหนือของประเทศจีน และภาคตะวันตกเฉียงเหนือของประเทศไทย ซึ่งชี้บอกว่า นอกจากการขับเคลื่อนโดยปริมาณรังสีดวงอาทิตย์แล้วนั้น ปฏิสัมพันธ์ที่เกิดขึ้นระหว่างทะเลและบรรยากาศที่เกิดขึ้นบริเวณมหาสมุทรแปซิฟิกเหนือด้านตะวันตกก็มีอิทธิพลต่อการเปลี่ยนแปลงทางอุทกวิทยาในสามพื้นที่นี้ (2) ในยุคโฮโลซีนตอนกลาง ข้อมูลที่บันทึกในหินงอกจากภาคใต้ของประเทศไทย ชี้บอกถึงปริมาณน้ำฝนที่มากในยุคโฮโลซีนตอนต้นและปริมาณน้ำฝนลดลงในยุคโฮโลซีนตอนปลาย ซึ่งสนับสนุนทฤษฎีที่รังสีดวงอาทิตย์มีอิทธิพลต่อการเคลื่อนที่ของร่องมรสุมจากทางตอนเหนือในยุคโฮโลซีนตอนต้น มายังทางตอนใต้ในช่วงระยะเวลาหลังจากนั้น และ (3) ในยุคโฮโลซีนตอนปลาย ข้อมูลการเปลี่ยนแปลงภูมิอากาศที่ได้รับจากข้อมูลไอโซโทปเสถียรของออกซิเจนในวงปีไม้สัก แสดงถึงความแห้งแล้ง โดยเฉพาะในช่วงศตวรรษที่ 18 ซึ่งปรากฏการณ์เอลนีโญและความผันแปรของระบบอากาศในซีกโลกใต้ (เอลโซ่) มีอิทธิพลต่อภูมิอากาศของประเทศไทยในช่วงปี ค.ศ. 1870-1906, 1907-1943, และ 1944-1980 มากกว่าช่วงปี ค.ศ. 1981-2015 ข้อมูลจากหลักฐานทางธรรมชาติจากโครงการนี้มีความเป็นไปได้ว่าเป็นข้อมูลที่มีความละเอียดสูงที่สุดและยาวนานที่สุด ซึ่งผลผลิตของโครงการนี้ช่วยสนับสนุนการประกอบรวมของข้อมูลลมมรสุมทวีปเอเชียที่มีคุณภาพสูงให้มีความสมบูรณ์

คำสำคัญ: โฮโลซีน / ลมมรสุมทวีปเอเชีย / หินงอก / สัก/ วงปีไม้ / อัตราการโต / ไอโซโทปเสถียรของออกซิเจน

CONTENTS

CONTENTS (cont.)

LIST OF TABLES

LIST OF FIGURES

LIST OF FIGURES (cont.)

LIST OF FIGURES (cont.)

LIST OF FIGURES (cont.)

LIST OF FIGURES (cont.)

LIST OF FIGURES (cont.)

LIST OF FIGURES (cont.)

LIST OF FIGURES (cont.)

LIST OF FIGURES (cont.)

LIST OF FIGURES (cont.)

LIST OF FIGURES (cont.)

LIST OF GLOSSARY AND ABBREVIATIONS

ß-/^{14}N: Emission of ß particle (electron) to nitrogen-14**.**

δ: *the delta notation*, a relative measure of the difference, typically ratios of molar concentrations of stable isotopes between a substance and an agreed-upon standard material.

^{14}δ, ^{14}A, ^{14}a, ^{14}Δ: notation used to express the value of the isotope of carbon-14**.**

δ^{13}C: notation used to express the value of the carbon isotope ratio ($^{13}C/^{12}C$) in a sample relative to that in a standard. Thus $\delta^{13}C = [(^{13}C/^{12}C_{sample})/(^{13}C/^{12}C_{standard})-1]x1000$, where s is the sample (unknown) and std is a standard that has been calibrated relative to the Pee Dee Bellemnite (PDB), usually expected as Vienna Pee Dee Bellemnite (VPDB).

δ^{18}O: notation used to express the value of the oxygen isotope ratio ($^{18}O/^{16}O$) in a sample relative to that in a standard. Thus $\delta^{18}O = [(^{18}O/^{16}O_{sample})/(^{18}O/^{16}O_{standard})-1]x1000$, where s is the sample (unknown) and std is a standard that has been calibrated relative to the Pee Dee Bellemnite (PDB), usually expected as Vienna Pee Dee Bellemnite (VPDB) or Vienna Standard Mean Ocean Water (VSMOW).

$\delta^{18}O_{atm}$: δ^{18}O from atmosphere.

$\delta^{18}O_{bio}$: δ^{18}O from biological activity.

$\delta^{18}O_c$: δ^{18}O in calcite.

$\delta^{18}O_p$: δ^{18}O from plant.

λ: *Lambda,* notation used to represent decay constant which is the probability that an atom will decay in unit time.

µg: *microgram,* is a unit of mass equal to 1/1,000,000 of a gram (1×10^{-6}), or 1/1000 of a milligram.

AD: *Anno Domini,* used to indicate that a time division falls within the Christian era.

LIST OF GLOSSARY AND ABBREVIATIONS (cont.)

Amino acid recemization: is a dating technique used to estimate the age of a specimen in paleobiology, archaeology, forensic science, and other fields. This technique relates changes in amino acid molecules to the time elapsed since they were formed.

AMS: *Accelerator Mass Spectrometry*

asl: *above mean sea level*

ASO: *August September October*

BP: *Before Present*, generally base on 1950 year.

Bq/gC: *Bequerel per gramme of Carbon*

^{12}C: *Carbon-12*, is the more abundant of the two stable isotopes of the element carbon, accounting for 98.89% of carbon; it contains 6 protons, 6 neutrons, and 6 electrons.

^{13}C: *Carbon-1*3, is a natural stable isotope of carbon and one of the environmental isotopes. It makes up about 1.1% of all natural carbon on Earth.

^{14}C: *Carbon-1*4, is a radioactive isotope of carbon with a nucleus containing 6 protons and 8 neutrons. Its presence in organic materials is the basis of the radiocarbon dating method to date archaeological, geological, and hydrogeological samples.

cm: *centimetre*, is a unit of length in the metric system, equal to one hundredth of a metre, which is the current SI base unit of length. Centi is the SI prefix for a factor of 10^{-2}**.**

C_3 plants: *Calvin cycle*, The C_3 pathway operates in about 85% of plant species and dominates in most terrestrial ecosystem. Most C_3 plants have $\delta^{13}C$ values that range from -24 to -30‰ with an average value of about -27‰. These differences are preserved as distinctive ranges in secondary carbonates, typically -14% to -6% for carbonates deposited in equilibrium with CO_2 respired from C_3 plants.

LIST OF GLOSSARY AND ABBREVIATIONS (cont.)

C_4 plants: *Hatch-Slack cycle,* C_4 species represent less than 5% of floral species, but dominate in hot open systems such as tropical and temperate grasslands, common agriculture. C_4 plants have $\delta^{13}C$ values that range from -10 to -16‰, mean value of about -12.5‰, however in secondary carbonates, typically -6% to +2% for carbonates deposited in equilibrium with CO_2 respired from C_4 plants.

DOC: *Dissolved Organic Carbon*

Dendrochronology: the study of climate and environmental change through analysis of tree and annual growth layer in wood.

DPI: *Dots Per Iinch,* is a measure of spatial printing or video dot density, in particular the number of individual dots that can be placed in a line within the span of 1 inch (2.54 cm). The DPI value tends to correlate with image resolution, but is related only indirectly.

Dpm/gC: *Disintegrations per minute per gramme of Carbon*

ENSO: *El Niño-Southern Oscillation*

Fission track: is a radiometric dating technique based on analyses of the damage trails, or tracks, left by fission fragments in certain uranium-bearing minerals and glasses.

Fractionation: partitioning of isotopes between substance or between two phases that results in a preferential uptake or release of one isotope (i.e., lighter or heavier) relative to another is termed ‘fractionation’.

Growth rate: is expressed as increasing laminae thickness per unit of time. Growth rate values are reported in mm/yr.

Half-life: is the time required for half the parent material to decay to daughter material.

Hiatus: gap or interruption in space, time, or continuity**.**

LIST OF GLOSSARY AND ABBREVIATIONS (cont.)

Holocene: is a geological epoch which began approximately 11,700 years ago. According to traditional geological thinking, the Holocene continues to the present. The Holocene is part of the Quaternary period. It has been identified with the current warm period, known as MIS 1, and can be considered an interglacial in the current ice age.

IAEA: *International Atomic Energy Agency*, is the world's center of cooperation in the nuclear field. It was set up as the world's "Atoms for Peace" organization in 1957 within the United Nations family. The secretariat is headquartered at the Vienna International Centre in Vienna, Austria.

ICP-MS: *Inductively Coupled Plasma- Mass Spectrometer*

Incidence reversals: is a change in the orientation of Earth's magnetic field such that the positions of magnetic north and magnetic south become interchanged. These events often involve an extended decline in field strength followed by a rapid recovery after the new orientation has been established. These events occur on a scale of tens of thousands of years or longer.

Isotopic equilibrium: is the partial separation of isotopes between two or more substances in chemical equilibrium. Equilibrium fractionation is strongest at low temperatures, and forms the basis of the most widely used isotopic paleothermometers (or climate proxies). It is thus important for the construction of geologic temperature records. Most equilibrium fractionations are thought to result from the reduction in vibrational energy (especially zero-point energy) when a more massive isotope is substituted for a less massive one. This leads to higher concentrations of the massive isotopes in substances where the vibrational energy is most sensitive to isotope substitution, i.e., those with the highest bond force constants.

ITCZ: *Intertropical Convergence Zone*, is the area encircling the earth near the equator where winds originating in the northern and southern hemispheres come together.

ka: *kiloannum*, is a unit of time equal to one thousand (10^3) years.

LIST OF GLOSSARY AND ABBREVIATIONS (cont.)

K/Ar: *Potassium-argon*, is a radiometric dating method used in geochronology and archeology. It is based on measurement of the product of the radioactive decay of an isotope of potassium (K), which is a common element found in many materials, such as micas, clay minerals, tephra, and evaporites, into argon. In these materials, the decay product ^{40}Ar is not trapped by the rock while it is liquid (molten), but starts to accumulate when the rock solidifies (recrystallises). Time since recrystallization is calculated by measuring the ratio of the amount of ^{40}Ar accumulated to the amount of ^{40}K remaining. The long half-life of ^{40}K allows the method to be used to calculate the absolute age of samples older than a few thousand years.

keV: *kiloelectron Volt*

Kinetic isotope fractionation effects: non-equilibrium fractionation, found for example in diffusion-controlled evaporation, or biologically-controlled process.

Lacustrine: relating with lake.

Lamina thickness: is the average distance between visible laminae along three different routes. Laminae thickness values are reported in mm.

Lichenometry: is a geomorphic method of geochronologic aging that uses lichen growth to determine the age of exposed rock.

Loess: an aeolian sediment formed by the accumulation of wind-blown silt and lesser and variable amounts of sand and clay that are loosely cemented by calcium carbonate. It is usually homogeneous and highly porous and is traversed by vertical capillaries that permit the sediment to fracture and form vertical bluffs.

LSS: *Liquid Scintillation Spectrometry*

m: *metre***,** is the basic unit of length in the International System of Units (SI).

Max. ß energy: *Maximum Beta Energy*, is The maximum energy of beta radiation from the majority of nuclides.

MC-ICPMS: *Multi-Collector Inductively Coupled Plasma Mass Spectrometry***.**

MJJ: *May June July*

LIST OF GLOSSARY AND ABBREVIATIONS (cont.)

mm: *millimetre*, is a unit of length in the metric system, equal to one thousandth of a metre, which is the SI base unit of length.

NIST: *National Institute of Standards and Technology*, is a federal technology agency that develops and promotes measurement, standards, and technology.

Obsidian hydration: is a geochemical method of determining age in either absolute or relative terms of an artifact made of obsidian.

Paleomagnetic dating: is the study of the record of the Earth's magnetic field preserved in various magnetic minerals through time. The study of paleomagnetism has demonstrated that the Earth's magnetic field varies substantially in both orientation and intensity through time.

***p*CO_2:** *partial pressure of carbon dioxide*, a measurement of the concentration of CO_2 in the atmosphere and water. The unit is atm.

Per mill (‰): literally parts per thousand, the conventional unit for expressing isotope delta (δ) value.

PGC: *Pyrolysis Gas Chromatography*

Phenological: the study of periodic plant and animal life cycle events and how these are influenced by seasonal and interannual variations in climate.

ppb: *part per billion*

ppm: *part per million*

Radioisotopic dating: is a technique used to date materials, usually based on a comparison between the observed abundance of a naturally occurring radioactive isotope and its decay products, using known decay rates.

Secular variations: studies look at small-scale changes in the direction and intensity of the Earth's magnetic field. The magnetic north pole is constantly shifting relative to the axis of rotation of the Earth. Magnetism is a vector and so magnetic field variation is made up of palaeodirectional measurements of magnetic declination and magnetic inclination and palaeointensity measurements.

LIST OF GLOSSARY AND ABBREVIATIONS (cont.)

SOI: *Southern Oscillation Index*

Speleothem: secondary carbonate accumulations such as stalagmites, stalactite and flowstones deposited in cave by degassing of cave drip-water that are supersaturated with respect to calcium carbonate.

SST: *Sea Surface Temperature*

Tephrochronology: is a geochronological technique that uses discrete layers of tephra-volcanic ash from a single eruption-to create a chronological framework in which paleoenvironmental or archaeological records can be placed.

^{229}Th: *Thorium-229*, is a radioactive isotope of Thorium that decays by alpha emission with a half life of 7340 years. ^{229}Th is produced by the decay of uranium-233, and its principal use is for the production of the medical isotopes actinium-225 and bismuth-213**.**

^{230}Th: *Thorium-230*, is a radioactive isotope of thorium which can be used to date corals and determine ocean current flux. Ionium was a name given early in the study of radioactive elements to the ^{230}Th isotope produced in the decay chain of ^{238}U before it was realized that ionium and thorium are chemically identical.

Thermoluminescence: is a radiometric dating technique which is determination by means of measuring the accumulated radiation dose of the time elapsed since material containing crystalline minerals was either heated (lava, ceramics) or exposed to sunlight (sediments). As the material is heated during measurements, a weak light signal, the thermoluminescence, proportional to the radiation dose is produced.

TIMS: *Thermal Ionisation Mass Spectrometry*

TM: *Thailand monsoon*

Trace element: chemical element. The concentration is less than 1000 ppm or 0.1% of a rock's composition. The term is used mainly in igneous petrology.

LIST OF GLOSSARY AND ABBREVIATIONS (cont.)

^{233}U: *Uranium-233,* is a fissile artificial isotope of uranium, part of the thorium fuel cycle which has been used in a few nuclear reactors and has been proposed for much wider use as a nuclear fuel. It has a half-life of 160,000 years. Uranium-233 is produced by the neutron irradiation of thorium-232.

^{236}U: *Uranium-236,* is an isotope of Uranium that is neither fissile with thermal neutrons, nor very good fertile material, but is generally considered a nuisance and long-lived radioactive waste. It is found in spent nuclear fuel and in the reprocessed uranium made from spent nuclear fuel. U-235 that absorbs a thermal neutron may go one of two ways. About 82% of the time, it will fission. About 18% of the time it will not fission, instead emitting gamma radiation and yielding U-236.

^{238}U: *Uranium-238,* is the most common isotope of uranium found in nature. When hit by a neutron, it eventually becomes plutonium-239 (Pu-239).

VPDB: *Vienna Pee Dee Bellemnite*

VSMOW: *Vienna Standard Mean Ocean Water*

WMO: *World Meteorological Organization*

Yr: *year*

CHAPTER I
INTRODUCTION

1.1 Rationales

The Asian Summer Monsoon (ASM) is an important component of global monsoons and is one of the dominant summer rainfall regimes in the world. Changes in the ASM activity have strong implications for the economy and livelihood of more than two billion people, which are directly or indirectly affected by the timing and amount of precipitation during the ASM season. Heavy rains brought by monsoon can cause severe floods and the most devastating drought caused by monsoon failures can also lead to severe famine in the Asian monsoon regions (Cook et al., 20010). In order to improve our adaptability to extreme climate, especially under the background of ongoing global warming, better understanding of the nature of ASM is necessary. These include long-term evolution, dynamics, and their associated mechanisms of the ASM on different timescales. Holocene, which means "entirely recent" or "wholly modern", is the geological epoch that starts from the most recent period of Earth history entirely to the present day, i.e. the past ~11,600 years (Wanner et al., 2008; Walker et al., 2009). The middle Holocene is warmer than present, and is looked upon as analogue of future global warming. This epoch is the most important period for studying the relationship between humanity and Earth's system (Wu et al., 2012). Therefore, Holocene climate has long been one of key focuses of climatologist and global change research community.

Previous works have drawn the general picture of the ASM history in the Holocene. However, some of key issues about the Holocene ASM dynamics are still under debate. For example, the exact connections and mechanisms among different components (i.e., the Indian summer monsoon (ISM), the East Asian summer monsoon (EASM), and the Western North Pacific summer monsoon (WNPSM) (Wang and Linho, 2002) of the ASM are never without debate (An et al., 2000; Wang et al., 2005). Improving our understanding of the ASM and its relations with oscillatory modes of coupled

ocean-atmosphere variability, thus requires the development of records from different ASM domains as well as different climate settings, including prehistoric times when these oscillatory modes and the Asian monsoon behaved differently from the present day.

Because of the limitation of long-term instrumental climate records, natural climate proxies have become vital dataset for exploring nature of Holocene (Wang et al., 2005, and references therein). Until now, a large number of studies have been performed to reconstruct the ASM history during the Holocene. Among all of them, stalagmites (Fleitmann et al., 2007; Cai et al., 2010), and tree rings (Buckley et al., 2007; Zhu et al., 2012) are the most important archives of the ASM. Stalagmite could provide well-dated and continuous climatic records over long time intervals (Fairchild et al., 2006), while tree-ring chronologies allow high-resolution (monthly to annual) calibration with climate and other factors (Jones et al., 2009). In addition, adequate understanding of the factors controlling speleothem (Fairchild et al., 2006) and tree ring's properties (Roden et al., 2000) have added the advantage over many other proxies.

Thailand is a country in the Southeast (SE) Asia, which is situated in the region where the IM converges with the WNP monsoons (Takahashi and Yasunari, 2006; Wang and Ho, 2002; Wei et al., 2018). As the boundary or transition, Thailand receives moisture from different sources associated with each monsoon regime (Aggarwal et al., 2004). Thus, climate data from the country is key for better understanding of monsoon climate in the transition zone area (Muangsong et al. 2016). Recent study shows that Indian, especially Bay of Bengal, and Northwestern Pacific warm pool are also major moisture sources for monsoon climatic region (Zhou et al., 2005). Fujian province is located in the south-eastern front of mainland China, which is typical of the EASM climatic zone. Consider that they share similar moisture sources originating from the North western Pacific Ocean, integrated study on stalagmites-based ASM records from Fujian, Yunnan China and Thailand, would allow us to explore interaction among the ISM, EASM, and WNPSM, as well as their relations with oscillatory modes of coupled ocean–atmosphere variability.

To this end, the main purposes of this project are; 1) to produce annual resolution records of Asian summer monsoon over the past few centuries based on

stalagmites and tree rings collected from Thailand in order to understand the short-term climatic variation, and 2) to combine climate records from stalagmites collected from the two Asian monsoon regions (Yunnan China as representing proxy from the ISM domain, and Fujian China as representing proxy from the EASM domain) and one transition region (Thailand) in order to synthesize the large-scale and long-term dynamic changes of the Holocene Asian monsoon, and 3) to investigate driving mechanisms of the Asian monsoon circulation and its teleconnection to global climate change. In this project, we took advantage of our previous well collaborative-studied works in Northwestern Thailand over the past years (Cai et al., 2010, Muangsong et al., 2011, Muangsong et al., 2014; Buajan et al., 2016; Muangsong et al., 2016), and our Chinese cooperation partner's preliminary works in Fujian and Yunnan China, to improve distribution of the Holocene climate records over the entire Asian monsoon region, hence to better understand the variability and associated mechanism by detailed comparisons of high-resolution, well-dated the ASM records. Thai proxy records of this study would probably be the most high-resolution and longest records for Thailand monsoon. High-quality and short term proxy records would have potentially significant implications to give a better understanding of teleconnections within the modern atmosphere as well as to quantify the climatological parameters in the long-term climate reconstruction. This project particularly focus on the areas where future study will most benefit to improve climate forecasts, especially in the monsoon transition area.

1.2 Objectives

1) To produce high-resolution composite records of Asian summer monsoon over the past few centuries based on stalagmites and tree rings collected from Northern, Northwestern, and Southern Thailand.

2) To reconstruct and synthesize the large-scale and long-term dynamic changes of the Holocene Asian monsoon based on stalagmites from the two Asian monsoon regions (Yunnan and Fujian, China) and one transition region (Mae Hong Son, Thailand).

3) To investigate both short-term and long-term driving mechanisms of the Asian monsoon circulation and its teleconnection to global climate change.

4) To carry out a systematic cave and climate monitoring program in Thailand for better understanding of climate signal derived from stalagmites and tree rings.

1.3 A brief literature review

The term "monsoon" typically refers to a seasonal wind shift between winter and summer (e.g. Wang et al., 2005), notably in tropical and subtropical Asia. The Asian summer monsoon (ASM) can be generally divided into three subsystems including the Indian summer monsoon (ISM), the East Asian summer monsoon (EASM), and the Western North Pacific summer monsoon (WNPSM) (Wang and Linho, 2002). The Asian summer monsoon (ASM) contributes most of precipitation totals in Asia and provides the water required for all agriculture and social activities. Heavy rains brought by monsoon can cause severe floods and the most devastating drought caused by monsoon failures can also lead to severe famine in the Asian monsoon regions (Cook et al., 2005). In order to improve our adaptability to extreme climate, especially under the background of ongoing global warming, better understanding of the nature of ASM is necessary. These include long-term evolution, dynamics, and their associated mechanisms of the ASM on different timescales.

Holocene, which means "entirely recent" or "wholly modern", is the geological epoch that starts from the most recent period of Earth history entirely to the present day, i.e. the past ~11,600 years (Wanner et al., 2008; Walker et al., 2009). There are several warm periods on difference time scales during the Holocene, for example, on orbital scale, the mid Holocene is much warmer than today, and on multi-centuries scale, the Middle age is as warm as present. On the other hands, the warm Holocene climate has been punctuated by a serial of abrupt "cold event" (Bond et al., 2001; Wang et al., 2005). The Holocene climate evolution history contains variability and their associated mechanisms on difference time scales. Therefore, the Holocene can be acted as a background of moden climate and as a resemblance of ongoing global warming (Wu et al., 2012). This epoch is the most important period for studying the relationship between humanity and Earth's system (Wu et al., 2012). Therefore, Holocene climate has long been one of key focuses of climatologist and global change research community.

Previous works have drawn the general picture of the ASM history in the Holocene. However, some of key issues about the Holocene ASM dynamics are still under debate. For example, the exact connections and mechanisms among different components (ISM, EASM, and WNPSM) of the ASM are never without debate. Cave records from the EASM (Wang et al., 2005) propose that their variability are synchronic through Holocene, while other studies (An et al., 2000) propose asynchronous trend in the Holocene. The response and associated mechanism of the ASM to millennium scale abrupt climate changes, which are sustain for few centuries and are original found in the North Atlantic Ocean (Bond et al., 2001), are still unclear. On seasonal to decadal time scales, oscillatory modes of coupled ocean-atmosphere variability, the Indian Ocean Dipole (IOD) (Saji, 1999; Abram et al., 2007), El Nino-Southern Oscillation (ENSO), as well as the Pacific Decadal Oscillation (PDO) (Kumar et al., 1999), could cause climatic extremes and socio-economic hardship. Their historic interactions and relationships with the ASM are under much debate. Given that regional monsoons are driven by annual cycle of solar radiation and bonded by the global divergent circulation, they should not be studied separately (Wang and Ding, 2011). Improving our understanding of the ASM and its relations with oscillatory modes of coupled ocean-atmosphere variability, thus requires the development of records from different ASM domains as well as different climate settings, including prehistoric times when these oscillatory modes and the Asian monsoon behaved differently from the present day.

Until now, however, distribution of high-resolution the Holocene ASM records are uneven. Most of them are from the ISM domain (Fleitmann et al., 2007; Sinha et al., 2011), Southern China (Wang et al., 2005; Hu et al., 2008; Cai et al., 2010), and Northern China (Cai et al., 2008; Xu et al., 2011). Furthermore, integrated studies on their interaction between subsystems of the ASM are rare for the Holocene. There have been relatively less attention paid to exploring the climate in the boundary area or transition zone among the different monsoon regions (Wang et al., 2010; Liu et al., 2012; Xu et al., 2015), including Thailand and Southern Yunnan, China. Even in the EASM domain, there are still no any reliable high-resolution monsoon records covering the whole Holocene in broadly Southeastern China, e.g. Fujian and surrounding area.

Because of the limitation of long-term instrumental climate records, natural climate proxies have become vital dataset for exploring nature of Holocene (Wang et al., 2005, and references therein). Until now, a large number of studies have been performed to reconstruct the ASM history during the Holocene. Among all of them, stalagmites (Fleitmann et al., 2004; 2005; Cai et al., 2008; Cai et al., 2010; Cai et al., 2015), and tree rings (Buckley et al., 2007; Borgaonkar et al., 2010; Zhu et al., 2012; Yang et al., 2014) are the most important archives of the ASM. Stalagmite could provide well-dated and continuous climatic records over long time intervals (Walker, 2005; Fairchild et al., 2006), while tree-ring chronologies allow high-resolution (monthly to annual) calibration with climate and other factors (Jones et al., 2009). In addition, adequate understanding of the factors controlling speleothem (Fairchild et al., 2006; Mickler et al., 2006; Van Rampelbergh et al., 2014) and tree ring's properties (Roden et al., 2000; McCarroll & Loader, 2004; OgÉE et al., 2009) have added the advantage over many other proxies.

Thailand is a country in the Southeast (SE) Asia. As the boundary or transition, Thailand receives moisture from different sources associated with each monsoon regime, the difference in the stable oxygen isotope ratios ($\delta^{8}O$) of seasonal monsoon rainfall originates from distinct moisture sources and is associated with large-scale monsoon circulations (Aggarwal et al., 2004). Thus, climate data from the country is key for better understanding of monsoon climate in the transition zone area (Muangsong et al. 2016). In our previous study, we reported evidence that changes in moisture sources and rainfall patterns, which we referred to as 'monsoon intensity', can affect the $\delta^{18}O$ of stalagmite NJ-1 collected from Namjang cave (19°40′30″N, 98°12′12″E) in the Mae Hong Son province of Northwestern Thailand (Cai et al., 2010). We therefore highlighted that seasonal variability of summer monsoon rainfall can affect the inter-annual variations of speleothem proxies (Cai et al., 2010; Muangsong et al., 2011). High-resolution dendro-isotope study by Muangsong et al. (2016) also confirmed the influence of the ISM and WNPSM on intra-annual (seasonal) variations in the $\delta^{8}O$ values of teak (*Tectona grandis* Linn.) tree-ring cellulose from Northwestern Thailand. Our recent study indicated that the Indian Ocean, especially over the Bay of Bengal, is the primary moisture source for precipitation during the early rainy season, while the western North Pacific Ocean and the South China Sea

probably contribute to the source of moisture for the late rainy season in Thailand (Muangsong et al. 2016). Unfortunately, high-resolution proxy climate data available from Thailand and surrounding China area are relatively rare compared to other monsoon regions. The longest, high-resolution (annual scale) chronologies from Thailand presently extend back only the past 448 years for tree rings and 387 years for stalagmite (Muangsong et al. 2014). Recent study shows that Indian, especially Bay of Bengal, and Northwestern Pacific warm pool are also major moisture sources for monsoon climatic region (Zhou et al., 2005). Fujian province is located in the south-eastern front of mainland China, which is typical of the EASM climatic zone. Consider that they share similar moisture sources originating from the North western Pacific Ocean, integrated study on stalagmites-based ASM records from Fujian, Yunnan China and Thailand, would allow us to explore interaction among the ISM, EASM, and NWPSM, as well as their relations with oscillatory modes of coupled ocean–atmosphere variability. Numeral geological climate records covering the Holocene have been reconstructed to explore the nature of ASM. However, the high-resolution robust records from some key sub-systems of ASM domain, e.g., Southeastern China, Western Yunnan, and Thailand, are still limited. Advance knowledge of the regional monsoons, especially in the transition area can result in a broad and complete understanding of the entire Asian monsoon circulation.

1.4 Conceptual Framework

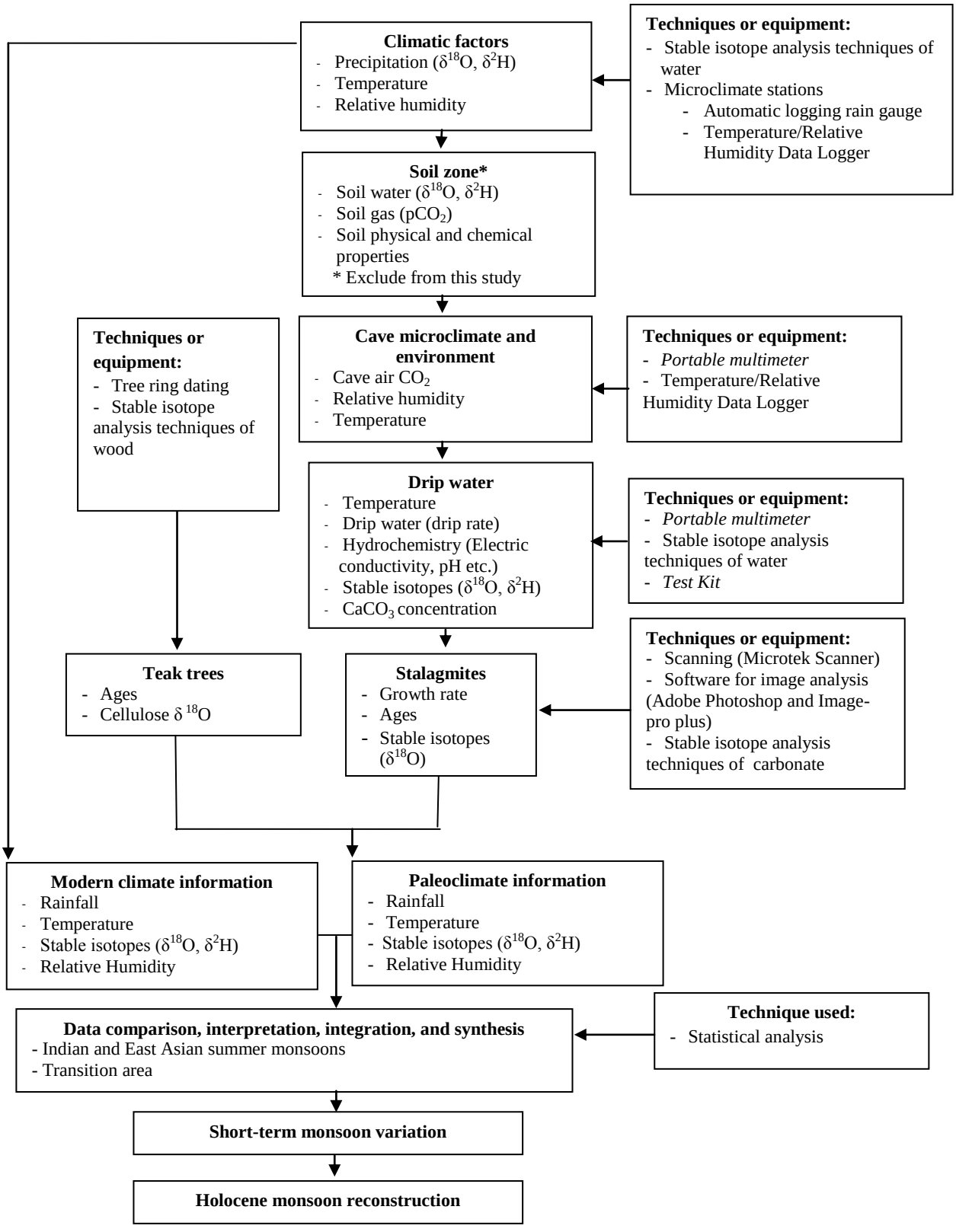

1.5 Scope of the study

1) Population/Samples scope

Stalagmites (approximately 2-10 samples of fallen or broken stalagmites available from previous works and current fieldwork in this projects). Thai teak trees (at least 10 living tree cores and 2 log coffin samples).

2) Variable scope

2.1) Parameters are stable oxygen isotopic compositions of stalagmites and tree-ring cellulose, ages, and growth rate for stalagmites (ring widths for trees).

2.2) For modern stalagmite precipitates, the parameters include stable oxygen isotopic compositions of modern aragonite precipitates, stalagmite growth rate as defined by the accumulated weight of glass plates.

2.3) For rainfall, the parameters include stable oxygen isotopic compositions of rainfall and rainfall amount.

2.4) For cave drip water, the parameters include stable oxygen isotopic compositions of cave drip water, drip rate, drip water temperature, Electrical Conductivity (EC), pH, carbonate hardness/alkalinity (as CaCO3 concentration).

2.5) Additional parameters for cave and climate conditions include air temperature, CO_2, and Relative Humidity (RH).

3) Timing scope from September 2016 to August 2019 (Duration three years)

4) Area scope

Study sites locate in Northern (Chiang Mai province), Northwestern (Mae Hong Son and Tak provinces), and Southern (Krabi and Satun provinces) parts of Thailand. In China, study sites locate in Beijing, Liaoning, Yunnan and Fujian provinces.

1.6 Project member

Name	University/Organization
Thai Principal Investigator	
Dr. Chotika Muangsong	Mahidol University
Chinese Principal Investigator	
Prof. Dr. Binggui Cai	Fujian Normal University
Co-researcher from Thailand	
Assoc. Prof. Dr. Nathsuda Pumijumnong	Mahidol University
Co-researcher from China	
Prof. Dr. Guoliang Lei Prof. Dr. Jiang Xiuyang Dr. Xiuling Chen	Fujian Normal University
Postdoctoral researcher	
Dr. Supaporn Buajan	Mahidol University
Research assistant	
Miss Kittapha Malimart	Mahidol University
Miss Tippawan Kunkoon	Mahidol University
Ph.D. candidate	
Miss Fang Wang	Fujian Normal Universiy
Mr. Miaofa Li	Fujian Normal Universiy
Mrs. Sineenart Preechamart	Mahidol University
Miss Kanokrat Buareal	Mahidol University
Co-researcher from the Ministry of Natural Resources and Environment in Thailand	
นายนิกร แก้วโมรา	เขตรักษาพันธุ์สัตว์ป่าลุ่มน้ำปาย
นายบำรุงรัตน์ พลอยดำ	เขตรักษาพันธุ์สัตว์ป่าเขาบรรทัด
นายพัทยา เท็กกิ้ม	เขตรักษาพันธุ์สัตว์ป่าสันปันแดน
นายศรัทธา กุนทอง	เขตรักษาพันธุ์สัตว์ป่าเชียงดาว
นายวีระ กอแก้ว	อุทยานแห่งชาติแม่เมย
นายสมศักดิ์ ฐิติชยาภรณ์	อุทยานแห่งชาติดอยผ้าห่มปก
นายสมชาย นุชนานนท์เทพ	สำนักจัดการทรัพยากรป่าไม้ที่ 12 สาขากระบี่

CHAPTER II
METHODOLOGY

2.1 Study area and sampling collection

1) Study area

Study sites are located in Northern (Chiang Mai and Phrae provinces), Northwestern (Mae Hong Son and Tak provinces), and Southern (Krabi and Satun provinces) parts of Thailand (Figure 2.1.1 and 2.1.2, and Table 2.1.1). For the study sites in China, some of stalagmite samples were chosen from Shanggan Cave (23° 30' N, 99° 40' E), Lincang city in the Southwest, Sharendong cave, Kunming city in the central, Qiwen cave (26° 31' N, 99° 36' E), Jianchuan city in the Northwest of Yunnan province, and Xinyan Cave (24° 50' N, 116° 10' E), Longyan city in the West of Fujian province (Figure 2.1.1). Samples (Teak trees and stalagmites) collected from Thailand and some locations from Yunnan representing proxies from the transition area, while samples collected from some sites from Yunnan and Fujian China representing proxies from ISM and EASM, respectively (Figure 2.1.1). Additional stalagmite samples were derived from pieces of fallen or broken stalagmites in caves available from previous projects. Details of studied samples were presented in Table 2.1.1 and 2.1.2.

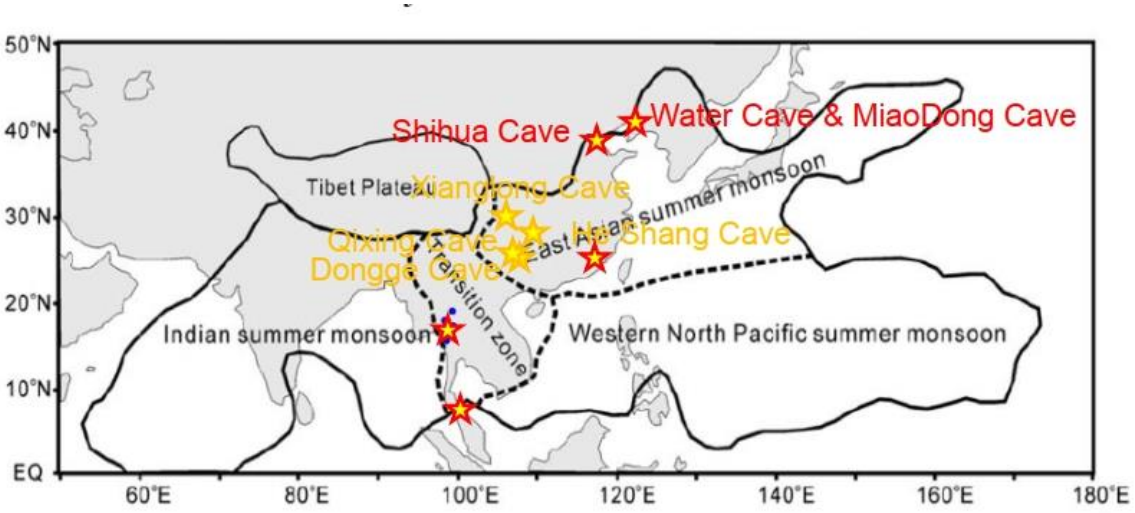

Figure 2.1.1 Map showing major subsystems of the Asian summer monsoon, transition region (after Wang and Lin (2002); Li et al. (2014)), and spatial distribution of stalagmites available for analysis from Thailand (red filled stars) and China (yellow filled stars).

Figure 2.1.2 Spatial distribution of tree rings and stalagmites available for analysis from Thailand (red filled circles)

Table 2.1.1 Details of studied stalagmite samples from China

Sample Name	Cave Name	Location	Length (mm)	Age covering (Yr BP)	Mineral composition
SGL1220	Sigangli (1)	Yunnan	1038	~9000-5500	aragonite
SGL01	Sigangli (1)	Yunnan	164	~ 628 - 43	calcite
SGL04	Sigangli (1)	Yunnan	160	~ 1289 -60	aragonite
XY-1701	Xianyun (2)	Fujian	150	~ 2931 - 2259	calcite
XY-1703	Xianyun (2)	Fujian	380	~ 9977 - 5767	calcite
XYIII-1	Xianyun (2)	Fujian	472	~3026 - 764	calcite
XYIII-4	Xianyun (2)	Fujian	200	~11413 - 9605	calcite
XY1720	Xianyun (2)	Fujian	160	~11404 - 8287	calcite
CS01C	Shihua (3)	Beijing	110	~11290 - 10200	calcite
SHD1311	Shihua (3)	Beijing	178	~10950-9900	calcite
MD11	Miao (4)	Liaoning	216	~4095 - 39	calcite
MD12	Miao (4)	Liaoning	178	~2924 - 329	calcite
TW02	Shuidong (5)	Liaoning	158	~5170 - 520	calcite
TW701	Shuidong (5)	Liaoning	256	~9620 - 3888	calcite
TW702	Shuidong (5)	Liaoning	304	~7470 - 2271	calcite
TW704	Shuidong (5)	Liaoning	234	~5820 - 4770	calcite
TW705	Shuidong (5)	Liaoning	186	~1252-50	calcite

Table 2.1.2 Study sites in Thailand and sample's details for this project*.

Regions	**Provinces**	**Districts**	**Cave/Site**	**Locations**
North	Chiang Mai	Chiang Dao	Khun Kong	19°26′03″N, 98°49′23″E
			Khi Mee	19°21′47″N, 98°43′ 25″E
			Nam Kong	19° 26'N, 98° 8'E
	Phrae	Mueang	Phrae	18°44'45"N, 100°11'45"E
Northwest	Mae Hong Son	Pang Ma Pha	Namjang	19°40′30″N, 98°12′12″E
			Mai Hung	19° 37' 51"N, 98° 11' 42"E
			Pha Peuak	19° 38' 59.61"N, 98° 12' 50.98"E
			Pang Kham	19° 40' 21.18"N, 98° 12' 10.34"E
			Pang Kham Branch	19° 40' 21.18"N, 98° 12' 10.34"E
			Huay Kham	19° 40' 21.12"N, 98° 12' 10.34"E
			Pha Mon 1	19° 30' 8.97"N, 98° 16' 41.90"E
			Tum Lod	19° 33' 54.64"N, 98° 16' 43.76"E
		Mueang	Susa	19°28'16"N, 98°7'41"E
	Tak	Mae Ramat	Mae Tuen	17°07′21″N, 98°39′22″E
South	Krabi	Ao Luek	Klang	8°20′N, 98°44′E
	Satun	Manung	Phu Pha Phet	7°07'35"N 99°59'49"E

*Noted that above sites were explored for their potential but samples were not collected from all sites.

2) Tree ring collection

Healthy teak (T. *grandis* Linn.) trees without signs of disease or physical damage were sampled. Two core samples per tree were taken at breast height (approximately 1.3 m above ground level) using a 5-mm-diameter core borer. Increment cores were fixed in the core holder and stored dry at room temperature. After one week, the fixed wood cores were sanded using progressively finer grits of sandpaper until they showed clear ring-growth patterns and structures.

3) Stalagmite preparation

Each stalagmite was cut into two halves along the growth axis and cleaned with distilled water. The cut surfaces were polished until exhibit clearly visible laminae.

2.2 Analyses of tree rings

1) Tree-ring width measurement and chronology

Tree-ring width measurement and yearly chronology were presented in Muangsong et al., (2020); Pumijumnong et al. (2020). Tree-ring widths (TRW) were measured using a LINTAB moving stage table equipped with a Leica GZ6 microscope at a resolution of 0.001 mm (RINNTECH®, Heidelberg, Germany). Ring-width series were analyzed and crossdated using the TSAP-Win software package (Rinn, 2011). Crossdating of the tree-ring series was statistically verified using COFECHA software (Holmes 1992). ARSTAN software (Cook et al., 2005) was used to produce the standard and residual chronologies. The raw TRW series were detrended by using linear negative slope or negative exponential curve fits to eliminate age trends (Cook and Kairiukstis 1990) and were followed by spline detrending with a 50% cutoff frequency. Next, the detrended data from TRW series were averaged using a bi-weight robust mean to produce the standard and residual chronologies (Cook and Kairiukstis 1990). A new TRW index representative of the site was constructed by using the

residual chronologies. To evaluate the quality of the chronology, the expressed population signal (EPS) and the mean interseries correlation (Rbar) were computed over a 40-year window, lagged by 20 years (Wigley et al. 1984). An EPS above a threshold of 0.85 is accepted (Wigley et al. 1984). Descriptive statistical parameters defined by Fritts (1976), including the mean ring width (MRW), ring standard deviation (SD), and mean ring sensitivity (MS), were also calculated using ARSTAN software (Cook et al. 2005).

Dating within the years, known as monthly or sub-annual chronologies, was previously performed using a linear interpolation technique (Muangsong et al., 2016). This technique has been widely used to estimate the monthly or seasonal chronologies in various natural proxies such as tree rings (Muangsong et al., 2016). The interpolation method was applied to build the sub-annual chronologies (covering the growing period in active monsoon months from May to October (Pumijumnong, 1995; Pumijumnong et al., 2013; Schollaen et al., 2013; Muangsong et al., 2016). Thus, we produced the monthly-scale resolution for tree-ring chronologies covering the growing period from May to October.

2) Stable isotopic ratio measurement

The stable oxygen isotope ratios ($\delta^{18}O$) from α-cellulose samples were analyzed at the Stable Isotope Centre of Fujian Normal University, China using a Thermo Scientific Flash 2000 HT Elemental Analyzer (EA) linked to a MAT-253 mass spectrometer (Thermo Electron Corporation, Bremen, Germany). The accuracy and precision were routinely checked by running the international standard for $\delta^{18}O$ (IAEA-601, 23.3‰) after every ten sample measurements. The analytical precision of the measurements was better than 0.1‰. All of the isotope values are reported in parts

per mil (‰) relative to the international standard, Vienna Standard Mean Ocean Water (VSMOW), in delta (δ) notation. The protocols followed were previously described in our previous studies (Buajan et al., 2016; Muangsong et al., 2016; Muangsong et al., 2018).

2.3 Analyses of stalagmites

1) Stalagmite chronology

Age-depth profiles of stalagmites were developed based mainly on lamina counting chronology and verified by ^{230}Th dating (Muangsong et al., 2014). Polished sections of stalagmites will be scanned using high resolution scanner under a 3200 dpi optical resolution and 48-bit RGB color. The digital images were used for laminae analysis, followed the protocols previously described in the works of Cai et al. (2010). The visible laminae were marked and counted with Adobe Photoshop software. Growth rates were measured via Image-Pro Plus 5.1 software. Powdered samples were drilled for ^{230}Th dating using a 0.9 mm carbide dental burr along their growth bands. The measurements were performed on a magnetic sector inductively coupled plasma mass spectrometer (ICP-MS, Finnigan Element) based on the procedure described by Shen et al. (2002). The ^{230}Th dating results were compared with those of lamina counting between dating points in order to obtain stalagmite ages.

2) Oxygen isotope analysis

On one section, powdered samples were manually drilled using dental drill with 0.5 mm carbide burrs or milled along its respective growth axis, and weighed approximately 150-250 μg for oxygen isotope analysis. Isotopic measurements will be performed following the standard procedures on a MAT-253 mass spectrometer linked to a Gas Bench-II (Thermo-Finnigan). Accuracy and precision will be routinely checked by running the carbonate standard NBS-19 after every six sample measurements. All oxygen isotope values are reported in parts per mil (‰) relative to the Vienna PeeDee Belemnite standard (VPDB) in delta (δ) notation.

2.4 Climate data sets and statistical analysis

The relationships between tree-ring and stalagmite's properties and climatic factors were explored using Pearson correlation analysis using the SPSS software (SPSS, Chicago, USA). For comparison and presentation purposes, annually resolved tree-ring isotope ($\delta^{18}O_{TR}$) series were transformed to a similar scale using Z-score normalization (Wilks, 1995). Scatter diagrams were developed to illustrate the linear relationship between variables. The area-averaged rainfall data obtained from local meteorological as well as the Climatic Research Unit (CRU) TS4.00 gridded precipitation fields derived from the Royal Netherlands Meteorological Institute (KNMI) Climate Explorer (available at http://www.knmi.nl/) (van Oldenborgh and Burgers 2005) were used to represent regional climate in Thailand. The $\delta^{18}O_{Rain}$ data at the Bangkok (BKK) station between AD 1968 and 2009 (IAEA/WMO, 2001) were used to test the influence of source water on $\delta^{18}O_{TR}$. To evaluate the influence of large-scale convection on the tree-ring and stalagmite's properties, spatial correlations were applied between our data and either the Climate Prediction Center (CPC) Outgoing Longwave Radiation (OLR) data (Liebmann and Smith, 1996) or Merged Analysis of Precipitation (CMAP) data (Xie and Arkin, 1997) obtained from the National Oceanic and Atmospheric Administration's Physical Sciences Division of the Earth System Research Laboratory, Boulder, Colorado, United States of America (USA) (available at http://www.esrl.noaa.gov/psd/) with a 0.5° × 0.5° spatial resolution. The OLR has been widely used as an indicator of atmospheric convection over particular regions (Zhu et al., 2012; Hu et al., 2018). The spatial correlations of tree-ring and/or stalagmite series with large-scale CMAP rainfall and OLR data were performed separately between the early rainy (MJJ) and the late rainy (ASO) seasons

to assess the relationship with large-scale convection associated with the monsoonal intraseasonal variations. A low OLR value is indicative of enhanced convective clouds and increased rainfall, and vice versa for a high OLR value (Wang and Xu, 1997). Air mass backward trajectory analyses were also performed to trace the source regions of air masses and moisture transportation into the study area (Hondula et al., 2010), using the free accessible Hybrid Single Particle Lagrangian Integrated Trajectory (HYSPLIT) model obtained from the National Oceanic and Atmospheric Administration (NOAA) Air Resources Laboratory, Silver Spring, Maryland, USA available at https://ready.arl.noaa.gov/HYSPLIT.php (Stein et al., 2015). The 72 h back trajectories at three different heights (500 m, 1,000 m, and 1,500 m above ground level) were produced for each rainy sub-season. The trajectories were calculated for May 1-31, 2012 and September 1-30, 2012 at the study site. These time periods that represent the early rainy (May) and late rainy (September) months, were selected based on a previous study where the $\delta^{18}O_{Rain}$ datasets collected from several locations in Thailand always exhibited a similar change in May and a different isotopic behavior in September (Wei et al., 2018).

2.5 Cave and climate monitoring

1) The precipitation

According to the project entitled “โครงการการเตรียมรับมือและป้องกันผลกระทบจากการเปลี่ยนแปลงสภาพภูมิอากาศที่อาจมีต่อระบบนิเวศและสิ่งแวดล้อมแหล่งธรรมชาติอันควรอนุรักษ์ประเภทถ้ำ (in Thai)” funded by Office of Natural Resources and Environmental Policy and Planning for a period for eight months from November 2015 to June 2016, surface climate and cave monitoring was previously conducted in Phu Pha Phet cave (hereafter referred to as “PPP” cave), from January to April 2016. The cave is located

in Satun province of Southern Thailand. For more in-depth understanding of factors controlling stalagmite's properties and microclimate dynamics in southern Thailand, the monitoring program at the cave has been continuing up to September, 2019 (Figure 2.5.1).

1) Present-day climate and rainfall monitoring

Present-day climate conditions of the study site has been monitored in Phu Pha Phet station (hereafter referred to as "PPP-00" station) which is approximately 20 meters away from Phu Pha Phet cave. The data between January and April, 2016 was previously reported in the project mentioned above. In this progress report, additional climate data from May, 2016 to September, 2019 was presented in this study. The ongoing monitoring program at Phu Pha Phet cave is performed on a monthly basis. Parameters includes rainfall amount, temperature, and relative humidity (RH). Rainfall amount was recorded automatically by HOBO® RG3 data logging rain gauge, while temperature and RH were measured by Onset HOBO® temperature/relative humidity data logger. Rainfall samples for stable isotopes analyses were collected for obtaining a cumulative monthly sample.

2) Cave monitoring

Monitoring work at PPP cave was perform on a monthly timescale from May, 2016 to September, 2019. The monitoring data includes cave environment, drip water hydrology-hydrochemistry and stable isotopes, as well as present-day stalagmite deposition. Thus, the data available in this [roject is the datasets of cave microclimate conditions, drip water hydrology-hydrochemistry, and the deposition rates of stalagmites from PPP cave.

2.1) Cave atmosphere

In order to study the cave meteorology, cave microclimate parameters including temperature and RH were recorded by Onset HOBO® temperature/relative humidity data logger installed in three sites along the cave passage. The first site (hereafter referred to as "PPP-01") is located near the cave entrance, while the second (hereafter referred to as "PPP-02") and third (hereafter referred to as "PPP-03") sites are located in the middle and the end of the main chamber, respectively.

2.2) Drip water hydrology

Drip water hydrology was defined by variations in drip rate which was measured from average continuous times between drips. Eight sampling locations (hereafter referred to as “P-1601 to P-1608”) were selected according to our previous project.

2.3) Drip water hydrochemistry

Carbonate hardness/alkalinity (as $CaCO_3$ concentration) of cave drip water, as one of the important hydrochemical properties to define stalagmite growth, was measured using the Aquamerck® carbonate hardness test kit (Merck Company, German). $CaCO_3$ concentrations for all sampling sites were presented.

2.4) Present-day stalagmite deposition

All glass plates were weighted prior to use, placed under drip sites, and changed every month. In laboratory, glass plates were kept in a clean room, dried at room temperature, and then weighted. The deposition of stalagmite is defined from the weight gain of glass plates.

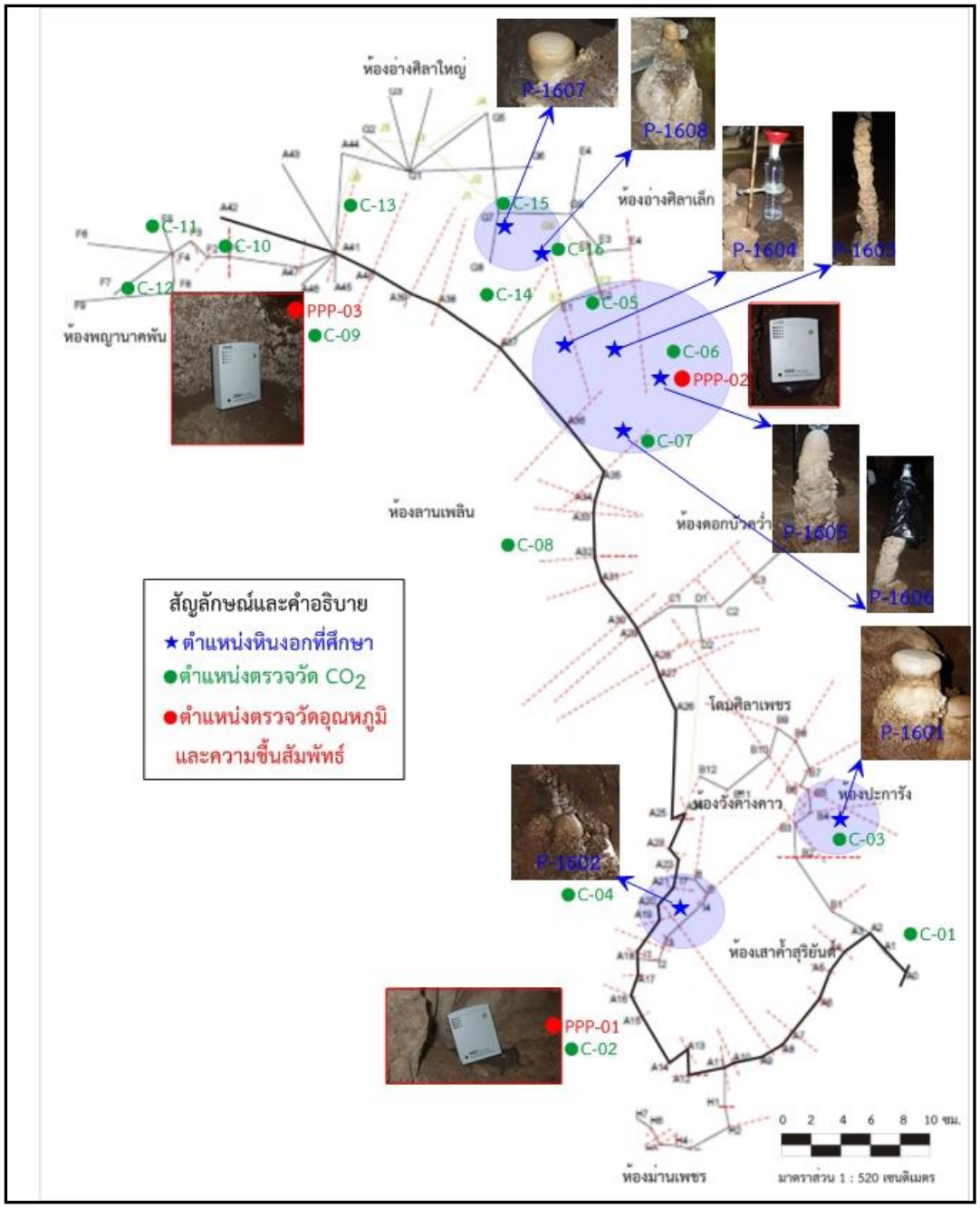

Figure 2.5.1 Map of Phu Pha Phet cave (modified from Russasarin et al. (2016)) showing the location of drip sampling sites (P-1601 to P-1608) (blue filled symboles) and cave microclimate monitoring location (PPP-01 to PPP-03) (red filled symboles).

CHAPTER III
RESULTS AND DISCUSSION

3.1 Dominant factors controlling the tree-ring properties

Thai teak tree-ring widths and $\delta^{18}O$ ($\delta^{18}O_{TR}$) typically records significant climatic parameters including rainfall amounts and seasonality (for example, Buajan et al., 2016) as well as large-scale changes in moisture sources and transport pathways (Muangsong et al., 2016). Furthermore, this species has demonstrated the potential for paleoclimate and paleoenvironmental studies. To assess how well Thai teak parameters (i.e. $\delta^{18}O_{TR}$ and widths) reflects rain signals and how teak tree-ring properties respond to their controlling factors on different timescales, the calibration with parameters controlling $\delta^{18}O_{TR}$ and ring widths at different temporal resolutions is required. Such calibration is necessary for further interpretation the isotopic and ring widths signals preserved in tree ring over a longer time period (i.e., Holocene).

3.1.1 Dominant factors controlling the tree-ring oxygen isotopic signal

The stable oxygen isotope analysis on seven teak trees collected from Phrae Province in northern Thailand at different temporal resolutions was presented. Analyses were carried out on teak trees collected from Phrae province in Northern Thailand at annual resolution as well as sub-annual resolution to test factors affecting tree-ring isotopes in this area (Muangsong et al., 2020). The inter-annual variation is year-to-year change in $\delta^{18}O$ values over several consecutive years. The terms "monthly, intra-annual, and sub-annual" resolutions are used to denoted the variation in monthly mean $\delta^{18}O$ values within a year (i.e., a ring). These results imply that variations in Thai teak cellulose $\delta^{18}O$ values are modulated not only by the local rainfall amount but also by large-scale convection, which varies between different seasons and over time. The results relating to the tree-ring oxygen isotopes and their controlling factors were previously shown in our publications (Muangsong et al., 2019; 2020; Pumijumnong et al., 2020; Xu et al., 2018).

1) Interannual oxygen isotope variations and controlling factors

1.1) Interannual time series of $\delta^{18}O_{TR}$

The oxygen isotopic composition of tree-ring α-cellulose ranged from 21.7‰ to 28.4‰. Generally, the interannual time series of $\delta^{18}O_{TR}$ were remarkably similar in their patterns and isotopic ranges (Figure 3.1.1 (a) and Table 3.1.1 and 3.1.2). The mean difference in $\delta^{18}O_{TR}$ values among series was within 0.1‰, except for GSP19B (0.7‰) (Figure 3.1.1 (c)). The running EPS values were approximately 0.8 (EPS = 0.76-0.84) throughout the entire period except between AD 1943-1962, which had an EPS value far below 0.85 (Figure 3.1.1 (b)). Although the threshold value of the mean EPS was 0.78 (Figure 3.1.1 (b)), there were several periods where the running EPS was greater than the commonly accepted value of 0.85, including AD 1934-1953, AD 1961-1980, and AD 1988-2007 (Figure 3.1.1 (b)). The running Rbar exhibited moderate (0.5) to high (0.8) values except the year around AD 1943 (Figure 3.1.1 (b)). The correlation coefficient (r) was higher than 0.6 ($p < 0.01$) among the series, except for PI03A ($r = 0.4$, $p < 0.01$) (Table 3.1.2), indicating that the $\delta^{18}O_{TR}$ of teak trees in this area was influenced by the same climatic factor. These findings confirm the strong common climatic signal recorded in teak tree rings and robust $\delta^{18}O_{TR}$ chronologies. In a recent study by Buras (2017) suggested that the EPS provides an estimation of how well tree-ring chronology represent population signal back through time and it is not an indicative of the reliability of a chronology. Considering a sufficiently replicated chronology (Figure 3.1.1 (a)), the effect of EPS values lower than 0.85 should be minimized and these tree-ring chronologies can thus be used.

To produce the first long-term record of Thailand Monsoon derived from teak $\delta^{18}O_{TR}$ in northern Thailand, the three $\delta^{18}O_{TR}$ chronologies, including GSP10A (AD 1871-2016), GSP19B (AD 1919-2016), and PI3A (AD 1933-2016), were combined to form a single chronology representing the site's $\delta^{18}O_{TR}$ chronology between AD 1871 and 2016 (hereafter referred to as "Phrae $\delta^{18}O_{Annual}$") (Table 3.1.1-3.1.2 and Figure 3.1.1 (c)). The Phrae $\delta^{18}O_{Annual}$ chronology demonstrated significantly high correlation coefficients with individual $\delta^{18}O_{TR}$ chronologies (r = 0.7-0.9, $p < 0.01$) (Table 3.1.2), which was comparable to the tree-ring records from northwestern (NW) Thailand, including the NK teak index (Pumijumnong, 2012) ($r = -0.38$, $p < 0.01$), the MHS teak

index (Buckley et al., 2007) (r = -0.28, p < 0.05), and the teak NJT-06 cellulose $\delta^{18}O$ record (Muangsong et al., 2019) (r = 0.26, p < 0.05).

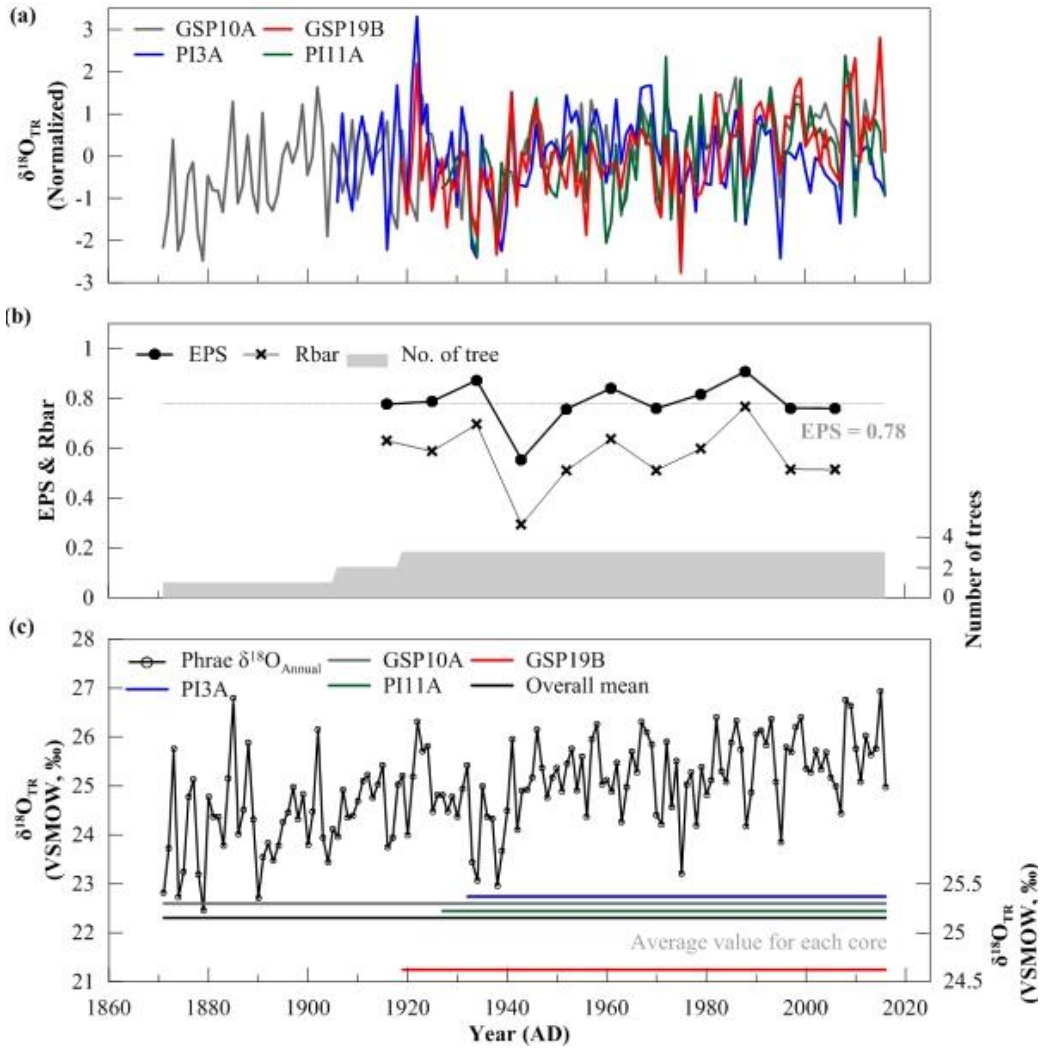

Figure 3.1.1 (a) Interannual cellulose $\delta^{18}O$ profiles of four individual cores including GSP10A (black solid line), GSP19B (red solid line), PI3A (blue solid line), and PI11A (green solid line). For presentation purposes, datasets were transformed into a similar scale using Z-score normalization. (b) The running EPS (black solid line with filled circles), Rbar (black solid line with asterisks) statistics over a 20-year window, lagged by 10 years as well as sample size (gray shading) (c) The Phrae $\delta^{18}O_{Monthly}$ series (black solid line with circles) was constructed by averaging the data of three teak trees (GSP10A, GSP19B, and PI3A) for the period between AD 1871 and 2016. The average $\delta^{18}O_{TR}$ values for GSP10A (gray solid line), GSP19B (red solid line), PI3A (blue solid line), PI11A (green solid line), and overall mean value (black solid line).

Table 3.1.1 Details of selected trees for annual and sub-annual analyses.

Resolutions	Tree no.	Sample codes	Chronology interval	Age (years)	Selected chronology	Number of years	$\delta^{18}O$ Range (‰)	Average $\delta^{18}O$ value (‰)	Standard deviation
Annual	1	GSP10A	1871-2016	146	1871-2016	146	22.5-28.4	25.3	1.15
	2	GSP19B	1890-2016	126	1919-2016	97	21.7-27.6	24.6	1.05
	3	PI03A	1906-2016	111	1933-2016	84	23.2-27.0	25.4	0.87
	4	PI11A	1927-2016	90	1927-2016	90	22.7-27.8	25.2	1.07
Sub-annual	5	GSP5A	1945-2016	72	1978-1987	10	22.2-29.2	25.7	1.60
		GSP5B	1948-2016	69	1978-1987	10	20.0-28.4	25.5	1.81
	6	GSP13A	1936-2015	80	1978-1987	10	21.8-28.3	25.5	1.71
	7	GSP22B	1958-2016	59	1978-1987	10	22.0-28.2	25.4	1.53

Table 3.1.2 Pearson's correlations (*r* Values) among tree-ring oxygen isotope series for annual (GSP10A, GSP19B, PI03A, PI11A, and Phrae $\delta^{18}O_{Annual}$) and monthly (GSP05A, GSP05B, GSP13A, GSP22B, and Phrae $\delta^{18}O_{Monthly}$) time scales. Statistically significant values are shown in italic font.

Cores	GSP10A	GSP19B	PI03A	PI11A	Phrae $\delta^{18}O_{Annual}$
GSP10A	1	*0.61*[b]	*0.44*[b]	*0.65*[b]	*0.91*[b]
GSP19B	*0.61*[b]	1	*0.41*[b]	*0.61*[b]	*0.85*[b]
PI03A	*0.44*[b]	*0.41*[b]	1	*0.48*[b]	*0.71*[b]
PI11A	*0.65*[b]	*0.61*[b]	*0.48*[b]	1	*0.70*[b]
Phrae $\delta^{18}O_{Annual}$	*0.91*[b]	*0.85*[b]	*0.71*[b]	*0.70*[b]	1
Cores	GSP05A	GSP05B	GSP13A	GSP22B	Phrae $\delta^{18}O_{Monthly}$
GSP05A	1	*0.64*[b]	*0.69*[b]	*0.68*[b]	*0.87*[b]
GSP05B	*0.64*[b]	1	*0.68*[b]	*0.49*[b]	*0.83*[b]
GSP13A	*0.69*[b]	*0.68*[b]	1	*0.73*[b]	*0.90*[b]
GSP22B	*0.68*[b]	*0.49*[b]	*0.73*[b]	1	*0.83*[b]
Phrae $\delta^{18}O_{Monthly}$	*0.87*[b]	*0.83*[b]	*0.90*[b]	*0.83*[b]	1

[a] Statistically significant at the 0.05 level

[b] Statistically significant at the 0.01 level

Table 3.1.3 Pearson's correlations (*r* Values) between monthly resolved $\delta^{18}O_{TR}$ values and current year rainfall data available from Phrae (PR: AD 1953-2016), Nan (NA: AD 1951-2016), and combined Phrae and Nan ($PN_{Combined}$: AD 1951-2016) meteorological stations (Thai Meteorological Department, 2013). Statistically significant values are shown in italic font.

Month and season	Single tree chronology												Three chronologies (GSP10A-GSP19B-PI03A)		
	PR				NA				$PN_{Combined}$				PR	NA	PN Combined
	GSP 10A	GSP 19B	PI 03A	PI 11A	GSP 10A	GSP 19B	PI 03A	PI 11A	GSP 10A	GSP 19B	PI 03A	PI 11A			
Jan	0.08	0.11	0.00	-0.00	-0.02	-0.02	-0.14	-0.15	0.02	0.04	-0.08	-0.08	0.09	-0.06	0.01
Feb	0.12	0.16	0.08	0.14	0.00	0.01	0.07	0.08	0.07	0.08	0.09	0.12	0.15	0.03	0.10
Mar	-0.09	-0.07	-0.04	0.16	0.02	0.01	0.05	0.14	-0.03	-0.05	0.04	0.16	-0.08	0.03	-0.02
Apr	*0.30*[a]	0.09	0.13	0.10	0.21	0.15	0.02	0.10	*0.28*[a]	0.13	0.08	0.11	0.22	0.16	0.21
May	-0.23	*-0.28*[a]	*-0.26*[a]	-0.20	-0.16	*-0.28*[a]	-0.12	-0.16	-0.22	*-0.31*[a]	-0.23	-0.20	*-0.33*[b]	*-0.25*[a]	*-0.34*[b]
Jun	0.01	-0.02	-0.07	0.00	*-0.26*[a]	*-0.26*[a]	-0.07	-0.14	-0.15	-0.15	-0.10	-0.08	-0.02	*-0.25*[a]	-0.16
Jul	*-0.30*[a]	-0.23	-0.35[b]	-0.17	-0.22	-0.20	*-0.27*[a]	-0.11	*-0.29*[a]	*-0.26*[a]	*-0.30*[a]	-0.15	*-0.37*[b]	*-0.30*[a]	*-0.36*[b]
Aug	*-0.42*[b]	-0.24	-0.14	*-0.32*[b]	*-0.27*[a]	-0.18	*-0.25*[a]	-0.17	*-0.38*[b]	*-0.25*[a]	-0.20	*-0.28*[a]	*-0.34*[b]	*-0.30*[a]	*-0.36*[b]
Sep	-0.04	-0.12	0.11	0.03	0.02	0.10	0.10	0.00	-0.02	-0.02	0.14	0.01	-0.04	0.09	0.02
Oct	-0.24	-0.08	-0.16	-0.11	*-0.35*[b]	-0.16	-0.09	*-0.31*[a]	*-0.33*[b]	-0.12	-0.17	-0.23	-0.21	*-0.27*[a]	*-0.27*[a]
Nov	-0.08	-0.08	*-0.25*[a]	-0.06	-0.14	-0.08	*-0.33*[b]	-0.14	-0.11	-0.06	*-0.32*[b]	-0.10	-0.15	-0.23	-0.20
Dec	0.15	-0.05	0.02	-0.00	0.21	*0.29*[a]	-0.01	-0.03	0.18	-0.25[a]	0.00	-0.02	0.16	0.22	*0.20*
Annual (Total)	*-0.34*[b]	*-0.30*[a]	*-0.28*[a]	-0.22	*-0.38*[b]	*-0.30*[a]	*-0.32*[b]	*-0.27*[a]	*-0.41*[b]	*-0.35*[b]	*-0.31*[a]	*-0.28*[a]	*-0.40*[b]	*-0.43*[b]	*-0.47*[b]
Mar-May	-0.04	-0.18	-0.14	-0.04	0.00	-0.13	-0.07	-0.01	-0.03	-0.18	-0.11	-0.03	-0.16	-0.09	-0.15

Month and season	Single tree chronology												Three chronologies (GSP10A-GSP19B-PI03A)		
	PR				NA				$PN_{Combined}$						
	GSP 10A	GSP 19B	PI 03A	PI 11A	GSP 10A	GSP 19B	PI 03A	PI 11A	GSP 10A	GSP 19B	PI 03A	PI 11A	PR	NA	PN Combined
(MAM)															
May-Jul (MJJ)	*-0.26*[a]	*-0.27*[a]	*-0.33*[b]	-0.18	*-0.37*[b]	*-0.42*[b]	*-0.29*[a]	-0.23	*-0.36*[b]	*-0.39*[b]	*-0.35*[b]	*-0.24*	*-0.36*[b]	*-0.46*[b]	*-0.47*[b]
Aug-Oct (ASO)	*-0.43*[b]	*-0.28*[a]	-0.10	*-0.26*[a]	*-0.20*[a]	-0.13	-0.16	-0.23	*-0.41*[b]	-0.24	-0.12	*-0.28*[a]	*-0.36*[b]	*-0.26*[a]	*-0.35*[b]
May-Oct (M-O)	*-0.47*[b]	*-0.38*[b]	*-0.31*[a]	*-0.30*[a]	*-0.46*[b]	*-0.38*[b]	*-0.30*[a]	*-0.32*[b]	*-0.54*[b]	*-0.45*[b]	*-0.40*[b]	*-0.36*[b]	*-0.50*[b]	*-0.50*[b]	*-0.58*[b]

[a] Statistically significant at the 0.05 level

[b] Statistically significant at the 0.01 level

1.2) Comparisons with precipitation isotopic data and local climatological data

Tree-ring isotopic data of individual chronologies were moderately correlated with the amounts of summer monsoon rainfall (Table 1.1.3). The GSP10A chronology showed the strongest relationship with total rainfall from May to October for both the PR (r = -0.47, $p < 0.01$) and NA (r = -0.46, $p < 0.01$) stations, whereas the PI11A displayed the weakest relationships with rainfall for both the PR (r = -0.30, $p < 0.05$) and NA (r = -0.32, $p < 0.01$) stations (Table 1.1.3). Correlation coefficients were improved when using combined rainfall data from both the meteorological stations ($PN_{Combined}$) (Table 3.1.3). In the long-term context, correlational analyses demonstrated significant influence of rainfall amount on the Phrae $\delta^{18}O_{Annual}$ series, particularly the entire summer monsoon period from May to October (r = -0.58, $p < 0.01$) (Table 3.1.2 and Figure 3.1.2 (a)), rather than $\delta^{18}O_{Rain}$ (r = 0.31, $p < 0.05$) (Figure 3.1.2 (b)). For the CRU precipitation data, the observed spatial correlation results strongly confirmed that interannual $\delta^{18}O_{TR}$ recorded the regional precipitation and represented climatology of the summer monsoon (M-O) over northern Thailand (Figure 3.1.2 (a)). The analysis revealed that there was no effect of rainfall in the previous years (data not shown) as well as no evidence of a humidity signal (Figure 3.1.2 (c)), signifying that there were fewer less biological influences (i.e., evaporation within tree leaves) on interannual $\delta^{18}O_{TR}$ at this site.

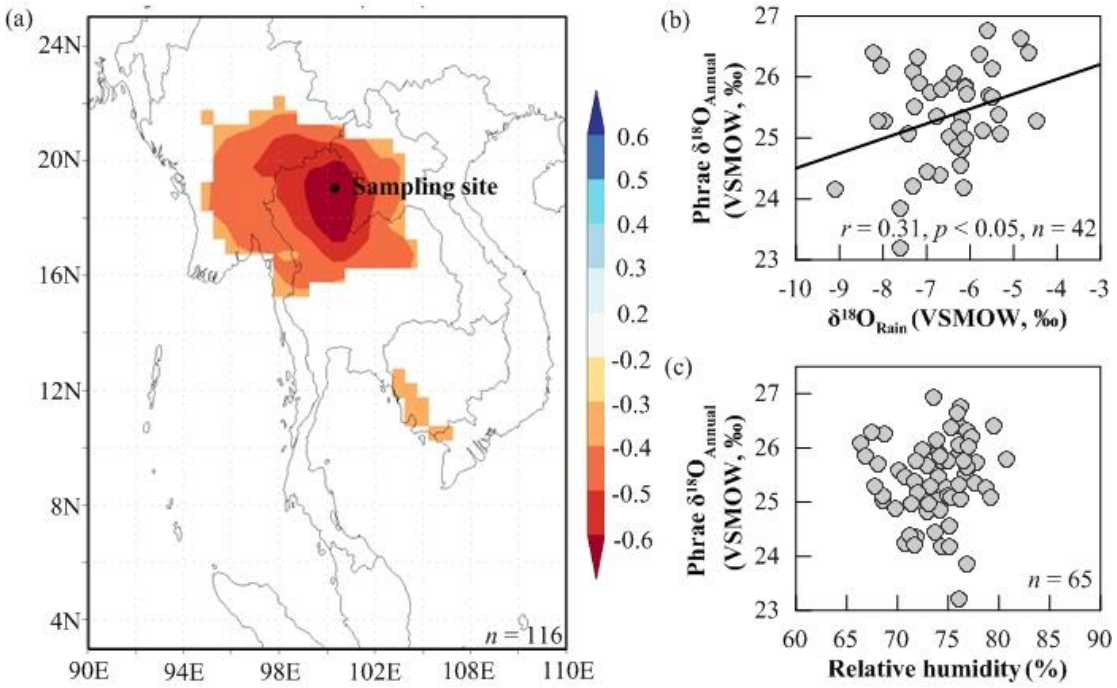

Figure 3.1.2 (a) Spatial correlation analysis between the Phrae $\delta^{18}O_{Annual}$ and summer monsoon precipitation (May to Oct), derived from the CRU TS4.00 gridded precipitation fields (van Oldenborgh and Burgers 2005) for the period between AD 1901-2016. Correlational analyses of interannual $\delta^{18}O_{TR}$ (Phrae $\delta^{18}O_{Annual}$) values with (b) rainfall $\delta^{18}O$ ($\delta^{18}O_{Rain}$) and (c) relative humidity at annual timescales. Linear regressions are shown in black lines, *r* represents the Pearson's correlation coefficient, *p* indicates a statistically significant value, and *n* is the number of samples.

2) Intraseasonal oxygen isotope variations and controlling factors

2.1) Intraseasonal time series of $\delta^{18}O_{TR}$

Overall, the high-resolution $\delta^{18}O_{TR}$ time series matched the patterns of the $\delta^{18}O_{Rain}$, indicating that the variations of $\delta^{18}O_{Rain}$ contributed significantly to the $\delta^{18}O_{TR}$ patterns (Figure 3.1.3 (a)). The more enriched $\delta^{18}O_{TR}$ values were generally observed at the early portions from the pith side and gradually depleted towards the late portions of the rings (Figure 3.1.3 (a)). The average $\delta^{18}O_{TR}$ values were 25.7‰ (varied from 22.2‰ to 29.2‰), 25.3‰ (varied from 20.0‰ to 28.2‰), 25.6‰ (varied from 21.8‰ to 28.3‰), and 25.4‰ (varied from 22.0‰ to 27.8‰) for GSP05A, GSP05B, GSP13A, and GSP22B, respectively.

Through the use of the interpolation technique, the measured $\delta^{18}O_{TR}$ chronologies were closely matched to the linearly interpolated $\delta^{18}O_{TR}$ series (ranged from $r = 0.79$ to $r = 0.87$, $p < 0.01$) (Figure 3.1.3 (b)). Monthly resolved $\delta^{18}O_{TR}$ chronologies exhibited highly correlations among individual trees (ranged from $r = 0.64$ to $r = 0.73$, $p < 0.01$), except between GSP5B and GSP 22B ($r = 0.49$, $p < 0.01$) (Table 3.1.2 and Figure 3.1.3 (a) and (b)). The average high-resolution $\delta^{18}O_{TR}$ values for all cores (hereafter referred to as "Phrae $\delta^{18}O_{Monthly}$") during the early rainy season was ~1.8‰ higher than the late rainy season (Figure 3.1.4 (b)). The maximum variation in intraseasonal $\delta^{18}O_{TR}$ between early and late rainy seasons as found in AD 1983 ranging between 3.8‰ and 4.2‰ for GSP05A, GSP13A, and GSP22B and in AD 1987 for GSP05B (4.2‰) (Figure 3.1.3 (b) and Figure 3.1.4 (a)). The $\delta^{18}O_{TR}$ variations clearly exhibited bimodal patterns (Figure 3.1.3 (a) and (b)).

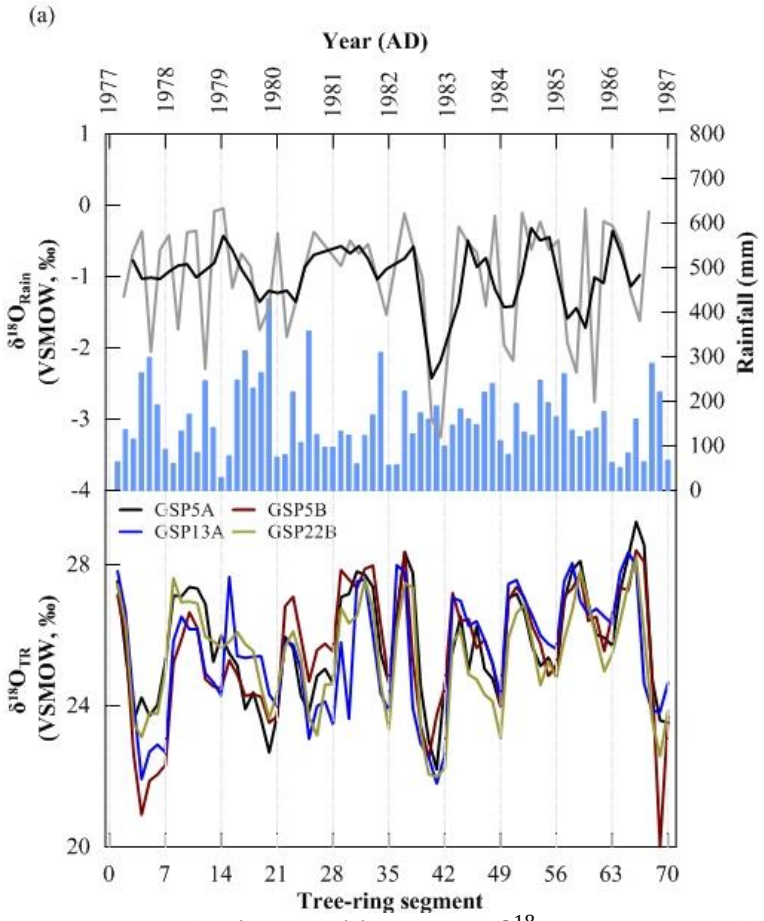

Figure 3.1.3 (a) *Top panel*: The monthly average $\delta^{18}O_{Rain}$ (gray solid line) and rainfall amount (blue vertical bar) at BKK station (black lines with open circles) (IAEA/WMO, 2001). The black solid line indicates the 3-year moving average trend. *Bottom panel*: Intra-annual cellulose $\delta^{18}O$ series of four individual cores, including GSP5A (black solid line), GSP5B (red solid line), GSP13A (blue solid line), and GSP22B (green solid line). The $\delta^{18}O_{TR}$ data were plotted as consecutive segments from the pith side. Years shown at the top are based on the result of the COFECHA analysis. (b) Time series of monthly mean interpolated (blue dashed lines) and measured (black solid lines with symbols) values of intraannual $\delta^{18}O_{TR}$ for individual four cores as well as $\delta^{18}O_{Rain}$ (gray solid line) profiles from the BKK station (IAEA/WMO, 2001). The interpolation method was applied to produce the monthly-scale resolution for tree-ring chronologies covering the growing period from May to October following Muangsong et al. (2016). *r* represents the Pearson's correlation coefficient, and *p* indicates a statistically significant value, and *n* is the number of samples.

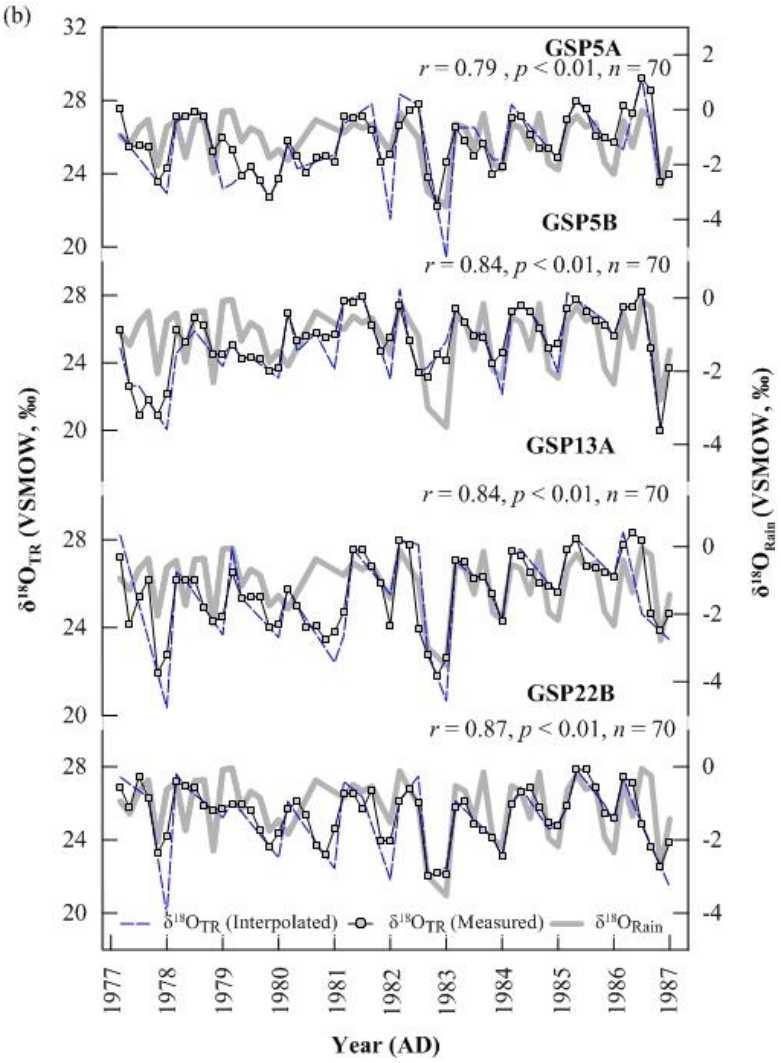

Figure 3.1.3 (cont.) (a) *Top panel*: The monthly average $\delta^{18}O_{Rain}$ (gray solid line) and rainfall amount (blue vertical bar) at BKK station (black lines with open circles) (IAEA/WMO, 2001). The black solid line indicates the 3-year moving average trend. *Bottom panel*: Intra-annual cellulose $\delta^{18}O$ series of four individual cores, including GSP5A (black solid line), GSP5B (red solid line), GSP13A (blue solid line), and GSP22B (green solid line). The $\delta^{18}O_{TR}$ data were plotted as consecutive segments from the pith side. Years shown at the top are based on the result of the COFECHA analysis. (b) Time series of monthly mean interpolated (blue dashed lines) and measured (black solid lines with symbols) values of intraannual $\delta^{18}O_{TR}$ for individual four cores as well as $\delta^{18}O_{Rain}$ (gray solid line) profiles from the BKK station (IAEA/WMO, 2001). The interpolation method was applied to produce the monthly-scale resolution for tree-ring chronologies covering the growing period from May to October following Muangsong et al. (2016). *r* represents the Pearson's correlation, and *p* indicates a statistically significant value, and *n* is the number of samples.

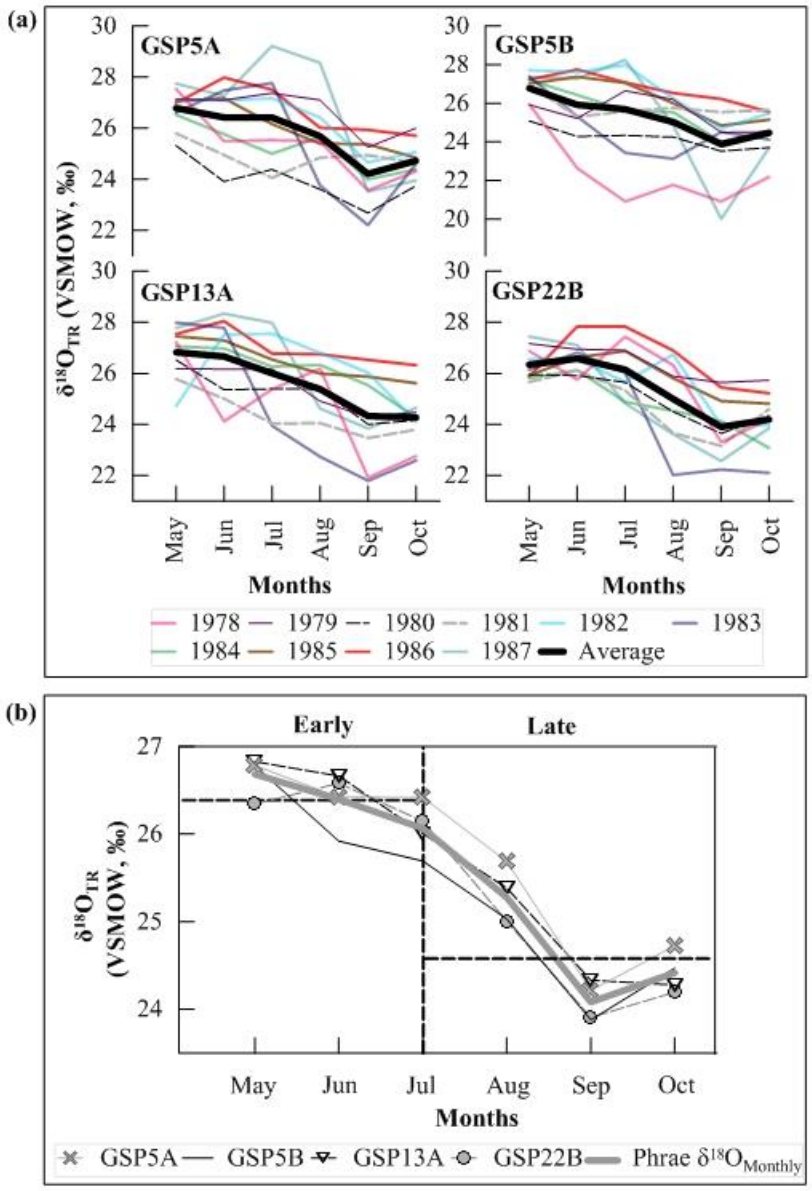

Figure 3.1.4 (a) Intra-annual $\delta^{18}O_{TR}$ variations of monthly average values of all cores (GSP5A, GSP5B, GSP13A, and GSP22B) for individual rings. Bold lines indicate monthly averaged values of the four individual cores. (b) Monthly average values of all individual cores, including GSP5A (gray solid line with asterisks), GSP5B (gray solid line), GSP13A (gray solid line with triangles), GSP22B (gray solid line with filled circles). The bold line indicates the Phrae $\delta^{18}O_{Monthly}$ series. The vertical dashed line indicates the boundary between early and late rainy seasons, whereas horizontal dashed lines indicate the average values of the Phrae $\delta^{18}O_{Monthly}$ values during the early (26.4‰) and late (24.6‰) rainy seasons, respectively.

2.2) Comparisons with precipitation isotopic data and local climatological data

Comparisons with the $\delta^{18}O_{Rain}$ indicated that the seasonal $\delta^{18}O_{TR}$ varied primarily in response to changes in the isotopic composition of precipitation (r = 0.63, p < 0.01) (Figure 3.1.5 (a)) and varied due to changes in RH (r = -0.53, p < 0.01) (Figure 3.1.5 (b)). In contrast to the annual timescale, there was no inverse correlation between $\delta^{18}O_{TR}$ and the local rainfall amount, thus implying that the $\delta^{18}O_{TR}$ signal was not sensitive to variations in the local rainfall amount at monthly to seasonal scales (Figure 3.1.5 (c)). The correlational analyses confirmed that the influence of source water isotopes observed in this study was relatively stronger than the influences of plant physiology and local climate on $\delta^{18}O_{TR}$.

2.3) Comparisons with large-scale convective activity

Variations in stable isotope ratios for monthly rainfall in Thailand was modulated by either local rainfall amount or large-scale convection, which may vary between different areas as well as over time (Aggarwal et al., 2004; 2016, Wei et al., 2018). The convective activity and convective rainfall indicated a positive correlation between $\delta^{18}O_{TR}$ with the OLR data as well as a negative correlation with the CMAP data over the convective areas. During the early rainy season (MJJ), the OLR datasets over the Indian Ocean Basin, in particular, the Bay of Bengal (BOB) region (Bellenger and Duvel, 2007), were more strongly correlated with the $\delta^{18}O_{TR}$ than over the Pacific Ocean Basin (Figure 3.1.6 (c)). Similar to the OLR data, spatial correlations of intraseasonal $\delta^{18}O_{TR}$ with CMAP rainfall showed that the strong correlations during the MJJ were observed in the northern, central, and western parts of the Indian Ocean (Fig. 8a). During the late rainy season (ASO), deep convection greatly increased convection and rainfall over the WNP Ocean and the South China Sea (SCS) region (Bellenger and Duvel, 2007) (Figure 3.1.6 (b) and (d)), and hence produced the late season rainfall at the study site. The strong correlation with the OLR data over the Indian Ocean was observed only over the Andaman Sea (Figure 3.1.6 (d)) and was rather weak compared to the early rainy season (Figure 3.1.6 (c)). The 72 h back trajectory analysis confirmed that moisture in the early rainy season, especially in May, was from the Indian Ocean (Figure 3.1.7 (a)). Major contributions to ASO

rainfall came from moisture originating from both the Indian and Pacific Oceans (Figure 3.1.6 (b, d) and Figure 3.1.7 (b)) as well as from the land (Figure 3.1.7 (b)).

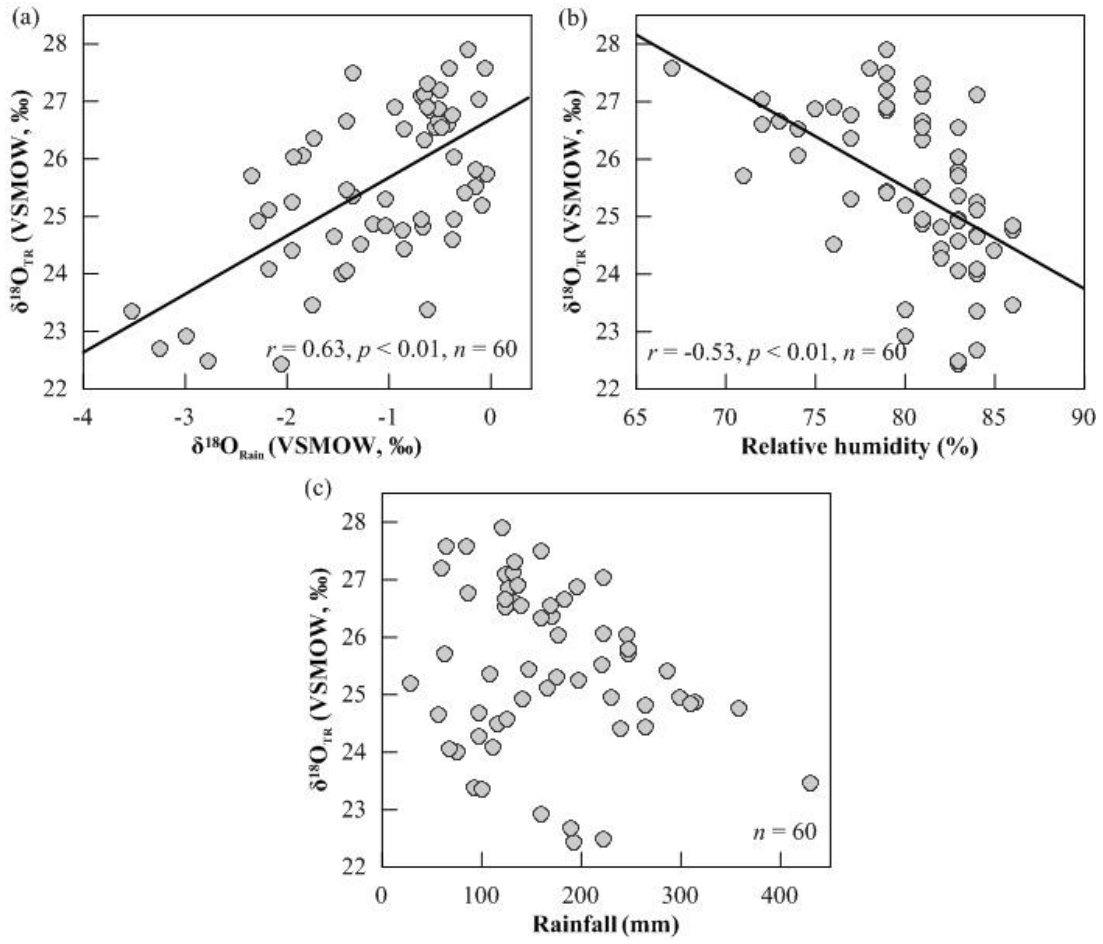

Figure 3.1.5 Correlational analyses of intra-annual $\delta^{18}O_{TR}$ values with (a) $\delta^{18}O_{Rain}$, (b) relative humidity, and (c) rainfall amount at monthly timescales. Linear regressions are shown in black lines, *r* represents the Pearson's correlation coefficient, *p* indicates a statistically significant value, and *n* is the number of samples.

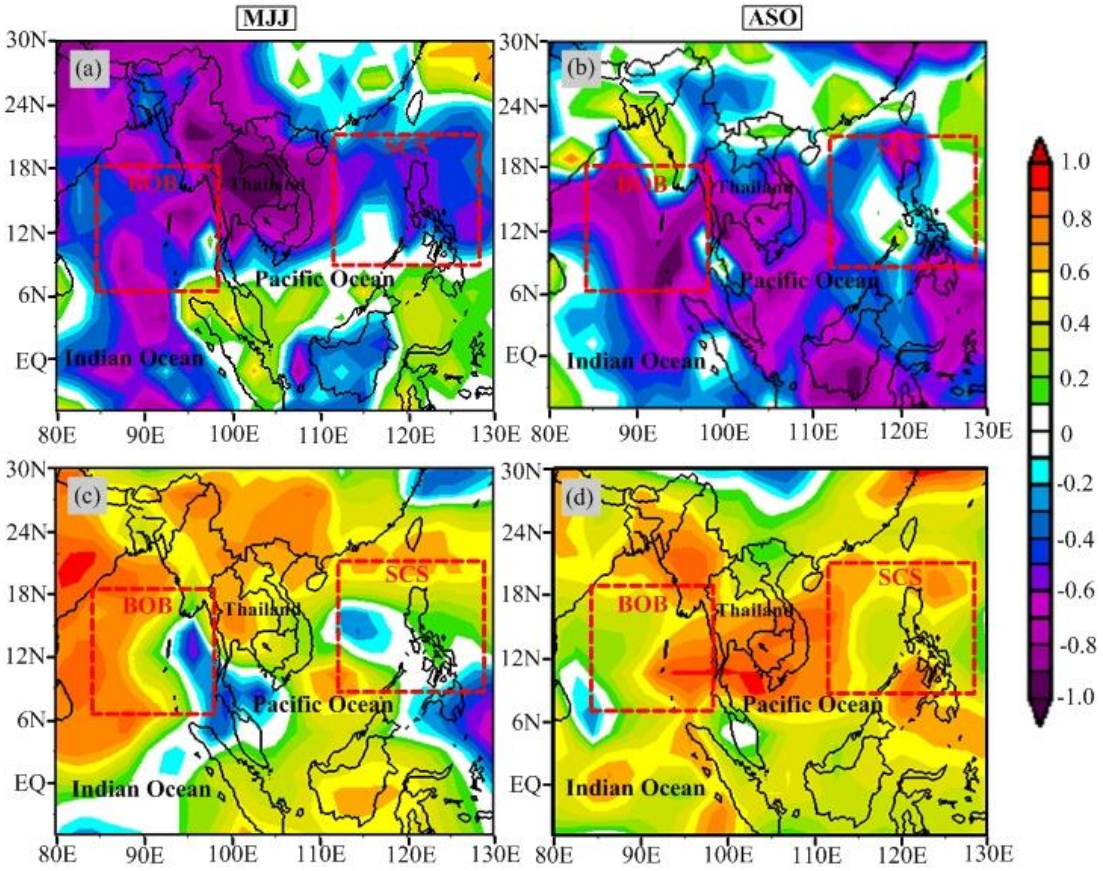

Figure 3.1.6 Spatial correlations of intra-annual $\delta^{18}O_{TR}$ with CMAP precipitation (Xie and Arkin, 1997) for (a) May to July and (b) August to October as well as with the OLR datasets (Liebmann and Smith, 1996) for (c) May to July and (d) August to October. The correlations are above the 95% significance level. The BOB and SCS regions are shown following Bellenger and Duvel (2007).

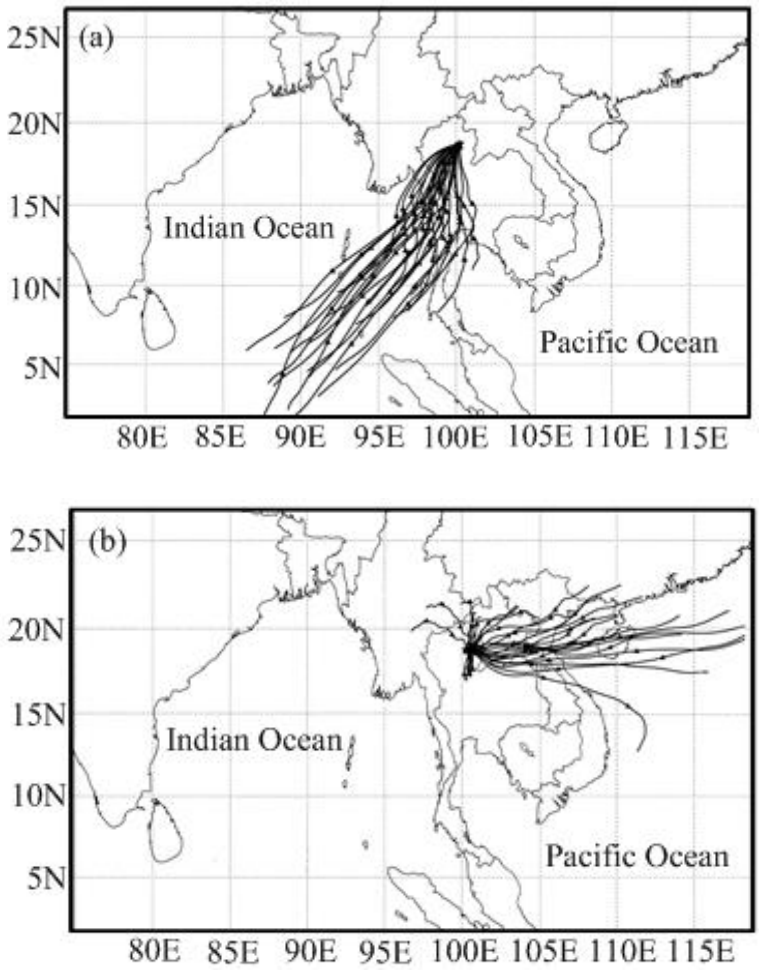

Figure 3.1.7 The 72 h back trajectories (Stein et al., 2015) at three different heights (500 m, 1,000 m, and 1,500 m above ground level) for (a) early rainy month (May) and (b) late rainy month (September) at the study location.

3) Imprints of source water isotopic signals in tree-ring $\delta^{18}O$

The oxygen isotope ratios of tree-ring cellulose are theoretically controlled by the isotopic composition of source water (i.e., atmospheric precipitation and soil water) and are modified by other processes such as the evapotranspiration causes heavy water isotopic enrichment in tree leaves during gas exchange (Roden et al., 2000; Waterhouse et al., 2002; Treydte et al., 2014). The $\delta^{18}O_{TR}$ is expected to be a proxy of source water isotopes (i.e., $\delta^{18}O_{Rain}$) (Brienen et al., 2013). Correlation analyses of $\delta^{18}O_{Rain}$ on annual (Figure 3.1.2 (b)) and monthly resolved $\delta^{18}O_{TR}$ (Figure 3.1.5 (a)) indicated that tree rings sampled at different temporal resolutions are likely to

reflect the isotopic composition of rainfall. The temporal variability of monthly resolved $\delta^{18}O_{TR}$ reproduced the variability of $\delta^{18}O_{Rain}$ than annually resolved $\delta^{18}O_{TR}$ more accurately, suggesting that higher sampling resolution could provide improved insights into the transfer of seasonal isotopic signals between $\delta^{18}O_{Rain}$ and $\delta^{18}O_{TR}$. The time series of monthly resolved $\delta^{18}O_{Rain}$ and $\delta^{18}O_{TR}$ exhibited clear trends of depletion in $\delta^{18}O$ values during the late rainy season, similar to the intraseasonal $\delta^{18}O_{TR}$ cycle observed in teak tree rings from NW Thailand (Muangsong et al., 2016).

Studying trees in various locations under different climatic conditions is necessary (Brienen et al., 2013) for an improved understanding of how the original isotopic signal ($\delta^{18}O_{Rain}$) is modified over time and space in response to effective rainfall (Muangsong et al., 2019), and how the $\delta^{18}O_{TR}$ is altered by the evapotranspiration process occurring in tree leaves. Variation in $\delta^{18}O_{TR}$ is dominated by the $\delta^{18}O$ of source water and also modified by plant physiological response to moisture-stressed conditions (i.e., the stomatal response to humidity), causing evaporative enrichment of leaf water $\delta^{18}O$ during evapotranspiration (McCarroll and Loader, 2004). The lack of significant correlation between the Phrae $\delta^{18}O_{Annual}$ and RH (Figure 3.1.2 (c)) clearly indicated that annual resolved $\delta^{18}O_{TR}$ values of Thai teak trees are less affected by plant physiological processes possibly due to abundant moisture under wet weather condition during the growing period in the rainy season (Pumijumnong, 1995, 2013, Muangsong et al., 2019). Variations in monthly resolved $\delta^{18}O_{TR}$ (Figure 3.1.5 (b)) can be modified by either plant physiological procession or the influence of rainfall-induced the moisture content of the air (i.e., RH). Given that the rainfall and RH in tropical countries are closely related (Thai et al., 2015), the observed correlation between RH and monthly resolved $\delta^{18}O_{TR}$ (Figure 3.1.5 (b)) might be related to rainfall to some extent. Our results confirmed the previous finding that rainfall oxygen isotopes (Brienen et al., 2013; Schollaen et al., 2013; Muangsong et al., 2016; 2019) play a key role in controlling inter-annual $\delta^{18}O_{TR}$ in tropical and subtropical regions (Brienen et al., 2013; Schollaen et al., 2013; Muangsong et al., 2019). However, intraseasonal variation in $\delta^{18}O_{TR}$ values varied primarily in response to changes in the $\delta^{18}O_{Rain}$, although possibly controlled by evaporation of water from leaves. It is also uncertain to what extent RH (i.e., plant physiology) controls variation in $\delta^{18}O_{TR}$ during the rainy season. To better understand isotopic signal retained in teak

tree rings, further plant physiology studies and models are needed. The ability of Thai teak $\delta^{18}O_{TR}$ to capture the $\delta^{18}O_{Rain}$ signal depends on temporal sampling resolution. The monthly resolved cellulose $\delta^{18}O$ in this study potentially provided a high-resolution biological archive for further rainfall $\delta^{18}O$ reconstruction in subtropical mainland Southeast Asia.

4) Local-scale atmospheric controls on tree-ring $\delta^{18}O$

Since the $\delta^{18}O_{Rain}$ in this area is controlled by several factors, the $\delta^{18}O_{TR}$ can be used to identify the atmospheric factors controlling $\delta^{18}O_{Rain}$, in particular, changes in the amounts of local and regional precipitation (Aggarwal et al., 2004; Wei et al., 2018). For long chronologies with annual resolution, the Phrae $\delta^{18}O_{Annual}$ series exhibited moderate negative relationships with both local (Table 3.1.3) and regional (Figure 3.1.2 (a)) rainfall amounts. Previous studies highlighted difficulties in using Thai teak tree-ring $\delta^{18}O$ (Buajan et al., 2016; Muangsong et al., 2018) for paleoclimate studies because it is not representative of the entire summer monsoon season and contains different seasonal rainfall signals. For example, teak $\delta^{18}O_{TR}$ collected close to Namjang Village (19°40'21"N, 98°12'14"E; 800-900 m asl.) in MHS Province of NW Thailand responded to changes in rainfall amount during the early rainy season from May to July (Muangsong et al., 2019). Conversely, teak $\delta^{18}O_{TR}$ collected in a nearby location (19°26'N, 98°8'E; 500-600 m asl.) responded to changes in rainfall amount during the late rainy season from August to October (Buajan et al., 2016). The authors suggested combining multiple climate proxy records, that are typically susceptible to seasonal climate, to create a single reconstruction that cover the entire summer monsoon period from May to October (e.g. Muangsong et al., 2019). The advantage of our annually resolved tree-ring records is that the Phrae $\delta^{18}O_{Annual}$ successfully captures rainfall signals during the entire summer monsoon season, which can be further used to quantify the amount of past monsoon rainfall over the whole period of summer monsoon season. Further development of long-term rainfall reconstructions based on tree-ring series collected from this site requires additional tree-ring stable isotope chronologies to improve the strength of the proxy signal. Although $\delta^{18}O_{Rain}$ data were unavailable for the study area, our interannual $\delta^{18}O_{TR}$ record indicated that the Phrae $\delta^{18}O_{Annual}$ series was sensitive to annual rainfall totals, thereby implying that its source water isotopes (i.e., soil water $\delta^{18}O$ and $\delta^{18}O_{Rain)}$ change in response to local

rainfall amounts. These results confirm the previous finding that interannual variation in Thai $\delta^{18}O_{TR}$ is dominated by the amount of rainfall (Buajan et al., 2016, Muangsong et al., 2019). The interpretation of intraseasonal $\delta^{18}O_{TR}$ as an indicator of rainfall amount appears inappropriate in most samples due to a lack of correlation between monthly resolved $\delta^{18}O_{TR}$ and the amount of rain. Results showed that interannual $\delta^{18}O_{TR}$ was more related (but not always) to variations in rainfall amount and more feasible for the local and regional rainfall reconstruction than intraseasonal $\delta^{18}O_{TR.}$ Data obtained from the GNIP database at the BKK station showed a record of monthly maximum amount of rainfall in September (335 mm), which reduced the $\delta^{18}O_{Rain}$ value to -8.13‰. However, the minimum $\delta^{18}O_{Rain}$ value was observed in October (-8.24‰) (IAEA/WMO, 2001). Similar to the BKK station, the $\delta^{18}O_{Rain}$ database at several stations such as Chiang Mai (CM) and Si Samrong Agromet (SA) stations in northern Thailand indicated the observed minimum $\delta^{18}O_{Rain}$ values in October, while the maximum rainfall was determined in September (Wei et al., 2018). Thus, variations in the isotopic composition of precipitation from this region could not be adequately explained only by changes in the amount of rainfall (i.e., amount effect). The absence of a correlation between the monthly resolved $\delta^{18}O_{TR}$ and rainfall amount indicated that seasonal $\delta^{18}O_{Rain}$ and $\delta^{18}O_{TR}$ could have been controlled by other factors.

5) Large-scale atmospheric controls on tree-ring $\delta^{18}O$

Besides the local amount effect, $\delta^{18}O_{Rain}$ in this region is strongly influenced by large-scale shifts in moisture regimes between two oceanic sources (i.e., Indian and Pacific Oceans) as well as moisture supply derived from land surface evapotranspiration (Wei et al., 2018). Delineating the relationship between $\delta^{18}O_{TR}$ and each moisture source locations is particularly important to correctly interpret teak $\delta^{18}O_{TR}$ as an indicator of past changes in moisture supply from different ocean basins. The bimodal patterns of the Phrae $\delta^{18}O_{Monthly}$ (Figure 3.1.4 (b)) suggested a strong degree of forcing by seasonal shifts in precipitation associated with changes in oceanic moisture supply from the Indian to Pacific Ocean. The monthly temporal $\delta^{18}O_{TR}$ patterns observed in northern Thailand teak are similar to those found in tree-ring records from NW Thailand (Muangsong et al., 2016) as well as observed patterns of a recent rainfall isotope-observation study (Wei et al., 2018).

The moderate to strong positive correlations with the OLR, and vice versa for the CMAP datasets, showed that convection mainly took place over the BOB in the Indian Ocean during the early rainy season (MJJ) (Figure 3.1.6 (a and c)), but the moisture originating from the Pacific Ocean, particularly the WNP and SCS, controlled the monsoon rainfall during the late rainy season (ASO) (Figure 3.1.6 (b and d)). Additionally, the HYSPLIT backward trajectories confirmed the intraseasonal changing in regional moisture pathways from the Indian Ocean source during the early rainy month to the Pacific Ocean source during the late rainy month (Figure 1.1.7 (a-b)). Although spatial correlations with the CMAP and OLR datasets in ASO indicated the integration of moisture originating from both oceanic (Indian and Pacific) and terrestrial sources (Figure 3.1.6 (b and d)), a majority of the trajectories originated from either the Pacific Ocean or the land surface (Figure 3.1.7 (b)). The moisture evaporated from the oceans was carried by the convective clouds and transported away to new regions. Consequently, the isotopic signals of falling precipitation dominantly mirrored $\delta^{18}O$ of the source water (i.e., oceanic sources) (Wei et al., 2018). The Indian Ocean-derived rainfall is characterized by its highly enriched isotopic values relative to that of rainfall originating from either the Pacific Ocean or the land surface (Wei et al., 2018). Gradually more depleted values of $\delta^{18}O_{Rain}$ signals embedded in $\delta^{18}O_{TR}$ during the late rainy season indicated a smaller proportion of moisture fraction originating from the Indian Ocean source associated with the progressive rainout (e.g.Wei et al., 2018). Therefore, the robust relationships of $\delta^{18}O_{TR}$ with OLR and CMAP data as well as the origin of air masses and moisture-delivery pathways defined by backward trajectory analyses confirmed that the intraseasonal variations in $\delta^{18}O_{TR}$ are controlled by large-scale atmospheric convection associated with different water vapor sources and transport trajectories between the early and late rainy seasons.

3.1.2 Dominant factors controlling the tree-ring widths

The climate-tree growth relationship was tested by using teak trees grew in the area of a famous tourist cave in the Lum Nam Pai Wildlife Sanctuary, namely, Susa cave. A tree-ring width (TRW) index representative of the site was referred to as the Susa index according to the site name (i.e., Susa cave). The results relating to the tree-ring widths and their controlling factors were previously shown in our publications (Buareal et al., 2020; Pumijumnong et al., 2020; Preechamart et al., 2018).

1) Tree-ring chronologies

Tree-ring characteristics and statistical parameters are given in Table 1. After the overall chronology-building process was completed, 7 trees were excluded, and 54 core samples from 39 living teak trees were used in this study (Table 3.1.4). The MRW was 0.31 cm (Table 3.1.4). The Susa index covered the chronology interval of AD 1824-2017, and the age of the sampled trees ranged from 50 to 195 years (Table 3.1.4). The ring-width chronology has an Rbar of 0.31, with some periods of EPS values lowering the threshold (Wigley et al. 1984) (e.g., AD 1864-1903) (Table 1.1.4 and Figure 3.1.8). Although the running EPS values varied between 0.74 and 0.92, the overall mean EPS value of 0.85 was considered acceptable and representative of the hypothetical population chronology (Wigley et al. 1984) (Table 3.1.4 and Figure 3.1.8). High-frequency growth patterns were observed from AD 1824 to 1905, and a lower growth rate was found from AD 1906 to the present (Figure 3.1.8).

Table 3.1.4 Details of tree-ring width characteristics and statistical parameters.

Parameters	TRW Values
Chronology interval	AD 1824-2017
Number of years	194
Number of trees	39
Number of cores	54
Mean ring widths (MRW)	0.31 cm
Standard deviation (SD)	0.15
Mean inter-series correlation (Rbar)	0.31
Mean ring sensitivity (MS)	0.35

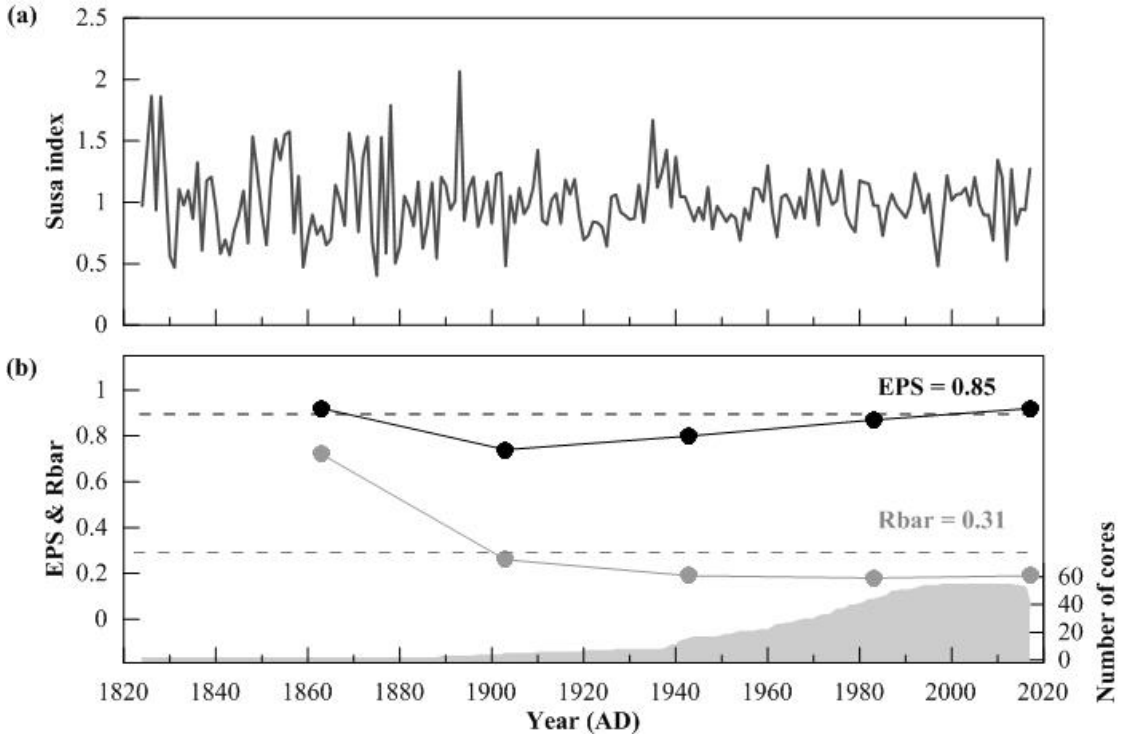

Figure 3.1.8 (a) Interannual variation in the tree-ring width index. (b) The running expressed population signal and mean interseries correlation statistics over a 40-year window, lagged by 20 years, and number of tree cores. The horizontal dashed lines indicate the overall mean EPS (0.85) and Rbar (0.31) values.

2) Correlations with meteorological data

The climate-tree growth relationship was tested by comparing the Susa index with local climate parameters (rainfall and air temperature) for the current, previous, and three-year moving averages of the rainfall data. Variations in the Susa index were coherent with the instrumental rainfall data for both the current year and three-year moving averages of the rainfall data (Table 3.1.5), whereas there was no association with air temperature (data not shown). For the comparisons with current-year rainfall, significant correlations were observed with the monthly rainfall total in September (r = 0.24, p < 0.016) and December (r = 0.23, p < 0.019), seasonal rainfall total during the early (MJJ: r = 0.31; p < 0.001) and late (ASO: r = 0.20; p < 0.043) rainy seasons, and the entire summer monsoon season (M-O: r = 0.28; p < 0.004) (Table 3.1.5). For the current-year rainfall, the Susa index was positively correlated with the previous-year rainfall from March to October (r = 0.20; p < 0.043) but not during other seasons

(Table 3.1.5). Relationships with the three-year moving averages of the rainfall data showed the greatest improvement in correlation coefficient values (Table 3.1.5 and Figure 3.1.9 (a-e)), particularly during the early rainy season (r = 0.58; p < 0.001) (Table 3.1.5 and Figure 3.1.9 (c)). Tree growth is likely dominantly affected by the average recharging rainfall amount in the early rainy season (Table 3.1.5) and better conserves low-frequency (e.g., multiannual to multidecadal climate variability) than high-frequency signals. The strongest correlations were observed with MJJ rainfall for either the current year or three-year average rainfall, indicating that rainfall in the early rainy season has a strong influence on teak tree growth at this site (Table 3.1.5).

Table 3.1.5 Pearson's correlational analysis of the tree ring-width index and rainfall amount. Correlation coefficient (r) and statistically significant (p) values are shown in the italic print.

Month/Season/Annual	Previous-year rainfall		Current-year rainfall		Three-year averaged rainfall	
	r	*p*	*r*	*p*	*r*	*p*
Jan	-0.18	0.077	-0.03	0.751	-0.11	0.294
Feb	-0.09	0.369	-0.04	0.677	-0.01	0.896
Mar	-0.03	0.804	0.04	0.717	0.14	0.175
Apr	-0.15	0.126	-0.01	0.316	*-0.23*	*0.023*
May	0.02	0.871	0.02	0.806	*0.29*	*0.003*
Jun	0.06	0.525	0.19	0.053	*0.42*	*0.001*
Jul	0.08	0.417	0.17	0.079	*0.44*	*0.001*
Aug	0.05	0.634	0.17	0.092	0.13	0.187
Sep	0.11	0.291	*0.24*	*0.016*	*0.32*	*0.001*
Oct	-0.02	0.884	0.14	0.154	0.13	0.212
Nov	-0.06	0.525	-0.03	0.755	*-0.21*	*0.034*
Dec	0.17	0.085	*0.23*	*0.019*	*0.35*	*0.001*
Mar-May (MAM)	-0.09	0.386	-0.03	0.748	0.10	0.312
May-Jul (MJJ)	0.08	0.404	*0.31*	*0.001*	*0.58*	*0.001*
Aug-Oct (ASO)	0.08	0.403	*0.20*	*0.043*	*0.32*	*0.001*
Mar-Oct (M-O)	*0.20*	*0.043*	*0.28*	*0.004*	*0.54*	*0.001*
Annual	0.05	0.618	*0.31*	*0.001*	*0.50*	*0.001*

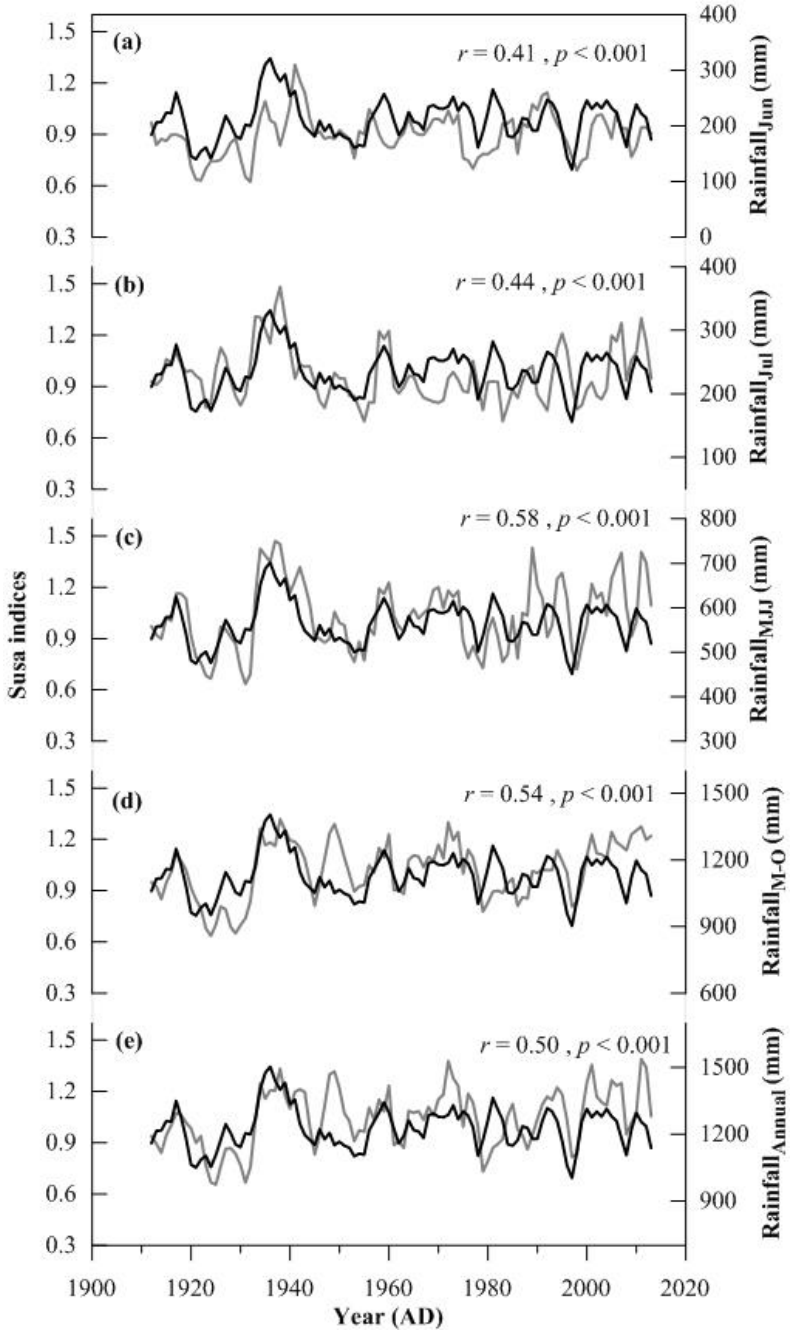

Figure 3.1.9 Comparisons between the Susa index (black lines) and MHS instrument record (gray lines) for total rainfall in (a) June, (b) July, **c** May to July (MJJ), and (d) May to October (M-O), and (e) annual rainfall. The black and gray lines represent three-year moving average values. *r* represents the Pearson's correlation coefficient, and *p* indicates a statistically significant value.

3) Comparisons with regional tree-ring records

Due to the small number of old teak trees at this site, the Susa index was compared with regional tree-ring records, including the Namkong teak TRW index between AD 1824 and 2009 (hereafter referred to as the NK teak index) (Pumijumnong, 2012) (Figure 3.1.10 (a)), the teak cellulose $\delta^{18}O$ chronologies between AD 1936 and 2004 from MHS province (hereafter referred to as NJT-06 $\delta^{18}O$) (Muangsong et al. 2019) (Figure 3.1.10 (b)) and Phrae province in northern Thailand (hereafter referred to as Phrae $\delta^{18}O_{Annual}$) (Muangsong et al., 2020) (Figure 3.1.10 (c)), to demonstrate that our tree-ring records are reliable and regionally representative. Moderate correlations were observed with other records based upon data smoothed with a five-point running-average filter (NK teak index: $r = 0.58$, $p < 0.001$; NJT-06 $\delta^{18}O$: $r = -0.42$, $p < 0.001$; Phare $\delta^{18}O_{Annual}$: $r = -0.52$, $p < 0.001$) and confirmed the reliability of the Susa index as a regional tree-ring record (Figure 3.1.10 (a-c)).

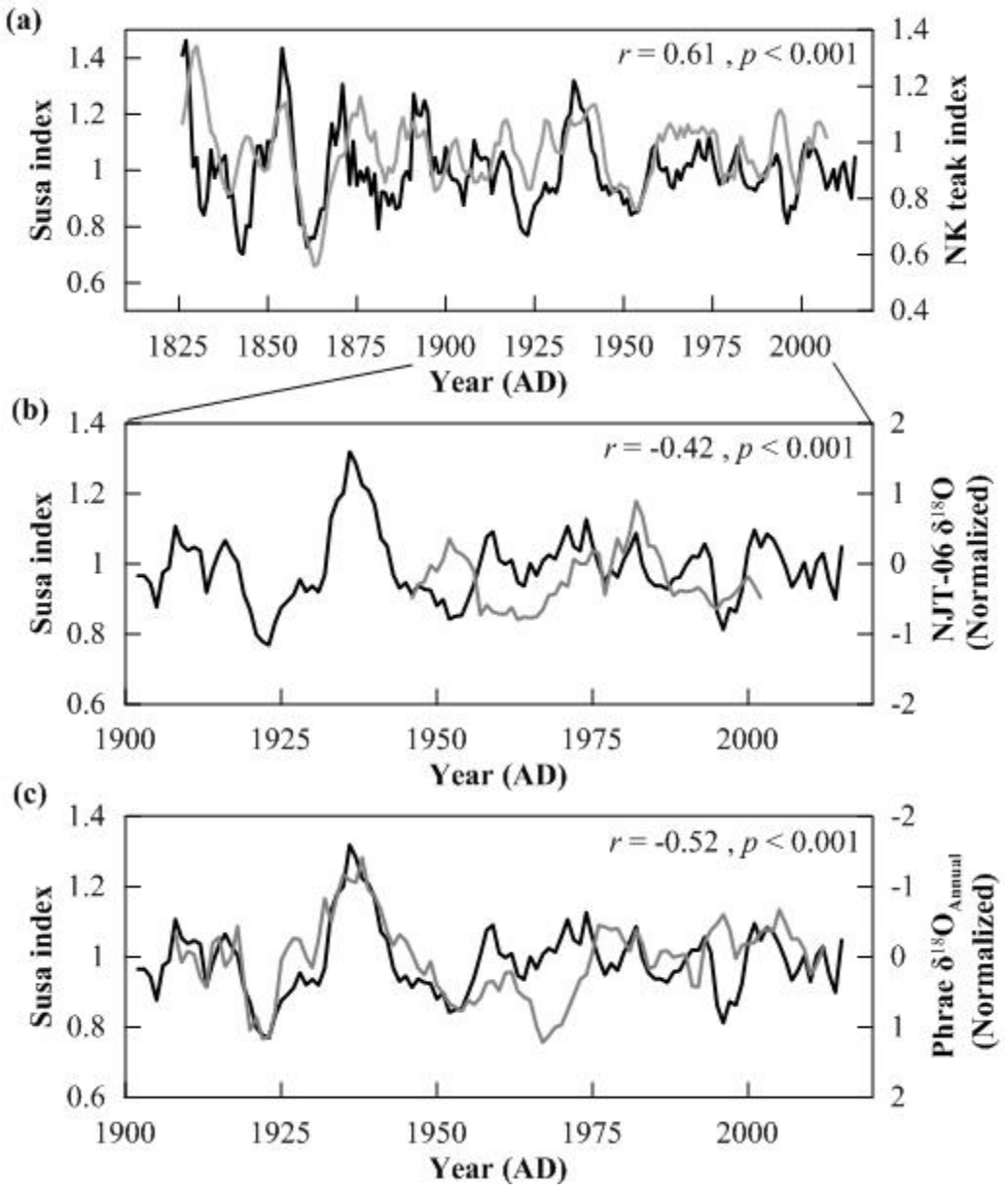

Figure 3.1.10 Comparisons between the Susa index (black lines) and regional tree-ring records (gray lines), including (a) the NK (Pumijumnong 2012), (b) the NJT-06 $\delta^{18}O$ chronology (Muangsong et al., 2019), and (c) the Phrae $\delta^{18}O_{Annual}$ (Muangsong et al., 2020) teak indices. For presentation purposes, the NJT-06 $\delta^{18}O$ the Phrae $\delta^{18}O_{Annual}$ values were transformed into a similar scale using Z-score normalization (Wilks, 1995). *r* represents the Pearson's correlation coefficient, and *p* indicates a statistically significant value.

4) Climatic significance of tree-ring width

The growing period of teak trees lasts for approximately eight months, from the late summer season (the premonsoon season) to the late rainy season (March-October) (Buckley et al., 2007; Buareal et al., 2020; Pumijumnong, 2012; Pumijumnong et al., 1995; Yoshifuji et al., 2006). Leaf fall occurs from November to February of the following year to minimize water use during the dry season (Buckley et al., 2007; Pumijumnong, 2012; Pumijumnong et al., 1995). However, only rainfall during the early stages of Thai teak tree growth (i.e., MAM and/or MJJ rainfall) is an important limiting factor in light of the high water demand during cambium cell division and expansion of newly formed wood after prolonged dormancy following the cessation of rain (Buckley et al., 2007; Pumijumnong, 2012; Pumijumnong et al., 1995; Yoshifuji et al., 2006). The growth of teak trees in this study was closely related to the variations in MJJ rainfall and was consistent with the early-season rain-sensitive tree-ring chronologies (Muangsong et al., 2019; Pumijumnong, 2012) in this region, suggesting that rainfall in the early rainy season is the dominant climatic factor affecting teak tree-ring growth in this area. The Susa index can therefore be regarded as a proxy for MJJ precipitation changes (hereafter referred to as Susa index-based TM rainfall) in NW Thailand over the past 194 years.

3.2 High-resolution composite records of Asian summer monsoon over the past few centuries

3.2.1 The late-Holocene Asian summer monsoon variability over the past 338 years derived from Thai teak trees

In this study, we presented the longest tree-ring oxygen isotope record in Thailand derived from Thai teak collected from Mae Hong Son province in Northwestern Thailand to capture the variations in the Asian summer monsoon system. Thailand monsoon rainfall was further reconstructed covering the period from AD 1678–2015. Note that only robust climate proxies were presented in this report.

1) Teak tree-ring $\delta^{18}O$ ($\delta^{18}O_{tr}$) chronology and its characteristics

Results indicated significant intercorrelations for the most of the individual tree-ring $\delta^{18}O$ ($\delta^{18}O_{tr}$) series and permitted for calculating the mean regional site chronology. The annually resolved $\delta^{18}O_{tr}$ mean values of tree-ring cellulose from 21 trees for the period AD 1678-2015 along with the running expressed population signal (EPS) and inter-series correlation (Rbar) statistics, through the use of 30-year windows, and when lagged 15 years were presented (Figure 3.2.1 (a-c)). The Rbar statistic for these data spans a range of 0.4-0.81, and EPS is in the range of 0.7-0.95 (Figure 3.2.1 (a)). For our $\delta^{18}O_{tr}$ series, the EPS value of ≥ 0.85 is generally accepted but fell below this criterion is associated with diminished the sample size (Wigley & Jones, 1984). Buras (2017) explained that EPS indicates how good a finite sample of tree-ring data is for an infinite population. Therefore, values that is lower than 0.85 do not mean that the chronology is unreliable. Due to the tree-ring $\delta^{18}O$ study, the number of samples taken is not as high as those for the tree ring width study. Therefore, at some times, an EPS value lowers than 0.85 does not mean that the value is unreliable. Teak $\delta^{18}O_{tr}$ values ranged between 20.81 and 26.90‰, and the long-term average was 24.44‰ (Figure 3.2.1 (b and c)).

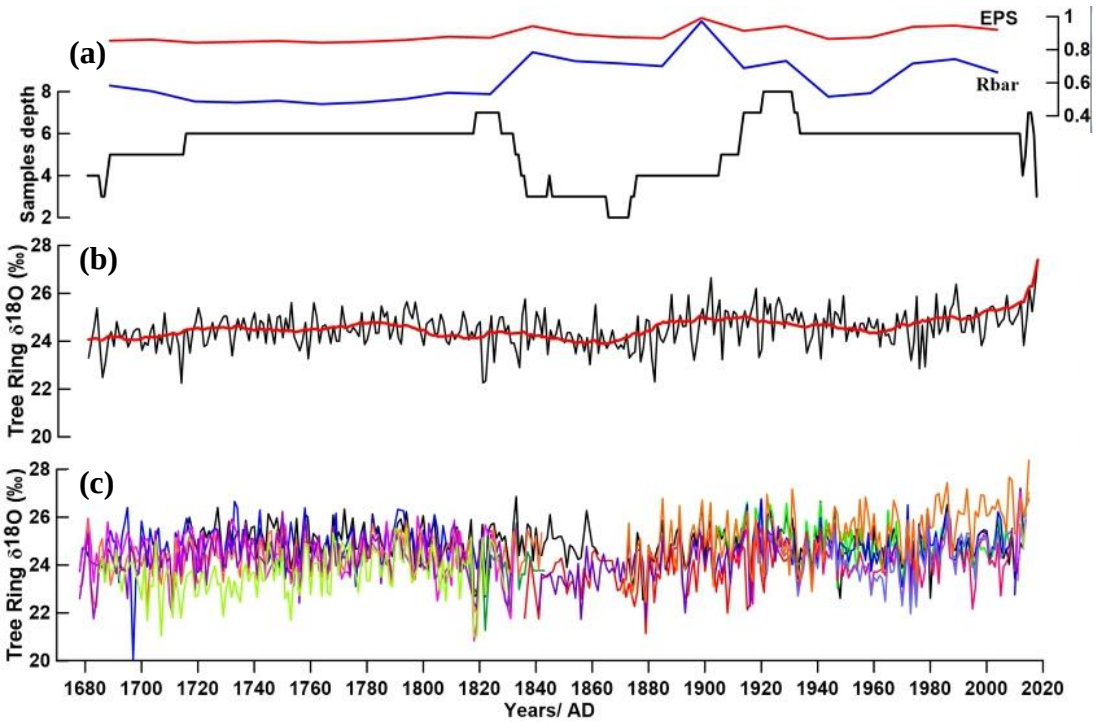

Figure 3.2.1 (a) Sample depth, running EPS, and Rbar statistics of the mean isotope chronology Thai teak tree-ring δ18O chronology (black line), (b) 11-year low pass filter (red line), and (c) individual teak tree-ring $\delta^{18}O$ series.

A 338-year-long teak oxygen isotope chronology for the period of AD 1678–2015 was developed, including data from 21 individual living teak trees from the Mae Hong Son Province, Northwestern Thailand. Instead of pooling the tree-ring material from several trees as mentioned above, we constructed the chronology by averaging the isotope series from individual trees that were well intercorrelated, allowing precise dating control on all individual $\delta^{18}O_{tr}$ values. For this approach, our chronology is covered by at least 4 trees after AD 1680; however, there is one particular period (ca. 1860–1870) where the chronology shows low replication. It is possible that the period was one of the heavy teak concessions, so old trees did not remain (Figure 3.2.1 (a-c)).

2) Teak $\delta^{18}O_{tr}$ and local and regional climate data

The relationships among $\delta^{18}O_{tr}$ and rainfall, humidity, and temperature at the Mae Hong Son meteorological station (hereinafter named the local climate), $\delta^{18}O_{rain}$ at Bangkok Station and CRU T4.03 rainfall and temperature (hereinafter named the

regional climate) were presented Figure 1.2.2. The $\delta^{18}O_{tr}$ has a negative correlation with the local rainfall (May–October (M–O), r = -0.413, p < 0.001), local humidity (May–June–July (MJJ), r = -0.439, p < 0.001) and regional rainfall (M–O, r = -0.593, p < 0.001) (Figure 3.2.2 (a-f)).

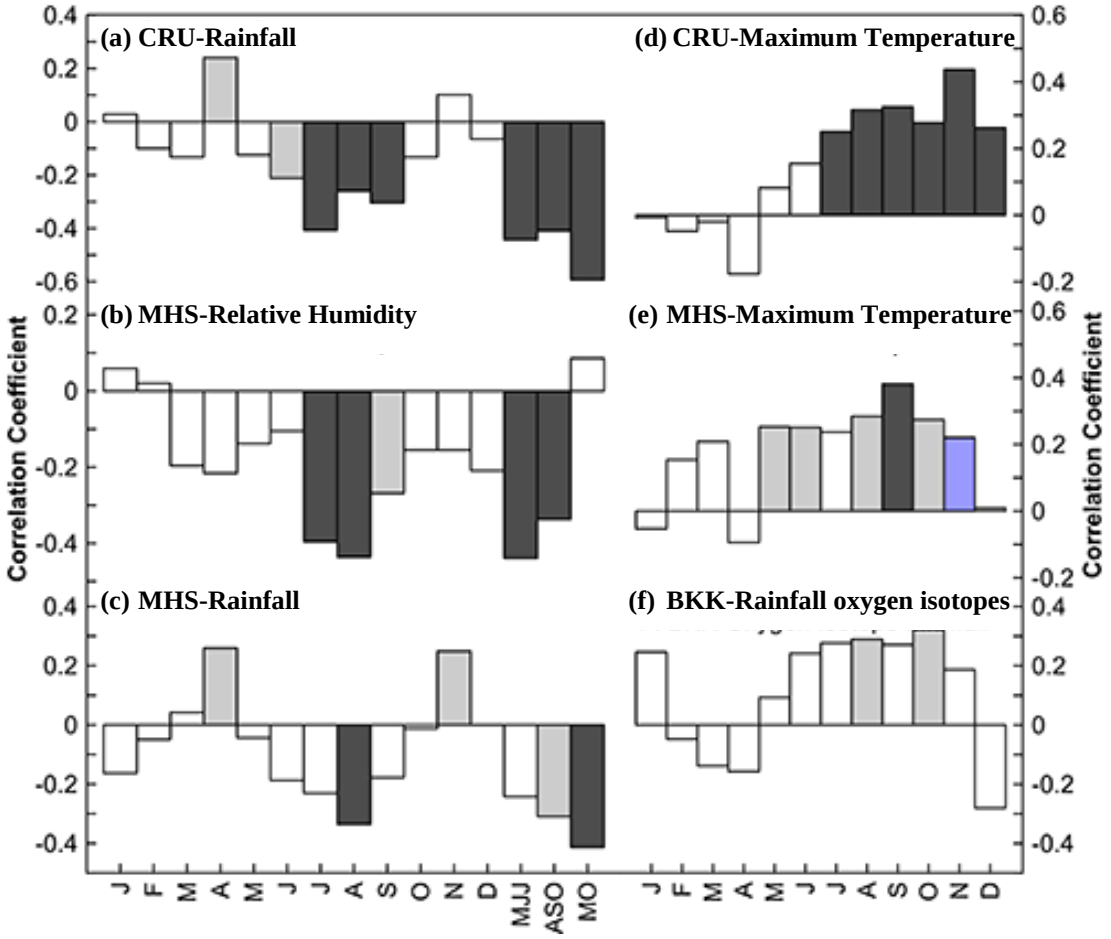

Figure 3.2.2 Correlations between tree-ring $\delta^{18}O$ and (a) rainfall obtained from the CRU TS4.03 during the period 1901–2015, (b) relative humidity (%) obtained from the Mae Hong Son meteorological station during the period 1950–2015, (c) rainfall obtained from the Mae Hong Son instrumental station during the period 1911–2015, (d) mean maximum temperature obtained from the CRU TS4.03 during the period of 1901–2015, (e) mean maximum temperature at Mae Hong Son meteorological station during the period of 1951–2015, and (f) $\delta^{18}O$ in rainfall in Bangkok. Black bars indicate correlations that are significant at the 99% level of confidence; light blue bars indicate correlations significant at the 95% level of confidence.

A spatial correlation analysis was performed to demonstrate the relationship between δ^{18}Otr and the amount of precipitation in the tropics. Regions showing significant negative correlations with the $\delta^{18}O_{tr}$ series appeared over wide areas in Southeast Asia as well as in the eastern parts of the Indian subcontinent. The correlation was strongest over northwestern Thailand and decreased toward the east (Figure 3.2.3).

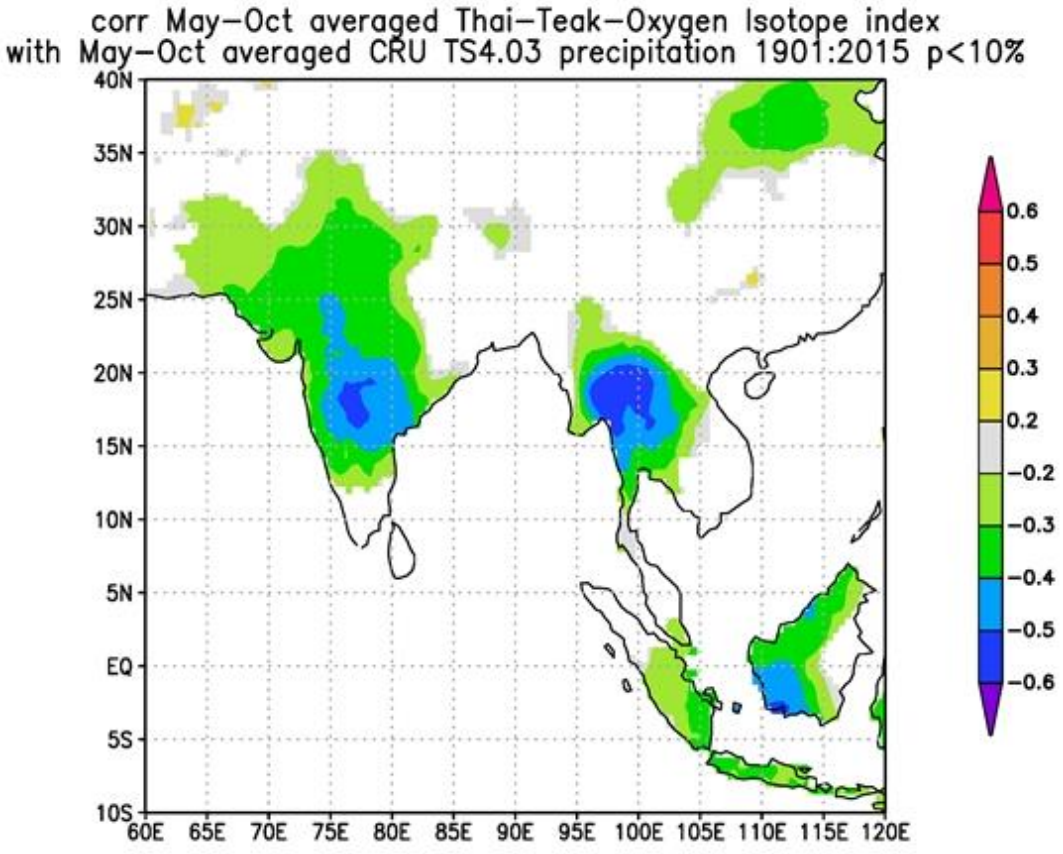

Figure 3.2.3 Spatial correlation pattern of Thai Teak $\delta^{18}O_{tr}$ *vs.* CRU TS4.03 May–October precipitation.

3) Possible mechanisms for the strong precipitation signal in $\delta^{18}O_{tr}$

Our $\delta^{18}O_{tr}$ chronology exhibits a stable inverse relationship with the local and regional rainy season (May to October) precipitation (r = -0.413, p < 0.001, n = 65 and r=-0.593, p<.001, n=112, respectively), probably as a result of the well-known "amount effect" (Dansgaard, 1964), and a positive relationship with the maximum temperature from June to December (highest in November, r = 0.437, p < 0.001, n = 112) during the dry season. It is possible that the source water signal of the soil is

dominated by seasonally changing $\delta^{18}O$ signatures in precipitation. As our study trees grew on mountain slopes, any groundwater impact on the tree-ring oxygen isotope signature can be excluded. In addition, teak has a shallow root system(Pumijumnong et al., 1995) and grows well on well-drained soils. Thus, variations in oxygen isotope series in teak wood are expected to reflect the variations in oxygen isotope ratios in seasonal rainfall, which is affirmed by the significant positive correlation between $\delta^{18}O_{tr}$ and annual $\delta^{18}O$ in rainfall from the Global Network of Isotopes in Precipitation (GNIP) station in Bangkok (August $r = 0.289$, $p < 0.045$, $n = 48$, October $r = 0.321$, $p < 0.030$, $n = 46$). Duy et al. (2018) concluded that the variation in oxygen isotopes in rainwater is 70% controlled by regional moisture regimes compared to local climatic conditions (30%), and regional and local factors vary in importance seasonally and have a large influence on the isotopic composition of rainfall. According to our results, local rainfall and regional rainfall are related to $\delta^{18}O_{tr}$ in the same direction, and seasonal rainfall quite clearly controls the signature in $\delta^{18}O_{tr}$. However, it is also clear that local precipitation throughout the rainy season (MO) has less relation to $\delta^{18}O_{tr}$ than regional rainfall. Rainfall in the Mae Hong Son Province is clearly influenced by the Indian Ocean at the beginning of the rainy season (MJJ) and by the South China Sea at the end of the rainy season (ASO). The results of this study have been confirmed by the studies of Cai et al. (2010), Muangsong et al. (2016), and Wei et al. (2018). We showed the moisture trajectory in May, which is the source of moisture from the Indian Ocean, in September, which is the source of moisture from the South China Sea (Figure 3.1.4) and the wind vector from 1981-2010 during May to July, August to September, and November to December. It is clear that the direction of the wind changed from the beginning of the rainy season to the dry season (Figure 3.1.5). However, the regional climate covers more extensive areas, which causes fluctuations in $\delta^{18}O_{rain}$ and the enrichment of oxygen isotopes in leaves until they accumulate in trees. Therefore, it is found that regional rainwater throughout the rainy season is associated with higher $\delta^{18}O_{tr}$ than local rainwater. Nevertheless, more research on the relationship of $\delta^{18}O_{rain}$ and amount of rainfall in the regions influenced by the Asian monsoon pointed out that it was controlled by convective heat transfer and terrain (Kumar et al., 2010; Shen and Poulsen, 2019). Therefore, we find that not every month of rainfall is associated with $\delta^{18}O_{tr}$.

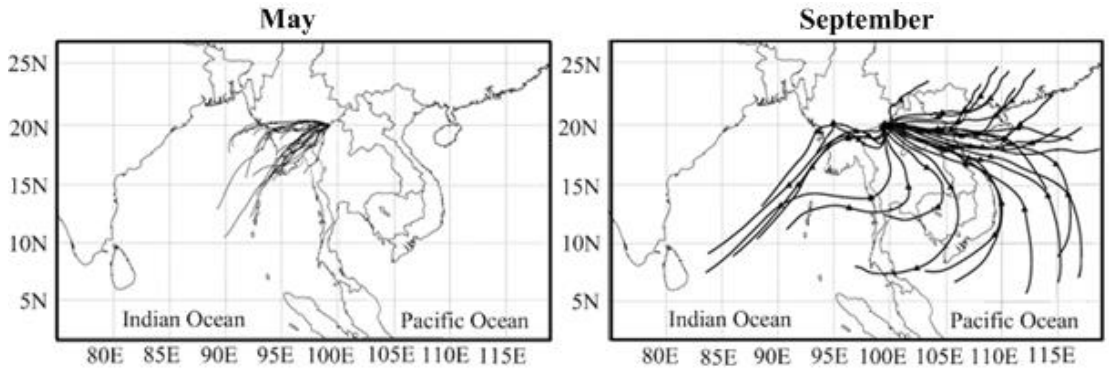

Figure 3.2.4 The 72-h back trajectories starting at 500, 1,000, and 1,500 m above ground level (Stein et al., 2015) for May and September at the study location.

Furthermore, our results correspond to the studies of Brienen et al. (2012) and Volland et al. (2016), which used $\delta^{18}O_{tr}$ in tree rings of *Cedrela spp.* from the Amazon basin and its surroundings and found significant positive correlations between $\delta^{18}O_{tr}$ and $\delta^{18}O$ in rainfall. The climate signals captured by our isotope record also agree with the studies of Muangsong et al. (2016 and 2019) and Schollaen et al. (2013). During the transitional months from the end of the dry season to the beginning of the rainy season (April), teak cambium becomes active (Enfield et al., 2001). However, evaporation during this time of the year is high, leading to ^{18}O-enriched leaf water. Hence, we found stronger correlations between $\delta^{18}O_{tr}$ and air humidity (July, August, and September, r = -0.396, $p < 0.001$, n = 66, r = -0.436, $p < 0.001$, n = 66, r = -0.269, $p < 0.029$, n = 65). Tree-ring $\delta^{18}O$ values in this region are not only controlled by total (or annual) rainfall but also by monthly and seasonal rainfall isotopic signatures. Hence, dominant variations in monthly and/or seasonal inputs of rainwater isotope signals are related to different humidity sources, which can be assigned values of $\delta^{18}O_{tr}$ in this region and may also result in different $\delta^{18}O_{tr}$ values, which may be the same species (Managave et al., 2011) or trees that grow in nearby areas (Buajan et al., 2016; Muangsong et al., 2016). In addition, an important process affecting $\delta^{18}O_{tr}$ is the fractionation of the oxygen isotope that occurs in leaves through the evapotranspiration process compliance with the maximum temperature control fluctuations in oxygen isotopes during warmer conditions, which enhances the

evaporation of the soil water and increases $\delta^{18}O$ in the source water (Sano et al., 2017), resulting in the abundance of the leaf water isotope (McCarroll & Loader, 2004).

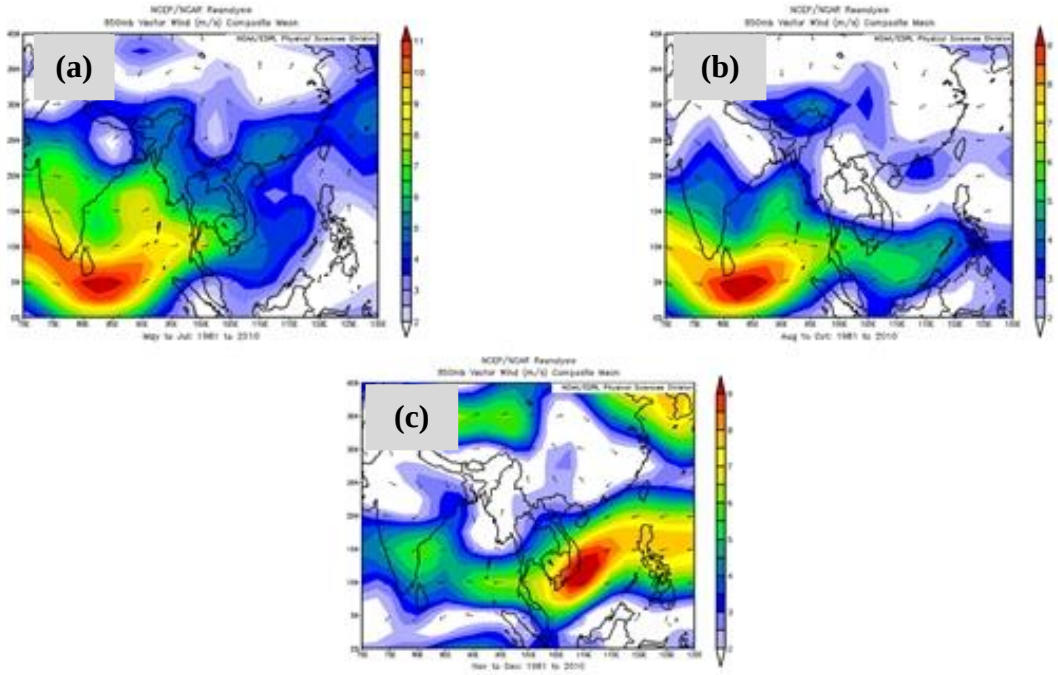

Figure 3.2.5 Composite averages of the 850-hPa wind vectors between AD 1981-2010 for (a) May to July of, (b) August to September, and (c) November to December. The NCEP/NCAR wind reanalysis data were obtained from NOAA/ESRL Physical Sciences Division (PSD), Boulder, Colorado (http://www.esrl.noaa.gov/psd/).

4) Comparison between $\delta^{18}O_{tr}$ and other proxies in nearby areas

The relationship between our teak $\delta^{18}O_{tr}$ and teak $\delta^{18}O_{tr}$ from the Phrae Province, which is approximately 400 km away, was 0.501, $p < 0.001$ (Muangsong et al., 2020), and Myanmar teak $\delta^{18}O_{tr}$ was 0.566, $p < 0.001$(Pumijumnong et al., 2020). We also found a relationship between our teak $\delta^{18}O_{tr}$ and *Pinus merkusii* $\delta^{18}O$ from Mae Hong Son *(*r = 0.646, $p < 0.001$*)* (Xu, et al., 2015) and from Umpang, Tak Province (r = 0.522, $p < 0.001$) (Xu, et al., 2018). This correlation coefficient was higher than the correlation found with the *Pinus kesiya* oxygen isotope series studied by Zhu et al. (2012), indicating that there was a common moisture source for the studied teak and *Pinus merkusii* trees. This has important implications for further studies on stable oxygen isotopes for both species to extend the existing records. It is interesting because the *Fokienia hodginsii* tree-ring $\delta^{18}O$ from Vietnam (r = 0.328, $p <$

0.001) (Sano et al., 2012) and the same species from Laos (r = 0.174, p < 0.005) (Xu et al., 2011) correlated with our teak $\delta^{18}O_{tr}$. The oxygen isotopes in tree rings are a great tool to study the hydrology cycle in Southeast Asia (Figure 3.2.6).

In addition to the tree-ring $\delta^{18}O$ that are extensively used in the study of monsoon dynamics, stalagmites in Thailand have also been studied for monsoon dynamics. We found that the teak $\delta^{18}O_{tr}$ has a positive relationship with high-resolution oxygen isotope record of stalagmites from Klang Cave in southern Thailand (Tan et al., 2019) after running a 31-point smoothing filter (r = 0.328, p < 0.001) as well as growth rate profile, derived from stalagmite NJ-0901, from Nam Jang Cave in Mae Hong Son province of northwestern Thailand (Muangsong et al., 2014) based upon data smoothed with a 7-point running-average filter (r = 0.430, p < 0.001) (Figure 3.2.7 (a)). Therefore, it is likely that we will gather proxies to be used to study the dynamics of the monsoon to unravel the complexity of the monsoon (Figure 1.2.7 (b)).

5) Teak $\delta^{18}O_{tr}$ and monsoon indices

The significant negative relationship between $\delta^{18}O_{tr}$ and ISM and the Webster and Yang Monsoon Index (WYM) was highest from June to August (JJA) (r = -0.544, p < 0.001) and highest from June to September (JJAS) (r = -0.459, p < 0.001) (data not shown).

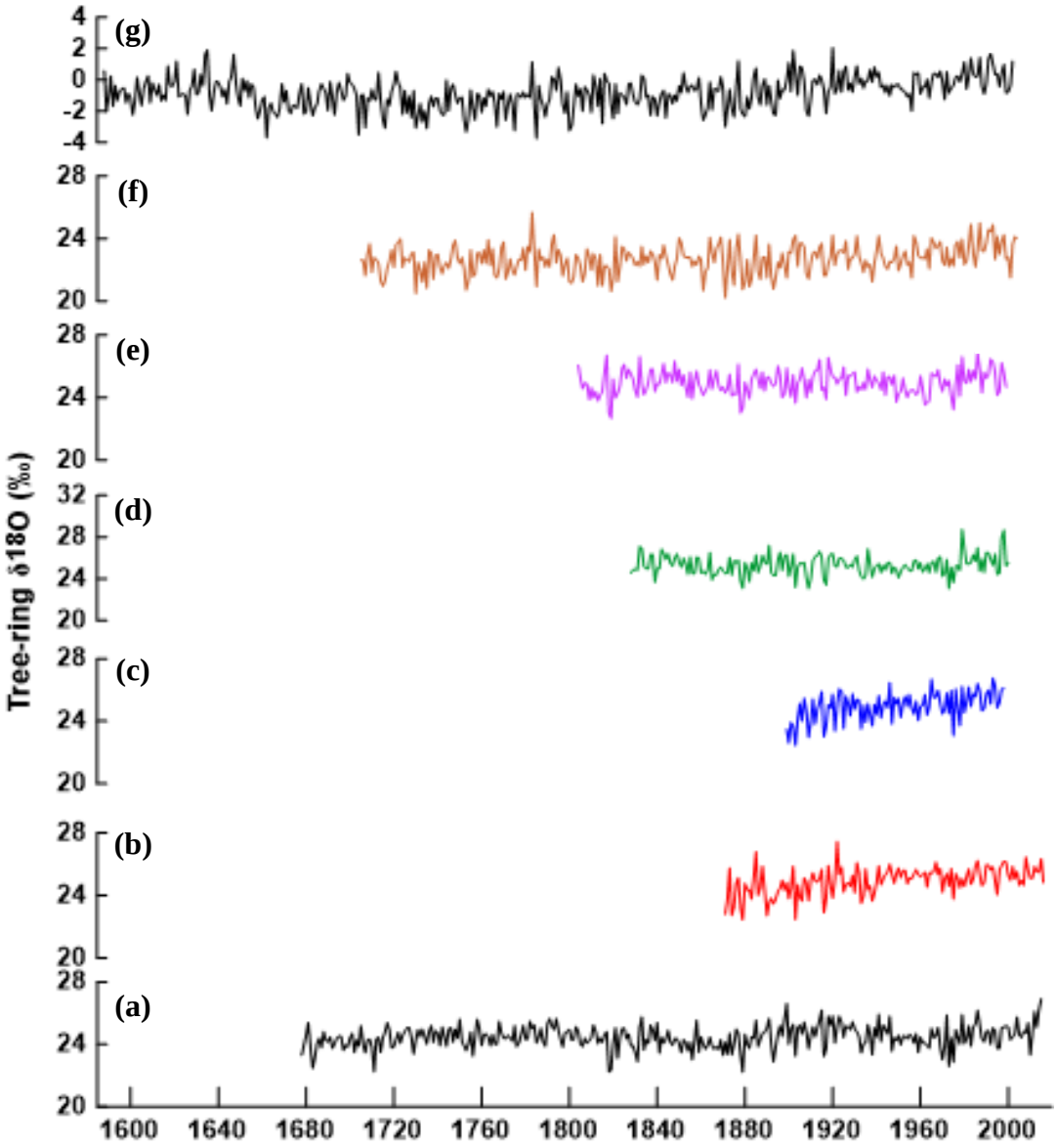

Figure 3.2.6 Comparisons of the oxygen isotope records of teak trees from (a) Mae Hong Son province in Thailand, (b) Phrae province in Thailand (Muangsong et al., 2020), (c) Myanmar (Pumijumnong et al., 2020), the oxygen isotope record of *Pinus merkusii* from (d) Mae Hong Son province in Thailand (Xu et al., 2015), (e) Tak province in Thailand (Xu et al., 2018), (f) the oxygen isotope record of *Fokienia hodginsii* from Vietnam (Sano et al., 2012), and (g) Laos (Xu et al., 2011).

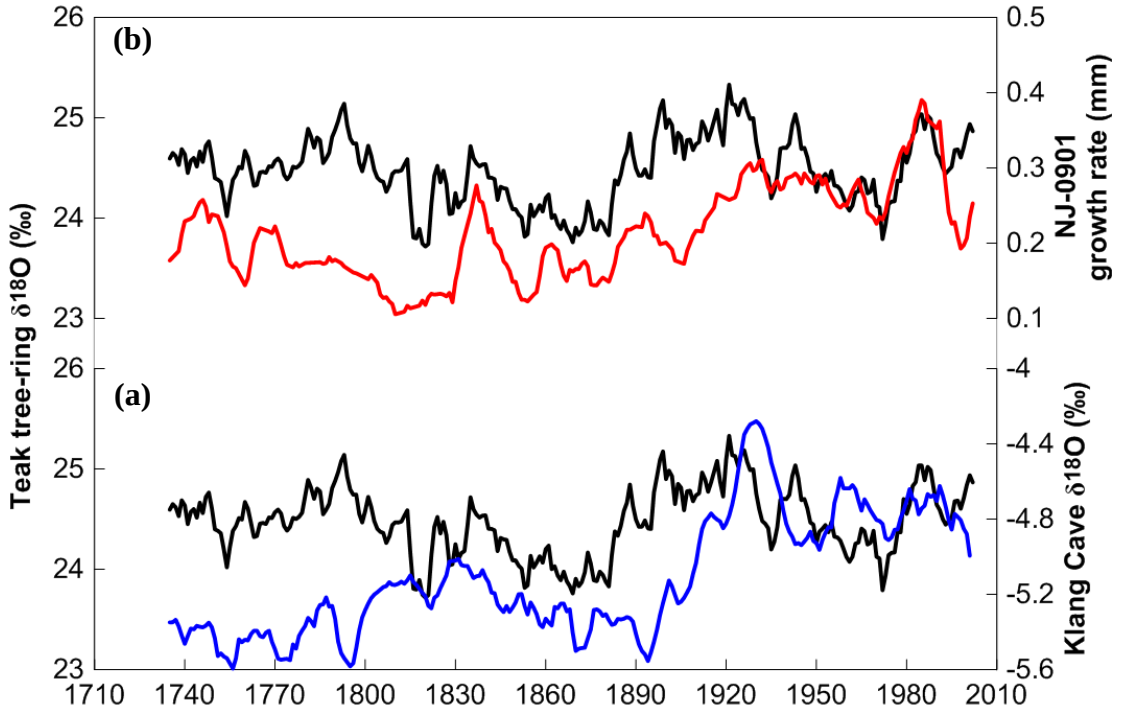

Figure 3.2.7 Comparisons of (a) the oxygen isotope record of stalagmites from Klang Cave in southern Thailand (blue solid line) (Tan et al., 2019) and (b) growth rate profile of stalagmite NJ-0901 from Namjang cave in Mae Hong Son province of northwestern Thailand (red solid line) (Muangsong et al., 2014) with the teak $\delta^{18}O_{tr}$ in this study (black line). All series were smoothed with a 7-point running-average filter.

6) Global correlation between $\delta^{18}O$ and sea surface temperature

We found significant positive relationships between our $\delta^{18}O_{tr}$ and the multivariate ENSO index (MEI). Correlations with the extended multivariate ENSO index (MEI_{ext} range of AD 1871–2005) were similar to MEI, in which the relationship began in May, with September showing the highest positive correlation (r = 0.565, $p < 0.001$). The same relationship was found between $\delta^{18}O_{tr}$ and both Niño3.4 and Niño4, with the highest positive correlation occurring in October for Niño4 (r = 0.577, $p < 0.001$) (Figure 3.2.8). Correlations between $\delta^{18}O_{tr}$ and Dipole Mode Index (DMI) over the entire period (AD 1870–2015) revealed significant positive relationships from June to October, with October being the month that had the highest correlation (r = 0.453, $p < 0.001$) (Figure 3.2.8 (a)). Furthermore, a positive relationship between $\delta^{18}O_{tr}$ and Pacific Decadal Oscillation (PDO) was found from

July to December, with the highest correlation in August (r = 0.258, p < 0.005). Our $\delta^{18}O_{tr}$ and Palmer Drought Severity Index (PDSI) showed significant negative correlations over the whole year, with the highest correlations being from October to December (r = -0.449, p < 0.001).

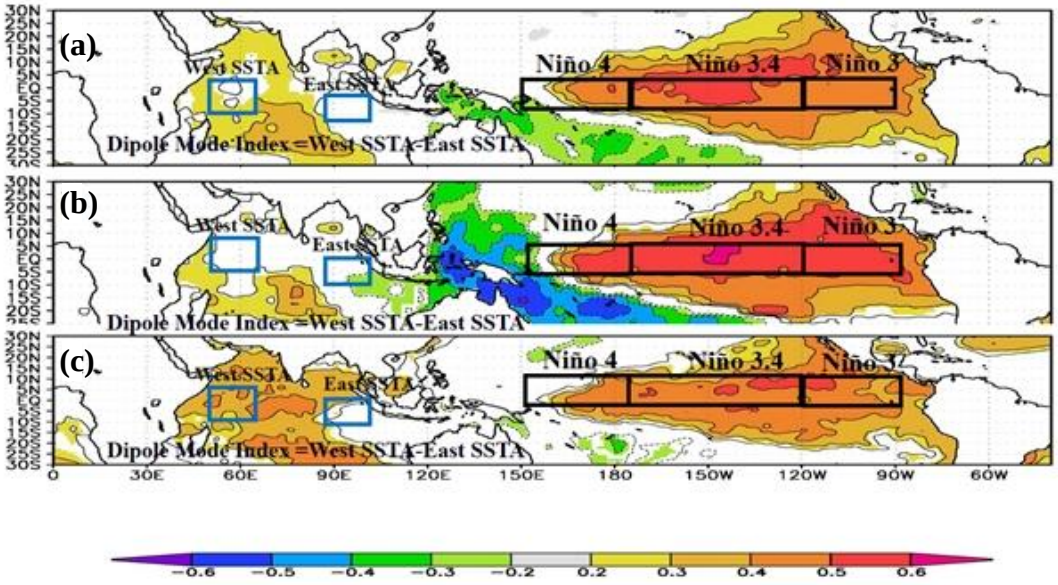

Figure 3.2.8 The correlation between average teak oxygen isotope values (May-December) and HadlSST (Niño3.4) in different time period, including (a) 1870-2015, (b) 1870-1942, and (c) 1943-2015. The blue frames are West SSTA and East SSTA and the black frames are Niño4, Niño3.4, and Niño3.

7) Reconstruction of May to October (M–O) rainfall

The correlation between $\delta^{18}O_{tr}$ and regional climate precipitation of M–O showed the highest value (r = -0.593, p < 0.001); therefore, precipitation during the ASM season was targeted for climate reconstruction. We used a simple regression model to develop a transfer function, which is shown as follows:

P_{MO} = 772.985+ (-21.250) * $\delta^{18}O_{tr}$,

where P_{MO} represents May–October rainfall. We divided this period into two subperiods, AD 1904–1959 and AD 1960–2015, for crosswise calibration and verification. The verification and calibration statistics were shown in Table 1.2.1. The values for Reduction of Error (RE) and Coefficient of Efficiency (CE) were positive in both subperiods, indicating the validity of the oxygen isotope record as a climate

estimate (Fritts, 1976). Finally, we reconstructed the precipitation from May–October based on the full dataset for calibration. The linear regression model explained 35.20% of the actual variance in the May-October precipitation (Figure 3.2.9).

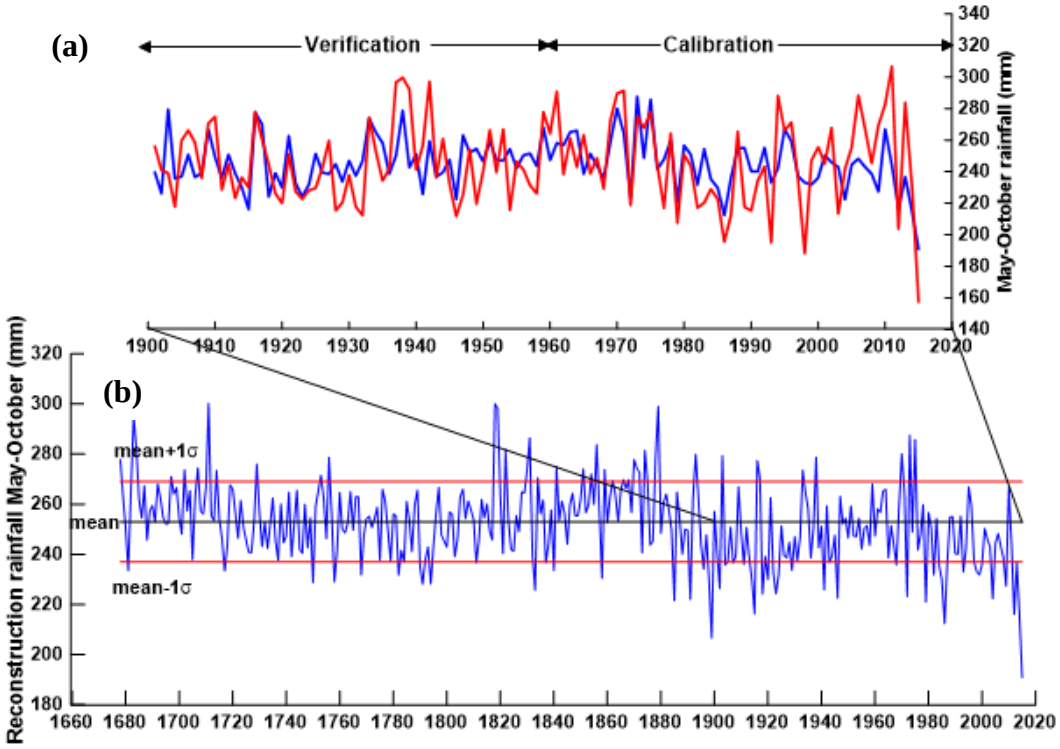

Figure 3.2.9 (a) May to October rainfall (mm), red line is actual CRU TS4.03 rainfall (mm) and blue line is reconstruction May-October rainfall (mm) and (b) reconstruction rainfall May–October black line is the average rainfall of 253 mm, read line (mean+1σ) is 269 mm, and (mean-1σ) is 237 mm.

Table 3.2.1 Calibration and verification of May to October precipitation reconstruction

Calibration				Verification				RE	CE
Period	r	r^2	ST	period	r	r^2	ST		
1904-1959	0.514	0.264	36/-20	1960-2015	0.643	0.413	35/-21	0.386	0.385
1960-2015	0.643	0.413	37/-19	1904-1959	0.514	0.264	35/-21	0.229	0.227
1904-2015	0.593	0.352	72/-40						

ST = sign test, RE = reduction of error, CE = coefficient of efficiency

Significant level at $p < 0.05$ level

8) The late-Holocene Asian summer monsoon variability over the past 338 years

Our May to October precipitation reconstruction revealed that over the entire period from AD 1678–2015, summer precipitation in northwestern Thailand had decreased, and the reconstructed long-term average of May–October (rainy season) average precipitation was 253 mm. The dry period mean minus the standard deviation was equal to 237 mm, and the wet period mean plus the standard deviation was equal to 269 mm. We found that during the 17th and 18th centuries, drought occurred during 8 years, respectively. In the 19th century, there was drought during 19 years. In the 17th, 18th, and 19th centuries, wet years occurred during 6, 10 and 1 years, respectively. Our May–October rainfall reconstruction corresponds to the findings of Xu et al. (2015) and (2018) using pine tree-ring oxygen isotopes, from both the Mae Hong Son and Tak Provinces. It was found that during the 17th century, rainfall tended to decrease, and the drought period continued more often than during periods of heavy rainfall. The mechanism that may support drought in Southeast Asia is the southward shift in the Intertropical Convergence Zone (ITCZ). The results of the rainfall reconstruction using stalagmite $\delta^{18}O$ from Klang Cave (Tan et al., 2019) found that the ITCZ has moved southward since the 18th century, and the most noticeable period is the 1980s.

In addition, our results are in line with the findings of Buckley et al. (2007) who built a teak growth index of living trees and stumps that covered 448 years. In particular, Buckley et al. (2007) proposed a relationship between teak growth and PDSI and highlighted the drought that was recorded by the teak index in the early and mid-1700s. Our study also found a significantly negative correlation between the $\delta^{18}O_{tr}$ of teak and PDSI, showing higher correlation coefficients than the teak ring width index. In addition, these findings are consistent with other reconstructed mega drought events, especially those found in the 18th century, such as the Strange Parallels drought (1756–1768) and the East India drought (1790–1796) (Cook et al., 2010). Anderson et al. (2002) found that during almost the entire 18th century, the weakening of the southwest monsoon was a result of cooler North Atlantic sea surface temperatures (SST).

9) Large-scale drivers of interannual to decadal variations in tree-ring oxygen isotopes

The significant positive relationships of our $\delta^{18}O_{tr}$ with MEI (AD 1950–2015), MEI extended (AD 1871–2005), Niño3.4 (AD 1870–2015) and Niño4 (AD 1870–2005) point to a strong impact of ENSO on rainfall variability in northwest Thailand.

We calculated the relationships between $\delta^{18}O_{tr}$ and Niño4 SSTs over different periods. During the four periods of AD 1870–1906, AD 1907–1943, AD 1944–1980, and AD 1981–2015, $\delta^{18}O_{tr}$ and SSTs showed strong positive correlations. The most affected time was in the period of 1870–1906, the relationship between $\delta^{18}O_{tr}$ and Niño4 showed a decrease in the positive relationship, and the month that appeared to be somewhat delayed but was still significant between AD 1981 and 2015. In general, the IM was strongly influenced by the ENSO during the first half of the 20th century, whereas since the 1980s, the IM has been increasingly influenced by the Indian Ocean Dipole (IOD) (Nakamura et al., 2009). Pratarastapornkul (2007) proposed that the IOD phenomenon affects annual rainfall in Thailand and that its impact varies depending on the combined effect and strength of the ENSO and IOD in the Pacific Ocean. As such, it is likely that excess rainfall and severe floods are to be expected in most regions of Thailand in cases of strong IOD events that combine with weak El Niño events.

The El Niño-Southern Oscillation (ENSO) is a major driver of global climate variability. The ENSO also interacts with other modes of climate variability, such as the Indian summer monsoon rainfall (ISMR). The easterly trade winds and SST gradients across the equatorial Pacific undergo a regime change, with enhanced trade winds and significant cooling (warming) over the tropical eastern (western) Pacific in the later period. Previous research has shown that the relationship between the ISRM and SSTs is variable (Achuthavarier et al, 2012; Malik et al., 2017). The strongest relationships were found on short timescales (interdecadal periodicity, 2–7 years) or decadal periodicity (10.5 years) but with varying significance levels (Varikoden and Babu, 2015). Several studies have examined the relationships between the ISM and ENSO phenomenon and/or variations in SST and sea surface pressure (SSP) in the Pacific Ocean (Roy and Tedeschi, 2016). This result suggests that $\delta^{18}O_{tr}$ records multiple ENSO phenomena. Several studies (Gadgil et al., 2004; Webster and Yang,

1992) have pointed to the fact that the influence of the ENSO phenomenon on the ASM varies over time.

Similar influences of ENSO on the isotopic signature in tree rings were observed in Laos (Xu et al., 2013), Thailand (Muangsong et al., 2020), Indonesia (Poussart et al., 2004), and China (Liu et al., 2011; 2014). However, the strength of the ENSO influence was variable throughout the study period. In Bolivia, a reduced influence of ENSO during 1950–1974 coincided with periods of lower variance in the Southern Oscillation Index. However, it was also found that the lowest correlations with Niño 4 events occurred between AD 1981 and 2015. There are multiple factors that make the relationship between our $\delta^{18}O_{tr}$ and El Niño lower. One probable factor is caused by rapid traversing of the ITCZ and/or the teleconnections with the northern Atlantic thermohaline circulation, which could weaken the Asian monsoon through the air-sea connection (Sinha et al., 2007). Singhrattna et al. (2005) found that in the past decade, Pacific SSTs have had a negative relationship with the summer monsoon in Thailand, but this relationship weakened prior to 1980 due to changes in the Walker circulation over the Thailand-Indonesian region. Therefore, variations in $\delta^{18}O_{tr}$ with El Niño periods could come from several factors and require a more in-depth analysis.

Ashok et al. (2001) explained the impact of the IOD on the IM and ENSO during the period of AD 1958–1997, stating that the IOD and ENSO have an integral effect on the Indian summer rainfall (ISR). Whenever the ENSO-ISR correlation was low (high), the IOD-ISR relationship was high (low). However, Ashok et al. (2003) and (2004) found that the IOD is a physical mode of the tropical Indian Ocean and that the evolution of the IOD is mostly independent from the Pacific's influence (Rao et al., 2002; Vinayachandran et al., 1999).

Based on the results presented in Figure 3.2.8 (a-c), SSTs in the central Pacific Ocean and Indian Ocean during the periods of AD 1870–2015, AD 1870–1942 and AD 1943–2015 showed that SSTs of both oceans are highly correlated with our $\delta^{18}O_{tr}$. Positive IOD phases occurred in 1961, 1963, 1972, 1982, 1983, 1994, 1997, 2006, and 2012. Furthermore, we found that Thailand's rainy season precipitation was below average in 1972, 1979, 1982, 1984, 1985, 1986, 1993, 1998, 1999, 2004, 2009, 2012, 2014, and 2015. Bridhikitti (2013) investigated the connection of ENSO/IOD with Thai rainfall anomalies during the period of AD 1980–2011 based on instrumental

data from 17 locations. He found that the effect of ENSO on summer monsoon rainfall was not obvious, but the negative (positive) IODs in October, November, and December corresponded with La Niña (El Niño) signals, which may be seen in increased (decreased) rainfall on the southeast coast during the months of December, January and February.

Severe IOD events in the summer monsoon season could affect rainfall in northern Thailand in the following year. Chansaengkrachang et al. (2015) studied the time lags between IOD and rainfall over Thailand during the period of AD 1979–2008 based on rainfall data derived from 80 meteorological stations spread throughout Thailand. It was found that signal consistency in years of strong IOD showed an offset of approximately 11 months. This indicates that the IOD leads the rainfall by approximately two months. In addition, Hochreuther et al. (2016) found positive correlations between Sikkim larch (*Larix griffithii*) $\delta^{18}O_{tr}$ during strong positive IOD phases in southeast Tibet, when heavy rains had occurred in the western part of the Indian Ocean and less rain/drought occurred in Indonesia and Australia.

Clearly, the ISM variability is complex and related to many phenomena, such as ENSO, differences in surface temperatures in the Indian Ocean (IOD) and the difference in North Atlantic SSTs (Mölg et al., 2017). Our $\delta^{18}O_{tr}$ captured the season of the ISM. Our $\delta^{18}O_{tr}$ showed a significant positive correlation with the ENSO phenomenon. As such, the creation of a network of oxygen isotope tree-ring cellulose chronologies to cover a wider area and extend the length of $\delta^{18}O_{tr}$ is needed and would help us to better understand long-term ASM variability and its interrelationships with other atmospheric circulation patterns and climate forcing factors. This holds particularly true for Thailand, since the currently existing tree-ring $\delta^{18}O$ are all from the Mae Hong Son Province in Northwestern Thailand. To better understand the influence of the monsoon nationwide, analyzing specimens from other areas and examining the consistency of monsoon influences over the entire country is needed. Additionally, there are good possibilities to further extend the length of the existing tree-ring $\delta^{18}O$ chronology through the use of ancient teak wood from archaeological sites.

3.3 Large-scale and long-term climate evolution in China, their driving mechanisms, and teleconnections to global climate change

1.3.1 The early-Holocene climate evolution in China

1) Multi-decadal variability of Eastern Asian Summer Monsoon during 2.8 ka cold event and its responding to solar activity and Greenland climate

The 2.8 ka cold event is one of well-known abruptly climate events during the late Holocene (Bond et al., 2001). Previous documents have shown weak Eastern Asian Summer Monsoon (EASM) (Wang et al., 2005) and less precipitation in the northern margin of EASM area during the 2.8 ka event. The forcing of this event has been pointed to Solar activity (Wang et al., 2005), but the detail forcing mechanism is still unclear. Considering the significantly negative excursion of solar activity during the 2.8 ka even, high resolution record of the EASM with well age constraining is helpful for us to better understand this mechanism.

In this study, stalagmites, namely MD11 and MD12, from Miaodong (MD) (41º03´N, 125º31´E), Northeastern China were analyzed. The Miaodong stalagmite oxygen isotope sequence covering 3.04-2.60 ka B.P, constrained by 7 high precise ^{230}Th ages, was built. The variability of Miaodong stalagmite oxygen isotopes was interpreted as change in the EASM intensity or monsoon precipitation in this area. Based on these ^{230}Th ages with low errors (two sigma, 18 to 23 years), the Miaodong record give a detail evolution of the EASM and precise transfer time of the 2.8 ka event. From 2.88 ka B.P. to 2.62 ka B.P., the Miaodong record exhibited two weak EASM intervals, 2.81-2.87 ka B.P. and 2.76-2.66 ka B.P., respectively (Figure 3.3.1 (a)). The later one covered approximately 100 year which was the key period of the 2.8 ka event, and exhibited symmetrical shifting processes (Figure 3.3.1 (a)). The EASM abruptly decreased at around 2.76 ka B.P., and reached its worst state at approximately 2.68 ka B.P., following by an abruptly strengthening process (Figure 3.3.1 (a)). This transfer point (2.68 ka B.P.) was little younger than those stalagmite records from southwestern China (ca. 2.71 ka B.P., Wang et al., 2005), but coincided very well with Solar Activity Index (Steinhilber et al., 2012) (Figure 3.3.1 (b-c)).

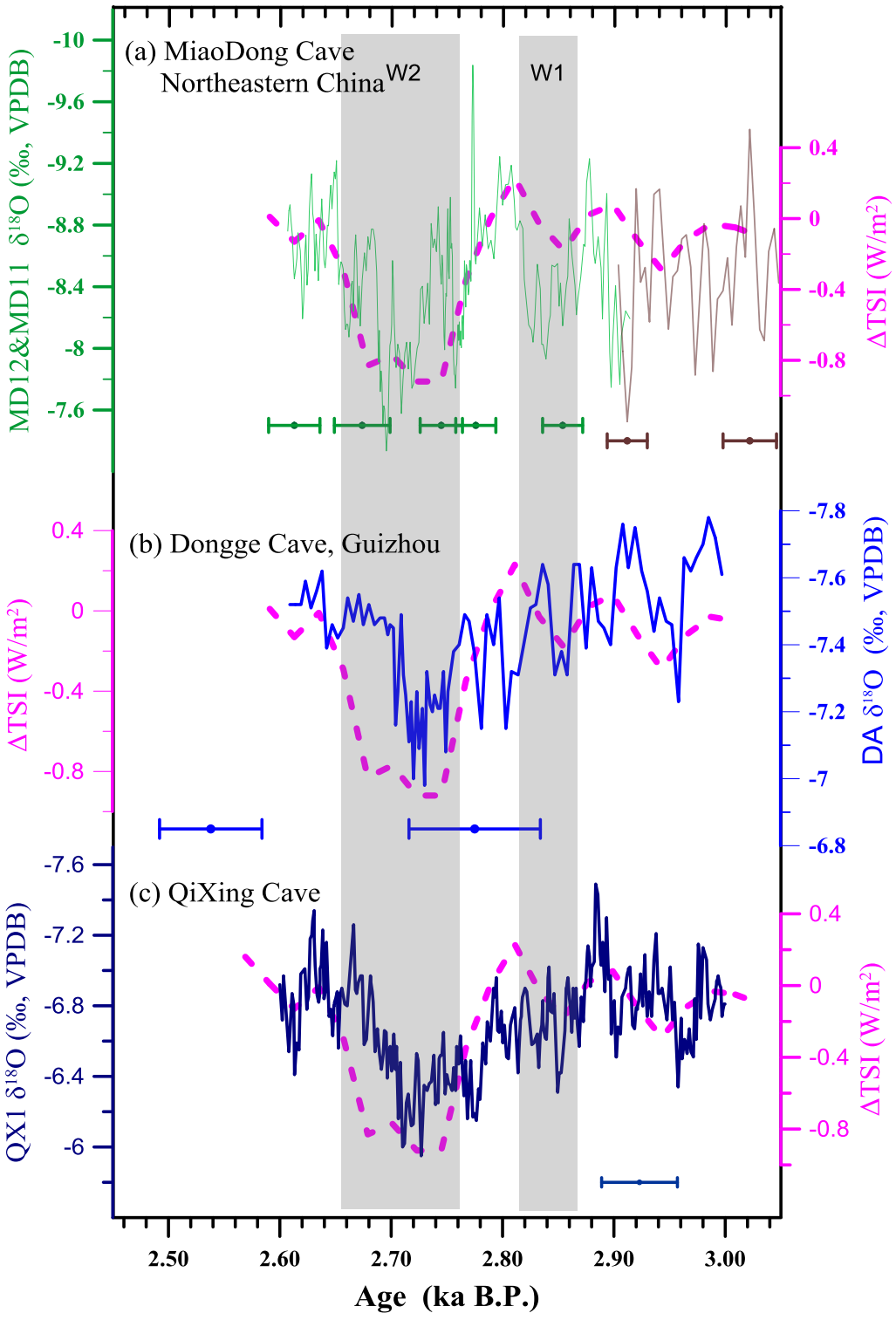

Figure 3.3.1 Comparisions of the Total solar irradiance (TSI) with stalagmite $\delta^{18}O$ sequences from (a) Miaodong cave (MD), (b) Dongge cave (DA) (Wang et al., 2005), and (c) Qixing cave (QX1) (Cai et al., 2001), showing the details of "2.8 ka" failure monsoon event and its robust correlation with solar activity (Steinhilber et al., 2012).

In general, the evolution of EASM indicated by Miaodong record coincides with those of total solar irradiance (ΔTSI) (Steinhilber et al., 2012) with any delay, indicating solar activity forcing via a fast dynamic mechanism. Unlike with southeastern records which show gradually decrease of EASM from 2.88 ka B.P. until ca. 2.71 ka B.P. and abruptly increase from then on, the instantaneously response of Miaodong record to ΔTSI without any delay indicates that the decrease of TSI (Steinhilber et al., 2012) maybe result in intense cold climate over North Atlantic Ocean (Bond et al., 2001) and high latitude area of North hemisphere (Grootes et al., 1993; Stuiver & Grootes, 1997), and then decrease the EASM via atmospheric remote-correlation (Figure 3.3.2).

2) Multi-decadal to centurial scale variability in East Asian Summer Monsoon around 5.5 ka event indicated by a stalagmite oxygen isotope record from Water cave, Liaoning, Northeastern China: links to ENSO and influence on the evolution of local civilization

The 5.5 ka events occurred in the middle Holocene, which were broadly thought to be dry and cold. However, the detailed nature of the EASM in 5.5 ka event remained unclear. Therefore, high resolution records, especially those records with high precise dating from typical monsoon region, are necessary. Northeastern China locates in the edge of the typical East Asian monsoon region. Based on the MC-ICP-MS- ^{230}Th dating and high resolution stable oxygen isotope analysis, stalagmite TW704 collected from Water cave, Northeastern China, were chosen to reconstruct high resolution proxy index of the EASM in this study.

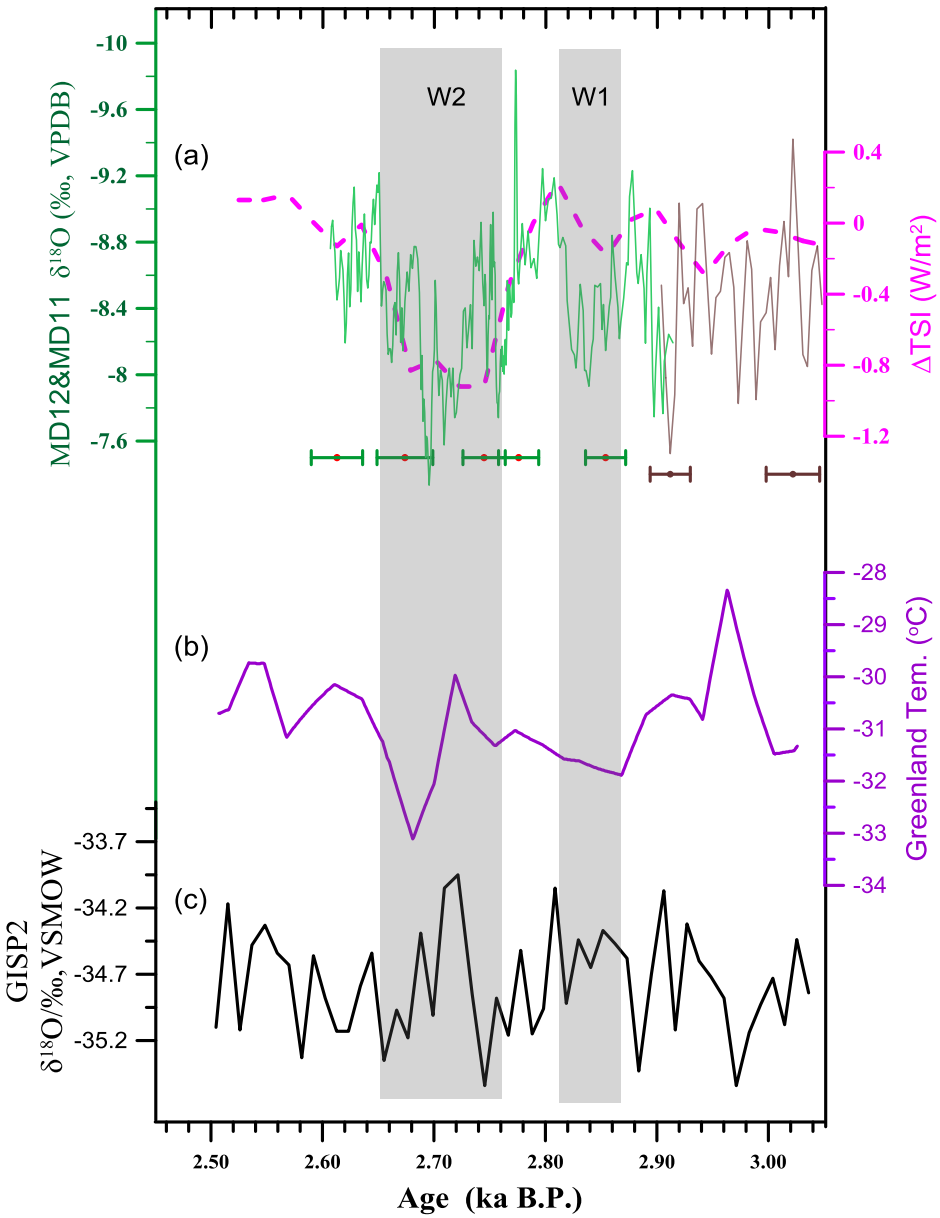

Figure 3.3.2 Comparisons between stalagmite MD oxygen isotope profiles (green solid line, the error bars indicate 2σ age error) and, (a) solar activity indexes (ΔTSI) (purple dashed line) (Steinhilber et al., 2012), (b) Greenland Temperature (Grootes et al., 1993) and (c) GISP2 oxygen record (GICC05 Chronology) (Stuiver and Grootes, 1997).

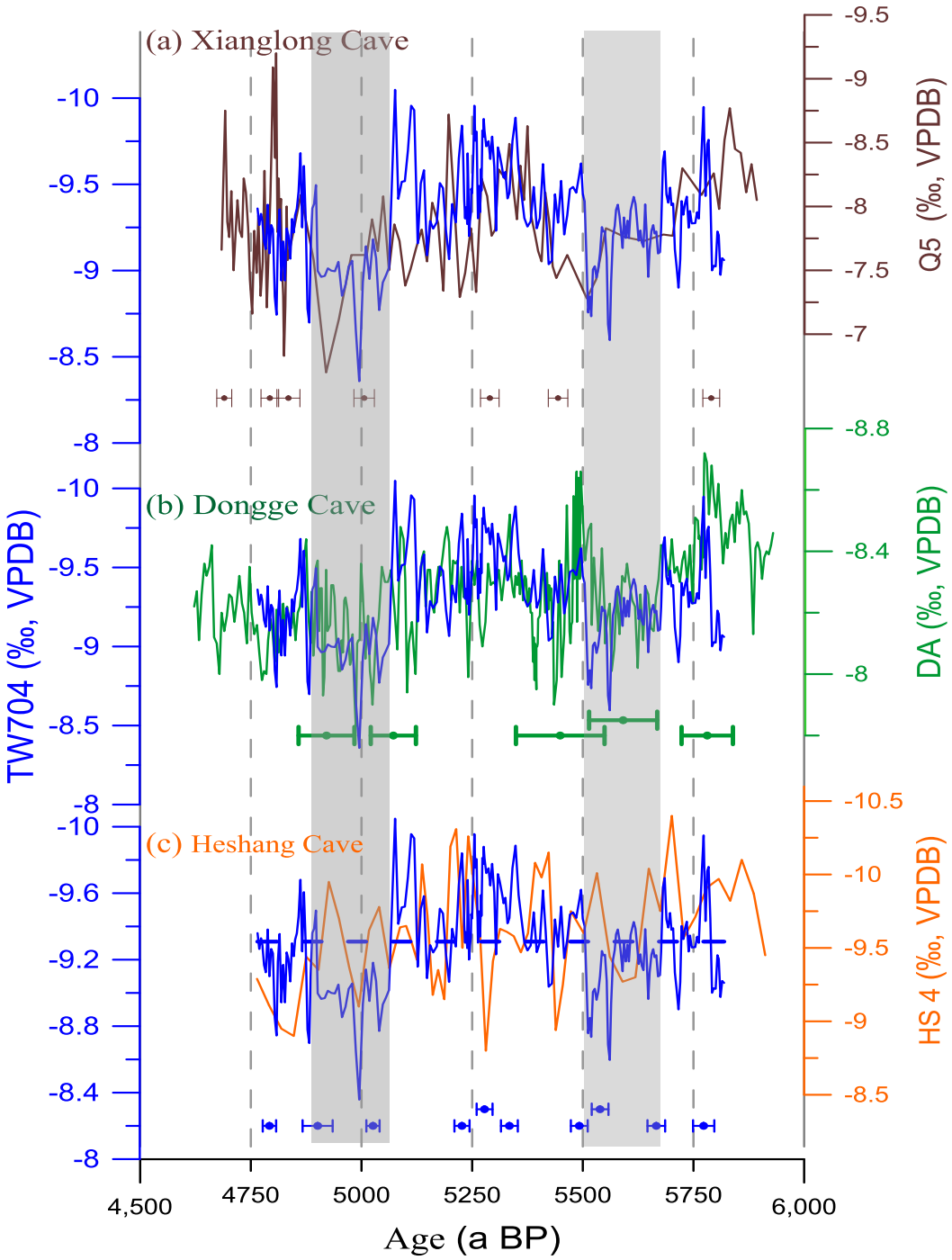

Figure 3.3.3 Comparisions of stalagmite $\delta^{18}O$ profiles collected from water cave (TW704) (blue solid lines) with those of stalagmites collected from (a) Xianglong cave in Sichuan province (blown solid line) (Tan et al., 2018), (b) Dongge cave in Guizhou province (green solid line) (Dykoski et al., 2005), (c) Heshang cave in Hubei province (orange solid line) (Hu et al., 2008), showing the similar evolution of the EASM around the "5.5 ka" event.

The TW704 record exhibited decade-scale and century-scale variability of the EASM, during a period from 5.82 ka B.P.to 4.77 ka BP (Figure 3.3.3). It showed a significant century-scale oscillation, including two weak monsoon intervals, centering at 5.54 and 4.95 ka BP, respectively (Figure 3.3.3). Results of the spectrum analysis showed a significant 11 and 22 years solar cycle. Comparing with solar activity indicators (Total Solar Irradiance, Sunspot Number and ^{10}Be) (Steinhilber et al., 2012), there was no obvious corresponding relation between them (Figure 3.3.4 (c)). The contrary trend in century-scale, especially weak monsoon stage (~5.0 ka BP), was observed, which was the strongest period of solar activity (Figure 1.2.4 (c)). Therefore, the evidence for the solar forcing was still limited. By contrast, TW704 records do agree well with ENSO event, indicating the ENSO forcing mechanism (Figure 3.3.4 (b)).

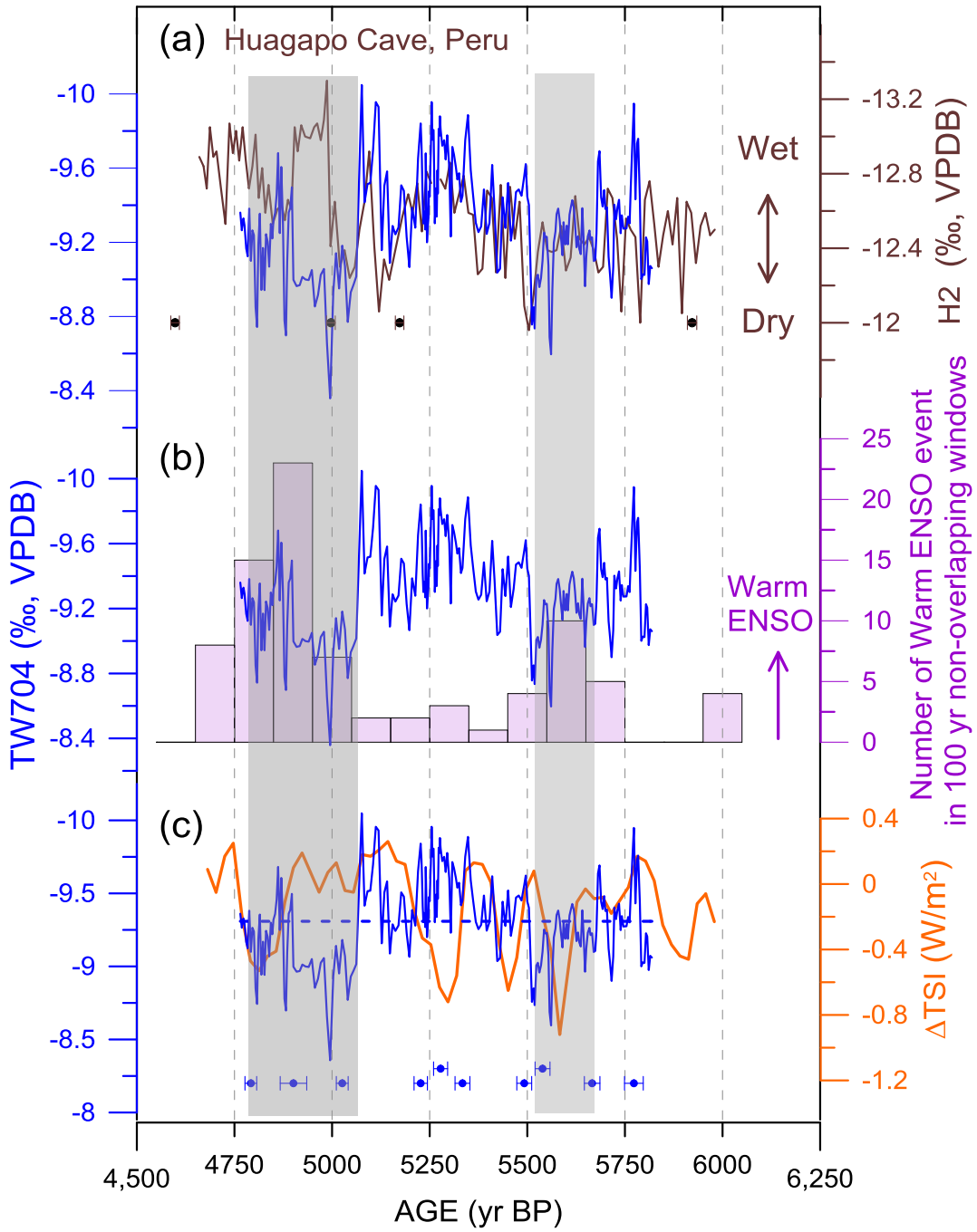

Figure 3.3.4 Comparisons of stalagmite TW704 record with (a) stalagmite records collected from Huagapo cave in Peru (Kanner et al., 2013), (b) frequency of the ENSO event, and (c) solar activities index (TSI) (Steinhilber et al., 2012).

3) Solar influence on the variability of East Asia Summer monsoon during Early Holocene: Annually-laminated stalagmite records from Beijing Shihua cave, Northern China

The precipitation variability of the EASM has a great significance on the lives of millions of people in this area. Understanding the early Holocene EASM dynamic during the demise of Northern Hemisphere continental ice sheets is crucial to assess the EASM behavior in the context of potential ice-sheet melting because of anthropogenic warming.

A well-dated high-resolution the EASM record from 11.3 ka BP to 9.9 ka BP based on a laminated stalagmite combined with another coeval stalagmite from the same cave, Northern China was presented (Figure 3.3.5 (a-c)). Four weak summer monsoon events (including Bond event 7) were identified, which were likely link to the cold events in Greenland (Figure 3.3.6)

Power spectra and Cross-wavelet analysis of stalagmite $\delta^{18}O$ sequence and annual band thickness both showed a statistically significant periodicity of approximately 200 years and indicated the anomalies climate events during the early Holocene, which were possibly triggered by solar activity. Solar changes may cause the cooling of high latitudes, and in turn, influence the EASM precipitation through atmospheric teleconnection.

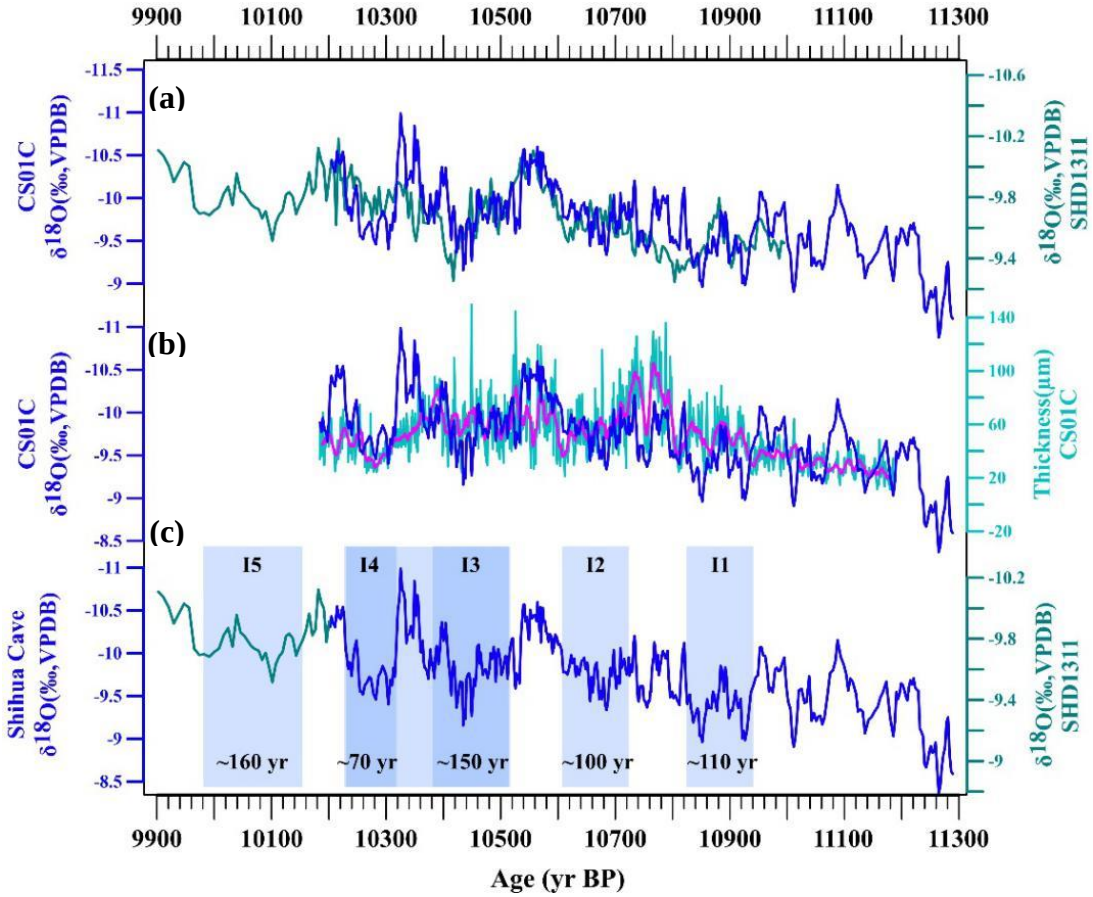

Figure 3.3.5 (a) The $\delta^{18}O$ values of stalagmite SHD1311 (green solid line) and CS01C (blue solid line), (b) The $\delta^{18}O$ (blue solid lines) and annual band thickness (green solid lines) profiles of stalagmite CS01C, and (c) the composite $\delta^{18}O$ profile for stalagmites SHD1311 and CS01C. Blue bars indicate intervals of positive excursion of $\delta^{18}O$.

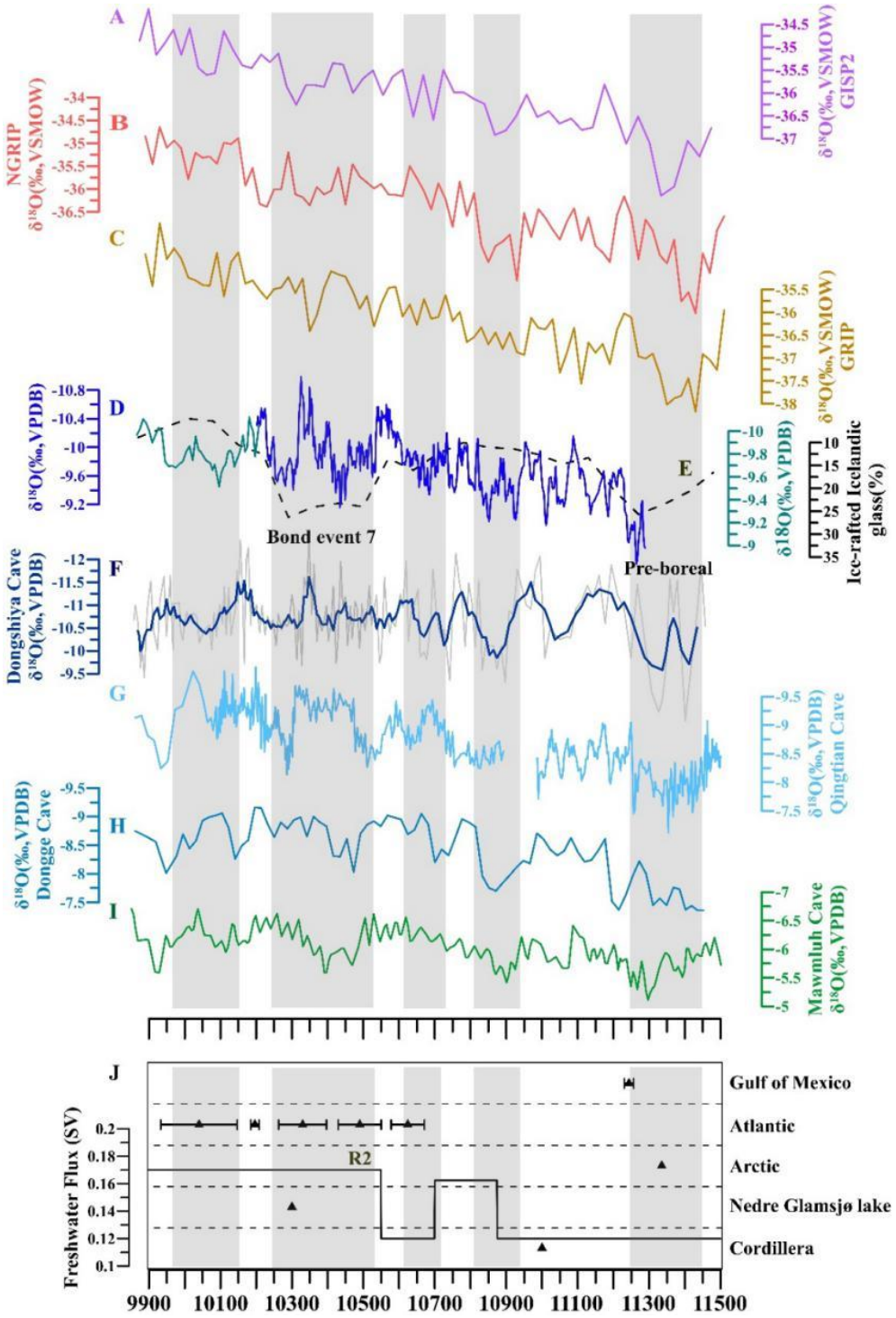

Figure 3.3.6 Comparison of Shihua cave $\delta^{18}O$ record with other records. Triangles mark freshwater outbursts from major ice-dammed lakes, error bars show chronological uncertainties of individual records. The solid dark black line marks the baseline flow of combined Hudson River and St. Lawrence River runoff, R2 denotes a rerouting event (Clark et al., 2001). The grey bars indicate four weak monsoon events.

1.3.2 The mid-Holocene climate evolution in China

1) The evolution of Asian Summer Monsoon during mid-Holocene recorded by a high-resolution stalagmite from western Yunnan

The Holocene optimum was the warmest and humid period of Holocene. However, there were also a series of centennial-millennial weak monsoon events. The 8.2 ka BP climate change event of the early-Holocene has the most extensive influence during this period. In this study, stalagmite record collected from Sigangli cave in western Yunnan, China was selected, with an average resolution of 3.7 years. The variability of the Sigangli cave $\delta^{18}O$ records can be regarded as a proxy index of the Indian summer monsoon (ISM). Results indicated the ISM variability at approximately from 5.4 to 8.9 ka BP. The $\delta^{18}O$ profile appeared to be a remarkable change on millennial timescale. The overall change trend of the stalagmite $\delta^{18}O$ records was positive, indicating that the Indian monsoon gradually became dry, consistent with the weakening of monsoon since the mid-Holocene (Figures 3.3.7 and 3.3.8)

Comparisions of the stalagmite record from Sigangli cave with other stalagmites in the Asian monsoon region (Figures 3.3.7) (Cheng et al., 2009; Liu et al., 2013) showed that the Asian monsoon subsystem in the Holocene optimum is synchronous on the orbital scale (Figures 3.3.7 and 3.3.8). The evolution of the Indian monsoon is mainly controlled by the changes of solar insolation (Berger and Loutre, 1991) in the northern hemisphere (Figures 3.3.7 and 3.3.8).

The $\delta^{18}O$ records clearly captured the 8.2 ka BP climate change event, it occurred at about 8.31～8.1ka BP The process of change is characterized by a slow start and a relatively sudden end. By analyzing the trend of $\delta^{18}O$ curves and comparing with the Greenland ice core records (Rasmussen et al.,2006), indicated that the stalagmite SGL1220 records basically consistent with the Greenland ice core records within the scope of error (Figures 3.3.8). It showed that the Indian monsoon climate is coupled with the northern latitude climate. The climate of the Indian monsoon region is teleconnected with the North Atlantic climate. Compared with the high resolution stalagmite records in the Asian monsoon area, we found that the overall trend of the three records is the same, but there are still differences in the internal structure, fluctuation amplitude and duration of events (Figures 3.3.8). The difference may be

due to the discrepancy in dating errors or the regional climate response. SGL1220 records basically consist with the north latitude climate records and Titanium (Ti) content in Cariaco Basin (Figures 3.3.8) (Haugh et al., 2001). It supports the north-south movement of the Inter Tropical Convergence Zone (ITCZ) affect the strength of the Asian monsoon.

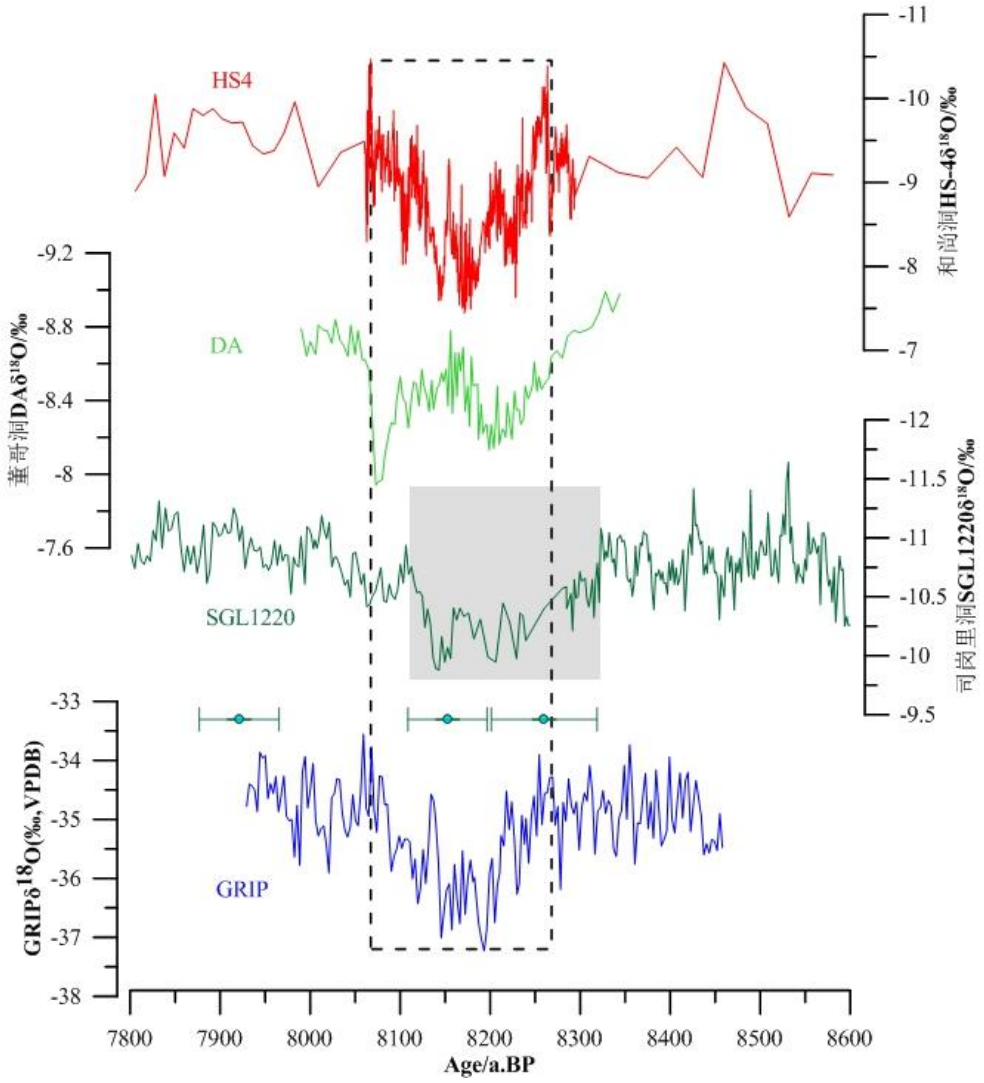

Figure 3.3.7 Stalagmite $\delta^{18}O$ sequences from cave Sigangli cave (dark green solid line) compared with those from Dongge cave (light green solid line) (Cheng et al., 2009), Heshang cave (red solid line) (Liu et al., 2013) and Greenland GRIP ice core (blue solid line) (Thomas et al., 2008) showing detail of "2.8 ka" failure monsoon event**.**

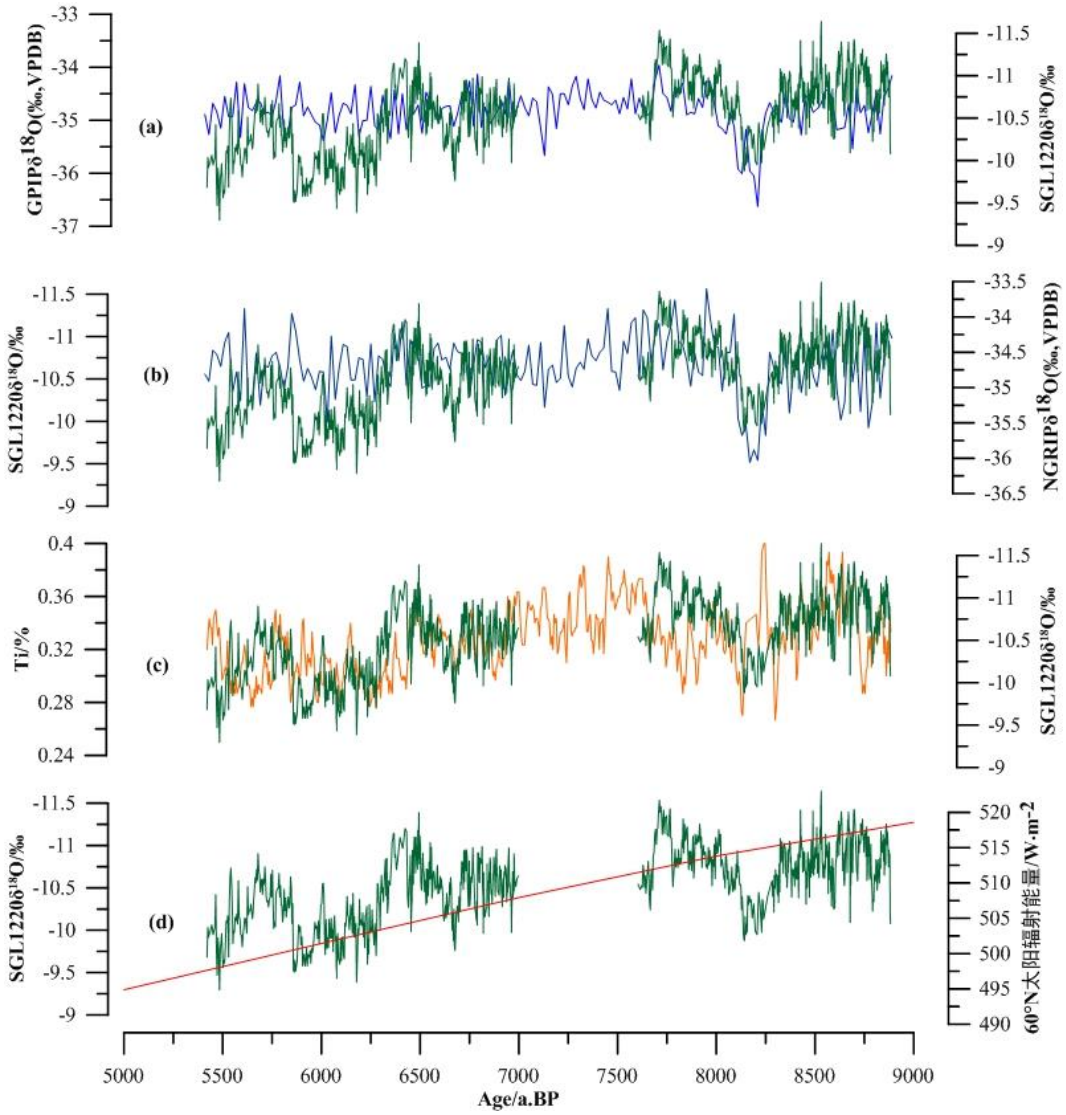

Figure 3.3.8 Comparisons between the $\delta^{18}O$ values of stalagmite SGL1220 (green solid lines) and (a) the 20-year average GRIP $\delta^{18}O$ record (blue solid line) (Rasmussen et al.,2006), (b) the 20-year average NGRIP $\delta^{18}O$ record (blue solid line) (Rasmussen et al.,2006), (c) the Ti concentration record derived from the core collected in Cariaco Basin (pink solid line) (Haugh et al., 2001), and (d) the solar radiation energy at 60° North latitude (red solid line) (Berger and Loutre, 1991).

1.3.3 Climate evolution in China covering the entire Holocene

1) Long-term EASM evolution through the Holocene: evidence from stalagmite isotope records from Northeastern China and Fujian, China

The entire Holocene climatic records from China were reconstructed using samples from Shuidong in northeastern China and Xianyun Cave in Fujian, southeastern China.

1.1) Northeastern China

The oxygen isotopic time series of stalagmites collected from Shuidong cave (Water cave) in Northeastern China were shown in Figure 3.3.9 (d). The time series were built using a total of five stalagmite samples, yielding a time resolution of ~20 years (Figure 3.3.9 (d)). The five sequences duplicated very well over contemporary time periods (Figure 3.3.9 (d)). This indicated that they were deposited under isotopic equilibrium fractionation, and the $\delta^{18}O$ values of stalagmites from the cave were equal to the $\delta^{18}O$ values in drip water feeding the stalagmites. The modern cave (i.e., Miaodong cave) monitoring results around this area demonstrated that the $\delta^{18}O$ values of cave drip water inherit $\delta^{18}O$ in water recharged the drip water which equal to averaged values of $\delta^{18}O$ in summer monsoon rainfall. This area located in northern margin of the EASM, the stronger EASM can carry more moisture to northern China, and results deplete $\delta^{18}O$ in rainfall. Therefore, the $\delta^{18}O$ values preserved in stalagmites from this area can be used as robust index of the EASM intensity and/or the EASM rainfall). The lighter value of $\delta^{18}O$ indicates stronger EASM and more rainfall in northern China.

In general, on orbital time scale, the stalagmite $\delta^{18}O$ record collected from Water cave exhibited gradually decreasing trend of the EASM intensity since 9.0 ka BP until about 8.3 ka BP, and interrupted by a deposition hiatus (Figure 3.3.9 (d)). Then, it reached a high platform of the EASM from 7.5 ka BP to 5.0 ka BP, followed by a gradually decreasing trend from 5.0 ka BP until 2.0 ka BP (Figure 3.3.9 (d)). After then, it lightly increases to the Medium Warm Period around 0.8 ka BP. This long term evolution pattern of the EASM is similar with those records from Qunf cave in Oman (Fleitmann et al., 2007) (Figure 3.3.9 (a)), Dongge cave in Guizhou, China (Cheng et al., 2009) (Figure 3.3.9 (b)) and Heshang cave in Hubei China (Liu et al., 2013) (Figure 3.3.9 (c)). The difference between northern China record and others was

that our records collected from Northern China showed a clear platform during the mid-Holocene (~7.5-5.0 ka BP). These stronger EASM stages correspond to mid-Holocene Climate Optimum (HCO) or mid-Holocene Thermal Optimum (HTO). Considering the deposition hiatus during 8.1-7.5 ka BP, our northern China stalagmite record reveals that the HTO in Northeastern China at least begins earlier than 7.5 ka BP, most likely begins at around 9.0 ka BP, and continues to 5.0 ka BP. The following one thousand years (5.0 - 4.0 ka BP) was a transitional period (Figure 3.3.9 (a-d)). It goes into the late-Holocene phase after approximately 4.0 ka BP. This beginning and ending of the HCO strongly support previous estimation of the HTO based on lake pollen records, which suggest that the HTO covers the time period of approximately 9-3.5 ka BP (Wang et al., 2001).

Previous stalagmite records from Southwestern China (Figure 3.3.9 (b)) (Cheng et al., 2009) and Oman (Fleitmann et al., 2007) (Figure 3.3.9 (a)) proposed that Holocene evolution of the Asian Summer Monsoon (ASM), including Indian Summer Monsoon (ISM) and the EASM, were synchronous. Their changes on orbital scale respond to solar insolation directly. Comparison between our stalagmite records from northern China with insolation in July at 65°N (Berger and Loutre, 1991), shows the EASM in northern China does respond to insolation change (Figure 3.3.9). However, unlike Oman (Fleitmann et al., 2007) and southwestern China (Cheng et al., 2009) records which gradually decline as early as 9 ka BP, northern China record shows the EASM keep strong until 5.0 ka BP. Its declining inflection point of 5.0 ka BP clearly lags behind isolation. These results indicated (1) the Asian Monsoon's sub-systems (e.g., EASM, ISM) may have their respective evolution history on sub-orbital scale during the Holocene. (2) Solar isolation is external forcing of the EASM, but other internal forcing, such as ice amount, ocean procession etc., may also be working.

Superposing on the sub-orbital trend of the EASM evolution, there are a serial of abrupt changes on centurial scale (Figure 3.3.9). The most clear abrupt climate events were 6.8 ka, 5.5 ka, 2.8 ka, and 0.4 ka. It should also be noted that the events identified from this record was limited due to the low resolution as well as subjective evaluate method. Additional stalagmite samples from the other cave in this region, namely Miaodong, were also studied. These samples covered two important abrupt climate events, occurred at 8.2 ka and 4.2 ka, respectively.

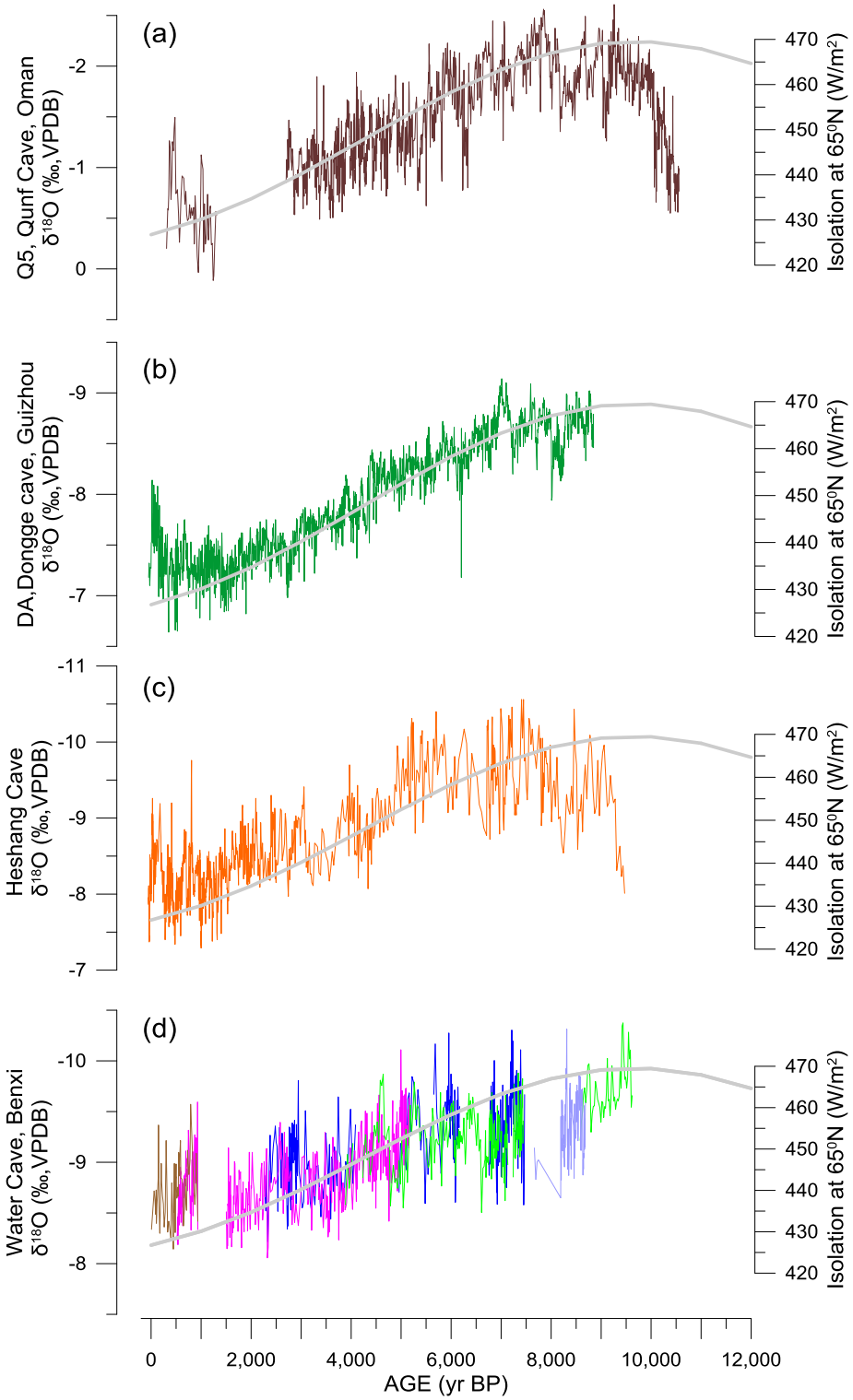

Figure 3.3.9 Stalagmite $\delta^{18}O$ sequences from (a) Oman (Fleitmann et al., 2007), (b) Guizhou, China (Cheng et al., 2009), (c) Hubei, China (Liu et al., 2013), and (d) Water cave (this study). Bold gray lines illustrate insolation in July at 65°N (Berger and Loutre, 1991). Note that all of $\delta^{18}O$ sequences were plotted on descending Y axis.

1.2) Southeastern China

This region is generally regarded as the typical EASM monsoonal region. Moisture from the Pacific Ocean contributes most of rainfall in this area. Climatic data derived from this area is essential for better understanding of the processes and dynamic mechanisms of the ASM systems under the context of global warming. However, up to date, convinced climate record from this region is very limited, partly due to the lack of appropriate materials. Southeastern China is mountainous region. There are nearly no nature lake or stable basin deposition in this area because of heavy rainfall and the high rates of erosion of the landscape. Tree ring from this area is one of important climate proxy records, but their chronology is short, normally less than 300 years. Therefore, stalagmites remaining in karst cave are very important material for paleoclimate study, even it also rare because limestone and caves in this region are also very sparse. In this study, stalagmites collected from Xianyun cave in Western Fujian province were collected. Mineral component of all stalagmite samples is pure calcite with high uranium and low thorium. These promised stalagmites allow us to obtain robust oxygen sequences with substantial age models.

The time series of $\delta^{18}O$ in stalagmites from cave Xianyun, Fujian, southeastern China were shown in Figure 3.3.10 (d). A total of nine stalagmite samples were employed to build the whole Holocene sequence from 11.5 ka BP to 0.5 ka BP. They were duplicated very well over contemporary time periods except two sequences covering the first few thousand years of the Holocene (Figure 3.3.10 (d)). It may due to small deposition hiatus and need to be further determined by more dating. However, the data presented here will not limit us to investigate long-term climate change in Southeastern China.

In general, the Xianyun $\delta^{18}O$ sequence (Figure 3.3.10 (d)) showed surprising Holocene evolution pattern compared to other records from Oman (Figure 3.2.10 (a)) (Fleitmann et al., 2007), Northern (Figure 3.3.10 (b)) (Cheng et al., 2009), and Southeastern China (Figure 3.3.10 (c)) (Liu et al., 2013). It deceases gradually since the beginning of Holocene (11.5 ka BP) until 6.5 ka BP. Then, it goes into a stage of lighter $\delta^{18}O$ values, with averaged $\delta^{18}O$ value of approximately -8.5 ‰. This stage forms a lighter platform from 6.5 ka BP to 3.5 ka BP on the long term evolution curve. Around 3.5 ka BP, it shift down to another stage with significant heavier $\delta^{18}O$ values,

and then gradually increase to its highest value at about 2.0 ka BP, followed by a slightly deceasing trend until 0.5 ka BP.

Climate in this area is dominated by Asian winter monsoon, i.e. EASM, as well as tropical cyclones (TCs, such as typhoons) that originate from the Western North Pacific Ocean (WNP). This region has abundant rainfall, with an average annual precipitation of 800-1900 mm. Most of the annual precipitation falls between March and September, with the first peak during May-June when the southeast (summer) monsoon brings large amounts of moisture from the ocean into this region, where it encounters cold fronts and yields heavy frontal rain. The typhoons contribute most of the rainfall from July to October to this region, which results in the second peak around August. In contrast, the winter is relatively mild and dry; the region is dominated by high pressure and frequent outbreaks of cold air associated with the northwest (winter) monsoon during the winter months.

Generally, the seasonal pattern of rainfall $\delta^{18}O$ in this region can be simplified as two components, related to the two rainfall peaks. The first rainfall peak has relative heavier $\delta^{18}O$ from late April to early June, and the second one shows significant lighter $\delta^{18}O$ from late June to early October, centering in August. The relative contribution of these two rainfall peak may play significant role on the annual mean value of $\delta^{18}O$. The more rainfall arising from TCs could yields negative $\delta^{18}O$ value, and vice versa. The other factor may also be considered that in the first rainfall peak, the rainfall amount effect could result a litter lighter $\delta^{18}O$ values in their rainfall water. The negative $\delta^{18}O$ indicates more rainfall fall arising from TCs, and vice versa.

Xianyun record showed clear negative peak of $\delta^{18}O$ during mid-Holocene and revealed that this area received more rainfall in the second rainfall peak arising from TCs. This stage begins at about 8.0 ka BP and end at about 3.5 ka BP, with a core interval between 6.5 ka BP and 3.5 ka BP. The heaver values of $\delta^{18}O$ indicated the contribution of TCs to local rainfall was quiet low during early Holocene. However, considering the high intensity of IM demonstrated by stalagmite record from Oman (Figure 3.3.10 (a)) and high intensity of the EASM indicated by stalagmite records from Southwestern China (Guizhou province, Figure 3.3.10 (b)) during this time period, the alternative explain was that rainfall in the first peak was high and rainfall in second peak was moderate or a little low. For the late-Holocene from 3.5 ka BP until

present, it looks like that both the first and the second raining seasons were mild, compared to the early-Holocene.

Climate change on orbital and sub-orbital scale has long been contributed to insolation change. The arguments among different hypothesis mechanisms have long been focused on how long climate responds to insolation change. Most of proxy records based on Loess, deep sea sedimentary, and lacustrine deposit suggest delay responding climate to insolation change. However, records derived from stalagmites, especially from China, demonstrated directly responding, without any delay (Figure 3.3.10 (a and b)). Our Xianyun record from Southeastern China Figure 3.3.10 (a and d)) showed different change pattern of the Holocene climate compared to other stalagmite records from Asian Monsoonal area. The most distinguish feature of our Xianyun record was that its mid-Holocene peak of negative $\delta^{18}O$, implied stronger activities of the TCs in Northwestern Pacific during mid-Holocene. Comparing with insolation in summer, whose maximum value occurred in the beginning of the Holocene and then gradually declined until present, with the peak of TCs delay at approximately five thousand years. This hysteretic responding indicated that the change of TC is not forced directly by insolation. There should have other processes, e.g. Ocean processes, ice volume etc., make essential role on the activity of TCs and climate around associated region. Furthermore, our record also indicated that the subsystems of the ASM may have their different behaviors during the Holocene. Its long-term evolution mechanisms on orbital scale should be different. More robust records from abroad area are essential for further understanding the nature of the ASM.

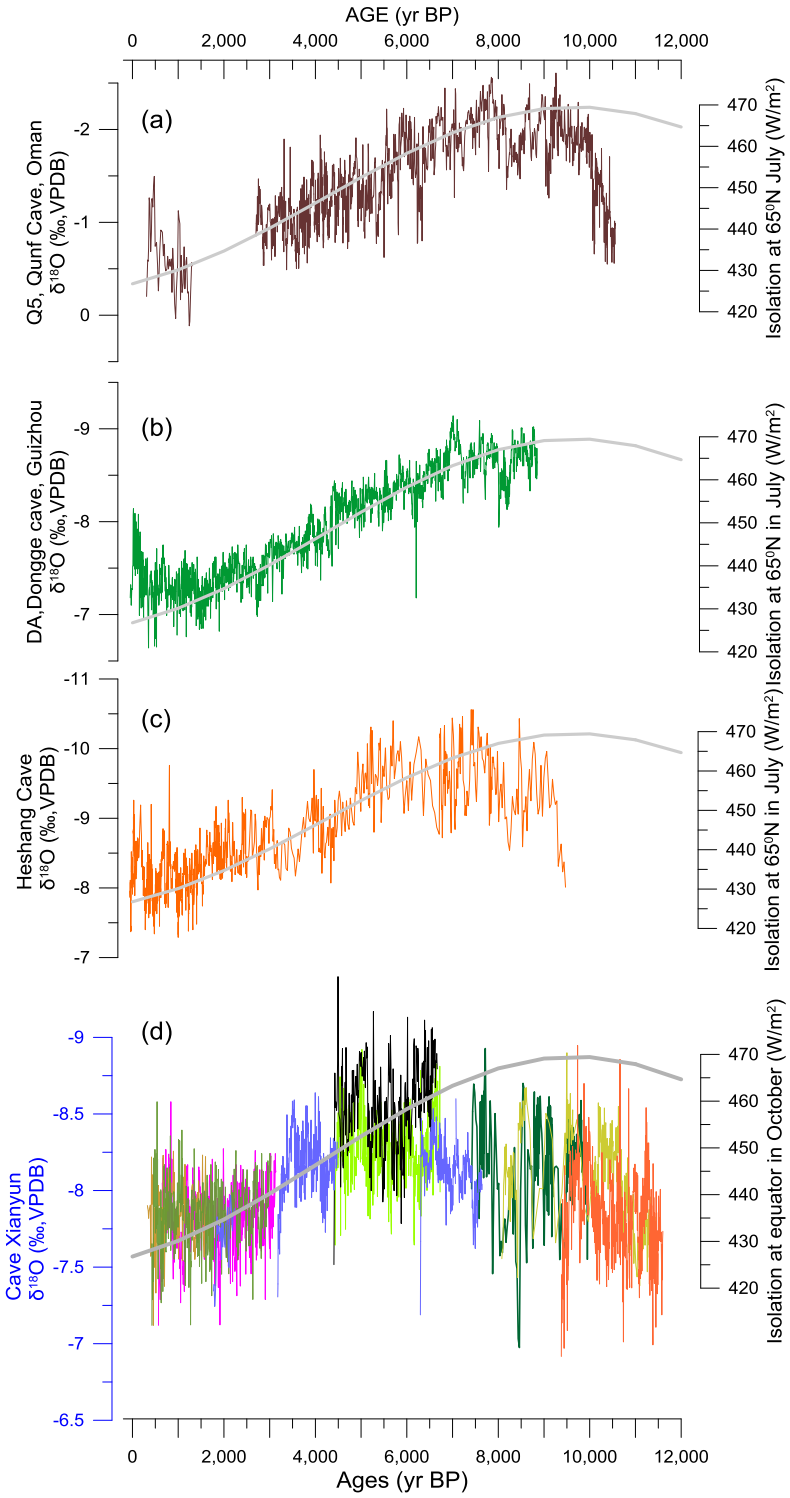

Figure 3.3.10 Stalagmite $\delta^{18}O$ sequences from (a) Oman (Fleitmann et al., 2007), (b) Guizhou, China (Cheng et al., 2009), (c) Hubei, China (Liu et al., 2013), and (d) Xianyun cave, Fujian (this study). Bold gray lines illustrate insolation in July at 65°N (Berger and Loutre, 1991). Note that all of $\delta^{18}O$ sequences were plotted on descending Y axis.

3.4 Large-scale and long-term climate evolution in Thailand, their driving mechanisms, and teleconnections to global climate change

3.4.1 Holocene climate evolution in Thailand: evidences from teak log coffins

1) Tree-ring widths and chronologies

Variations in coffin ring widths are shown in Figure 3.4.1 (a). The number of rings ranged from 59 for core NJ15A to 217 for core NJ11A (Figure. 3.4.1 (a)). C-14 ages indicated that the studied ancient teak trees grew between approximately 2147-1996 BP and 1697-1646 BP (Figure 3.4.2 and Table 3.4.1). According to the C-14 ages, the oldest teak tree (NJ11A) grew from 2147-1996 BP to 1751-1746 BP, whereas the youngest tree (NJ15A) grew from 1812-1605 BP to 1637-1544 BP (Figure 3.4.2 and Table 3.4.1). The overall chronology of the Namjang coffin index (i.e., $Coffin_{NJ}$ index) was developed from a combination of C-14 ages and the crossdating of ten coffin cores covering a 477-year period from 106 BC to AD 371 (Figure 3.4.1 (b)). The statistical descriptions are summarized in Table 1.3.2. The EPS and Rbar values were 0.704 and 0.517, respectively (Table 3.4.2 and Figure 3.4.1 (c)). Periods of low growth were observed during 45 BC-AD 55 and AD 100-179, whereas a period of high growth was found in AD 180-371 (Figure 3.4.1 (b)).

2) Spectral analysis

The spectral periodicities of the $Coffin_{NJ}$ index displayed cycles at millennial (637 years), decadal (11.2 years), and annual (5.1, 5.9, and 7.5 years) time scales (Figure 3.4.3 (a)). The decadal periodicity of approximately 11.2 years of the $Coffin_{NJ}$ index was almost identical to the well-known 11-year periodic change in the sunspot cycle (Foukal, 1990), which was evident in several previously tree-ring records (Kurths et al., 1993; Murphy and Palmer 1992; Rigozo et al., 2005). The short-term periods, of approximately 5–7 years of the log CoffinNJ index were found to be likely associated with El Niño–Southern Oscillation (ENSO) event (D'Arrigo et al., 2005).

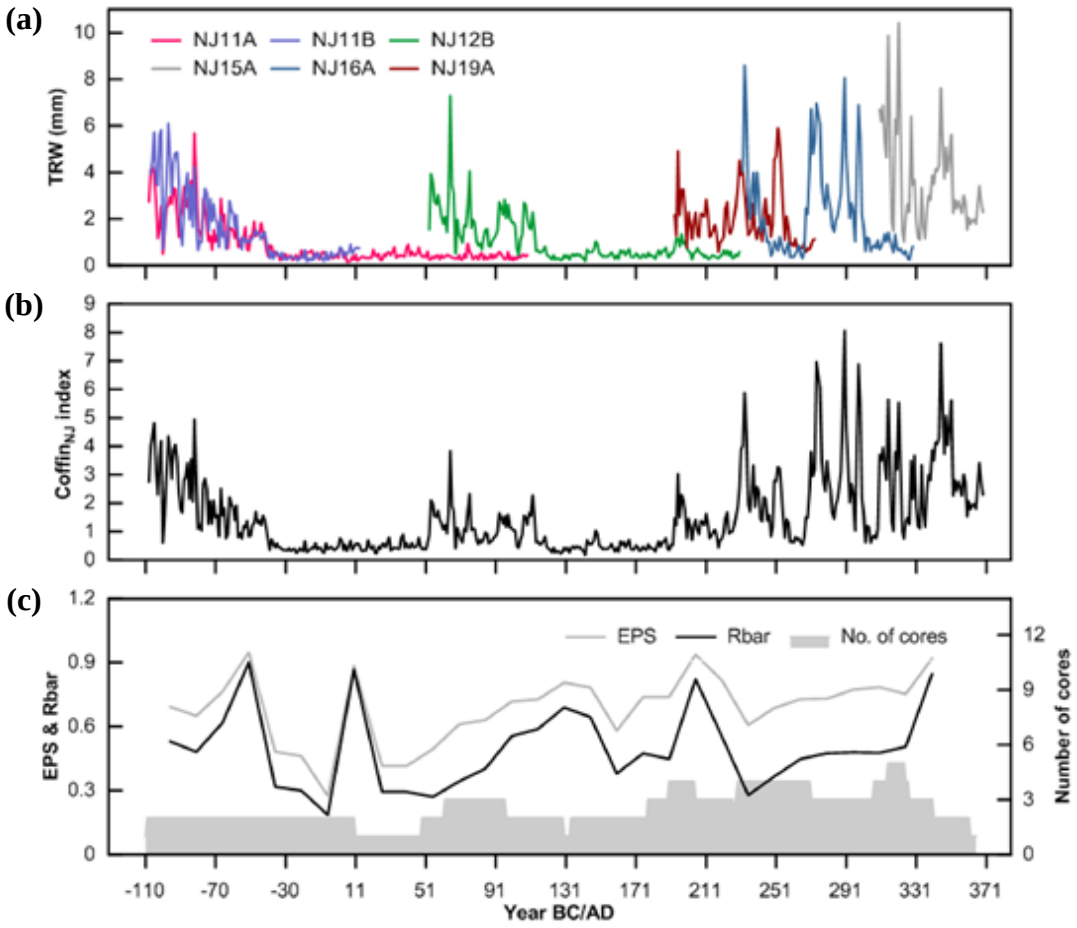

Figure 3.4.1 (a) Ring width variation and cross-dating position according to the C-14 dating data of each Namjang log coffin sample, the Coffin$_{NJ}$ index, and (c) the number of cores (gray shed area), EPS (gray line) and running Rbar (black line).

Table 3.4.1 The conventional radiocarbon age and calendar calibration at probability (%) of each sample.

Sample no.	Position	Conventional age (± 30 BP)	Calendar calibration at Probability (%)	IRMS $\delta^{13}C‰$
NJ11A	Pith side	2100	198 - 47 cal BC (95.4%) (2147 - 1996 cal BP)	-23.9
NJ11A	Bark side	1920	2 - 138 cal AD (95.1%) (1948 - 1812 cal BP) 199 - 204 cal AD (0.3%) (1751 - 1746 cal BP)	-26.3
NJ11B	Pith side	2020	107 cal BC - 58 cal AD (95.4%) (2056 - 1892 cal BP)	-23.2
NJ11B	Bark side	1940	0 cal BC - 130 cal AD (94.2%) (1950 - 1820 cal BP) 20 - 12 cal BC (1.2%) (1969 - 1961 cal BP)	-24.0
NJ12B	Bark side	1960	40 cal BC - 87 cal AD (91.9%) (1989 - 1863 cal BP) 104 - 120 cal AD (3.5%) (1846 - 1830 cal BP)	-25.3
NJ16A	Pith side	1850	85 - 235 cal AD (95.4%) (1865 - 1715 cal BP)	-25.2
NJ16A	Bark side	1780	137 - 334 cal AD (95.4%) (1813 - 1616 cal BP)	-25.2
NJ19A	Pith side	1840	86 - 242 cal AD (95.4%) (1864 - 1708 cal BP)	-24.6
NJ19A	Bark side	1860	80 - 230 cal AD (95.4%) (1870 - 1720 cal BP)	-24.9
NJ15A	Pith side	1770	138 - 345 cal AD (95.4%) (1812 - 1605 cal BP)	-25.3
NJ15A	Bark side	1700	313 - 406 cal AD (71.8%) (1637 - 1544 cal BP) 253 - 304 cal AD (23.6%) (1697 - 1646 cal BP)	-24.6

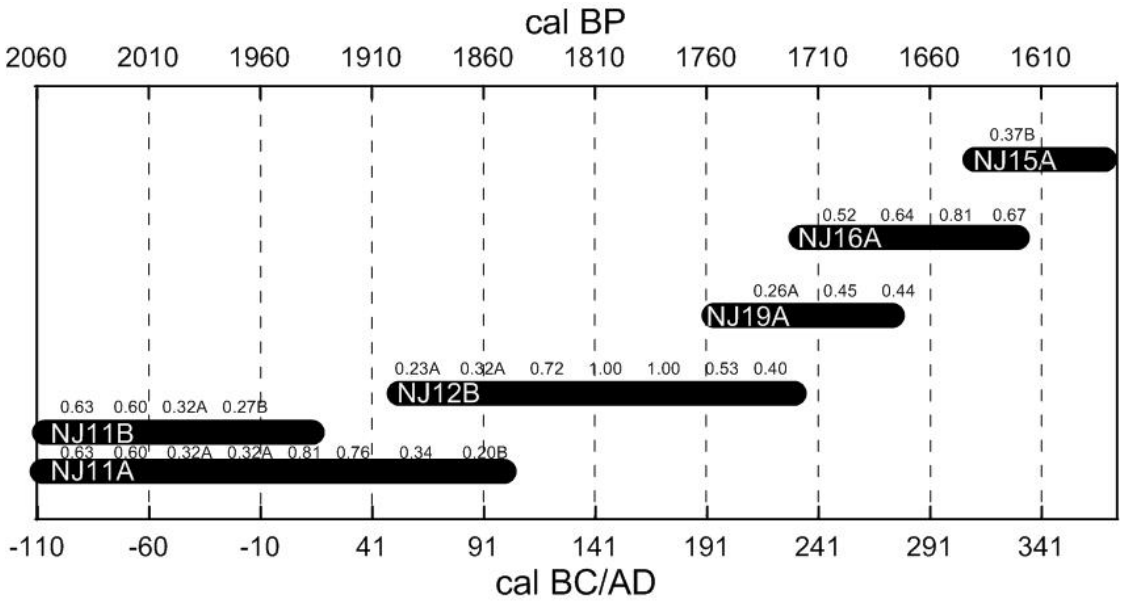

Figure 3.4.2 NJ log coffin chronological series; the time spans of the tree-ring series are in cross-dated position according to the C-14 dating data. Numbers above the bar chats indicates the correlations of 50-year dated segments, lagged 25 years, flags: A = correlation under 0.3281 but highest as dated; B = correlation higher at other than dated position.

Table 3.4.2 Statistic description of NJ log coffin chronology

Statistic	**Statistic value**
Time-span	1- 477
Year	477
Average ring width (mm)	1.51
Series intercorrelation	0.505
Mean sensitivity	0.346
Autocorrelation	0.759
Standard deviation (SD)	0.127
EPS	0.704
Rbar	0.515

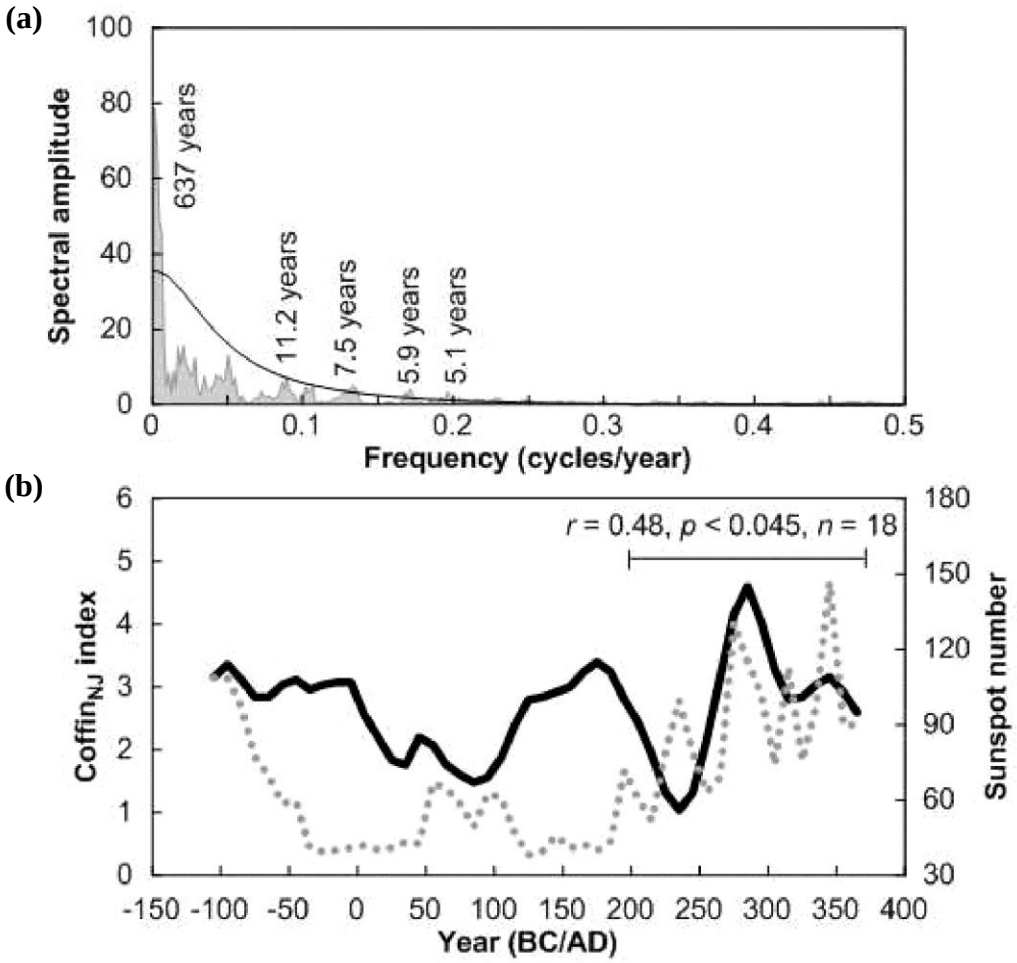

Figure 3.4.3 (a) Spectral analysis of the Coffin$_{NJ}$ index using REDFIT (Schulz and Mudelsee, 2002). The gray area indicates the power spectrum of the ring width. The black lines represent the 95% confidence limits, relative to the red-noise spectrum. The confidence limits were estimated using a Monte Carlo simulation. Significant peaks are labeled for each period. (b) The sunspot number index with a 10-year average (black line) (Wu et al., 2018) and Coffin$_{NJ}$ index (dashed line)

3) Comparisons with solar proxies

The significant periodicity of tree-ring chronologies of approximately 11 years has been commonly linked with the Schwab solar cycle (Clark and Clark, 2007). The alternating phase between solar minima and maxima over an 11-year period is usually given in terms of the variation in the number of sunspots (Clark and Clark, 2007; Foukal, 1990). To further investigate the relationship between solar variability and tree growth, the Coffin$_{NJ}$ index was compared with sunspot numbers with an average

resolution of 10 years (Wu et al., 2018), as well as natural proxies sensitive to variations in solar activity including layer thickness (Tan et al., 2003) and the stable oxygen isotopic ($\delta^{18}O$) (Zhang et al., 2008) properties of speleothems from the Shihua (Tan et al., 2003) and Wangxiang (Zhang et al., 2008) Caves, China.

A positive relationship (r = 0.31, p < 0.035) was observed between the $Coffin_{NJ}$ index and sunspot number (Wu et al., 2018) for the entire period between 110 BC and AD 370, particularly during the period of AD 191-370 (r = 0.48, p < 0.045) (Figure 3.4.3 (b)). Because the relationship between tree rings and solar activity is generally nonlinear and remains unstable over time (Li et al., 2019), anti-phase periods between the $Coffin_{NJ}$ index and sunspot number were also observed, for example from 110 to 21 BC (Figure 3.4.3 (b)). Moderate negative (r = -0.50, p < 0.001) and positive (r = 0.40, p < 0.001) correlations were found in comparison to stalagmite layer thickness (Tan et al., 2003) (Figure 3.4.4 (a)) and $\delta^{18}O$ (Zhang et al., 2008) (Figure 3.4.4 (b)), respectively. Our results confirmed that the variations in the ancient teak trees in this study were associated with solar activity.

4) Log Coffin Culture

Log Coffin Culture in NW Thailand was first explored during 1965-1966 by Gorman, an American archaeologist who found many log coffins in the so-called Spirit Cave (Gorman, 1970). Extensive studies relating to Log Coffin Culture have been conducted in that area since then (Hayes et al., 2017; Pumijumnong and Wannasri 2015; Wannasri et al., 2007). NJ Cave is one of the many coffin caves distributed in the PMP district of MHS province in NW Thailand. Although NJ Cave has not had detailed archaeological excavations, unlike other archaeological sites in this area, such as Ban Rai rock shelter, Tham Rod rock shelter, and Long Long Rak Cave (Shoocongdej, 2016), NJ Cave is regarded as one of the most suitable caves for archaeology and paleoclimate studies because it contains more than 20 wooden coffins and its entrance can be easily reached (Ellis, 2017). In addition, the location of NJ Cave is close to the hill tribe communities that settled in the north of Thailand.

The most interesting about log coffin is the head style of the log coffin, the samples from 18 archeological sites in PMP district found 12 styles of log coffin head (Shoocongdej, 2014). Those log coffins have been dated by C-14 dating and shown

the age from 3160-430 BP (Shoocongdej, 2003). The date of log coffin was not related to the head style indicating the development from simple to complex style of log coffin head was not depend on time. The style of log coffin head might be related to the status of the buried individual (Wannasri et al., 2007). The log coffin style found in NJ Cave is similar to the style of coffins remaining in other caves or rock shelters nearby (Wannasri 2004; Wannasri et al., 2007). Age comparing with the same style of log coffin found form Lod Cave (Grave et al., 1994) and our samples (NJ11A and NJ11B). Both samples from two caves are the same style (2A). Age of our samples (2060 ± 30 BP) were older than log coffin from Lod Cave (1240 ± 90 BP) (Grave et al., 1994). Previous studies reported that the period of Log Coffin Culture ranged from approximately 2200 BP to the nineteenth century, which is comparable to the Iron Age (Shoocongdej, 2004; Shoocongdej, 2016). The ages of the NJ log coffins approximately fall within the Log Coffin Culture period in NW Thailand (Shoocongdej, 2004; Shoocongdej, 2016). The result of the C-14 dating of six log coffin cores in this study indicated that the teak trees were cut down approximately between 1937 to 1582 BP for ancient human burials (Figure 3.3.2). The NJ coffins are considered to belong to the Log Coffin Culture period in NW Thailand, which began from approximately 2100 BP to 1200 BP; same as, coffins found in the Ban Rai rock shelter. This period related to the phase of human activity within the late Holocene (Treerayapiwat, 2005b). A log coffin, namely, BR5A which is the 2B style, collected from the Ban Rai rock shelter was dated back to AD 265 (Pumijumnong and Wannasri, 2015), which was similar to the ages of the NJ log coffins in this study (i.e., NJ16A and NJ15A) (Figure 3.4.2). These two samples of log coffin are the same style with BR5A from the Ban Rai rock shelter indicated that the studied caves and rock shelters in the PMP area were used for burial rituals in the same period. The oldest age of our NJ coffin samples was dated back to approximately 106 BC (NJ11A) (Figure 3.4.2) and confirmed that the burial ritual existed in that area, at least during the studied period. Older log coffins were found in Spirit Cave in NW Thailand and dated from 500 BC to AD 800 (Lampert et al., 2003). The log coffin found from distributed caves in NW Thailand indicating the population growth of ancient people, the system of relatives and society. The different styles of log coffin with different ages can be cross dated and continued was not related to the development of log coffin style but might

be related to the capability of log coffin maker or user needs. However, the simple styles (1A, 1B, 2A, 2B) were more common than the complex style. The Log Coffin Culture existed not only in NW but also in Western Thailand during the same time period. Log coffins from Ongbah Cave in Kanchanaburi province, Western Thailand, had ages of approximately 2180 ± 100 BP (Sørensen, 1973), similar to the NJ coffins, indicating that the Log Coffin Culture was not only found in NW Thailand but also disseminated to Western Thailand. The Coffin Culture in MHS province occurred during the same time period as the Jar Burials (AD 1300-1656) found in the southern part of Tak province in Western Thailand (Hotchkis et al., 1994). Moreover, wood utilization of ancient people to make a coffin, people choose a good quality of wood especially, teak represented the abundance of forest resources in the past.

In Southeast (SE) Asia, the Log Coffin Culture expanded from south of Southeast Asia in the islands of Borneo and the Philippines to Northern Vietnam, Cambodia, and NW Thailand (Hotchkis et al., 1994). Log coffins found in Borneo have been dated back to 3150 ± 40 BP in Samang Buat Cave (Abdullah, 2017) and between 3080 ± 40 BP (Harrisson, 1975) and 2460 ± 65 BP in Niah Cave (Sørensen, 1988). In Vietnam, the log coffin ages collected from archaeological sites in Viet Khe and Chau Chan of Northern Vietnam ranged from 2500 to 2200 BP (Higham, 1989). The log coffins collected from Viet Khe and Chau Chan of Northern Vietnam had ages ranging from 2500 to 2200 BP (Higham, 1989). Other coffin samples from Niah Cave in Borneo have earlier dates (2460±65 BP) (Sørensen, 1988). These coffins were generally made from trees that were abundant in the local areas. For example, the coffins found in Samang Buat Cave, Brunei were made from Belian trees *Eusideroxylon zwageri*), which belong to the dominant tree species in the evergreen forest, suggesting that an evergreen forest occupied that area during the period in which the coffins were made (Abdullah, 2017). Ancient people usually used the most available and suitable trees to make log coffins. Similar to other caves, most of the log coffins from NJ Cave were made from the dominant tree species (i.e., teak), indicating that a deciduous forest occupied NW Thailand during that time period. A wide variety and quality of coffin types have been reported in a total of 26 archaeological sites in MHS province, which suggested that the people of this province had various coffin-making skills over time (Hotchkis et al., 1994). Our log coffin samples from NJ Cave

are therefore regarded as one of many pieces of evidences describing the Log Coffin Culture in NW Thailand.

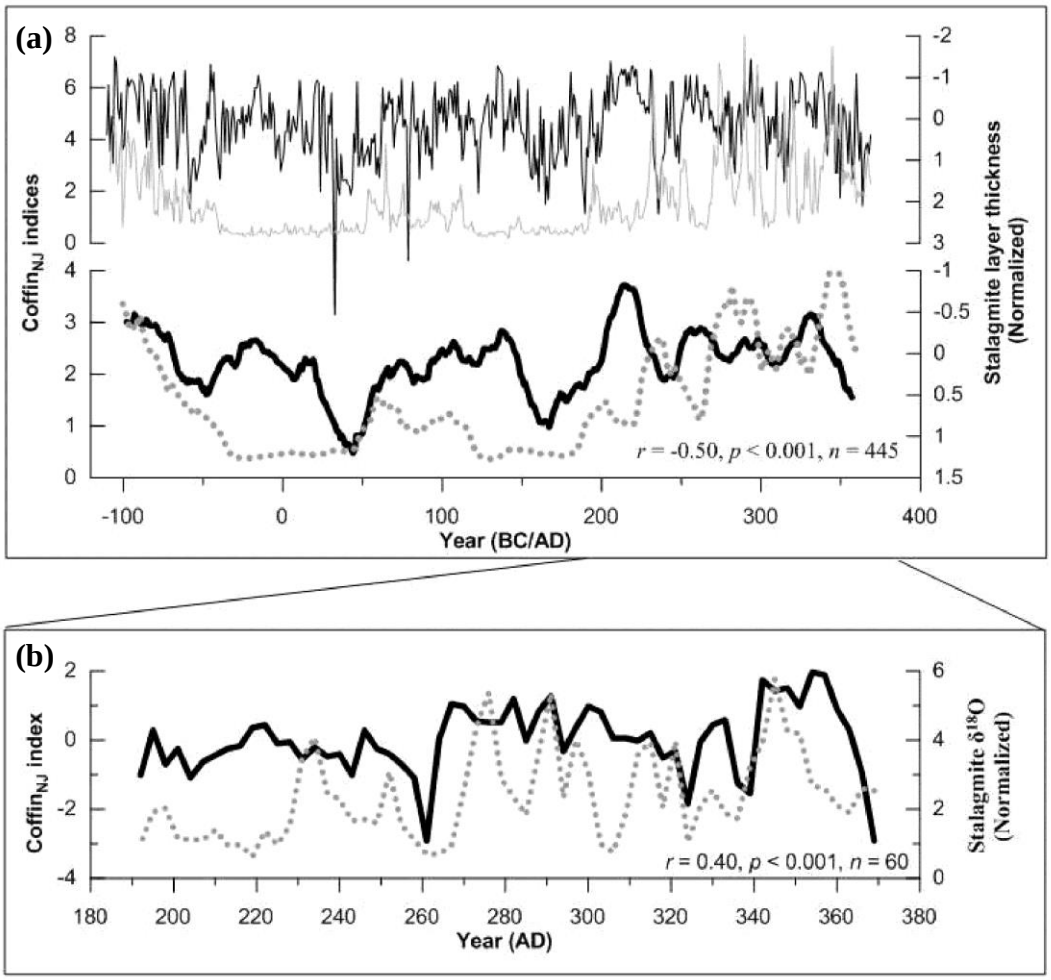

Figure 3.4.4 (a) the stalagmite thickness index with a 21-year running average (black line) (Tan et al., 2003) and Coffin$_{NJ}$ index (dashed line). (b) The stalagmite $\delta^{18}O$ index (Zhang et al., 2008) and Coffin$_{NJ}$ index (dashed line); *r* represents the Pearson's correlation coefficient, *p* indicates a statistically significant value, and *n* indicates the number of samples.

5) The imprint of solar signals in tree-ring width

Solar activity, especially during phase changes of the solar cycle (Gizani et al., 2011), plays an important role in moderating the Earth's climate system (e.g., (Tsiropoula, 2003). A decline (incline) in solar irradiance possibly leads to a drop (rise) in global temperatures and causes extreme climate events in many regions (Owens et al., 2017; Reddy and Reddy, 2016). Tree rings are among the best natural proxies to capture the past variability of solar signals (Muraki et al., 2011; Rigozo et al., 2007). The present 11-year solar cycle has been extensively recorded in tree-ring widths of living trees from several sites, such as Brazil (Rigozo et al., 2004), Chile (Rigozo et al., 2005), and China (Wang and Zhang, 2011), spanning from the past few thousand years (Rigozo et al., 2005; Wang and Zhang, 2011) to the present several hundred years (Rigozo et al., 2004; Rigozo et al., 2007), with fossil trees (e.g., Murphy and Palmer, 1992) extending back to the Miocene epoch (e.g., Kurths et al., 1993).

The 11.2-year cyclicity found in the $Coffin_{NJ}$ index (Figure 3.4.3 (a)) could be related to the well-known periodic 11-year change in the solar activity (i.e., the Schwab solar cycle) (Clark and Clark, 2007). A positive correlation ($r = 0.31$, $p < 0.035$) indicated a possible relationship between tree growth and sunspot number (Figure 3.4.3 (b)). There was an obvious increase in teak tree growth during an interval of high sunspot numbers at AD 191-370 ($r = 0.48$, $p < 0.045$) (Figure 3.4.3 (b)). Comparisons with speleothem proxies sensitive to changes in solar activity (Figure 3.4.4 (a and b)) confirmed that the teak trees in this study might respond, at least partly, to the same external factors (i.e., solar variation). Because tropical and subtropical regions, particularly Thailand, generally receive greater heat through solar radiation than any other places (Satoh, 2014), variations in solar energy are closely related to climate changes in this area (Medvigy and Beaulieu, 2012). Studies have reported that the influence of solar energy on plant growth is probably due to the photosynthetic process (Dorotovič et al., 2014; Prestes et al., 2018). The effect of solar energy can also be indirect through the regulation of factors limiting tree growth, such as ambient temperature and rainfall conditions (Wang and Zhang, 2011). However, the detailed mechanisms of solar forcing on teak trees growth in the past are complicated and beyond the scope of this study. Coupled ecosystem-climate models and longer

continuous tree-ring chronologies are needed to further identify the past sun-tree growth relationships and their mechanisms.

The annual-scale cycles of approximately 5-7 years observed in the $Coffin_{NJ}$ index (Figure 3.4.3 (a)) were likely associated with the regular periodic variation in the ENSO cycles between 2 and 8 years (D'Arrigo et al., 2005; Li et al., 2011; Torrence and Webster, 1999). Teak tree-ring records from several sites within Southeast Asia, including living teak trees collected from Thailand (AD 1558-2005) (Buckley et al., 2007; Pumijumnong, 2012), Myanmar (AD 1613-2009) (D'Arrigo et al., 2013), and Indonesia (AD 1514-1929) (Cook et al., 2000), have also shown the spectral coherence of the ENSO periodicity ENSO has affected the monsoon climate of Thailand over the past four centuries (Buckley et al., 2007; Muangsong et al., 2014), and this effect probably extends as far back as at least 191 BC. The spectral peak at approximately 637 years is outside the scope of our focus and might be related to other factors.

Although preliminary, this study confirmed the potential of teak tree-ring widths derived from log coffins as a potential proxy indicator for past climate variation in this area. Further studies will be necessary to continually extend tree-ring sequences from living trees in the present to the past using fossil trees.

3.4.2 Holocene climate evolution in Thailand: evidences from stalagmites

1) Northern and Northwestern Thailand

Caves are broadly developed in Northern (N) and Northwestern (NW) Thailand, especially ChiangMai and Mae Hong Son (MHS) provinces, respectively. We had explored many caves in these areas. Most of stalagmite samples were collected from MHS province in NW Thailand and only few samples were collected from ChiangMai. Unfortunately, these few stalagmite samples from ChiangMai were suffering from big age error, confirming by U-Th dating results. Thus, only the samples collected from MHS can be used in this study. Several caves in MHS have been explored including the longest one in N Thailand. Some of them have few speleothems because of influence from seasonal underground river. The useful samples were mainly collected from three caves, namely Lahu, Maihung and Susa, and additional few samples collected from Mae La Na cave. Most of these samples were short and some of them were broken into several pieces. Many U-Th dating were performed for these samples in order to select some promised stalagmites for Holocene climate reconstruction. Unlike those from China, nearly all of stalagmites collected from N and NW Thailand were formed with aragonite with fast growth rate, resulting in short growing period for each sample. These features made us more trouble to getting long-term record, because most of samples were broken in cave and normally were short. Based on large amount of U-Th dating results, we found that only stalagmite samples collected from Lahu cave in MHS province in NW Thailand can be used to get long record covering the Holocene.

Lahu cave locates in hill closed to small town, namely Ban Mae Pha, in PMP district in MHS province. It is a shallow wildly cave with big entrance, allowing people to access easily. Speleothems in the cave have been broken by local children who playing in the cave. Even the samples from this cave were also short and some of them were broken into several parts. With a lot of dating, we found they are mostly growing during the Holocene (Figure 3.4.5). Limited to cost and time consumed by laboratory for U-Th dating, we have provided preliminary results of stalagmite's ages covering parts of the Holocene (Figure 3.4.5). The densities of stalagmite growing through the Holocene were calculated (Figure 3.4.6). This result allows us to evaluate long-term moisture changes in this region because the overlaying back rock and soil of

Lahu cave is shallow. This means that the drip water feeding the stalagmites respond fast to outside rainfall. Thus, the higher stalagmite's growing rates in the cave could indicate higher rainfall in this region.

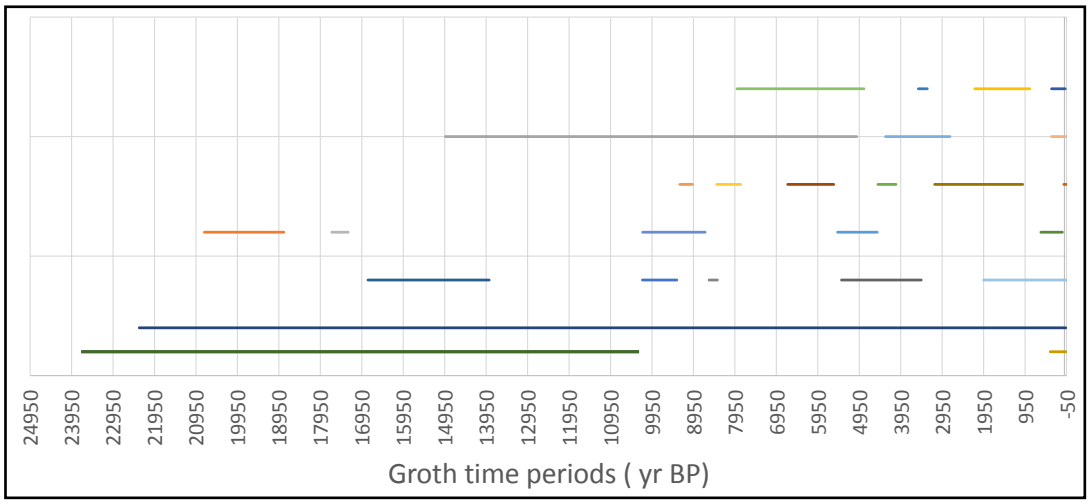

Figure 3.4.5 Growing periods of stalagmites collected from Lahu cave in Mae Hong Son province of Northwestern Thailand.

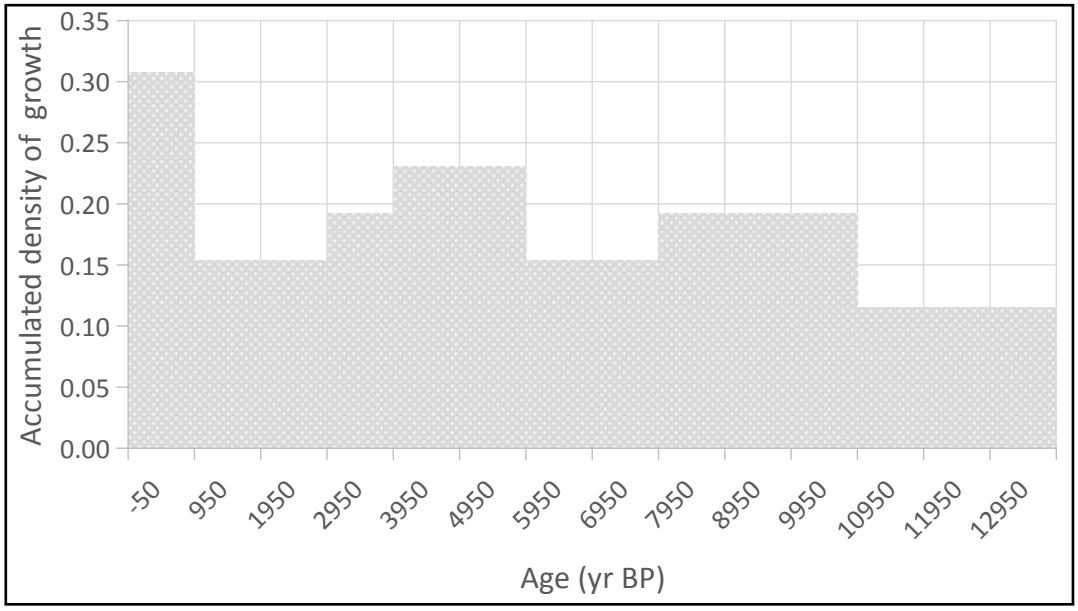

Figure 3.4.6 Accumulated density of stalagmite growth through the Holocene for stalagmites collected from Lahu cave. Note that the stalagmite laminae were counted at interval of 1,000 years.

In general, the accumulated density of stalagmite was low during the early Holocene, and then it increased to a peak from 11.0 ka BP until 8.0 ka BP (Figure 1.4.6). With a little decease, the second peak was found during time period between 6.0 and 3.0 ka BP. The last and the highest peak appeared in the last one thousand years (Figure 3.4.6). There were coffin preserved in the cave, indicating strong human influence of speleothem in the last one thousand years. This last high peak may be a result of human activity. The stalagmite, stalactites, and straw tube were broken by human when they put coffins into this cave, and thus stalagmite's drip points were changed in their direction and re-growing new stalagmites were generally observed. Therefore, take the uncertain of the last highest peak into account; the second peak of stalagmite growing period during the mid-Holocene is robust.

This indicated that moisture situation during the mid-Holocene was higher compared to the early-Holocene. The moisture was increased since 8.0 ka BP, and its peak was observed during the interval between 6.0 and 3.0 ka BP. This Holocene moisture evolution pattern in NW Thailand similar with that of in Southeastern China (Figure 1.3.10), indicating a teleconnection between these two regions. There should be a large scale atmospheric component linkage behind this teleconnection. Our studies on stalagmite records from Namjang cave, another cave in PMP district, demonstrated that the later rainy season from August to early October contribute most of water feeding the drip water in the cave, and maintain the drip in following dry season (Cai et al., 2010; Muangsong et al., 2020). Higher rainfall in the late rainy season will result in higher growth rate of stalagmites (Cai et al., 2010; Muangsong et al., 2020). The variability of rainfall in the late rainy season is sensible to Northwestern Pacific Ocean, which also influence the TCs rainfall in Southeastern China as discussed in section 3.3. The teleconnection of Holocene moisture changing pattern in Northern Thailand and that in Southeastern China can be explained by the large atmospheric circle derived from sea-air interaction processes over the Northwestern Pacific Ocean.

It should be noted that our preliminary results from Lahu cave is still very limited with details of U-Th dating. However, these results allows us to evaluate details of Holocene moisture change in northern Thailand, hence, to show the

teleconnections among climate in Northern Thailand, Southeastern China, and sea-air interaction process over the Northwestern Pacific Ocean.

2) Southern Thailand

Modern climate in southern Thailand is different from those of Northern and Northwestern regions. Because this area locates in northern margin of the ITCZ, rainfall in this area exhibits much less clear dry season as it behaves in Northern and Northwestern Thailand. Many documents have demonstrated that the ITCZ dynamic on orbital scale driven by insolation change (for examples, Liu et al., 2013). The long-term stalagmite oxygen records from Oman (Fleitmann et al., 2007), China (Cheng et al., 2009; Liu et al., 2013), Thailand (Tan et al., 2019), and South American (Novello et al., 2017) reveal summer insolation directly force the ITCZ move northward or southward. When summer insolation at the North Hemisphere reach its highest values, the ITCZ belt move northward and results in strong ASM and weak South American Monsoon (SAM), and vice versa (Cheng et al., 2009; Liu et al., 2013; Novello et al., 2017). Considering the strong effect of ITCZ on southern Thailand, the record from this area can be employed to be an index of ITCZ, and can therefore be a powerful evidence to test the forcing mechanism of insolation on the ITCZ, hence on the ASM changing on orbital scale.

Based on our large efforts of field cave exploring and preliminary U-Th dating results, we finally focused on the two caves in Southern Thailand. One of caves, namely Klang, locates in Krabi province. The other cave, namely Phu Pha Phet, locates in Satun province. However, only samples from Klang cave can be used. Klang cave was developed in a karst peak closed to Ao Luk district. There are two natural entrances, the first one is large entrance with underground river flowing out and easily be accessed. The other is small window opens to atmosphere outside locating at the end of the cave with higher elevation. Therefore, it forms cross ventilation, which can significantly influence the isotope fractionation for stalagmites growing along the main passage connect two entrances. This feature of cave requires for carefully choosing promised stalagmite samples in order to reconstruct robust oxygen isotope-based climate record.

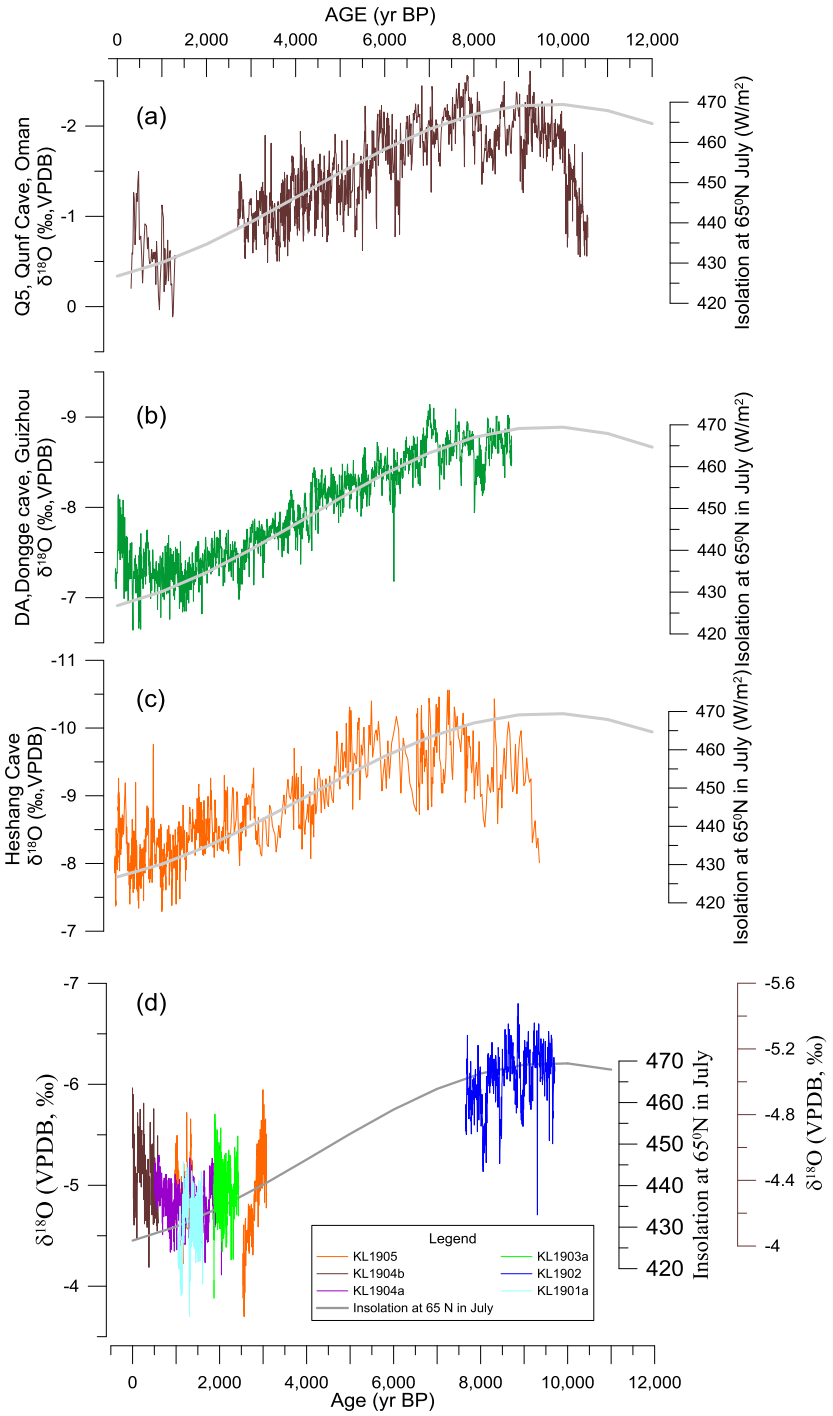

Figure 3.4.7 Stalagmite $\delta^{18}O$ sequences from (a) Oman (Fleitmann et al., 2007), (b) Guizhou, China (Cheng et al., 2009), (c) Hubei, China (Liu et al., 2013), and (d) Klang cave, Krabi, Southern Thailand. Bold gray lines illustrate insolation in July at 65°N (Berger and Loutre, 1991). Note that all of $\delta^{18}O$ sequences were plotted on descending Y axis. For (d), $\delta^{18}O$ sequence of stalagmite KL1904a (brown solid line) was plotted

on individual Y axis on the right side (brown solid axis), others were plotted on Y axis on the left (black solid axis).

A total of five broken stalagmite (or pieces) samples were collected and used in this study. Four of them covered the last 3.2 ka, and the others covered the time period between 9.5 ka BP and 7.5 ka BP. Time series of $\delta^{18}O$ for these samples were showed in different color in Figure 3.4.7 (d). In general, the stalagmite $\delta^{18}O$ values (Figure 3.4.7 (d)) were much lighter during the early to mid-Holocene than those in the late-Holocene. For the long-term change trend during episode of 9.5-7.5 ka BP, the most negative stalagmite $\delta^{18}O$ values were found in the first thousand years from 9.5 ka BP to 8.5 ka BP (Figure 3.4.7 (d)). Then it slightly increased to the end of this interval at approximately 7.5 ka BP. For the last 3.2 ka, the sequences of $\delta^{18}O$ showed gradually increasing trend from 3.2 ka BP until 1.5 ka BP, followed by decreasing trend through the present.

In this low latitude area without clear seasonal shift of moisture sources, the $\delta^{18}O$ in rainfall is dominated by rainfall amount, because weak rain event will result in rain water rich in $\delta^{18}O$ values due to evaporation effect when rain drop falling down. Therefore, the oxygen isotopic compositions of stalagmites collected in this Southern region can be regarded as an index of rainfall amount. The negative value of $\delta^{18}O$ indicates higher rainfall, and vice versa. The lighter value of $\delta^{18}O$ in Klang record implies more rainfall during the early-mid Holocene. Limited to missing data covering mid-Holocene, we can't present assessment in-depth on long-term trend through the Holocene. However, taking Holocene as a whole, it is reasonable to deduce that our Klang record coincided very well with those records from Oman (Figure 3.4.7 (a)) (Fleitmann et al., 2007), Guizhou province in Southwestern China (Figure 3.4.7 (b)) (Cheng et al., 2009), and Hubei province in central China (Figure 3.4.7 (c)) (Liu et al., 2013). All of these records respond to summer insolation change over the North Hemisphere (Figure 3.4.7) (Berger and Loutre, 1991) without delay. Further work involved in reconstructing integrated Holocene record will finally confirm this observation.

The strong connections among these stalagmite records and their fast responding to isolation agrees with the view that insolation directly force the ITCZ

belt move northward or southward, resulting in advancing or shrinking of ASM (especially ISM) on orbital scale (Tan et al., 20019). It should be noted that the long-term variability of Holocene climate in the EASM and NWPSM dominated zones are quite different from those of the ISM, if we compared stalagmite records collected from Southern Thailand (Klang cave) (Figure 3.4.7 (d)), Oman (Figure 3.4.7 (a)) (Fleitmann et al., 2007), and Southwestern China (Dogge cave in Guizhou province) (Figure 3.4.7 (b)) (Cheng et al., 2009) with Southeastern China (Heshang cave in Hubei province) (Figure 3.4.7 (c)) ((Liu et al., 2013)) and Northern Thailand as discussed above (Figure 3.4.6). This implies special evolution feature of the EASM and NWPSM, which may have more complex mechanism of insolation respond.

3.5 Cave and climate monitoring program in Thailand

Climate and cave monitoring programs under this project were carried out in both Thailand for Namjang (NJ) cave in Mae Hong Son province and Phu Pha Phet (PPP) cave in Satun province and China for Miaodong cave in Benxi province and Xianyun cave in Fujian province (Figure 3.5.1). Climate and cave monitoring in Namjang cave were previously performed by Muangsong (2016) and consequently reanalyzed and published under this project in 2020 (Muangsong et al., 2020). According to the project's objectives, only results from PPP cave was presented in this report. Monitoring work at PPP cave was performed from May 2016 to September 2019.

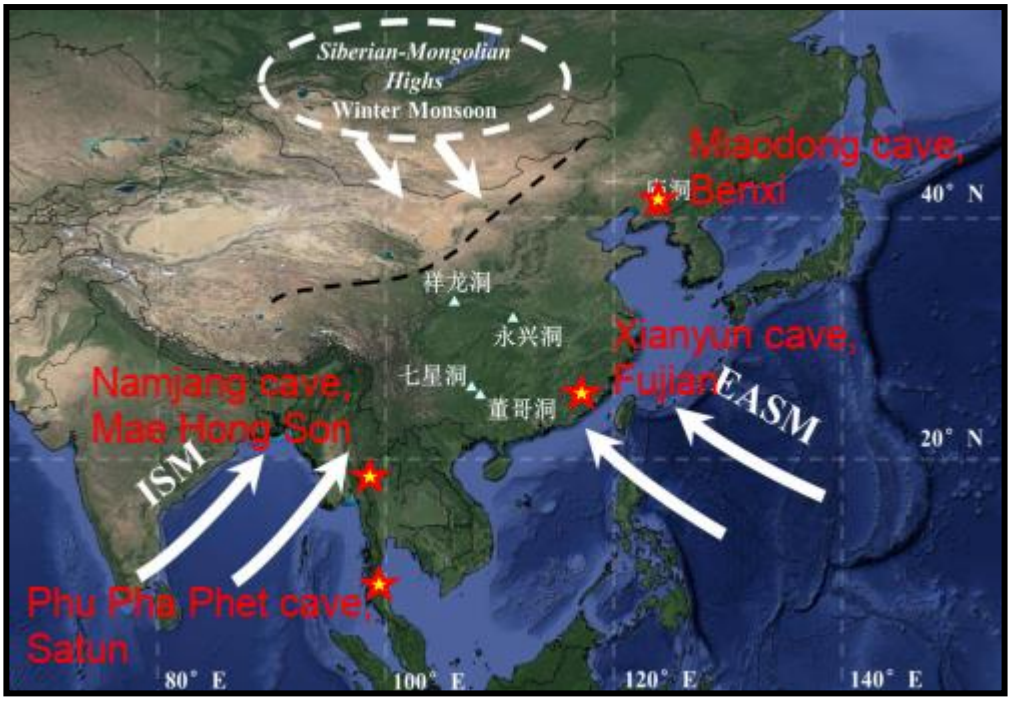

Figure 3.5.1 Schematic map showing location of caves (red filled star) under monitoring program in this project from Thailand (Namjang cave, Mae Hong Son province and Phu Pha Phet cave, Satun province) and China (Miaodong cave, Benxi and Xianyun cave, Fujian).

3.5.1 Present-day climate monitoring

1) Rainfall

Monitoring results of monthly rainfall from May, 2016 to September, 2019 for PPP-00 stations were shown in Figures 3.5.2 (a). Discontinuous rainfall record was shown in some periods because there was a problem with the automatic rain gauge operating at the PPP-00 station. The monthly rainfall amounts reached a maximum of 325.6 mm in September, 2018. Annual averaged rainfall in 2018 (continuous data) was approximately 1572 mm. The highest numbers of consecutive rainy days (raining continually) were 16-17 days in October. Overall, these observation data exhibited rainy period from May until the following next year in January to February.

2) Temperature and RH

Yearly averaged temperature was 27.1 °C. The monthly temperatures generally decreased in January to February and increased in ~March-April. However, these variations were quite stable during the rainy periods (Figures 3.5.2 (a)). Yearly averaged RH was 85%. The monthly averaged RH values ranged from 70% in April to 93% in August (Figure 3.5.2 (a)).

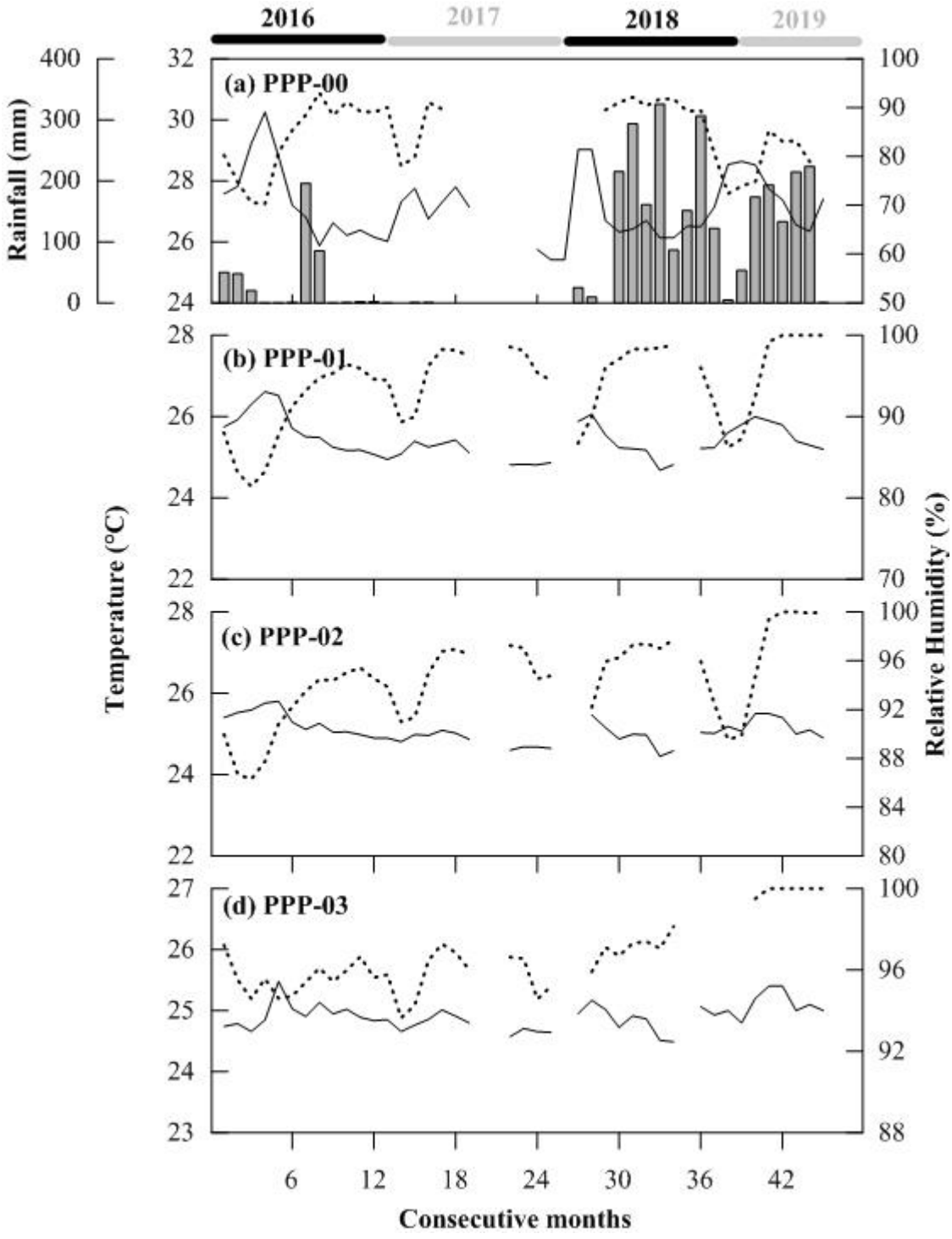

Figure 3.5.2 Time series of (a) monthly averaged surface temperature (black solid lines), RH (black dashed lines), and monthly rainfall total (grey vertical bars) for (a) PPP-00 climate station, and (b) monitoring sites inside the cave (PPP-00 to PPP-03).

3.5.2 Cave monitoring

1) Cave microclimate monitoring

The average monthly cave air temperature and RH were presented in Figure 3.5.2 (b-d) for three sites along the cave passage, including the first site near the cave entrance (PPP-01) (Figure 3.5.2 (b)), the second (PPP-02) (Figure 3.5.2 (c)), and third PPP-03) (Figure 3.5.2 (d)) sites are located in the middle and the end of the main chamber, respectively. Temperature and RH data available at PPP-00 station was used to represent the modern climate condition outside PPP cave (Figures 3.5.2 (a). Monthly averaged temperature near the cave entrance ranged between 24.7 °C and 26.6 °C. High-resolution time intervals temperature recording near cave entrance (showed a pronounced daily fluctuation which was similar to the variations seen in temperature outside the cave for both wet and dry seasons. It displayed a very close relationship with temperature outside the cave (Figure3.5.2 (a and b)). The deeper chamber (PPP-02 and PPP-03) maintained more constant temperature and less variable throughout the year compared to PPP-01 (Figure 3.5.2 (c-d)). The monthly averaged RH values varied from 81% to almost 100% in PP-01 and 81% to 100% in the deeper chamber (PPP-02 and PPP-03).

In order to show the possible connection between climate conditions outside and inside cave, present-day climate parameters (rainfall amount, temperature, and RH) outside Phu Pha Phet (PPP) cave were correlated with cave monitoring parameters (temperature and relative humidity) representing micro-climate conditions inside the cave. These temperature and relative humidity datasets cover a period between 2016 and 2019. Variations in cave air RH for all locations inside cave showed similar variations and closely related to climate conditions outside the cave (Figures 3.5.2 (b)). It showed significantly positive correlations with rainfall amount at PPP-00 station for PPP-01 ($r = 0.51$, $p < 0.001$), PPP-02 ($r = 0.53$, $p < 0.001$), and PPP-03 ($r = 0.52$, $p < 0.001$).

For outdoor temperature (PPP-00), significantly positive correlations were found with cave indoor conditions for both air temperature (PPP-01: $r = 0.73$, $p < 0.003$, PPP-02: $r = 0.65$, $p < 0.011$) and relative humidity (PPP-01: $r = -0.67$, $p < 0.008$, PPP-02: $r = -0.62$, $p < 0.018$). Correlations were also observed between relative humidity outside the cave and micro-climate parameters inside the cave for air

temperature (PPP-01: $r = 0.73$, $p < 0.003$, PPP-02: $r = 0.65$, $p < 0.027$) and relative humidity (PPP-01: $r = 0.89$, $p < 0.000$, PPP-02: $r = 0.87$, $p < 0.000$). However, there was less observed correlation at deep location inside cave (PPP-03) where this monitoring site was located at the end of the main chamber with close environment conditions. Cross-correlation analysis showed the time-delay response of inside cave temperature to outside climate conditions of approximately 60-95 minutes for the PPP-01 location near cave entrance (Table 3.5.1). After that, the cave air temperature at PPP-02 in the middle of cave passage was changed in the next 10-65minutes after PPP-01. For the PPP-03, it took approximately 20 minutes to one day for the time delay. Correlation results for monthly averaged data showed that climate conditions outside the cave apparently control micro-climate conditions inside cave, especially the locations near cave entrance (PPP-01) and the middle part of the main chamber (PPP-02).

Table 3.5.1 Time delay of cave air temperature at the three locations inside the cave to the external temperature.

Lead	Lag	Time delay
PPP station	PPP-01	60-95 นาที
PPP-01	PPP-02	10-65 นาที
PPP-01	PPP-03	1 วัน 12 ชั่วโมง
PPP-02	PPP-03	10-20 นาที

2) Drip water hydrology, hydrochemistry and isotopic properties

Averaged monitoring results of drip water properties from May, 2016 to September, 2019 for all drip sites (P-1201 to P-1208) were shown in Figures 3.5.3.

2.1) Drip rates

Monthly averaged drip rates for the eight drip sources (P-1601, P-1602, P-1603, P-1604, P-1605, P-1606, P-1607, and P-1608) were presented in Figure 3.5.3 (a-h). During the monitoring period, results demonstrated that only drip sources at P-1605 (Figure 3.5.3 (e)), P-1607 (Figure 3.5.3 (g)), and P-1608 (Figure 3.5.3 (h)). remain hydrological active for the whole years. The other drip sites were generally stopped periodically during the dry months (February to April) (Figure 3.5.3 (a-d, and

f)). Generally, the drip rates were slow or stop dripping during the dry months from (~January-February) to the beginning of the rainy months (~June), and gradually increases until reach its maximum rate in August-October for P-1601, P-1602, P-1603, P-1604, P-1605 or November-December for P-1608 (Figure 3.5.3 (a-h)), except for P-1606 and P-1607 (Figure 3.5.3 (a-h)). These indicated that variations in drip rates for PPP cave were likely caused and triggered by local rainfall amount, in particular from August to December. The monthly averaged drip rates were 0.32 drips/minute for P-1601, 0.45 drips/minute for P-1602, 0.23 drips/minute for P-1603, 0.09 drips/minute for P-1604, 0.13 drips/minute for P-1605, 0.17 drips/minute for P-1606, 0.56 drips/minute for P-1607, and 0.07 drips/minute for P-1608.

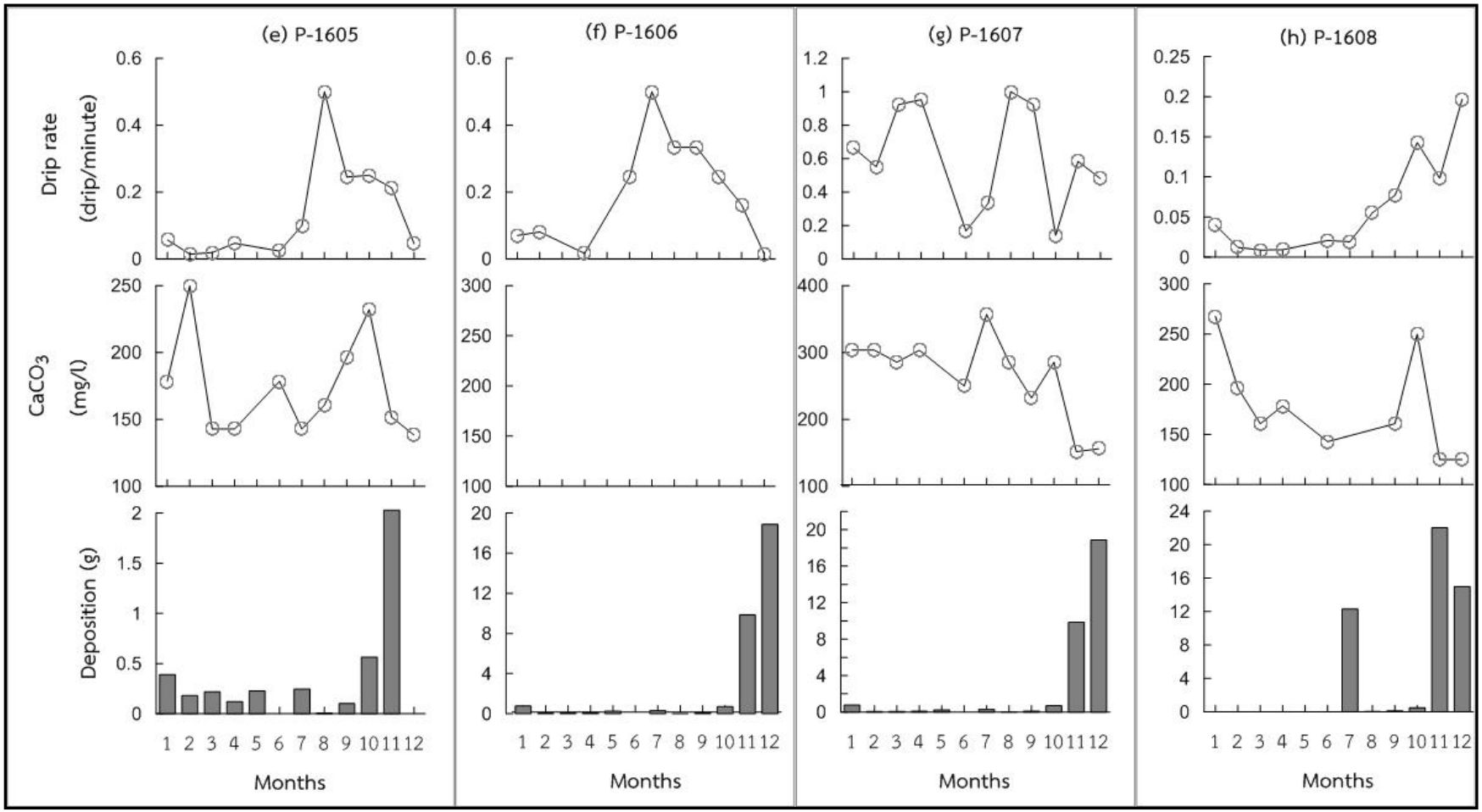

Figure 3.5.3 Time series of monthly averaged of drip rate, drip water hydrochemistry ($CaCO_3$ concentration), and modern aragonite growth rate for eight sampling sites in Phu Pha Phet cave including (a) P-1601, (b) P-1602, (c) P-1603, (d) P-1604, (e) P-1605, (f) P-1606, (g) P-1607, (h) P-1608.

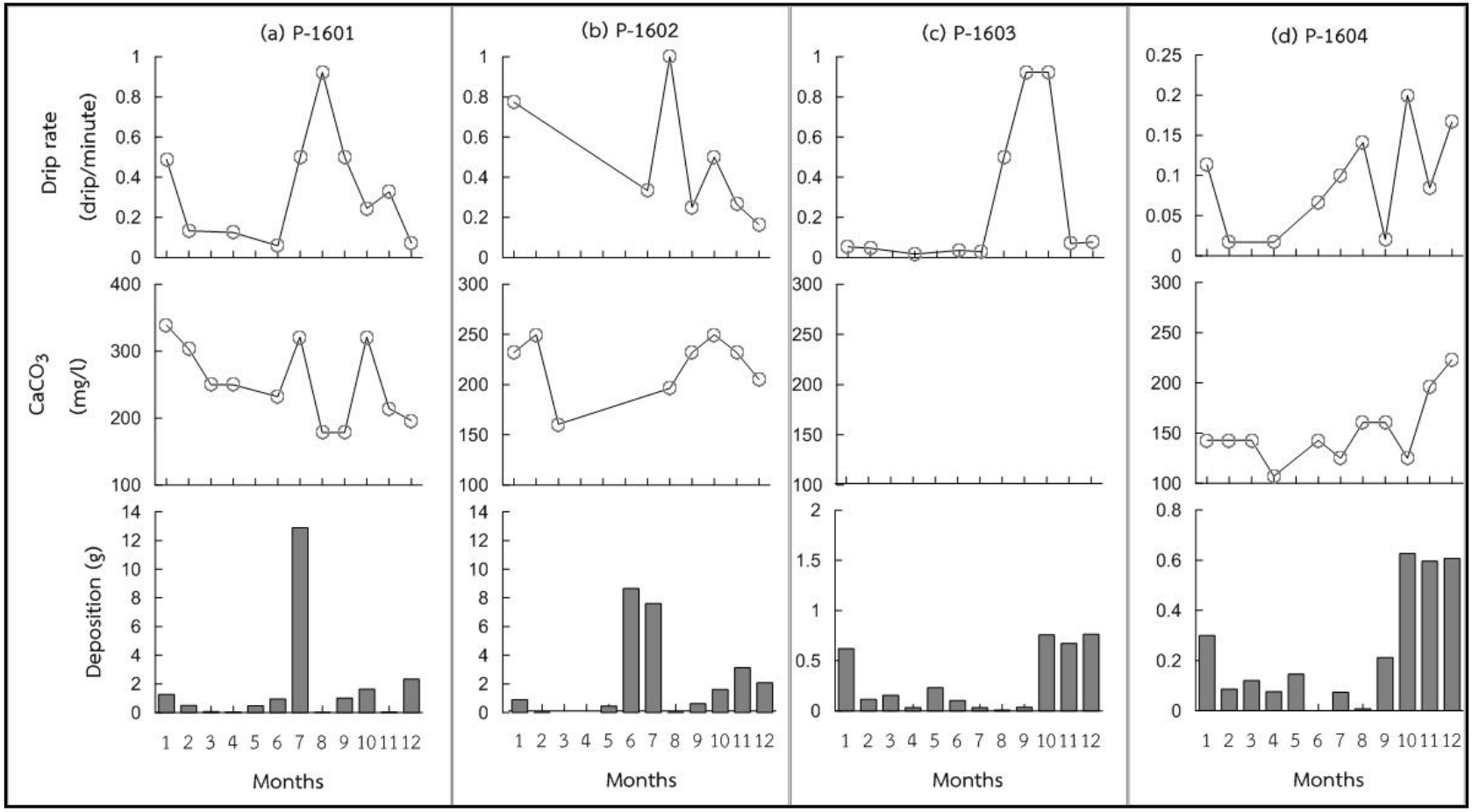

Figure 3.5.3 (cont.) Time series of monthly averaged of drip rate, drip water hydrochemistry ($CaCO_3$ concentration), and modern aragonite growth rate for eight sampling sites in Phu Pha Phet cave including (a) P-1601, (b) P-1602, (c) P-1603, (d) P-1604, (e) P-1605, (f) P-1606, (g) P-1607, (h) P-1608.

2.2) Drip water hydrochemistry

Results of cave drip water hydrochemistry including $CaCO_3$ concentration, pH, and Electrical Conductivity (EC) were presented in Figure 3.5.3. $CaCO_3$ concentration as represented carbonate hardness/alkalinity in cave drip likely exhibited the highest $CaCO_3$ concentration From August to the end of year (Figure 3.5.3). The lowest concentration was found in dry months, for examples in April for P-1601 (Figure 1.5.3 (a)), P-1603 (Figure 3.5.3 (c)), P-1604 (Figure 3.5.3 (d)), P-1605 (Figure 3.5.3 (e)), P-1606 (Figure 3.5.3 (f)), and P-1608 (Figure 3.5.3 (h)). The concentration ranged from 170 to 339 mg/l with an averaged value of 237 mg/l for P-1601, from 125 to 250 mg/l with an averaged value of 215 mg/l for P-1602, from 71 to 223 mg/l with an averaged value of 141 mg/l for P-1604, from 107 to 250 mg/l with an averaged value of 165 mg/l for P-1605, from 152 to 357 mg/l with an averaged value of 244 mg/l for P-1607, and from 125 to 268 mg/l with an averaged value of 171 mg/l for P-1608.

Monthly averaged of pH values were 8.07 for P-1601, 7.98 for P-1602, 7.63 for P-1604, 7.84 for P-1605, 8.37 for P-1607, and 8.06 for P-1605. The EC values of cave drip water vary and likely inconsistent among sampling sites. The values ranged from 256 to 497 µS/cm for P-1601, from 267 to 420 µS/cm for P-1602, from 1605 to 2150 µS/cm for P-1604, from 857 to 2850 µS/cm for P-1605, from 300 to 318 µS/cm for P-1607, and from 286 to 554 µS/cm for P-1608. The CO_2 concentration in cave varied from 300-500 ppm which is suitable for tourism.

3) Stalagmite growth rate dynamics

Stalagmite deposition rates for all sampling sites were shown in Figure 3.5.3 (a-h). The monthly deposition rates ranged from 0.03 g to 12.9 g with an averaged value of 1.94 g for P-1601, from 0.03 g to 8.64 g with an averaged value of 2.38 g for P-1602, from 0.01 g to 0.76 g with an averaged value of 0.30 g for P-1603, from 0.01 g to 0.63 g with an averaged value of 0.27 g for P-1604, from 0.01 g to 2.80 g with an averaged value of 0.62 g for P-1605, from 0.01 g to 18.86 g with an averaged value of 2.83 g for P-1606, from 0.03 g to 19.23 g with an averaged value of 5.07 g for P-1607, and from 0.01 g to 22.03 g with an averaged value of 4.59 g for P-1608. The highest deposition rates were generally found in June-July (P-1601 and P-1602), in October (P-1603 and P-1604), and in November-December (P-1605, P-1606, P-1607, and P-1608) (Figure 3.5.3). The extreme maximums in their growth rates were found during

the rainy months in, and likely constant for the other months with a minimum growth in dry periods. It thus seemed that stalagmite growth rates were dominated by rainfall/drip water during the rainy season.

We noted that we did not collect active stalagmites under monitoring drips in this cave for climate reconstruction as proposed earlier due to the permission from the Ministry of Natural Resources and Environment. Stalagmites from other locations and other caves were used instead as presented above.

CHAPTER IV
CONCLUSIONS

The Asian Summer Monsoon (ASM) is an important component of global monsoons and is one of the dominant summer rainfall regimes in the world. Changes in the ASM activity have strong implications for the economy and livelihood of more than two billion people, which are directly or indirectly affected by the timing and amount of precipitation during the ASM season. A better understanding of the nature of the ASM is necessary to improve our adaptability to extreme climate, especially under the background of ongoing global warming. History of the ASM during the Holocene (recent 11.6 ka) has long been one of key focuses of climatologist and global change research community. This epoch is the most important period for studying the relationship between humanity and Earth's system. Regional monsoons are driven by annual cycle of solar radiation and bonded by the global divergent circulation. They are closely correlated because of the large-scale Asian monsoon circulation. Synthetic study on the ASM variability based on proxies derived from high-resolution. Because of the limitation of long-term instrumental climate records, natural climate proxies have become vital dataset for exploring nature of Holocene. Until now, a large number of studies have been performed to reconstruct the ASM history during the Holocene. Among all of them, stalagmites and tree rings are the most important archives of the ASM. Stalagmite could provide well-dated and continuous climatic records over long time intervals, while tree-ring chronologies allow high-resolution (monthly to annual) calibration with climate and other factors. In addition, adequate understandings of the factors controlling speleothem and tree ring's properties have added the advantage over many other proxies.

The objectives of this project are; 1) To produce high-resolution composite records of Asian summer monsoon over the past few centuries based on stalagmites and tree rings collected from Northern, Northwestern, and Southern Thailand, and 2) To reconstruct and synthesize the large-scale and long-term dynamic changes of the Holocene Asian monsoon based on stalagmites from the two Asian monsoon regions

(Yunnan and Fujian, China) and one transition region (Mae Hong Son, Thailand), 3) To investigate both short-term and long-term driving mechanisms of the Asian monsoon circulation and its teleconnection to global climate change, and 4) To carry out a systematic cave and climate monitoring program in Thailand for better understanding of climate signal derived from stalagmites and tree rings.

Research methodologies can be divided into three parts as follows: 1) For analyses of stalagmites, stalagmite chronologies were developed based on either U-Th dating or lamina counting chronology. The measurements were performed on a magnetic sector inductively coupled plasma mass spectrometer. Growth rates were measured via Image-Pro Plus 5.1 software. Oxygen isotopic ($\delta^{18}O$) measurements were performed following the standard procedures on a MAT-253 mass spectrometer linked to a Gas Bench-II. 2) Cave and climate monitoring were carried on a monthly or seasonal timescales during both dry and wet seasons in order to understand the factors controlling stalagmite properties. Examples of selected parameters were stalagmite drip water properties (drip rate, Electrical Conductivity, pH, carbonate hardness, modern aragonite precipitates ($\delta^{18}O$, growth rate), and cave air conditions (relative humidity, temperature, and CO_2). 3) For tree rings, tree ring chronologies were performed using COFCHA program. Pure α-cellulose was extracted by a modified Jayme-Wise method. The cellulose $\delta^{18}O$ composition was determined with a continuous flow system by a pyrolysis-type elemental analyzer connected to a MAT-253 mass spectrometer via an open split interface.

Based on these results, observations and knowledge relating to climate changes during the Holocene epoch can be summarized as follows:

1) The early to mid-Holocene climate evolution in Thailand and China

1.1) In the early-Holocene, long-term pattern of summer monsoon in different regions are different. In Northern China, stalagmite isotope sequence showed the East Asian Summer Monsoon (EASM) was strong during the early-Holocene until 5.0 ka BP, followed by gradually declining trend. In Southeastern China, there also have a more moisture interval during mid-Holocene from approximately 6.5 ka BP to 4.5 ka BP. This wetter mid-Holocene was also observed in Northwestern Thailand. The accumulated density of stalagmites from Northwestern Thailand was low during the early Holocene, and then it increased to a peak from 11.0 ka BP until 8.0 ka BP.

The second peak was found during time period between 6.0 and 3.0 ka BP. This indicated that moisture situation during the mid-Holocene was higher compared to the early-Holocene. The moisture was increased since 8.0 ka BP, and its peak was observed during the interval between 6.0 and 3.0 ka BP. The Holocene moisture evolution pattern in Northwestern Thailand was similar with that of in Southeastern China, indicating a teleconnection between these two regions. The wetter mid-Holocene in these regions was different from those in the Indian Summer Monsoon (ISM) dominated region as observed by stalagmite records from Oman and Southwestern China. By comparing our results with insolation, we suggested that there were more regional precipitation in Northern China, Southeastern China, and Northwestern Thailand in the mid-Holocene when the ISM has shrunk since the early-Holocene. This indicated that hydrological changes in these three regions were not only influenced by orbital-driven insolation, but also by the sea-air interaction processes over the Western North Pacific Ocean.

1.2) Stalagmite isotopic records from Southern Thailand indicated higher rainfall in the early-Holocene, lower in the late-Holocene. Its long-term trend was similar to those in Oman and Southwestern China. Their Holocene change pattern were closely correlated with insolation in the Northern Hemisphere, supporting the hypothesis of insolation directly forcing mechanism via the Inter Tropical Convergence Zone (ITCZ) shifting northward at the early-Holocene and gradually moving southward then after.

1.3) For the millennium cold events in the Holocene, we investigated in-deep the cold events occurred at 2.8 ka BP, 5.5 ka BP and those occurred at the early-Holocene, depending on high-resolution stalagmite records from Northern China. We found that not all of cold events responding to solar activity. For the 2.8 ka event, the EASM indicated by Miaodong cave’s stalagmite record coincided with those of the total solar irradiance without any delay, indicating solar activity forcing via a fast dynamic mechanism, such as atmospheric remote-correlation. However, for the cold event 5.5 ka, our stalagmite records collected from Northeastern China exhibited two weak monsoon intervals, centering at 5.54 and 4.95 ka BP, respectively. There was no obvious corresponding relation between the EASM and solar activity indicators. We propose that the evidence of solar forcing on the EASM at 5.5 ka event

was still limited. Inversely, the EASM indicated by our record do agree well with the El Niño–Southern Oscillation (ENSO) event, indicating the ENSO forcing mechanism.

2) The late-Holocene climate evolution in Thailand

A 338-year oxygen isotope record from teak tree-ring cellulose revealed that over the entire period from AD 1678-2015, summer precipitation in Northwestern Thailand had decreased, and the reconstructed long-term average of May-October (rainy season) average precipitation was 253 mm. We found that during the 17^{th} and 18^{th} centuries, drought occurred during 8 years, respectively. In the 19^{th} century, there was drought during 19 years. In the 17^{th}, 18^{th}, and 19^{th} centuries, wet years occurred during 6, 10 and 1 years, respectively. The mechanism that may support drought in Southeast Asia is the southward shift in the ITCZ. In addition, these findings are consistent with other reconstructed mega drought events, especially those found in the 18^{th} century, such as the Strange Parallels drought (AD 1756-1768) and the East India drought (AD 1790-1796). Spatial correlations and spectral analyses revealed a strong impact of the ENSO on tree-ring $\delta^{18}O$. The ENSO influenced the tree-ring $\delta^{18}O$ more strongly in the AD 1870-1906, AD 1907-1943, and AD 1944-1980 periods than in the AD 1981-2015 period, which corresponded to periods of weaker and stronger ISM intensity.

Finally, proxy records of this study would probably be the most high-resolution and longest records for Thailand monsoon. High-quality and short term proxy records would have potentially significant implications to give a better understanding of teleconnections within the modern atmosphere as well as to quantify the climatological parameters in the long-term climate reconstruction. This study will most benefit to improve climate forecasts, especially in the monsoon transition area.

REFERENCES

Abdullah, J. (2017). Mansuli Valley, Lahad Dalu, Sabah in the Prehistory of Southeast Asia. Penerbit University Sains Malaysia, Pulau Pinang, Malaysia

Abram, N. J., Gagan, M. K., Liu, Z., Hantoro, W. S., McCulloch, M. T., & Suwargadi, B. W. (2007). Seasonal characteristics of the Indian Ocean Dipole during the Holocene epoch. *Nature, 445*(7125), 299-302. doi: http://www.nature.com/nature/journal/v445/n7125/suppinfo/nature05477_S1.html

Achuthavarier, D., Krishnamurthy, V., Kirtman, B. P., & Huang, B. (2012). Role of the Indian Ocean in the ENSO–Indian summer monsoon teleconnection in the NCEP Climate Forecast System. *Journal of Climate*, *25*(7), 2490-2508. doi:https://doi.org/10.1175/JCLI-D-11-00111.1

Aggarwal, P. K., Fröhlich, K., Kulkarni, K. M., & Gourcy, L. L. (2004). Stable isotope evidence for moisture sources in the asian summer monsoon under present and past climate regimes. *Geophysical Research Letters, 31(L08203)*(8), 1-4. doi:10.1029/2004GL019911

Aggarwal, P.K., Romatschke, U., Araguas-Araguas, L., Belachew, D., Longstaffe, F.J., Berg, P., Schumacher, C., Funk, A. (2016). Proportions of convective and strati-form precipitation revealed in water isotope ratios. *Nature Geoscience, 9*, 624–629. doi.org/10.1038/ngeo2739.

An, Z., Porter, S. C., Kutzbach, J. E., Xihao, W., Suming, W., Xiaodong, L., . . . Weijian, Z. (2000). Asynchronous Holocene optimum of the East Asian monsoon. *Quaternary Science Reviews, 19*(8), 743-762. doi: http://dx.doi.org/10.1016/S0277-3791(99)00031-1

Anderson, D. M., Overpeck, J. T., & Gupta, A. K. (2002). Increase in the Asian southwest monsoon during the past four centuries. *Science, 297*(5581), 596-599. doi:doi: 10.1126/science.1072881

REFERENCES) (cont.)

Ashok, K., Guan, Z., Saji, N., & Yamagata, T. (2004). Individual and combined influences of ENSO and the Indian Ocean dipole on the Indian summer monsoon. *Journal of Climate, 17*(16), 3141-3155. doi:https://doi.org/10.1175/1520-0442(2004)017<3141:IACIOE>2.0.CO;2

Ashok, K., Guan, Z., & Yamagata, T. (2001). Impact of the Indian Ocean dipole on the relationship between the Indian monsoon rainfall and ENSO. *Geophysical Research Letters, 28*(23), 4499-4502. doi:https://doi.org/10.1029/2001GL013294

Ashok, K., Guan, Z., & Yamagata, T. (2003). A look at the relationship between the ENSO and the Indian Ocean dipole. *Journal of the Meteorological Society of Japan. Ser. II, 81*(1), 41-56. doi:https://doi.org/10.2151/jmsj.81.41

Bellenger, H., & Duvel, J. P. (2007). Intraseasonal Convective Perturbations Related to the Seasonal March of the Indo-Pacific Monsoons. *Journal of Climate, 20*(12), 2853-2863. doi:10.1175/JCLI4182.1

Berger, A., & Loutre, M. F. (1991). Insolation values for the climate of the last 10 million years. *Quaternary Science Reviews, 10*(4), 297-317. doi:https://doi.org/10.1016/0277-3791(91)90033-Q

Bond, G., Kromer, B., Beer, J., Muscheler, R., Evans, M. N., Showers, W., . . . Bonani, G. (2001). Persistent Solar Influence on North Atlantic Climate During the Holocene. *Science, 294*(5549), 2130. doi:10.1126/science.1065680

Borgaonkar, H. P., Sikder, A. B., Ram, S., & Pant, G. B. (2010). El Niño and related monsoon drought signals in 523-year-long ring width records of teak (*Tectona grandis* L.F.) trees from south India. *Palaeogeography, Palaeoclimatology, Palaeoecology, 285*(1–2), 74-84. doi: http://dx.doi.org/10.1016/j.palaeo.2009.10.026

REFERENCES) (cont.)

Brienen, R. J., Helle, G., Pons, T. L., Guyot, J.-L., & Gloor, M. (2012). Oxygen isotopes in tree rings are a good proxy for Amazon precipitation and El Niño-Southern Oscillation variability. *Proceedings of the National Academy of Sciences, 109*(42), 16957-16962. doi:www.pnas.org/cgi/doi/10.1073/pnas.1205977109

Brienen, R.J.W., Hietz, P., Wanek, W., Gloor, M. (2013). Oxygen isotopes in tree rings record variation in precipitation $\delta^{18}O$ and amount effects in the south of Mexico, *Journal of Geophysical Research: Biogeosciences, 118,* 1604–1615, https://doi:10.1002/2013JG002304.

Buajan, S., Pumijumnong, N., Li, Q., & Liu, Y. (2016). Oxygen isotope ($\delta^{18}O$) of teak tree-rings in north-west thailand. *Journal of Tropical Forest Science,* 396-405. doi:https://www.jstor.org/stable/43956806

Buareal, K., Buajan , S., Preechamart, S., Muangsong, C., & Pumijumnong, N. (2020). A 177 Years Extended of Teak Chronology Revealing to the Climate Variability in Phrae Province, Northern of Thailand. *Applied Environmental Research, 42*(1), 85-100. https://doi.org/10.35762/AER.2020.42.1.7

Buckley, B.M., Palakit, K., Duangsathaporn, K., Sanguantham, P., & Prasomsin, P. (2007). Decadal scale droughts over northwestern Thailand over the past 448 years: links to the tropical Pacific and Indian Ocean sectors. *Climate Dynamics* 29, 63-71

Buras, A. (2017). A comment on the expressed population signal. *Dendrochronologia, 44,* 130-132. doi:https://doi.org/10.1016/j.dendro.2017.03.005

Cai, B., Edwards, R. L., Cheng, H., Tan, M., Wang, X., & Liu, T. (2008). A dry episode during the Younger Dryas and centennial-scale weak monsoon events during the early Holocene: A high-resolution stalagmite record from southeast of the Loess Plateau, China. *Geophysical Research Letters, 35*(2), n/a-n/a. doi: 10.1029/2007GL030986

REFERENCES) (cont.)

Cai, B., Pumijumnong, N., Tan, M., Muangsong, C., Kong, X., Jiang, X., & Nan, S. (2010). Effects of intraseasonal variation of summer monsoon rainfall on stable isotope and growth rate of a stalagmite from northwestern Thailand. *Journal of Geophysical Research: Atmospheres, 115*(D21). doi:10.1029/2009JD013378

Cai, Y., Zhang, M., Peng, Z., Lin, Y., An, Z., Zhang, Z., & Cao, Y. (2001). The $\delta^{18}O$ variation of a stalagmite from Qixing Cave, Guizhou Province and indicated climate change during the Holocene. *Chinese Science Bulletin, 46*(22), 1904-1908. doi:10.1007/BF02901169

Cai, B., Pumijumnong, N., Tan, M., Muangsong, C., Kong, X., Jiang, X., & Nan, S. (2010). Effects of intraseasonal variation of summer monsoon rainfall on stable isotope and growth rate of a stalagmite from northwestern Thailand. *Journal of Geophysical Research: Atmospheres, 115*(D21). doi:https://doi.org/10.1029/2009JD013378

Chansaengkrachang, K., Luadsong, A., & Aschariyaphotha, N. (2015). A study of the time lags of the Indian ocean dipole and rainfall over Thailand by using the cross wavelet analysis. *Arabian Journal for Science and Engineering, 40*(1), 215-225. doi:https://doi.org/10.1007/s13369-014-1480-1

Cheng, H., Edwards, R. L., Broecker, W. S., Denton, G. H., Kong, X., Wang, Y., . . . Wang, X. (2009). Ice Age Terminations. *Science, 326*(5950), 248. doi:10.1126/science.1177840

Clark, P. U., Marshall, S. J., Clarke, G. K. C., Hostetler, S. W., Licciardi, J. M., & Teller, J. T. (2001). Freshwater Forcing of Abrupt Climate Change During the Last Glaciation. *Science, 293*(5528), 283. doi:10.1126/science.1062517

Clark, S. & Clark, S.G. (2007). The Sun Kings: the unexpected tragedy of Richard Carrington and the tale of how modern astronomy began. Princeton University Press.

REFERENCES) (cont.)

Cook, E.R., Cole, J.E., D'Arrigo, R.D., Stahle, D.W., & Villalba, R. (2000). Tree-ring records of past ENSO variability and forcing. In: Diaz, H., & Markgraf, V. (eds) El Niño and the Southern Oscillation: Multiscale variability and Global and Regional impacts. Cambridge University Press, London, pp 297-324.

Cook, E. R., Anchukaitis, K. J., Buckley, B. M., D'Arrigo, R. D., Jacoby, G. C., & Wright, W. E. (2010). Asian monsoon failure and megadrought during the last millennium. *Science, 328*(5977), 486-489. doi: 10.1126/science.1185188

Cook, E.R., Kairiukstis, L.A. (1990). Methods of Dendrochronology Applications in the Environmental Sciences. Springer, Dordrecht.

D'Arrigo, R., Cook, E.R., Wilson, R.J., Allan, R., & Mann, M.E. (2005). On the variability of ENSO over the past six centuries. *Geophysical Research Letters 32*.

Dansgaard, W. (1964). Stable isotopes in precipitation. *Tellus, 16*(4), 436-468. doi:https://doi.org/10.3402/tellusa.v16i4.8993

Dykoski, C. A., Edwards, R. L., Cheng, H., Yuan, D., Cai, Y., Zhang, M., . . . Revenaugh, J. (2005). A high-resolution, absolute-dated Holocene and deglacial Asian monsoon record from Dongge Cave, China. *Earth and Planetary Science Letters, 233*(1), 71-86. doi:https://doi.org/10.1016/j.epsl.2005.01.036

Dorotovič, I., Louzada, J., Rodrigues, J., & Karlovsky, V. (2014). Impact of solar activity on the growth of pine trees: Case study. *European Journal of Forest Research, 133*, 639-648 doi:DOI: 10.1007/s10342-014-0792-8

Ellis, M. (2017). The cave of Thailand 2- Northern of Thaialnd vol 2. Martin Ellis Shepton Mallet Somerste UK, United Kingdom.

REFERENCES) (cont.)

Enfield, D. B., Mestas- Nuñez, A. M., & Trimble, P. J. (2001). The Atlantic multidecadal oscillation and its relation to rainfall and river flows in the continental US. *Geophysical Research Letters*, *28*(10), 2077-2080. doi:https://doi.org/10.1029/2000GL012745

Fairchild, I. J., Smith, C. L., Baker, A., Fuller, L., Spötl, C., Mattey, D., . . . E.I.M.F. (2006). Modification and preservation of environmental signals in speleothems. *Earth-Science Reviews, 75*(1–4), 105-153. doi: http://dx.doi.org/10.1016/j.earscirev.2005.08.003

Fleitmann, D., Burns, S. J., Mangini, A., Mudelsee, M., Kramers, J., Villa, I., . . . Matter, A. (2007). Holocene ITCZ and Indian monsoon dynamics recorded in stalagmites from Oman and Yemen (Socotra). *Quaternary Science Reviews, 26*(1), 170-188. doi:https://doi.org/10.1016/j.quascirev.2006.04.012

Foukal, P. (1990). Solar Astrophysics. Wiley, New York.

Fritts, H. (1976). Tree rings and climate New York: Academic Press.

Gadgil, S., Vinayachandran, P., Francis, P., & Gadgil, S. (2004). Extremes of the Indian summer monsoon rainfall, ENSO and equatorial Indian Ocean oscillation. *Geophysical Research Letters*, *31*(12). doi:https://doi.org/10.1029/2004GL019733

Gizani, N.A.B., Papathanasopoylos, K., Vatikiotis, L., & Zervas, E. (2011). Impact of solar activity on climate changes in Athens region, Greece. *Atmospheric and Oceanic Physics*:1-9.

Gorman, C.F. (1970). Excavation of spirit cave, North Thailand. *Asian Perspective 13,* 81-108.

Grave, P., Spies, J., Barrbetti, M., & Hotchkis, M. (1994). Dating of log coffins of northwestern Thailand. In: IPPA Conference chiang Mai, Thailand, 5-12 Jan 1994. pp 5-12

REFERENCES) (cont.)

Grootes, P. M., Stuiver, M., White, J. W. C., Johnsen, S., & Jouzel, J. (1993). Comparison of oxygen isotope records from the GISP2 and GRIP Greenland ice cores. *Nature, 366*(6455), 552-554. doi:10.1038/366552a0

Harrisson, T. (1975). Early dates for "seated" burial and burial matting at Niah Caves, Sarawak (Borneo) *Asian Perspective XVIII* (2):161-165

Hayes, S., Shoocongdej, R., Pureepatpong, N., Sangvichien, S., & Chintakanon, K. (2017). A Late Pleistocene woman from ThamLod, Thailand: the influence of today on a face from the past. *Antiquity, 91*, 289–303

Haug, G. H., Hughen, K. A., Sigman, D. M., Peterson, L. C., & Röhl, U. (2001). Southward Migration of the Intertropical Convergence Zone Through the Holocene. *Science, 293*(5533), 1304. doi:10.1126/science.1059725

Higham, C. (1989). The Archaeology of Mainland Southeast Asia from 10000 BC to the Fall of Angkor Cambridge University Press,

Hochreuther, P., Wernicke, J., Grießinger, J., Mölg, T., Zhu, H., Wang, L., & Bräuning, A. (2016). Influence of the Indian Ocean Dipole on tree-ring δ 18 O of monsoonal Southeast Tibet. *Climatic Change, 137*(1-2), 217-230. doi:https://doi.org/10.1007/s10584-016-1663-8

Hotchkis, M.A.C., Fink, D., Jacobsen, G.E., Lawson, E.M., Shying, M., A.M. S, &Tuniz, C. (1994). 14C analysis at the ANTARES AMS center: dating the long coffin of northern Thailand Nuclear Instruments and Methods in Physics Research B 92, 27-30

Hu, C., Henderson, G. M., Huang, J., Xie, S., Sun, Y., & Johnson, K. R. (2008). Quantification of Holocene Asian monsoon rainfall from spatially separated cave records. *Earth and Planetary Science Letters, 266*(3), 221-232. doi:https://doi.org/10.1016/j.epsl.2007.10.015

IAEA/WMO, 2001. Global network of isotopes in precipitation. The GNIP Database. http://www-naweb.iaea.org/napc/ih/IHS_resources_gnip.html.

REFERENCES) (cont.)

Jones, P. D., Briffa, K. R., Osborn, T. J., Lough, J. M., van Ommen, T. D., Vinther, B. M., . . . Xoplaki, E. (2009). High-resolution palaeoclimatology of the last millennium: a review of current status and future prospects. *The Holocene, 19*(1), 3-49. doi: 10.1177/0959683608098952

Kanner, L. C., Burns, S. J., Cheng, H., Edwards, R. L., & Vuille, M. (2013). High-resolution variability of the South American summer monsoon over the last seven millennia: insights from a speleothem record from the central Peruvian Andes. *Quaternary Science Reviews, 75*, 1-10. doi:https://doi.org/10.1016/j.quascirev.2013.05.008

Kumar, B., Rai, S., Kumar, U. S., Verma, S., Garg, P., Kumar, S. V., . . . Pande, N. (2010). Isotopic characteristics of Indian precipitation. *Water Resources Research, 46*(12). doi:https://doi.org/10.1029/2009WR008532

Kumar, K. K., Rajagopalan, B., & Cane, M. A. (1999). On the Weakening Relationship Between the Indian Monsoon and ENSO. *Science, 284*(5423), 2156-2159.

Kurths, J., Spiering, C., Müller-Stoll, W., & Striegler, U. (1993). Search for solar periodicities in Miocene tree ring widths. *Terra Nova* 5:359–363.

Lampert, C.D. et al. (2003). Dating resin coating on pottery: the Spirit Cave early ceramic dates revised. *Antiquit, 77*, 126-133

Le Duy, N., Heidbüchel, I., Meyer, H., Merz, B., & Apel, H. (2018). What controls the stable isotope composition of precipitation in the Mekong Delta? A model-based statistical approach. *Hydrology and Earth System Sciences, 22*, 1239-1262. doi:doi:10.5194/hess-22-1239-2018

Li, G., Zheng, M., & Yang, H. (2019). Cycle Analysis Method of Tree Ring and Solar Activity Based on Variational Mode Decomposition and Hilbert Transform. *Advances in Meteorology* 2019:8.

REFERENCES) (cont.)

Li, Y., Wang, N. a., Zhou, X., Zhang, C., & Wang, Y. (2014). Synchronous or asynchronous Holocene Indian and East Asian summer monsoon evolution: A synthesis on Holocene Asian summer monsoon simulations, records and modern monsoon indices. *Global and Planetary Change, 116*, 30-40. doi: http://dx.doi.org/10.1016/j.gloplacha.2014.02.005

Liu, W., Y, W., CY, H., HM, S., QF, C., H, T., & HW, S. B. a. L. (2011). Tree-ring-based annual precipitation reconstruction in Kalaqin Inner Mongolia for the last 238 years. *Chinese Science Bulletin, 56,* 2995-3002. doi:https://doi.org/10.1007/s11434-011-4706-6

Liu, X., An, W., Treydte, K., Shao, X., Leavitt, S., Hou, S., . . . Qin, D. (2012). Tree-ring $\delta^{18}O$ in southwestern China linked to variations in regional cloud cover and tropical sea surface temperature. *Chemical Geology, 291,* 104-115. doi: http://dx.doi.org/10.1016/j.chemgeo.2011.10.001

Liu, Y., Wang, Y., Li, Q., Song, H., Linderholm, H. W., Leavitt, S. W., . . . An, Z. (2014). Tree-ring stable carbon isotope-based May–July temperature reconstruction over Nanwutai, China, for the past century and its record of 20th century warming. *Quaternary Science Reviews, 93,* 67-76. doi:https://doi.org/10.1016/j.quascirev.2014.03.023

Liu, Y. H., Henderson, G. M., Hu, C. Y., Mason, A. J., Charnley, N., Johnson, K. R., & Xie, S. C. (2013). Links between the East Asian monsoon and North Atlantic climate during the 8,200 year event. *Nature Geoscience, 6*(2), 117-120. doi:10.1038/ngeo1708

Malik, A., Brönnimann, S., Stickler, A., Raible, C. C., Muthers, S., Anet, J., . . . Schmutz, W. (2017). Decadal to multi-decadal scale variability of Indian summer monsoon rainfall in the coupled ocean-atmosphere-chemistry climate model SOCOL-MPIOM. *Climate dynamics, 49*(9-10), 3551-3572. doi:https://doi.org/10.1007/s00382-017-3529-9

REFERENCES) (cont.)

Managave, S., Sheshshayee, M., Ramesh, R., Borgaonkar, H., Shah, S., & Bhattacharyya, A. (2011). Response of cellulose oxygen isotope values of teak trees in differing monsoon environments to monsoon rainfall. *Dendrochronologia*, 29(2), 89-97. doi:https://doi.org/10.1016/j.dendro.2010.05.002

McCarroll, D., & Loader, N. J. (2004). Stable isotopes in tree rings. *Quaternary Science Reviews, 23*(7-8), 771-801. doi:https://doi.org/10.1016/j.quascirev.2003.06.017

Medvigy, D., & Beaulieu, C. (2012). Trends in daily solar radiation and precipitation coefficients of variation since 1984. *Journal of Climate, 25*, 1330-1339

Mickler, P. J., Stern, L. A., & Banner, J. L. (2006). Large kinetic isotope effects in modern speleothems. *Geological Society of America Bulletin, 118*(1-2), 65-81. doi: 10.1130/b25698.1

Mölg, T., Maussion, F., Collier, E., Chiang, J. C., & Scherer, D. (2017). Prominent midlatitude circulation signature in High Asia's surface climate during monsoon. *Journal of Geophysical Research: Atmospheres*, *122*(23), 12,702-712,712. doi:https://doi.org/10.1002/2017JD027414

Muangsong, C., 2016. Asian monsoon variability over the last two thousand years as inferred from stalagmites and tree rings from Northwestern Thailand. Ph.D. Thesis, China University of Geosciences (Wuhan).

Muangsong, C., Cai, B., Pumijumnong, N., Hu, C., & Cheng, H. (2014). An annually laminated stalagmite record of the changes in Thailand monsoon rainfall over the past 387 years and its relationship to IOD and ENSO. *Quaternary International, 349*, 90-97

Muangsong, C., Cai, B., Pumijumnong, N., Hu, C., & Lei, G. (2016). Intra-seasonal variability of teak tree-ring cellulose δ18O from northwestern Thailand: A potential proxy of Thailand summer monsoon rainfall. *The Holocene, 26*(9), 1397-1405. doi:https://doi.org/10.1177/0959683616640045

REFERENCES) (cont.)

Muangsong, C., Cai, B., Pumijumnong, N., Lei, G., & Wang, F. (2019). A preliminary study on teak tree ring cellulose $\delta^{18}O$ from northwestern Thailand: the potential for developing multiproxy records of Thailand summer monsoon variability. *Theoretical and applied climatology*, *136*(1-2), 575-586. doi:https://doi.org/10.1007/s00704-018-2499-0

Muangsong, C., Pumijumnong, N., Cai, B., & Tan, M. (2011). Stalagmite grey level as a proxy of the palaeoclimate in northwestern Thailand. *ScienceAsia*, *37*(3), 262. doi: 10.2306/scienceasia1513-1874.2011.37.262

Muangsong, C., Pumijumnong, N., Cai, B., Buajan, S., Lei, G., Wang, F., . . . Payomrat, P. (2020). Effect of changes in precipitation amounts and moisture sources on inter-and intra-annual stable oxygen isotope ratios ($\delta^{18}O$) of teak trees from northern Thailand. *Agricultural and Forest Meteorology*, *281*, 107820. doi:https://doi.org/10.1016/j.agrformet.2019.107820

Muraki, Y., Masuda, K., Nagaya, K., Wada, K., & Miyahara, H. (2011). Solar variability and width of tree ring. *Astrophysics and Space Sciences Transactions*, *7*, 395-401

Murphy, J.O. & Palmer, J.G. (1992). Ring Width Variation in Sub-Fossil Wood Samples as an Indicator of Shortterm Solar Variability 2000-YR B.P. *AStronomical Society of Australia*, *10*, 68-70

Nakamura, N., Kayanne, H., Iijima, H., McClanahan, T. R., Behera, S. K., & Yamagata, T. (2009). Mode shift in the Indian Ocean climate under global warming stress. *Geophysical Research Letters*, *36*(23). doi:https://doi.org/10.1029/2009GL040590

REFERENCES) (cont.)

Novello, V. F., Cruz, F. W., Vuille, M., Stríkis, N. M., Edwards, R. L., Cheng, H., Emerick, S., de Paula, M. S., Li, X., Barreto, E. S., Karmann, I., & Santos, R. V. (2017). A high-resolution history of the South American Monsoon from Last Glacial Maximum to the Holocene. *Scientific reports*, *7*, 44267. https://doi.org/10.1038/srep44267

OgÉE, J., Barbour, M. M., Wingate, L., Bert, D., Bosc, A., Stievenard, M., . . . Dewar, R. C. (2009). A single-substrate model to interpret intra-annual stable isotope signals in tree-ring cellulose. *Plant, Cell & Environment*, *32*(8), 1071-1090. doi: 10.1111/j.1365-3040.2009.01989.x

Owens, M.J. et al. (2017). The Maunder minimum and the Little Ice Age: an update from recent reconstructions and climate simulations. *J Space Weather Space Clim*,*7* , 10

Poussart, P. F., Evans, M. N., & Schrag, D. P. (2004). Resolving seasonality in tropical trees: multi-decade, high-resolution oxygen and carbon isotope records from Indonesia and Thailand. *Earth and Planetary Science Letters*, *218*(3-4), 301-316. doi:https://doi.org/10.1016/S0012-821X(03)00638-1

Pratarastapornkul, T. (2007). An apparent effect of Indian Ocean Dipole phenomenon on annual rainfall variability of Thailand. Paper presented at the IOGOOS Workshop and the fifth annual meeting.

Preechamart, S., Pumijumnong, N., Payomrat, P., & Buajan, S. (2018). Variation in Climate Signals in Teak Tree-Ring Chronologies in Two Different Growth Areas. *Forests*, *9*(12), 772. doi:10.3390/f9120772

Prestes, A., Klausner, V., Rojahn da Silva, I., Ojeda-González, A., & Lorensi, C. (2018). Araucaria growth response to solar and climate variability in South Brazil. In: Annales Geophysicae, vol 3. Copernicus GmbH, pp 717-729

Pumijumnong, N. (1995). Dendrochrnologie mit Teak (*Tectona grandis* L.) in Nord-Thailand. Jahrringbildung—Chronologiennetz—Klimasignal. Diss. Univ. Hamburg, 104.

REFERENCES) (cont.)

Pumijumnong, N. (2012). Teak tree ring widths: Ecology and climatology research in Northwest Thailand. *Journal of Science, Technology and Development, 31*, 165-174

Pumijumnong, N. (2013). Dendrochronology in Southeast Asia. *Trees. 27*, 343–358. https://doi.org/10.1007/s00468-012-0775-7.

Pumijumnong, N. & Wannasri, S. (2015). Teak Log Coffins in Northwest Thailand: Dated by Dendrochronology and ^{14}Cwiggle Matching. *Applied Environmental Research, 37*, 1-16

Pumijumnong, N., Muangsong, C., Buajan, S., Sano, M., & Nakatsuka, T. (2020). Climate variability over the past 100 years in Myanmar derived from tree-ring stable oxygen isotope variations in Teak. *Theoretical and applied climatology*, *139*(3-4), 1401-1414. doi:https://doi.org/10.1007/s00704-019-03036-y

Rasmussen, S. O., Andersen, K. K., Svensson, A. M., Steffensen, J. P., Vinther, B. M., Clausen, H. B., . . . Ruth, U. (2006). A new Greenland ice core chronology for the last glacial termination. *Journal of Geophysical Research: Atmospheres*, *111*(D6). doi:10.1029/2005JD006079

Rao, S. A., Behera, S. K., Masumoto, Y., & Yamagata, T. (2002). Interannual subsurface variability in the tropical Indian Ocean with a special emphasis on the Indian Ocean dipole. Deep Sea Research Part II: *Topical Studies in Oceanography, 49*(7-8), 1549-1572. doi:https://doi.org/10.1016/S0967-0645(01)00158-8

Reddy, P.R. & Reddy, D.V. (2016). Impact due to sunspot activity on climate change: some salient results. *International Journal of Earth Sciences and Engineering, 9*, 1-4

REFERENCES) (cont.)

Rigozo, N.R., Nordeman, D.J.R., Echer, E., Vieira, L.E.A., Echer, M.P.S. & Prestes, A. (2005). Tree-ring width wavelet and spectralanalysis of solar variability and climaticeffects on a Chilean cypress during thelast two and a half millennia. *Climate of the Past Discussion, 1,* 121-135

Rigozo, N.R., Nordemann, D.J.R., Echer, E., Vieira, L.E.A. (2004). Search for Solar Periodicities in Tree-ring Widths from Conco´ rdia (S.C., Brazil). *Pure and Applied Geophysics, 161*, 221-233

Rigozo, N.R., Nordemann, D.J.R., Silva, H.E.d, Echer, M.P.d.S, Echerc, E. (2007). Solar and climate signal records in tree ring width from Chile (AD 1587–1994). *Planetary and Space Science, 55*, 158-164

Rinn, F. (2011). TSAP-WinTM: Time Series Analysis and Presentation for Dendrochronology and Related Applications. Version 4.64 for Microsoft Windows User Reference. 4.64 ed. Rinntech, Heidelberg

Roden, J. S., Lin, G., & Ehleringer, J. R. (2000). A mechanistic model for interpretation of hydrogen and oxygen isotope ratios in tree-ring cellulose. *Geochimica et Cosmochimica Acta, 64*(1), 21-35. doi: http://dx.doi.org/10.1016/S0016-7037(99)00195-7

Roy, I., & Tedeschi, R. G. (2016). Influence of enso on regional indian summer monsoon precipitation—local atmospheric influences or remote influence from pacific. *Atmosphere, 7*(2), 25. https://doi.org/10.3390/atmos7020025

Saji, N. H., Goswami, B. N., Vinayachandran, P. N., & Yamagata, T. (1999). A dipole mode in the tropical Indian Ocean. *Nature, 401*(6751), 360-363.

Sano, M., Dimri, A., Ramesh, R., Xu, C., Li, Z., & Nakatsuka, T. (2017). Moisture source signals preserved in a 242-year tree-ring $\delta^{18}O$ chronology in the western Himalaya. *Global and Planetary Change, 157*, 73-82. doi:https://doi.org/10.1016/j.gloplacha.2017.08.009

REFERENCES) (cont.)

Sano, M., Xu, C., & Nakatsuka, T. (2012). A 300- year Vietnam hydroclimate and ENSO variability record reconstructed from tree ring $\delta^{18}O$. *Journal of Geophysical Research: Atmospheres*, *117*(D12). doi:https://doi.org/10.1029/2012JD017749

Satoh, M. (2014). Latitudinal energy balance. In: Atmospheric Circulation Dynamics and General Circulation Models. Springer, pp 353-369

Schollaen, K., Heinrich, I., Neuwirth, B., Krusic, P. J., D'Arrigo, R. D., Karyanto, O., & Helle, G. (2013). Multiple tree-ring chronologies (ring width, δ13C and δ18O) reveal dry and rainy season signals of rainfall in Indonesia. *Quaternary Science Reviews*, *73*, 170-181. doi:https://doi.org/10.1016/j.quascirev.2013.05.018

Shen, H., & Poulsen, C. J. (2019). Precipitation δ18O on the Himalaya-Tibet orogeny and its relationship to surface elevation. *Clim Past*, *15*, 169-187. doi:https://doi.org/10.5194/cp-2018-117

Shoocongdej, R. (2003). Open site in northwest thailand: a preliminary report. In: The highland archaeological project roundtable conference, 2003. pp 21-34

Shoocongdej, R. (2004). Preliminary Report on the Archaeology Investigations of the Highland Archaeology Project in Pang Mapha (HAPP), Mae Hong Son Province Between 1998-2004. Southeast Asian Archaeology International Newsletter

Shoocongdej, R. (2014). Craft-Specialization in Iron Age Log Coffin Culture on Highland Pang Mapha District, Mae Hong Son Province. *Journal of the Faculty of Archaeology, 13*, 75-106

Shoocongdej, R. (2016). Log coffin culture of Thailand in the Southeast Asian context. Faculty of Archaeology, Silpakorn University, Bangkok, Thailand

Singhrattna, N., Rajagopalan, B., Kumar, K. K., & Clark, M. (2005). Interannual and interdecadal variability of Thailand summer monsoon season. *Journal of Climate, 18*(11), 1697-1708. doi:https://doi.org/10.1175/JCLI3364.1

REFERENCES) (cont.)

Sinha, A., Cannariato, K. G., Stott, L. D., Cheng, H., Edwards, R. L., Yadava, M. G., . . . Singh, I. B. (2007). A 900 year (600 to 1500 AD) record of the Indian summer monsoon precipitation from the core monsoon zone of India. *Geophysical Research Letters, 34*(16). doi:http://doi: 10.1029/2007GL030431

Sinha, A., Berkelhammer, M., Stott, L., Mudelsee, M., Cheng, H., & Biswas, J. (2011). The leading mode of Indian Summer Monsoon precipitation variability during the last millennium. *Geophysical Research Letters, 38*(15), n/a-n/a. doi: 10.1029/2011GL047713

Stein, A.F., Draxler, R.R, Rolph, G.D., Stunder, B.J.B., Cohen, M.D., Ngan, F. (2015). NOAA's HYSPLIT atmospheric transport and dispersion modeling system. *Bulletin of the American Meteorological Society, 96,* 2059-2077. https://doi.org/10.1175/BAMS-D-14-00110.1.

Steinhilber, F., Beer, J., & Fröhlich, C. (2009). Total solar irradiance during the Holocene. *Geophysical Research Letters, 36*(19). doi:10.1029/2009GL040142

Stuiver, M., & Grootes, P. M. (2000). GISP2 Oxygen Isotope Ratios. *Quaternary Research, 53*(3), 277-284. doi:https://doi.org/10.1006/qres.2000.2127

Sørensen, P. (1973). Prehistoric Iron Imprements from Thailand. *Asian Perspective XVII* (2):134-172

Sørensen, P. (1988). Archaeological Excavations in Thailand. Surface Finds and Minor Excavations,Scandinavian Institute of Asian Studies Occasional Paper no. 1, Copenhagen

Takahashi, H.G., Yasunari, T. (2006). A climatological monsoon break in rainfall over Indochina – A singularity in the seasonal March of the Asian summer monsoon. *Journal of Climate, 19,* 1545–1556. https://doi.org/10.1175/JCLI3724.1.

REFERENCES) (cont.)

Tan, M., Liu, T.S., Hou, J., Qin, X., Zhang, H. & Li, T. (2003). 2650-Year Beijing Stalagmite Layer Thickness and Temperature Reconstruction. *Geophysical Research Letters, 30*, 1617

Tan, L., Cai, Y., Cheng, H., Edwards, L. R., Gao, Y., Xu, H., . . . An, Z. (2018). Centennial- to decadal-scale monsoon precipitation variations in the upper Hanjiang River region, China over the past 6650 years. *Earth and Planetary Science Letters, 482*, 580-590. doi:https://doi.org/10.1016/j.epsl.2017.11.044

Tan, L., Shen, C.C., Löwemark, L., Chawchai, S., Edwards, R. L., Cai, Y., . . . Duerrast, H. (2019). Rainfall variations in central Indo-Pacific over the past 2,700 y. Proceedings of the National Academy of Sciences, *116*(35), 17201-17206. doi:https://doi.org/10.1073/pnas.1903167116

Thai, P.Q., Choisy, M., Duong, T.N., et al. (2015). Seasonality of absolute humidity explains seasonality of influenza-like illness in Vietnam. *Epidemics, 13*, 65–73. https://doi.org/10.1016/j.epidem.2015.06.002.

Thomas, E. R., Mulvaney, R., & Wolff, E. W. (2008). A change in seasonality in Greenland during a Dansgaard–Oeschger warming. *Annals of Glaciology, 48*, 19-24. doi:10.3189/172756408784700590

Torrence, C. & Webster, P.J. (1999). Interdecadal changes in the ENSO–monsoon system. *Journal of climate, 12*, 2679-2690

Treerayapiwat, C. (2005). Patterns of habitation and burial activity in the Ban Rai Rock Shelter, Northwestern Thailand. *Asian Perspectives*, 231-245

Tsiropoula, G. (2003). Signatures of solar activity variability in meteorological parameters. *Journal of Atmospheric and Solar-Terrestrial Physics, 65*, 469– 482

REFERENCES) (cont.)

Van Rampelbergh, M., Verheyden, S., Allan, M., Quinif, Y., Keppens, E., & Claeys, P. (2014). Monitoring of a fast-growing speleothem site from the Han-sur-Lesse cave, Belgium, indicates equilibrium deposition of the seasonal δ18O and δ13C signals in the calcite. *Climate of the Past, 10*(5), 1871-1885. doi: 10.5194/cp-10-1871-2014

Varikoden, H., & Babu, C. (2015). Indian summer monsoon rainfall and its relation with SST in the equatorial Atlantic and Pacific Oceans. *International Journal of Climatology,* 35(6), 1192-1200. doi:https://doi.org/10.1002/joc.4056

Vinayachandran, P., Saji, N., & Yamagata, T. (1999). Response of the equatorial Indian Ocean to an unusual wind event during 1994. *Geophysical Research Letters*, *26*(11), 1613-1616. doi: https://doi.org/10.1029/1999GL900179

Volland, F., Pucha, D., & Braeuning, A. (2016). Hydro-climatic variability in southern Ecuador reflected by tree-ring oxygen isotopes. *Erdkunde*, 69-82. doi:https://www.jstor.org/stable/24892591

Walker, M., Johnsen, S., Rasmussen, S. O., Popp, T., Steffensen, J.-P., Gibbard, P., . . . Schwander, J. (2009). Formal definition and dating of the GSSP (Global Stratotype Section and Point) for the base of the Holocene using the Greenland NGRIP ice core, and selected auxiliary records. *Journal of Quaternary Science, 24*(1), 3-17. doi: 10.1002/jqs.1227

Wang, B., & Ho, L. (2002). Rainy season of the Asian-Pacific summer monsoon. *Journal of Climate, 15*, 386–398. doi: 10.1175/1520-0442(2002)015<0386:RSOTAP>2.0.CO;2

Wang B, & Q, D. (2011). *The global monsoon system: research and forecast* (Chang C-P, Wang B & L. GN-C Eds. 2ed.): World Scientific Publication Company.

REFERENCES) (cont.)

Wang, Y., Cheng, H., Edwards, R. L., He, Y., Kong, X., An, Z., . . . Li, X. (2005). The Holocene Asian Monsoon: Links to Solar Changes and North Atlantic Climate. *Science, 308*(5723), 854. doi:10.1126/science.1106296

Wang, Y., Liu, X., & Herzschuh, U. (2010). Asynchronous evolution of the Indian and East Asian Summer Monsoon indicated by Holocene moisture patterns in monsoonal central Asia. *Earth-Science Reviews, 103*(3–4), 135-153. doi: http://dx.doi.org/10.1016/j.earscirev.2010.09.004

Wang, X. & Zhang, Q.B. (2011). Evidence of solar signals in tree rings of Smith fir from Sygera Mountain in southeast Tibet. *Journal of Atmospheric and Solar-Terrestrial Physics, 73*, 1959-1966

Wannasri, S., Pumijumnong, N. & Shoocongdej, R. (2007). Teak log coffin head styles in northern Thailand: time sequencing with dendrochronology. *Sci Asia, 33*, 47-56

Wanner, H., Beer, J., Bütikofer, J., Crowley, T. J., Cubasch, U., Flückiger, J., . . . Widmann, M. (2008). Mid- to Late Holocene climate change: an overview. *Quaternary Science Reviews, 27*(19–20), 1791-1828. doi: http://dx.doi.org/10.1016/j.quascirev.2008.06.013

Webster, P. J., & Yang, S. (1992). Monsoon and ENSO: Selectively interactive systems. *Quarterly Journal of the Royal Meteorological Society, 118*(507), 877-926. doi:https://doi.org/10.1002/qj.49711850705

Wei, Z., Lee, X., Liu, Z., Seeboonruang, U., Koike, M., & Yoshimura, K. (2018). Influences of large-scale convection and moisture source on monthly precipitation isotope ratios observed in Thailand, Southeast Asia. *Earth and Planetary Science Letters, 488*, 181-192. doi:https://doi.org/10.1016/j.epsl.2018.02.015

REFERENCES) (cont.)

Wigley, T. M. L., Briffa, K. R., & Jones, P. D. (1984). On the Average Value of Correlated Time Series, with Applications in Dendroclimatology and Hydrometeorology. *Journal of Climate and Applied Meteorology, 23*(2), 201-213. doi:10.1175/1520-0450(1984)023<0201:OTAVOC>2.0.CO;2

Wilks, D.S. (1995). Statistical Methods in Atmospheric Sciences: an Introduction, San Diego, Academic Press.

Wu, C.J., Usoskin, I.G., Krivova, N., Kovaltsov, G.A., Baroni, M., Bard, E. & Solanki, S.K. (2018). Solar activity over nine millennia: A consistent multi-proxy reconstruction. *Astronomy & Astrophysics,* 1-13

Wu, L., Li, F., Zhu, C., Li, L., & Li, B. (2012). Holocene environmental change and archaeology, Yangtze River Valley, China: Review and prospects. *Geoscience Frontiers, 3*(6), 875-892. doi: http://dx.doi.org/10.1016/j.gsf.2012.02.006

Xie, P., Arkin, P.A. (1997). Global Precipitation: A 17-year monthly analysis based on gauge observations, satellite estimates, and numerical model outputs. *Bulletin of the American Meteorological Society, 78*, 2539–2558.

Xu, C., Pumijumnong, N., Nakatsuka, T., Sano, M., & Guo, Z. (2018). Inter-annual and multi-decadal variability of monsoon season rainfall in central Thailand during the period 1804–1999, as inferred from tree ring oxygen isotopes. International Journal of Climatology, *38*(15), 5766-5776. doi:https://doi.org/10.1002/joc.5859

Xu, C., Pumijumnong, N., Nakatsuka, T., Sano, M., & Li, Z. (2015). A tree-ring cellulose δ^{18}O-based July–October precipitation reconstruction since AD 1828, northwest Thailand. *Journal of Hydrology*, 529, 433-441. doi:https://doi.org/10.1016/j.jhydrol.2015.02.037

Xu, C., Sano, M., & Nakatsuka, T. (2011). Tree ring cellulose δ^{18}O of Fokienia hodginsii in northern Laos: A promising proxy to reconstruct ENSO? *Journal of Geophysical Research: Atmospheres*, *116*(D24). doi:https://doi.org/10.1029/2011JD016694

REFERENCES) (cont.)

Xu, C., Sano, M., & Nakatsuka, T. (2013). A 400-year record of hydroclimate variability and local ENSO history in northern Southeast Asia inferred from tree-ring $\delta^{18}O$. *Palaeogeography, Palaeoclimatology, Palaeoecology, 386*, 588-598. doi:https://doi.org/10.1016/j.palaeo.2013.06.025

Xu, H., Yeager, K. M., Lan, J., Liu, B., Sheng, E., & Zhou, X. (2015). Abrupt Holocene Indian Summer Monsoon failures: A primary response to solar activity? The Holocene, 25(4), 677-685. doi: 10.1177/0959683614566252

Yang, B., Qin, C., Wang, J., He, M., Melvin, T. M., Osborn, T. J., & Briffa, K. R. (2014). A 3,500-year tree-ring record of annual precipitation on the northeastern Tibetan Plateau. *Proceedings of the National Academy of Sciences of the United States of America, 111*(8), 2903-2908. doi: 10.1073/pnas.1319238111

Yoshifuji, N., Kumagai, T. o., Tanaka, K., Tanaka, N., Komatsu, H., Suzuki, M., & Tantasirin, C. (2006). Inter-annual variation in growing season length of a tropical seasonal forest in northern Thailand. *Forest Ecology and Management, 229*(1), 333-339. doi:https://doi.org/10.1016/j.foreco.2006.04.013

Zhang, P. et al. (2008). A test of climate, sun, and culture relationships from an 1810-year Chinese cave record. *Science, 322*, 940-942

Zhou, T.-J., & Yu, R.-C. (2005). Atmospheric water vapor transport associated with typical anomalous summer rainfall patterns in China. *Journal of Geophysical Research: Atmospheres, 110*(D8), n/a-n/a. doi: 10.1029/2004JD005413

Zhu, M., Stott, L., Buckley, B., & Yoshimura, K. (2012). 20^{th} century seasonal moisture balance in Southeast Asian montane forests from tree cellulose $\delta^{18}O$. *Climatic Change, 115*(3-4), 505-517. doi:https://doi.org/10.1007/s10584-012-0439-z

APPENDICES

APPENDIX A

Publications

Publication No. 1: Inter-annual and multi-decadal variability of monsoon season rainfall in central Thailand during the period 1804–1999, as inferred from tree ring oxygen isotopes.

Xu, C., Pumijumnong, N., Nakatsuka, T., Sano, M., Guo, Z. (2018). Inter-annual and multi-decadal variability of monsoon season rainfall in central Thailand during the period 1804–1999, as inferred from tree ring oxygen. *International Journal of Climatology*, *38*, 5766-5776. https://doi.org/10.1002/joc.5859.

Received: 24 October 2017 | Revised: 13 July 2018 | Accepted: 31 August 2018 | Published on: 24 September 2018
DOI: 10.1002/joc.5859

International Journal of Climatology RMetS

RESEARCH ARTICLE

Inter-annual and multi-decadal variability of monsoon season rainfall in central Thailand during the period 1804–1999, as inferred from tree ring oxygen isotopes

Chenxi Xu[1,2] | Nathsuda Pumijumnong[3] | Takeshi Nakatsuka[4] | Masaki Sano[4,5] | Zhengtang Guo[1,2,6]

[1]Key Laboratory of Cenozoic Geology and Environment, Institute of Geology and Geophysics, Chinese Academy of Sciences, Beijing, China
[2]CAS Center for Excellence in Life and Paleoenvironment, Beijing, China
[3]Faculty of Environment & Resource Studies, Mahidol University, Nakhon Pathom, Thailand
[4]Research Institute for Humanity and Nature, Kyoto, Japan
[5]Faculty of Human Sciences, Waseda University, Tokorozawa, Japan
[6]University of Chinese Academy of Sciences, Beijing, China

Correspondence
Nathsuda Pumijumnong, Faculty of Environment & Resource Studies, Mahidol University, Nakhon Pathom 73170, Thailand.
Email: nathsuda@gmail.com

Funding information
National Natural Science Foundation of China, Grant/Award Number: 41672179; the Strategic Priority Research Program of Chinese Academy of Sciences, Grant/Award Number: XDB26020000; the Chinese Academy of Sciences (CAS) Pioneer Hundred Talents Program, the National Key R&D Program of China, Grant/Award Number: 2016YFA0600502; Ministry of Science and Technology of China, Grant/Award Number: 2017YFE0112000; Research Institute of Humanity and Nature, Kyoto, Japan; Japan Society for the Promotion of Science Fellows, Grant/Award Number: 23242047 and 23-10262; Asian summer monsoon variability during the Holocene: a synthesis study on stalagmites and tree rings from Thailand and China by the Thailand Research Fund (TRF), Grant/Award Number: RDG5930014

Long-term records of precipitation in Thailand are necessary to evaluate the robustness of the relationship between El Niño–Southern Oscillation (ENSO) and rainfall. This study presents a tree ring-cellulose oxygen isotope ($\delta^{18}O$) record, based on *Pinus merkusii*, for the period 1804–1999 in Thailand. Response and spatial correlation analyses reveal that tree ring $\delta^{18}O$ is significantly correlated with regional monsoon season (May–October) precipitation. Tree ring $\delta^{18}O$, which explains 50.1% of the variability in regional precipitation, was employed to reconstruct monsoon season rainfall back to 1804. Relatively wet periods occurred in 1809–1821, 1876–1882, 1897–1908, and 1944–1975, while the periods 1825–1850, 1913–1925, and 1979–1997 were relatively dry. During the periods 1854–1930 and 1970–1999, inter-annual variability of precipitation was modulated by the ENSO. In contrast, the absence of this relationship between 1930 and 1970 might relate to the reduced variance of ENSO.

KEYWORDS
central Thailand, ENSO, monsoon season rainfall, tree ring oxygen isotopes

1 | INTRODUCTION

The global monsoon precipitation provides water resources to about two thirds of the world's population, and a better understanding of mechanism of monsoon changes will be of great societal importance (Liu *et al*., 2009). In particular, almost 80% of the annual rainfall in Thailand occurs during the summer monsoon season (May–October), which has important implications for agriculture and the economy. For instance, 67% of the national rice crop originates

Funding information for Xu et al. (2018)

Source: https://rmets.onlinelibrary.wiley.com/doi/abs/10.1002/joc.5859

Funding information
National Natural Science Foundation of China, Grant/Award Number: 41672179; the Strategic Priority Research Program of Chinese Academy of Sciences, Grant/Award Number: XDB26020000; the Chinese Academy of Sciences (CAS) Pioneer Hundred Talents Program, the National Key R&D Program of China, Grant/Award Number: 2016YFA0600502; Ministry of Science and Technology of China, Grant/Award Number: 2017YFE0112800; Research Institute of Humanity and Nature, Kyoto, Japan; Japan Society for the Promotion of Science Fellows, Grant/Award Number: 23242047 and 23-10262; Asian summer monsoon variability during the Holocene: a synthesis study on stalagmites and tree rings from Thailand and China by the Thailand Research Fund (TRF), Grant/Award Number: RDG5930014

Publication No. 2: Variation in Climate Signals in Teak Tree-Ring Chronologies in Two Different Growth Areas

Preechamart, S., Pumijumnong, N., Payomrat, P., Buajan, S. (2018). Variation in Climate Signals in Teak Tree-Ring Chronologies in Two Different Growth Areas. *Forests*, *9*(772), 1-12. https://doi.org/10.3390/f9120772.

forests

MDPI

Article

Variation in Climate Signals in Teak Tree-Ring Chronologies in Two Different Growth Areas

Sineenart Preechamart [1], Nathsuda Pumijumnong [1,*], Paramate Payomrat [2] and Supaporn Buajan [2]

[1] Faculty of Environment and Resource Studies, Mahidol University, Nakhon Pathom 73170, Thailand; sineenart.pre@student.mahidol.ac.th

[2] Tree-Ring and Climate Change Research Center, Faculty of Environment and Resource Studies, Mahidol University, Nakhon Pathom 73170, Thailand; paramate.ohm@gmail.com (P.P.); buajan_s@hotmail.com (S.B.)

* Correspondence: nathsuda.pum@mahidol.ac.th; Tel.: +66-244-15000 (ext. 2311)

Received: 30 November 2018; Accepted: 11 December 2018; Published: 14 December 2018

check for updates

Abstract: We developed two tree-ring chronologies of teak (*Tectona grandis* L.f.) from Mae Tuen (462-year, 1555–2016) and Umphang (165-year, 1852–2016) in Tak province, northwestern Thailand. The chronologies were based on 67 and 71 living teak trees, respectively. We used crossdating methods to check and verify the tree-ring width data and tree-ring chronology construction using the ARSTAN program. In this study, the two teak tree-ring chronologies from two different growth areas could not be crossdated. The relationship among these chronologies is, thus, relatively low ($r = 0.33$, $n = 165$, $p < 0.01$). This result shows that the growth of tree-ring structure from two sites can be affected by a variety of non-climatic patterns due to site variation, such as topography, nutrient, light, and internal factors. However, these chronologies have a significant positive correlation with rainfall, during the pre-monsoon season (April to May). As demonstrated by the spatial correlation patterns, these chronologies represent April to May rainfall, which was a limiting factor of teak growth from northwestern Thailand. While the difference in surface temperatures of the Indian Ocean Dipole (IOD) might not be affected by rainfall, its unstable relationship with the El Niño-Southern Oscillation (ENSO) was noted to have occurred.

Keywords: dendroclimatology; ring-width; teak (*Tectona grandis* L.f.)

1. Introduction

The Asian monsoon system (AMS) is a key variable for global climate change and plays a significant role in large-scale climate variability [1]. The AMS is primarily driven by convective, radiative, and sensible heat sources/sinks [2,3]. Southwest monsoons are formed due to intense low pressure systems formed over the Tibetan plateau. Northeast monsoons are associated with high pressure cells over the Tibetan and Siberian plateaus. Countries like India, Indonesia, Bangladesh, Myanmar, and Thailand receive most of the annual rainfall during the southwest monsoon season [4]. AMS is composed of three inter-linked components: Indian summer monsoon (ISM), East Asian summer monsoon (EASM), and Southeast Asian summer monsoon (SASM) [5]. Studies on the past AMS have sought to explain the ISM or EASM and the interaction between the two monsoons [6–8]. In addition, recent studies have focused on the influence of the El Niño phenomena and its effect on the amount of rainfall or drought in Southeast Asia [9,10]. The interaction between the El Niño phenomenon and the variation in sea surface temperatures in the Indian Ocean influences the amount of rainfall that will fall on land [11–13]. In contrast, currently, there are not many studies on the SASM. Indeed, to better understand the influence of climate in Southeast Asian countries, long climate information and extensive weather stations coverage area are required. These are limitations of the

Funding information for Preechamart et al. (2018)

Source: https://www.mdpi.com/1999-4907/9/12/772

Funding: This research was funded by the Royal Golden Jubilee Ph.D. (RGJ-PHD) Program under the Thailand Research Fund (TRF) (Grant No. PHD/0076/2560) (For RGJ-PHD) and a project of Asian summer monsoon variability during the Holocene: A synthesis study on stalagmites and tree rings from Thailand and China by the Thailand Research Fund (TRF) (Grant No. RDG5930014).

Acknowledgments: We would like to thank forestry officers and co-workers for sample collection and preparation. Thanks to Kritsadapan Palakit, Faculty of Forest, Kasetsart University for encouragement and suggestion, Thomas Neal Stewart, Voravart Ratanadilok Na Bhuket and Kanokrat Buareal, Faculty of Environment and Resource Studies, Mahidol University for editing this manuscript and wonderful help.

Conflicts of Interest: The authors declare no conflict of interest.

Publication No. 3: A preliminary study on teak tree ring cellulose $\delta^{18}O$ from northwestern Thailand: the potential for developing multiproxy records of Thailand summer monsoon variability

Muangsong, C., Cai, B., Pumijumnong, N., Lei, G., Wang, F. (2019). A preliminary study on teak tree ring cellulose $\delta^{18}O$ from northwestern Thailand: the potential for developing multiproxy records of Thailand summer monsoon variability. *Theoretical and Applied Climatology*, *136*, 575-586. https://doi.org/10.1007/s00704-018-2499-0.

Theoretical and Applied Climatology (2019) 136:575–586
https://doi.org/10.1007/s00704-018-2499-0

ORIGINAL PAPER

A preliminary study on teak tree ring cellulose $\delta^{18}O$ from northwestern Thailand: the potential for developing multiproxy records of Thailand summer monsoon variability

Chotika Muangsong[1] · Binggui Cai[2,3] · Nathsuda Pumijumnong[4] · Guoliang Lei[2,3] · Fang Wang[2,3]

Received: 4 September 2017 / Accepted: 30 April 2018 / Published online: 23 May 2018
© Springer-Verlag GmbH Austria, part of Springer Nature 2018

Abstract
Thailand monsoon is located in the transition zone between the Indian and western North Pacific monsoons. Assuredly, proxy climate data from this area could improve our understanding of the nature of Asian monsoon. Tree rings and stalagmites from this area are two potential materials for high-resolution paleoclimate reconstructions. However, a comprehensive understanding of these multiproxy records is still a challenge. In this study, a 76-year tree ring cellulose oxygen isotope value ($\delta^{18}O$) of a teak tree from northwestern Thailand was developed to test its climatic significance and potential for multiproxy climate reconstruction. The results indicate that the interannual variability of cellulose $\delta^{18}O$ can be interpreted as a proxy of rainfall in the early monsoon season (May to July rainfall) as well as a proxy of relative humidity. Comparisons with speleothem proxies from the same locality and tree ring records from wider geographical areas provide a basis for developing a multiproxy approach. The results from a teleconnection analysis reveal that the El Niño-Southern Oscillation (ENSO) is an important climate mode that impacts monsoon rainfall in Thailand. High-quality proxy records covering recent decades are critically important not only to improve proxy data calibrations but also to provide a better understanding of teleconnections within the modern atmosphere. Preliminary findings demonstrated the potential of tree ring stable isotopes from Thai teak to develop multiproxy climate reconstruction.

1 Introduction

Thailand monsoon (TM) is located in the transition zone between the Indian monsoon (IM) and western North Pacific (WNP) monsoon (WNPM) (Wang and Ho 2002) and receives moisture from different sources related to each monsoon regime (Aggarwal et al. 2004). A unique characteristic of TM is the seasonal changes in rainfall patterns (Takahashi and Yasunari 2006) and its isotopic composition (Aggarwal et al. 2004). Improving our understanding of the Asian summer monsoon (ASM) requires the development of climatic data from the entire ASM domain, especially in the transition area. However, compared to the IM and the East Asian summer monsoon (EASM), much less attention has been paid to the monsoon climate in the boundary area or transition zone among the different monsoon regions (e.g., Singhrattna et al. 2005a, b; Limsakul et al. 2010).

Because of the limitations of long-term instrumental climate records, indirect or proxy indicators of climate have become vital data sets for exploring the nature of TM (Cai et al. 2010, and references therein). More recent works that have attempted to study the prior climate of Thailand are based on tree rings (Buajan et al. 2016; Muangsong et al. 2016), speleothems (Cai et al. 2010; Muangsong et al. 2011; Muangsong et al. 2014), corals (Muangsong et al. 2012), and lake sediments (Chawchai et al. 2015a, b; Wohlfarth et al. 2016). Although TM history has recently been the key focus, knowledge about TM is still limited, partly owing to the scarcity of high-resolution and long-term records with equivalent qualities. Tree rings have great potential for

✉ Binggui Cai
bingguicai@qq.com; bg-cai@fjnu.edu.cn

[1] Innovation for Social and Environmental Management, Mahidol University, Amnatcharoen Campus, Amnatcharoen 37000, Thailand
[2] Institute of Geography, Fujian Normal University, Fuzhou 350007, China
[3] Key Laboratory of Humid Subtropical Eco-geographical Processes, Ministry of Education, College of Geographical Sciences, Fujian Normal University, Fuzhou 350007, China
[4] Faculty of Environment and Resource Studies, Mahidol University, Nakhon Pathom 73170, Thailand

Funding information for Muangsong et al. (2019)

Source: https://link.springer.com/article/10.1007/s00704-018-2499-0

Funding information This research was funded under a project of Asian summer monsoon variability during the Holocene: a synthesis study on stalagmites and tree rings from Thailand and China by the Thailand Research Fund (TRF) (grant No. RDG5930014), the Natural Science Foundation of China (award number 41661144021, 41272197) and the Inovation Research Team Fund of Fujian Normal University (IRTL1705) as well as was supported by Mahidol University, Amnatcharoen campus.

Publication No. 4: A 177 years extended of teak chronology revealing to the climate variability in phrae province, northern of Thailand.

Buareal, K., Buajan,S., Preechamart, S., Muangsong, C., Pumijumnong, N., (2020) A 177 Years Extended of Teak Chronology Revealing to the Climate Variability in Phrae Province, Northern of Thailand. *Applied Environmental Research*, *42*(1), 85-100. https://doi.org/10.35762/AER.2020.42.1.7.

App. Envi. Res. 42(1) (2020): 85-100

Applied Environmental Research

Journal homepage : http://www.tci-thaijo.org/index.php/aer

A 177 Years Extended of Teak Chronology Revealing to the Climate Variability in Phrae Province, Northern of Thailand

Kanokrat Buareal[1], Supaporn Buajan[1], Sineenart Preechamart[1] Chotika Muangsong[2], Nathsuda Pumijumnong[1,*]

[1] Faculty of Environment and Resource Studies, Mahidol University, Nakhon Pathom, Thailand
[2] Innovation for Social and Environmental Management, Mahidol University, Amnatcharoen campus, Amnatcharoen, Thailand
[*] Corresponding author: Email: nathsuda.pum@mahidol.ac.th

Article History
Submitted: 20 November 2019/ Revision received: 9 March 2020/ Accepted: 11 March 2020/Published online: 25 March 2020

Abstract

Teak ring-width is one of the promising paleoclimate proxies in the tropical region. Tree-ring chronology spanning from 1840 to 2016 (177 years) was derived from 76 trees from Phrae Province, northern Thailand. A total of 141 core samples were cross-dated, a standardized master was constructed, and the tree residual master chronology was developed by ARSTAN program. The tree-ring chronology has a significant positive correlation with the monthly rainfall and relative humidity during the monsoon season (May–June). In addition, the growth of tree-ring width also significantly inversely correlated with Niño 3, Niño 3.4, and Niño 4 indices during the second half of the dry season (January–March). We reconstructed summer monsoon season (May–June) rainfall based on a linear regression model which explained 21.95% of the actual rainfall variance. The trend of the reconstructed rainfall record shows a decrease of 0.6 mm per decade and substantially showed four wet periods and five dry periods. These results suggest that this teak chronology has a good potential to be a high-resolution proxy for reconstructing the past local climate in northern Thailand.

Keywords: Teak (*Tectona grandis* L.f.); Dendrochronology; Tree-ring width

Introduction

Paleoclimatic studies are desirable to find out the dynamics of past climate, in order to composite information to explain past historical evidence, or help in predicting future climate. In Thailand, the climate data are relatively limited. Natural paleoclimate proxy information provides a past record of climate data (e.g. precipitation, temperature, and humidity) when recorded data from meteorological instruments is lacking [1]. The paleoclimatological proxies could be extracted from various kinds of natural sources such as sediments from lakes or oceans, ice cores, pollen, speleothems, coral reefs, and tree-ring [2-5].

https://doi.org/10.35762/AER.2020.42.1.7

Funding information for Buareal et al. (2020)

Source: https://ph01.tci-thaijo.org/index.php/aer/article/view/226085

Acknowledgments

We would especially like to thank Dr. Paramate Payomrat for professional guidance and insightful comments throughout this research, and Dr. Thomas Neal Stewart for editing the manuscript. Finally, we also would like to thank Mae Yom National Park for permitting the sample collection. This research was partially supported by a postdoctoral fellowship award from Mahidol University, as well as the project of Asian summer monsoon variability during the Holocene: a synthesis study on stalagmites and tree rings from Thailand and China by the Thailand Research Fund (TRF) (grant number RDG5930014); the National Natural Science Foundation of China (grant number 41661144021 and 41272197); the National Key Research and Development Program of China (2017YFA0603401); the Innovation Research Team Fund of Fujian Normal University (grant number IRTL1705); the grant number RSA6280017; and Mahidol University, Amnatcharoen campus.

Publication No. 5: Effect of changes in precipitation amounts and moisture sources on inter-and intra-annual stable oxygen isotope ratios ($\delta^{18}O$) of teak trees from northern Thailand

Muangsong, C., Pumijumnong, N., Cai, B., Buajan, S., Lei, G., Wang, F., Li, M., Payomrat, P., (2020). Effect of changes in precipitation amounts and moisture sources on inter- and intra-annual stable oxygen isotope ratios ($\delta^{18}O$) of teak trees from northern Thailand. *Agricultural and Forest Meteorology. 281*(107820), https://doi.org/10.1016/j.agrformet.2019.107820.

Agricultural and Forest Meteorology 281 (2020) 107820

Contents lists available at ScienceDirect

Agricultural and Forest Meteorology

journal homepage: www.elsevier.com/locate/agrformet

Effect of changes in precipitation amounts and moisture sources on inter- and intra-annual stable oxygen isotope ratios ($\delta^{18}O$) of teak trees from northern Thailand

Chotika Muangsong[a], Nathsuda Pumijumnong[b,*], Binggui Cai[c,d], Supaporn Buajan[b,e], Guoliang Lei[c,d], Fang Wang[c,d], Miaofa Li[c,d], Paramate Payomrat[b]

[a] Innovation for Social and Environmental Management, Mahidol University, Amnatcharoen campus, Amnatcharoen 37000, Thailand
[b] Faculty of Environment and Resource Studies, Mahidol University, Nakhon Pathom 73170, Thailand
[c] Key Laboratory for Humid Subtropical Eco-geographical Processes of the Ministry of Education, Fujian Normal University, Fuzhou 350007, China
[d] Institute of Geography, Fujian Normal University, Fuzhou 350007, China
[e] Key Laboratory of Environment Change and Resources Use in Beibu Gulf, Ministry of Education, Nanning Normal University, Nanning 530002, China

ARTICLE INFO

Keywords:
Teak
Tree rings
Thailand monsoon
Rainfall
Oxygen isotope
Moisture source

ABSTRACT

Thailand is situated in a transition zone of overlap between the Indian monsoon (IM) and the western North Pacific (WNP) monsoon. The region serves as an important area to study the influences of different moisture sources. This study presents the first stable oxygen isotope analysis on seven teak (*Tectona grandis* Linn.) trees collected from Phrae Province in northern Thailand at different temporal resolutions. Isotopic analyses of teak tree rings at both annual and sub-annual timescales reflected the variations in their source water oxygen isotope ratios ($\delta^{18}O$, i.e., rainfall) to different degrees (Annual scale: $r = 0.31$, $p < 0.05$, Monthly scale: $r = 0.63$, $p < 0.01$). A 146-year-long annually resolved tree-ring cellulose $\delta^{18}O$ series, spanning between AD 1871 and 2016, exhibited moderate negative relationships with both local ($r = -0.58$, $p < 0.01$) and regional rainfall amounts, representing the climatology of rainfall totals during the entire summer monsoon period from May to October. A spatial correlation analysis between monthly resolved tree-ring cellulose $\delta^{18}O$ with large-scale Climate Prediction Center (CPC), Outgoing Longwave Radiation (OLR), and Merged Analysis of Precipitation (CMAP) datasets, as well as an air mass backward trajectory analysis, indicated that the intraseasonal tree-ring cellulose $\delta^{18}O$ values reflected changes in moisture originating from the Indian and Pacific Oceans, rather than the amount of local precipitation. These results imply that variations in northern Thai teak cellulose $\delta^{18}O$ values are modulated not only by the local rainfall amount but also by large-scale convection, which varies between different seasons and over time. Advance knowledge of the regional monsoons in the transition area can therefore lead to a broad and complete understanding of the entire Asian monsoon circulation.

1. Introduction

The hydrological cycle plays a key role in the regulation and evolution of the Earth's climate and biological systems (Salazar et al., 2009). The atmospheric moisture transport is an essential process in hydrological cycle as it produces large quantities of water for agricultural, environmental, and domestic uses. Thailand is situated in the region where the Indian monsoon (IM) converges with the western North Pacific (WNP) monsoon (WNPM) (Takahashi and Yasunari, 2006; Wang and Ho, 2002; Wei et al., 2018). The Thailand monsoon (TM) is a part of the Asian monsoon system, which is characterized by a high degree of seasonal rainfall variability (Takahashi and Yasunari, 2006). With unique features that differ distinctly from the IM and WNPM in certain aspects such as seasonality, intensities, timing of onset, and retreat, the TM is regarded as a boundary or transition zone of overlap between these two tropical monsoon regimes (Takahashi and Yasunari, 2006; Wang and Ho, 2002; Wei et al., 2018).

The oxygen isotopic composition ($\delta^{18}O$) of meteorological precipitation is an effective tool for studying various hydrological processes (Dansgaard, 1964), more specifically, to trace water vapor sources (Krklec and Domínguez-Villar, 2014; Srivastava et al., 2015). Interpreting the rainfall $\delta^{18}O$ signal is difficult due to a combination of factors affecting the rainfall isotopes in this area (Aggarwal et al., 2004). Dansgaard (1964) and Rozanski et al. (1993) observed the

* Corresponding author.
E-mail addresses: bg-cai@fjnu.edu.cn (B. Cai), guolianglei@fjnu.edu.cn (G. Lei).

https://doi.org/10.1016/j.agrformet.2019.107820
Received 5 April 2019; Received in revised form 14 October 2019; Accepted 17 October 2019
0168-1923/ © 2019 Elsevier B.V. All rights reserved.

Funding information for Muangsong et al. (2020)

Source: https://www.sciencedirect.com/science/article/pii/S0168192319304368

Acknowledgements

This work was supported under a project of Asian summer monsoon variability during the Holocene: a synthesis study on stalagmites and tree rings from Thailand and China by the Thailand Science Research and Innovation (TSRI) (grant number RDG5930014); the National Natural Science Foundation of China (grant number 41661144021 and 41272197); the National Key Research and Development Program of China (2017YFA0603401); Innovation Research Team Fund of Fujian Normal University (grant number IRTL1705); Mahidol University, Amnatcharoen campus (2016-2019); and Postdoctoral fellowship award from Mahidol University (2018-2019). We thank the anonymous reviewers for their helpful comments.

Publication No. 6: Effects of the Pacific Decadal Oscillation on Thailand monsoon rainfall derived from a 194-year tree ring width chronology of teak trees from northwestern Thailand

Pumijumnong, N., Muangsong, C., Buajan, S., Cai, B., Kunkoon, T., Malimart, K. (2020). Effects of the Pacific Decadal Oscillation on Thailand monsoon rainfall derived from a 194-year tree ring width chronology of teak trees from northwestern Thailand. *International Journal of Biometeorology*. *64*, 1481–1495, https://doi.org/10.1007/s00484-020-01926-9.

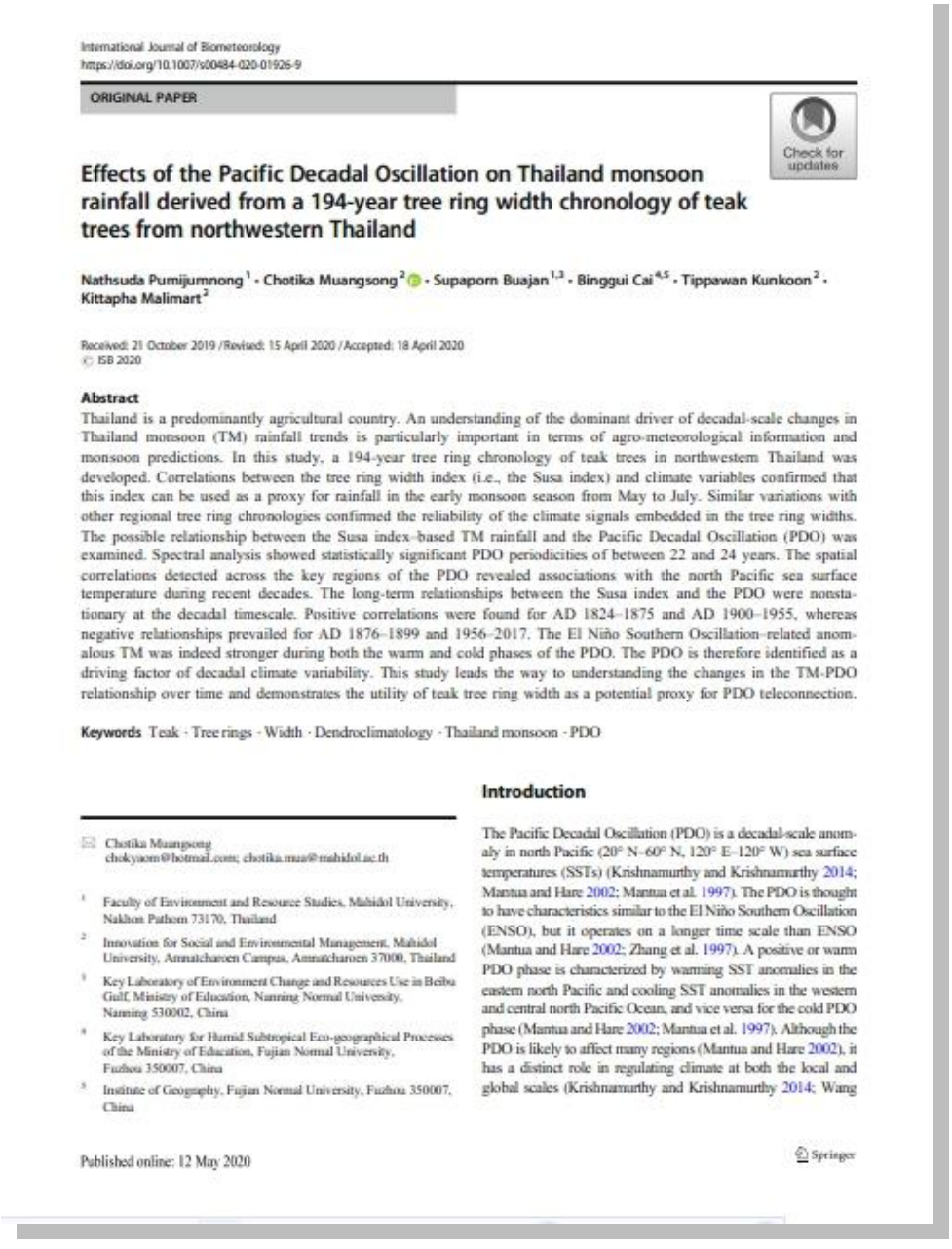

International Journal of Biometeorology
https://doi.org/10.1007/s00484-020-01926-9

ORIGINAL PAPER

Check for updates

Effects of the Pacific Decadal Oscillation on Thailand monsoon rainfall derived from a 194-year tree ring width chronology of teak trees from northwestern Thailand

Nathsuda Pumijumnong [1] · Chotika Muangsong [2] · Supaporn Buajan [1,3] · Binggui Cai [4,5] · Tippawan Kunkoon [2] · Kittapha Malimart [2]

Received: 21 October 2019 / Revised: 15 April 2020 / Accepted: 18 April 2020
© ISB 2020

Abstract
Thailand is a predominantly agricultural country. An understanding of the dominant driver of decadal-scale changes in Thailand monsoon (TM) rainfall trends is particularly important in terms of agro-meteorological information and monsoon predictions. In this study, a 194-year tree ring chronology of teak trees in northwestern Thailand was developed. Correlations between the tree ring width index (i.e., the Susa index) and climate variables confirmed that this index can be used as a proxy for rainfall in the early monsoon season from May to July. Similar variations with other regional tree ring chronologies confirmed the reliability of the climate signals embedded in the tree ring widths. The possible relationship between the Susa index–based TM rainfall and the Pacific Decadal Oscillation (PDO) was examined. Spectral analysis showed statistically significant PDO periodicities of between 22 and 24 years. The spatial correlations detected across the key regions of the PDO revealed associations with the north Pacific sea surface temperature during recent decades. The long-term relationships between the Susa index and the PDO were nonstationary at the decadal timescale. Positive correlations were found for AD 1824–1875 and AD 1900–1955, whereas negative relationships prevailed for AD 1876–1899 and 1956–2017. The El Niño Southern Oscillation–related anomalous TM was indeed stronger during both the warm and cold phases of the PDO. The PDO is therefore identified as a driving factor of decadal climate variability. This study leads the way to understanding the changes in the TM-PDO relationship over time and demonstrates the utility of teak tree ring width as a potential proxy for PDO teleconnection.

Keywords Teak · Tree rings · Width · Dendroclimatology · Thailand monsoon · PDO

Introduction

The Pacific Decadal Oscillation (PDO) is a decadal-scale anomaly in north Pacific (20° N–60° N, 120° E–120° W) sea surface temperatures (SSTs) (Krishnamurthy and Krishnamurthy 2014; Mantua and Hare 2002; Mantua et al. 1997). The PDO is thought to have characteristics similar to the El Niño Southern Oscillation (ENSO), but it operates on a longer time scale than ENSO (Mantua and Hare 2002; Zhang et al. 1997). A positive or warm PDO phase is characterized by warming SST anomalies in the eastern north Pacific and cooling SST anomalies in the western and central north Pacific Ocean, and vice versa for the cold PDO phase (Mantua and Hare 2002; Mantua et al. 1997). Although the PDO is likely to affect many regions (Mantua and Hare 2002), it has a distinct role in regulating climate at both the local and global scales (Krishnamurthy and Krishnamurthy 2014; Wang

✉ Chotika Muangsong
chokyaom@hotmail.com; chotika.mua@mahidol.ac.th

[1] Faculty of Environment and Resource Studies, Mahidol University, Nakhon Pathom 73170, Thailand
[2] Innovation for Social and Environmental Management, Mahidol University, Amnatcharoen Campus, Amnatcharoen 37000, Thailand
[3] Key Laboratory of Environment Change and Resources Use in Beibu Gulf, Ministry of Education, Nanning Normal University, Nanning 530002, China
[4] Key Laboratory for Humid Subtropical Eco-geographical Processes of the Ministry of Education, Fujian Normal University, Fuzhou 350007, China
[5] Institute of Geography, Fujian Normal University, Fuzhou 350007, China

Published online: 12 May 2020

Springer

Funding information for Pumijumnong et al. (2020)

Source: https://link.springer.com/article/10.1007/s00484-020-01926-9

Acknowledgments We thank the editor and two anonymous reviewers for their valuable and helpful comments.

Funding information

This work was supported under a project of Asian summer monsoon variability during the Holocene: a synthesis study on stalagmites and tree rings from Thailand and China by the Thailand Science Research and Innovation (TSRI) (grant number RDG5930014); the TSRI (grant number RSA6280017); the German Academic Exchange Service (DAAD); the National Natural Science Foundation of China (grant numbers 41661144021 and 41272197); Postdoctoral fellowship award from Mahidol University (2018-2020); the National Key Research and Development Program of China (2017YFA0603401); Innovation Research Team Fund of Fujian Normal University (grant number IRTL1705); and Mahidol University, Amnatcharoen campus (2016-2020).

Publication No. 7: Climate variability over the past 100 years in Myanmar derived from tree-ring stable oxygen isotope variations in Teak.*

Pumijumnong, N., Muangsong, C., Buajan, S., Sano, M., Nakatsuka, T. (2020). Climate variability over the past 100 years in Myanmar derived from tree-ring stable oxygen isotope variations in Teak. *Theoretical and Applied Climatology, 139*, 1401-1414. https://doi.org/10.1007/s00704-019-03036-y.

*Note that study area is out of scope in this project but with the analysis and funds were provided by Chinese member under this project.

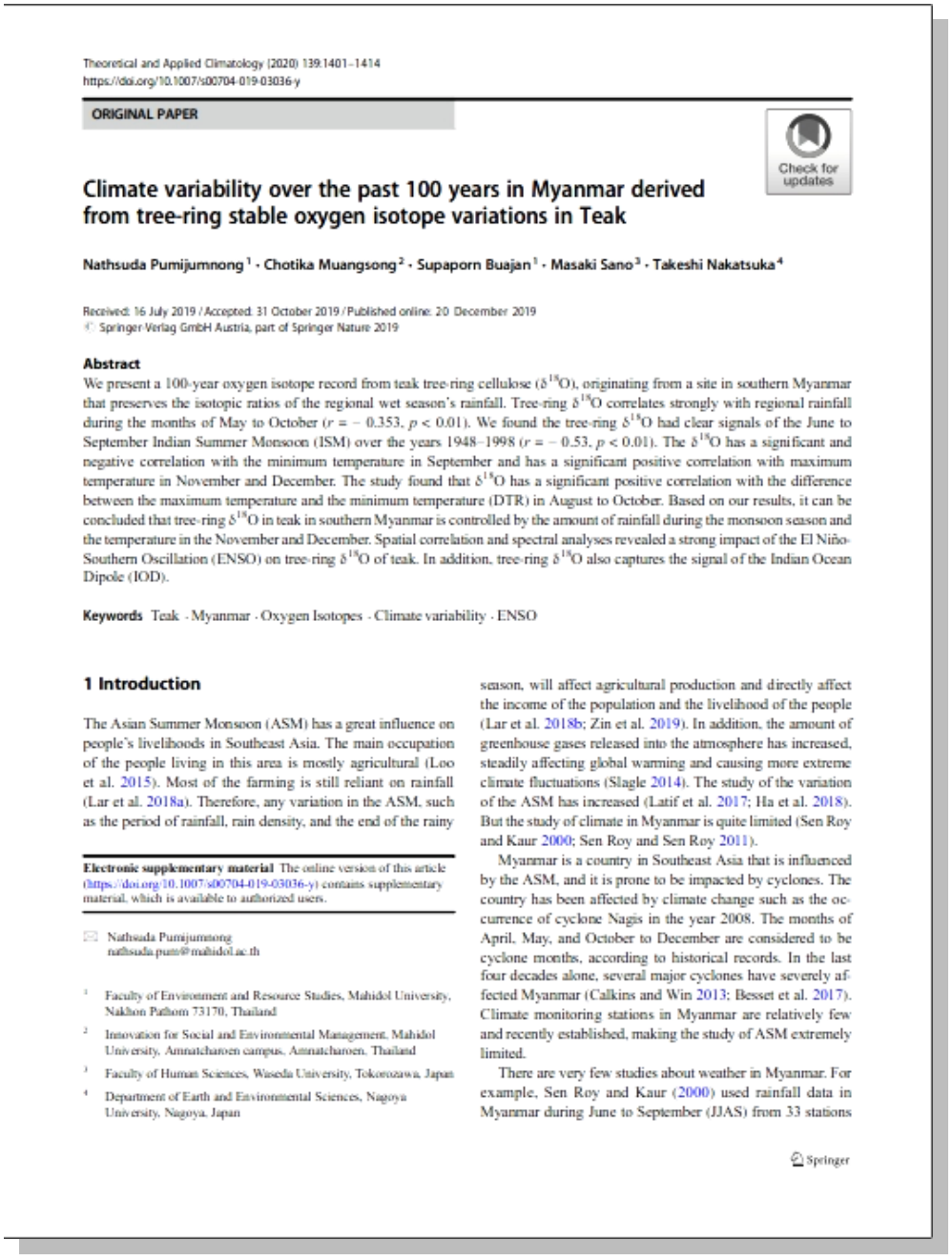

Theoretical and Applied Climatology (2020) 139:1401–1414
https://doi.org/10.1007/s00704-019-03036-y

ORIGINAL PAPER

Check for updates

Climate variability over the past 100 years in Myanmar derived from tree-ring stable oxygen isotope variations in Teak

Nathsuda Pumijumnong[1] · Chotika Muangsong[2] · Supaporn Buajan[1] · Masaki Sano[3] · Takeshi Nakatsuka[4]

Received: 16 July 2019 / Accepted: 31 October 2019 / Published online: 20 December 2019
© Springer-Verlag GmbH Austria, part of Springer Nature 2019

Abstract
We present a 100-year oxygen isotope record from teak tree-ring cellulose ($\delta^{18}O$), originating from a site in southern Myanmar that preserves the isotopic ratios of the regional wet season's rainfall. Tree-ring $\delta^{18}O$ correlates strongly with regional rainfall during the months of May to October ($r = -0.353$, $p < 0.01$). We found the tree-ring $\delta^{18}O$ had clear signals of the June to September Indian Summer Monsoon (ISM) over the years 1948–1998 ($r = -0.53$, $p < 0.01$). The $\delta^{18}O$ has a significant and negative correlation with the minimum temperature in September and has a significant positive correlation with maximum temperature in November and December. The study found that $\delta^{18}O$ has a significant positive correlation with the difference between the maximum temperature and the minimum temperature (DTR) in August to October. Based on our results, it can be concluded that tree-ring $\delta^{18}O$ in teak in southern Myanmar is controlled by the amount of rainfall during the monsoon season and the temperature in the November and December. Spatial correlation and spectral analyses revealed a strong impact of the El Niño-Southern Oscillation (ENSO) on tree-ring $\delta^{18}O$ of teak. In addition, tree-ring $\delta^{18}O$ also captures the signal of the Indian Ocean Dipole (IOD).

Keywords Teak · Myanmar · Oxygen Isotopes · Climate variability · ENSO

1 Introduction

The Asian Summer Monsoon (ASM) has a great influence on people's livelihoods in Southeast Asia. The main occupation of the people living in this area is mostly agricultural (Loo et al. 2015). Most of the farming is still reliant on rainfall (Lar et al. 2018a). Therefore, any variation in the ASM, such as the period of rainfall, rain density, and the end of the rainy season, will affect agricultural production and directly affect the income of the population and the livelihood of the people (Lar et al. 2018b; Zin et al. 2019). In addition, the amount of greenhouse gases released into the atmosphere has increased, steadily affecting global warming and causing more extreme climate fluctuations (Slagle 2014). The study of the variation of the ASM has increased (Latif et al. 2017; Ha et al. 2018). But the study of climate in Myanmar is quite limited (Sen Roy and Kaur 2000; Sen Roy and Sen Roy 2011).

Myanmar is a country in Southeast Asia that is influenced by the ASM, and it is prone to be impacted by cyclones. The country has been affected by climate change such as the occurrence of cyclone Nagis in the year 2008. The months of April, May, and October to December are considered to be cyclone months, according to historical records. In the last four decades alone, several major cyclones have severely affected Myanmar (Calkins and Win 2013; Besset et al. 2017). Climate monitoring stations in Myanmar are relatively few and recently established, making the study of ASM extremely limited.

There are very few studies about weather in Myanmar. For example, Sen Roy and Kaur (2000) used rainfall data in Myanmar during June to September (JJAS) from 33 stations

Electronic supplementary material The online version of this article (https://doi.org/10.1007/s00704-019-03036-y) contains supplementary material, which is available to authorized users.

✉ Nathsuda Pumijumnong
nathsuda.pum@mahidol.ac.th

[1] Faculty of Environment and Resource Studies, Mahidol University, Nakhon Pathom 73170, Thailand
[2] Innovation for Social and Environmental Management, Mahidol University, Amnatcharoen campus, Amnatcharoen, Thailand
[3] Faculty of Human Sciences, Waseda University, Tokorozawa, Japan
[4] Department of Earth and Environmental Sciences, Nagoya University, Nagoya, Japan

Funding information for Pumijumnong et al. (2020)

Source: https://link.springer.com/article/10.1007/s00704-019-03036-y

Acknowledgements This study was supported by the Thailand Science Research and Innovation (TSRI) grant nr. RDG5930014 and TSRI grant nr. RSA6280017. We also thank the anonymous referees for their valuable input and critical regarding for the manuscript. We express our thanks to Kuaw Tint, Director General, Forest Department, Mehm Ko Ko Gyi, former Coordinator of TEAKNET (Asia Pacific Region), Saw Eh Dah, Coordinator, Forest Department Yangon/Myanmar, for cooperation during the sampling expedition in March 1999. We also thank Mr. Tin Ko OO for making a clear map of the study area.

Publication No. 8: Oxygen isotopic compositions of meteoric precipitation, drip water, and aragonitic stalagmite deposition from the Namjang cave in northwestern Thailand: implications for multi-proxy climate reconstruction

Muangsong, C., Pumijumnong, N., Cai, B., Hu, C. (2020). Oxygen isotopic compositions of meteoric precipitation, drip water, and aragonitic stalagmite deposition from the Namjang cave in northwestern Thailand: implications for multi-proxy climate reconstruction. *Theoretical and Applied Climatology*. https://doi.org/10.1007/s00704-020-03245-w.

Theoretical and Applied Climatology
https://doi.org/10.1007/s00704-020-03245-w

ORIGINAL PAPER

Check for updates

Oxygen isotopic compositions of meteoric precipitation, drip water, and aragonitic stalagmite deposition from the Namjang cave in northwestern Thailand: implications for multi-proxy climate reconstruction

Chotika Muangsong[1] · Nathsuda Pumijumnong[2] · Binggui Cai[3,4] · Chaoyong Hu[5]

Received: 3 April 2019 / Accepted: 27 April 2020
© Springer-Verlag GmbH Austria, part of Springer Nature 2020

Abstract
Stalagmites provide one of the few high-quality proxy records of the Thailand monsoon. The Namjang (NJ) cave (19°40′30″N, 98°12′12″E; 923 m a.s.l.), which is situated in the data-scarce region of northwestern Thailand, serves as a unique and important site that offers great potential for multi-proxy climate reconstruction. We present new data on stable oxygen isotopic ($\delta^{18}O$) compositions and growth rates of aragonite stalagmites based on an in situ cave and climate monitoring study performed between August 2012 and October 2013. The dominant factors that control the variations in the $\delta^{18}O$ values of rainfall, drip water, and modern aragonite precipitate as well as the variations in the modern speleothem deposition rates and drip water hydrochemical properties were determined to correctly interpret the climatic signals of the parameters that are derived from speleothems. The intraseasonal variations in rainfall $\delta^{18}O$ values were faithfully recorded from cave drip water isotopic signals. The monthly mean values of $\delta^{18}O$ in cave drip water were lower in the rainy season and higher in the dry seasons and shifted from approximately − 4 in the early rainy months to approximately − 6‰ in the late rainy months. These variations have implications for the use of speleothem $\delta^{18}O$ from the NJ cave as a proxy of the seasonal variations in monsoon rainfall $\delta^{18}O$ and changes in moisture source trajectories. The deposition rates of modern speleothem deposits are primarily controlled by drip water flow rates, which are linked to the amount of water recharge in the cave during the summer monsoon season. There was a significant correlation between the drip rate and amount of carbonate precipitation for the drip sites NJ-1 ($r = 0.54$, $p < 0.040$) and NJ-1202 ($r = 0.76$, $p < 0.004$). Combinations of different parameters and proxies from this area could provide the potential for the further development of multi-proxy climate reconstructions over different time scales.

1 Introduction

Monsoon rainfall provides a vital supply of water for most Asian monsoon countries. Tropical and subtropical regions, where the vast amount of atmospheric moisture originates in this region, are of particular interest for paleoclimate studies (Cobb et al. 2007; Lewis et al. 2010). Thailand is a country in Southeast Asia (Fig. 1a). Thailand monsoon (TM) is regarded as a tropical monsoon climate and is located in a transition zone between the Indian monsoon (IM) and western North Pacific (WNP) monsoon (WNPM) (Wang and Ho 2002; Wei et al. 2018). The stable oxygen isotopic ($\delta^{18}O$) signature of water is an important tracer for hydrological and ecological processes (Clark and Fritz 1997; West et al. 2006; Kumar et al. 2010). Among many applications, $\delta^{18}O$ and δD have been used extensively to determine the origin and pathway of atmospheric water vapor (Srivastava et al. 2015) and to interpret

✉ Nathsuda Pumijumnong
nathsuda@gmail.com; nathsuda.pum@mahidol.ac.th

[1] Innovation for Social and Environmental Management, Mahidol University, Amnatcharoen campus, Amnatcharoen 37000, Thailand
[2] Faculty of Environment and Resource Studies, Mahidol University, Nakhon Pathom 73170, Thailand
[3] Key Laboratory for Humid Subtropical Eco-geographical Processes of the Ministry of Education, Fujian Normal University, Fuzhou 350007, China
[4] Institute of Geography, Fujian Normal University, Fuzhou 350007, China
[5] State Key Laboratory of Biogeology and Environmental Geology, China University of Geosciences, Wuhan 430074, China

Published online: 12 May 2020

Funding information for Muangsong et al. (2020)

Source: https://link.springer.com/article/10.1007%2Fs00704-020-03245-w

Funding information This work was supported under a project of Asian summer monsoon variability during the Holocene: a synthesis study on stalagmites and tree rings from Thailand and China by the Thailand Science Research and Innovation (TSRI) (grant number RDG5930014); the National Natural Science Foundation of China (grant number 41661144021 and 41272197); the National Key Research and Development Program of China (2017YFA0603401); Innovation Research Team Fund of Fujian Normal University (grant number IRTL1705); and Mahidol University, Amnatcharoen campus (2015–2020).

Publication No. 9: A 338-year tree-ring oxygen isotope record from Thai teak captures the variations in the Asian summer monsoon system

Pumijumnong, N., Bräuning, A., Sano, M., Nakatsuka, T., Muangsong, C.,Buajan, S. (2020). A 338-year tree-ring oxygen isotope record from Thai teak captures the variations in the Asian summer monsoon system. *Scientific Reports*, *10*, 8966. https://doi.org/10.1038/s41598-020-66001-0

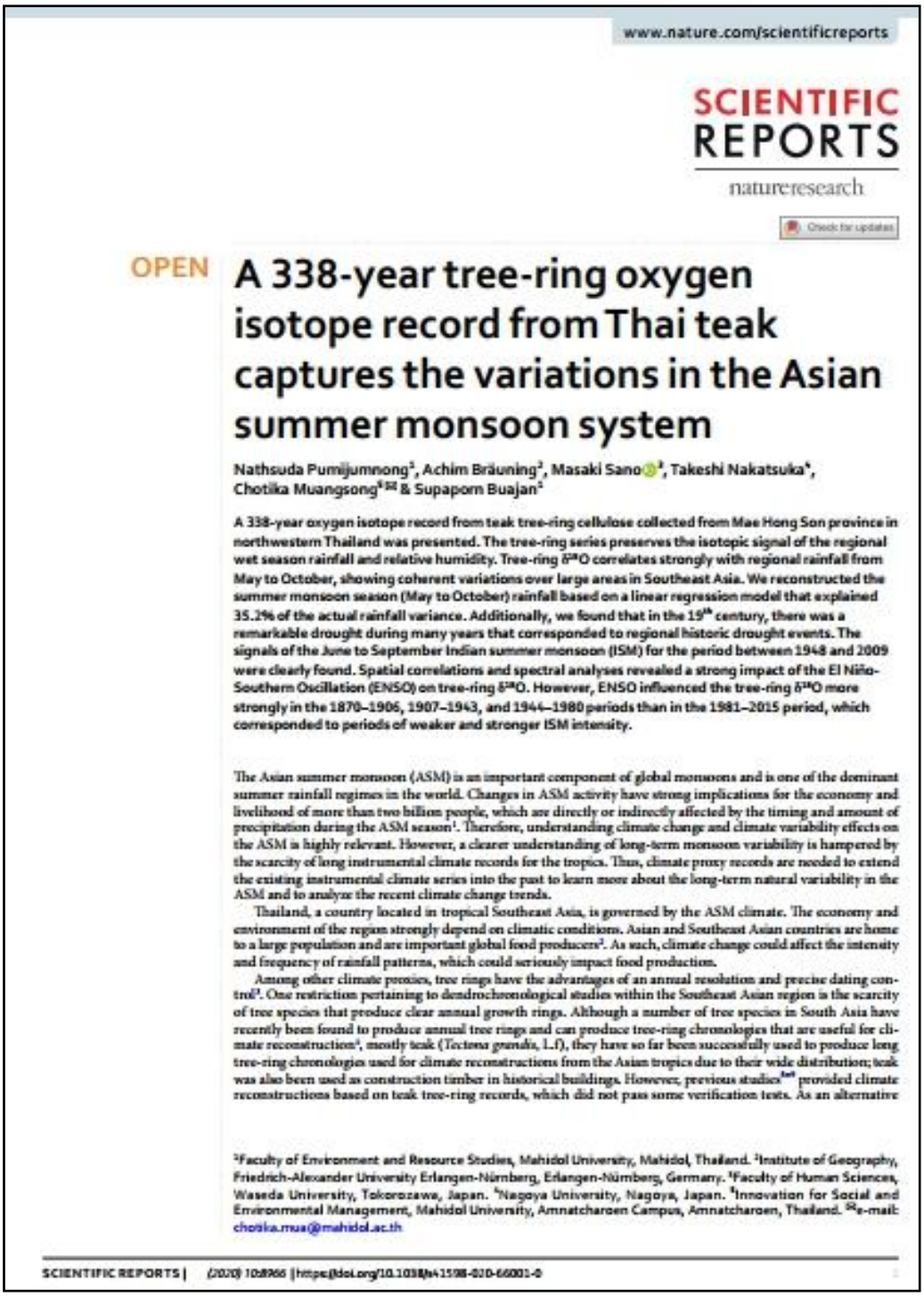

www.nature.com/scientificreports

SCIENTIFIC REPORTS

nature research

OPEN

A 338-year tree-ring oxygen isotope record from Thai teak captures the variations in the Asian summer monsoon system

Nathsuda Pumijumnong[1], Achim Bräuning[2], Masaki Sano[3], Takeshi Nakatsuka[4], Chotika Muangsong[1*] & Supaporn Buajan[1]

A 338-year oxygen isotope record from teak tree-ring cellulose collected from Mae Hong Son province in northwestern Thailand was presented. The tree-ring series preserves the isotopic signal of the regional wet season rainfall and relative humidity. Tree-ring $\delta^{18}O$ correlates strongly with regional rainfall from May to October, showing coherent variations over large areas in Southeast Asia. We reconstructed the summer monsoon season (May to October) rainfall based on a linear regression model that explained 35.2% of the actual rainfall variance. Additionally, we found that in the 19th century, there was a remarkable drought during many years that corresponded to regional historic drought events. The signals of the June to September Indian summer monsoon (ISM) for the period between 1948 and 2009 were clearly found. Spatial correlations and spectral analyses revealed a strong impact of the El Niño-Southern Oscillation (ENSO) on tree-ring $\delta^{18}O$. However, ENSO influenced the tree-ring $\delta^{18}O$ more strongly in the 1870–1906, 1907–1943, and 1944–1980 periods than in the 1981–2015 period, which corresponded to periods of weaker and stronger ISM intensity.

The Asian summer monsoon (ASM) is an important component of global monsoons and is one of the dominant summer rainfall regimes in the world. Changes in ASM activity have strong implications for the economy and livelihood of more than two billion people, which are directly or indirectly affected by the timing and amount of precipitation during the ASM season[1]. Therefore, understanding climate change and climate variability effects on the ASM is highly relevant. However, a clearer understanding of long-term monsoon variability is hampered by the scarcity of long instrumental climate records for the tropics. Thus, climate proxy records are needed to extend the existing instrumental climate series into the past to learn more about the long-term natural variability in the ASM and to analyze the recent climate change trends.

Thailand, a country located in tropical Southeast Asia, is governed by the ASM climate. The economy and environment of the region strongly depend on climatic conditions. Asian and Southeast Asian countries are home to a large population and are important global food producers[2]. As such, climate change could affect the intensity and frequency of rainfall patterns, which could seriously impact food production.

Among other climate proxies, tree rings have the advantages of an annual resolution and precise dating control[3]. One restriction pertaining to dendrochronological studies within the Southeast Asian region is the scarcity of tree species that produce clear annual growth rings. Although a number of tree species in South Asia have recently been found to produce annual tree rings and can produce tree-ring chronologies that are useful for climate reconstruction[4], mostly teak (*Tectona grandis*, L.f), they have so far been successfully used to produce long tree-ring chronologies used for climate reconstructions from the Asian tropics due to their wide distribution; teak was also been used as construction timber in historical buildings. However, previous studies[5,6] provided climate reconstructions based on teak tree-ring records, which did not pass some verification tests. As an alternative

[1]Faculty of Environment and Resource Studies, Mahidol University, Mahidol, Thailand. [2]Institute of Geography, Friedrich-Alexander University Erlangen-Nürnberg, Erlangen-Nürnberg, Germany. [3]Faculty of Human Sciences, Waseda University, Tokorozawa, Japan. [4]Nagoya University, Nagoya, Japan. [5]Innovation for Social and Environmental Management, Mahidol University, Amnatcharoen Campus, Amnatcharoen, Thailand. [*]e-mail: chotika.mua@mahidol.ac.th

Funding information for Pumijumnong et al. (2020)

Source: https://www.nature.com/articles/s41598-020-66001-0

Acknowledgements

This study was supported by the German Academic Exchange Service (DAAD), the Thailand Science Research and Innovation (TSRI) grant nr. RDG5930014 and TSRI grant nr. RSA6280017, the National Natural Science Foundation of China (NSFC) grant nr. 41661144021 and 41272197, the National Key Research and Development Program of China grant nr. 2017YFA0603401, Innovation Research Team Fund of Fujian Normal University grant nr. IRTL1705, Mahidol University, Amnatcharoen campus grant 2016-2020, and Postdoctoral fellowship award from Mahidol University for 2018-2020. We are deeply thankful to Dr. Thomas Neal Stewart for editing and proofing the English language of this manuscript. We also thank the anonymous referees for their valuable input and critical regarding for the manuscript.

Publication No. 10: The potential of teak log coffins collected from Namjang Cave in Northwestern Thailand for studying the Coffin Culture and paleoclimate in Southeast Asia

Buajan, S., Pumijumnong, N., Muangsong, C., Cai. B., Wang, F., Li, F. (2020). The potential of teak log coffins collected from Namjang Cave in Northwestern Thailand for studying the Coffin Culture and paleoclimate in Southeast Asia. *Archaeological and Anthropological Sciences*, *12*, 137, https://doi.org/10.1007/s12520-020-01105-2

Archaeological and Anthropological Sciences (2020) 12: 137
https://doi.org/10.1007/s12520-020-01105-2

ORIGINAL PAPER

The potential of teak log coffins collected from Namjang Cave in Northwestern Thailand for studying the coffin culture and paleoclimate in Southeast Asia

Supaporn Buajan[1,2] · Nathsuda Pumijumnong[1] · Chotika Maungsong[3] · Binggui Cai[4,5] · Fang Wang[4,5] · Miaofa Li[4,5]

Received: 30 July 2019 / Accepted: 1 June 2020 / Published online: 17 June 2020
© Springer-Verlag GmbH Germany, part of Springer Nature 2020

Abstract
Ancient teak log coffins found in Namjang (NJ) Cave, Pang Ma Pha district of Mae Hong Son province in Northwestern (NW) Thailand, were dated using a combination of C-14 dating and cross-dating techniques. The longest tree-ring width chronology (i.e., the $Coffin_{NJ}$ index) in Thailand covered a 477-year period from 106 BC to AD 371. The ages of the NJ log coffins fell within the log coffin culture epoch in NW Thailand. The NJ coffins are considered to belong to the second component of the log coffin culture period in NW Thailand, which began from approximately 2100 BP to 1200 BP. Spectral analysis of the $Coffin_{NJ}$ index displayed a decadal periodicity of 11.2 years, similar to the well-known 11-year periodic change in the sunspot cycle. A positive relationship ($r = 0.31$, $p < 0.035$) was observed between the $Coffin_{NJ}$ index and sunspot number for the entire period from 110 BC to AD 370, particularly during the period of AD 191–370 ($r = 0.48$, $p < 0.045$). Comparisons with speleothem proxies sensitive to changes in solar activity showed relationships between the $Coffin_{NJ}$ index and speleothem parameters (layer thickness: $r = -0.50$, $p < 0.001$ and $\delta^{18}O$: $r = 0.40$, $p < 0.001$). The results confirmed that the ancient teak trees in this study might have responded, at least partly, to solar variation. The ring widths of the teak log coffins proved to be a promising proxy for studying the evolution of coffin culture and past climate change in this area.

Keywords Teak · Log coffin · Ring width · Carbon-14 · Solar · Thailand

Introduction

The Asian monsoon (AM) is a key component of the global monsoon system (Wang 2006), which has a significant impact on billions of people in Asia because it produces a vital supply of rainwater feeding the agricultural, economic, and social sectors (Loo et al. 2015). Thailand is located in a transition region among different AM subsystems, including the South Asia-Indian monsoon and the East Asia-East Asian and Western North Pacific monsoons (Takahashi and Yasunari 2006; Wang and Lin 2002). This area is regarded as a strategically important location for studying the interplay of different monsoon subsystems (Aggarwal et al. 2004; Wei et al. 2018). However, the meteorological record derived from instrumental equipment is generally limited in space and time, making it difficult to assess the long-term changes in global climate conditions (Hansen et al. 2016). Paleoclimatology is the study of changes in ancient climates by using natural climate archives, known as natural climate proxies (e.g., sediments, ice cores, tree rings, and corals), to determine past climate states (Bender 2013). Monsoon variations in terms of climate change have a long history, occurring not only in the last few decades but also in the past several thousand years. Learning from past climate change is particularly important to improve understanding of present and future climate changes.

✉ Nathsuda Pumijumnong
nathsuda@gmail.com; nathsuda.pum@mahidol.ac.th

[1] Faculty of Environment and Resource Studies, Mahidol University, Nakhon Pathom 73170, Thailand
[2] Key Laboratory of Environment Change and Resources Use in Beibu Gulf, Ministry of Education, Nanning Normal University, Nanning 530002, China
[3] Innovation for Social and Environmental Management, Mahidol University, Amnatcharoen campus, Amnatcharoen 37000, Thailand
[4] Key Laboratory for Humid Subtropical Eco-geographical Processes of the Ministry of Education, Fujian Normal University, Fuzhou 350007, China
[5] Institute of Geography, Fujian Normal University, Fuzhou 350007, China

Funding information for Buajan et al. (2020)

Source: https://link.springer.com/article/10.1007/s12520-020-01105-2

Funding information This research was partially supported by a postdoctoral fellowship award from Mahidol University, as well as the project of Asian summer monsoon variability during the Holocene: a synthesis study on stalagmites and tree rings from Thailand and China by the Thailand Research Fund (TRF) (grant number RDG5930014); the National Natural Science Foundation of China (grant number 41661144021 and 41272197); the National Key Research and Development Program of China (2017YFA0603401); the Innovation Research Team Fund of Fujian Normal University (grant number IRTL1705); the grant number RSA6280017; and Mahidol University, Amnatcharoen campus.

APPENDIX B

Books

Book No. 1

1. หนังสือ คู่มือการตรวจวัดระบบถ้ำ (Cave Monitoring Handbook)

คู่มือการตรวจวัดระบบถ้ำ (Cave Monitoring Handbook) นี้ เป็นส่วนหนึ่งของโครงการ “ความผันแปรของลมมรสุมฤดูร้อนในทวีปเอเชียสมัยโฮโลซีน: การศึกษาเพื่อสังเคราะห์ข้อมูลที่บันทึกในหินงอกและวงปีไม้จากประเทศไทยและจีน (Asian summer monsoon variability during the Holocene: a synthesis study on stalagmites and tree rings from Thailand and China)” ซึ่งเป็นโครงการความร่วมมือระหว่างประเทศไทยและสาธารณรัฐประชาชนจีน โดยได้รับทุนสนับสนุนสำนักงานคณะกรรมการส่งเสริมวิทยาศาสตร์ วิจัยและนวัตกรรม (สกสว.) ฝ่ายสวัสดิภาพสาธารณะ และ The National Natural Science Foundation of China (NSFC) สำหรับคู่มือฉบับนี้จัดทำขึ้นเพื่อให้นักศึกษา นักวิชาการ และบุคคลทั่วไป สามารถนำไปใช้เป็นจุดเริ่มต้นในการพัฒนาการศึกษาพลวัฒน์ของการเปลี่ยนแปลงถ้ำในประเทศไทยอย่างเป็นระบบและถูกต้องตามหลักวิชาการ รวมถึงสร้างความรู้ความเข้าใจให้กับสาธารณชนใน ด้านการศึกษาด้านการเปลี่ยนแปลงสภาพภูมิอากาศในอดีตโดยอาศัยหลักฐานทางธรรมชาติ (Natural climate proxy) ทางธรณีวิทยา ซึ่งได้แก่ หินงอก (Stalagmite)

คู่มือการตรวจวัดระบบถ้ำ

Cave Monitoring Handbook

สนับสนุนการวิจัย โดย
สำนักงานกองทุนสนับสนุนการวิจัย (สกว.) ฝ่ายสวัสดิภาพสาธารณะ
National Natural Science Foundation of China (NSFC)

ตุลาคม 2561

ข้อมูลบรรณานุกรม

คู่มือการตรวจวัดระบบถ้ำ (Cave Monitoring Handbook)

ผู้เขียน

- ดร. โชติกา เมืองสง Chotika Muangsong, Ph.D.
  โครงการจัดตั้งวิทยาเขตอำนาจเจริญ มหาวิทยาลัยมหิดล
  โทรศัพท์ 0 62826 4220, 0 98126 5040
  อีเมล์: Chotika.mua@mahidol.ac.th หรือ Chokyaom@hotmail.com

ฝ่ายประสานการผลิต/ศิลปกรรม

- นางสาว กิตตาภา มะลิมาตร
- นางสาว ชญานิษฐ์ เมืองสง

คณะผู้ศึกษา

- โครงการจัดตั้งวิทยาเขตอำนาจเจริญ มหาวิทยาลัยมหิดล
  เลขที่ 259 ม.13 ถ.ชยางกูร ต.โนนหนามแท่ง อ.เมือง จ.อำนาจเจริญ 37000
- คณะสิ่งแวดล้อมและทรัพยากรศาสตร์ มหาวิทยาลัยมหิดล
  เลขที่ 999 ถ.พุทธมณฑล สาย 4 ต.ศาลายา อ.พุทธมณฑล จ.นครปฐม 73170
- College of Geographical Sciences, Fujian Normal University
  NO. 8 Shangsan Road, Cangshan District, Fuzhou 350007, China

จัดพิมพ์โดย

- โครงการ "ความผันแปรของลมมรสุมฤดูร้อนในทวีปเอเชียสมัยโฮโลซีน : การศึกษาเพื่อสังเคราะห์ข้อมูลที่บันทึกในหินงอกและวงปีไม้จากประเทศไทยและจีน (Asian summer monsoon variability during the Holocene: a synthesis study on stalagmites and tree rings from Thailand and China)"
  โครงการจัดตั้งวิทยาเขตอำนาจเจริญ มหาวิทยาลัยมหิดล
  โทรศัพท์ 045 523 211 หรือ 0 98126 5040 โทรสาร 045 523 211

สนับสนุนจัดพิมพ์โดย

- สำนักงานกองทุนสนับสนุนการวิจัย (สกว.) ฝ่ายสวัสดิภาพสาธารณะ

คำสืบค้น : การตรวจวัดระบบถ้ำ, การเปลี่ยนแปลงสภาพภูมิอากาศ, ยุคโฮโลซีน

พิมพ์ครั้งที่หนึ่ง : ตุลาคม 2561 **พิมพ์ที่ :** บริษัท จรัลสนิทวงศ์การพิมพ์ จำกัด
219 ซอย 102/2 ถนนเพชรเกษม
แขวงบางแคเหนือ เขตบางแค กรุงเทพฯ 10160

จำนวนพิมพ์ : 125 เล่ม **ISBN:**


รายชื่อคณะผู้ศึกษา
มหาวิทยาลัยมหิดล
ดร. โชติกา เมืองสง หัวหน้าโครงการ
หลักสูตรศิลปศาสตรบัณฑิต (นวัตกรรมการจัดการสังคมและสิ่งแวดล้อม)
โครงการจัดตั้งวิทยาเขตอำนาจเจริญ มหาวิทยาลัยมหิดล
รองศาสตราจารย์ ดร. นาฏสุดา ภูมิจำนงค์ ผู้ร่วมวิจัย
คณะสิ่งแวดล้อมและทรัพยากรศาสตร์ มหาวิทยาลัยมหิดล
นางสาว กิตตาภา มะลิมาตร ผู้ช่วยนักวิจัย
โครงการจัดตั้งวิทยาเขตอำนาจเจริญ มหาวิทยาลัยมหิดล
นางสาว พิมพ์ผจี บัวเพ็ชร์ นักศึกษาปริญญาโท
คณะสิ่งแวดล้อมและทรัพยากรศาสตร์ มหาวิทยาลัยมหิดล
Fujian Normal University
Prof. Dr. Binggui Cai หัวหน้าโครงการ
Assoc. Prof. Dr. Xiuyang Jiang ผู้ร่วมวิจัย
Assoc. Prof. Dr. Guoliang Lei ผู้ร่วมวิจัย
Dr. Xiuling Chen ผู้ร่วมวิจัย
คณะผู้วิจัยจากพื้นที่อนุรักษ์
นายพัทยา เท็กกิ้ม ผู้ร่วมวิจัย
หัวหน้าเขตรักษาพันธุ์สัตว์ป่าสันป่าแดน จังหวัดแม่ฮ่องสอน
นายนิกร แก้วโมรา ผู้ร่วมวิจัย
หัวหน้าเขตรักษาพันธุ์สัตว์ป่าลุ่มน้ำปาย จังหวัดแม่ฮ่องสอน
นายสมชาย บริสุทธิ์ ผู้ร่วมวิจัย
หัวหน้าศูนย์ศึกษาธรรมชาติและสัตว์ป่าถ้ำน้ำลอด จังหวัดแม่ฮ่องสอน
นายวีระ กอแก้ว ผู้ร่วมวิจัย
หัวหน้าอุทยานแห่งชาติแม่เมย จังหวัดตาก
นายสมศักดิ์ ฐิติชยาภรณ์ ผู้ร่วมวิจัย
หัวหน้าอุทยานแห่งชาติดอยผ้าห่มปก จังหวัดเชียงใหม่
นายศรัทธา กุลทอง ผู้ร่วมวิจัย
หัวหน้าเขตรักษาพันธุ์สัตว์ป่าเชียงดาว จังหวัดเชียงใหม่
นายดำรงค์ หาญภักดีนิยม ผู้ร่วมวิจัย
หัวหน้าวนอุทยานถ้ำหลวง-ขุนน้ำนางนอน จังหวัดเชียงราย
องค์การบริหารส่วนตำบลปาล์มพัฒนา
นายรัฐพงศ์ วรวรรณสงคราม ผู้ร่วมวิจัย
รองปลัดองค์การบริหารส่วนตำบลปาล์มพัฒนา จังหวัดสตูล

Book No. 2

2. หนังสือ: ความรู้เรื่องการศึกษาภูมิอากาศในอดีตในประเทศไทย (Introduction to Paleoclimate Research in Thailand)*

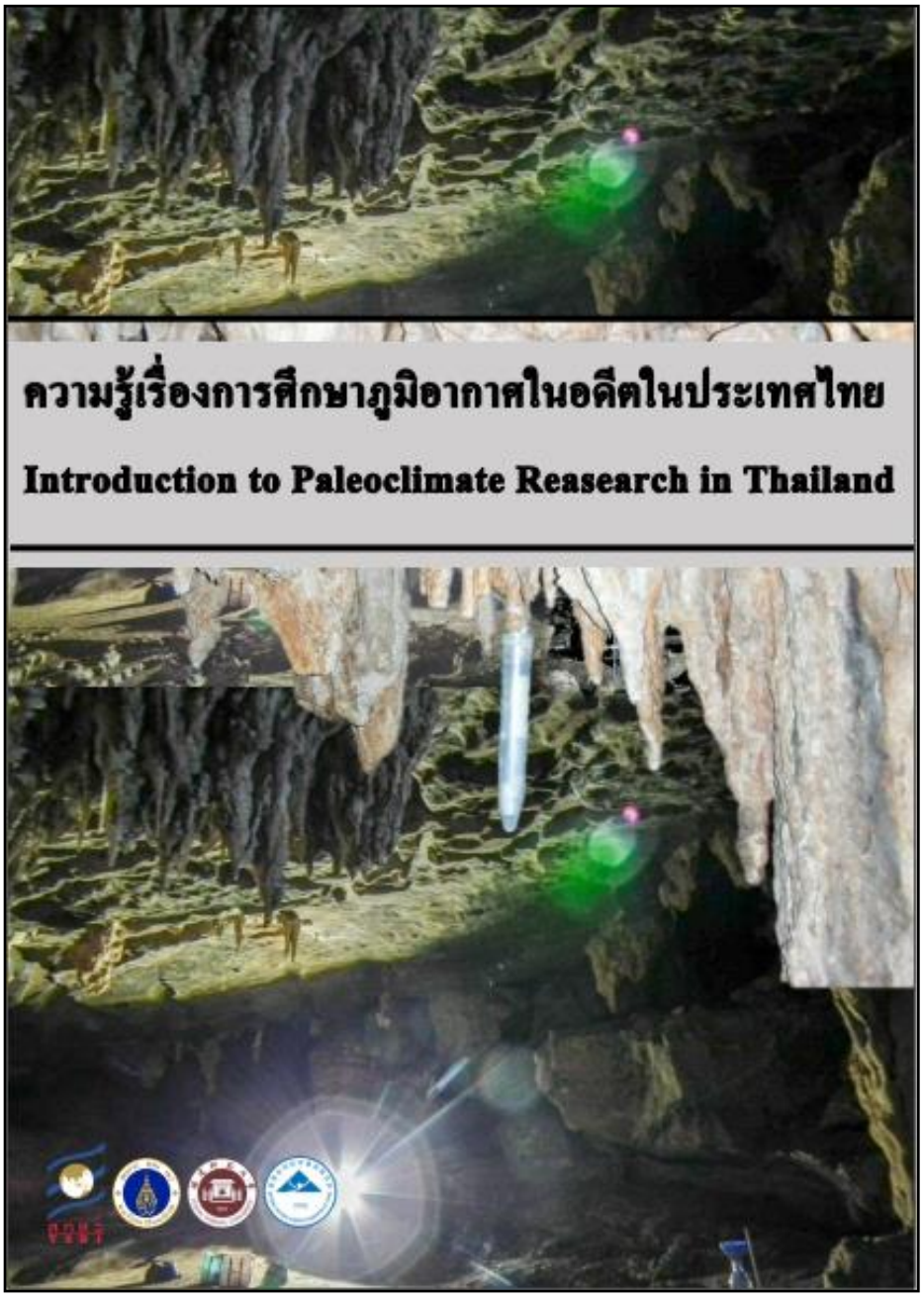

APPENDIX C

Website

Website is available at www.holocenceclimate-project.com with more than 20,000 visitors

APPENDIX D

Brochure

APPENDIX D

Brochure

APPENDIX D

Brochure

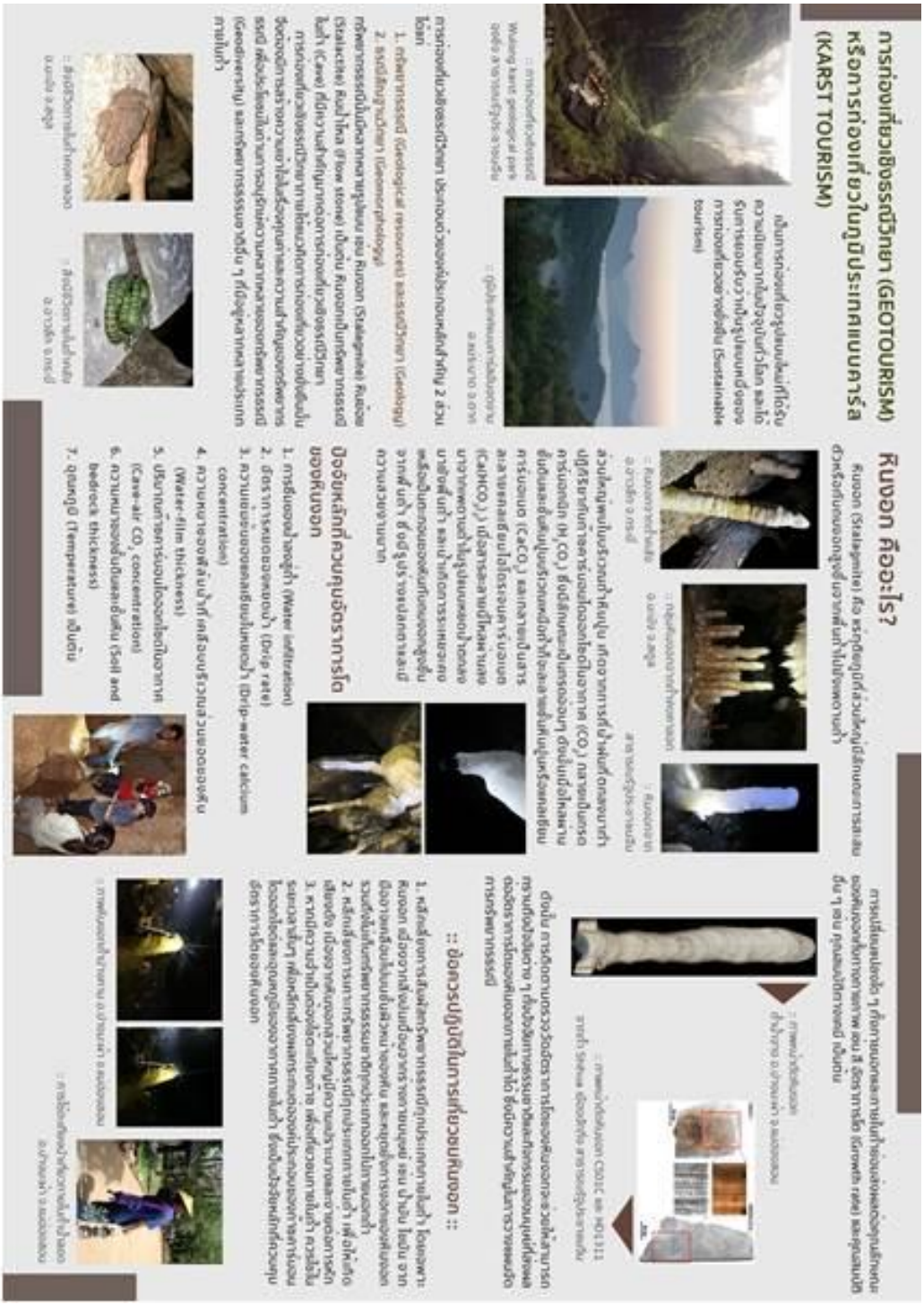

APPENDIX E

Conferences

APPENDIX E

Conferences

Thailand

27-29 November 2017: The 5th China-Thailand Joint Seminar on climate Change, Chiang Mai, Thailand.

31 August 2018: The National GEOTHAI 2018, Bangkok, Thailand

8-11 November 2018: The 6th China-Thailand Joint Seminar on climate Change, Chongqing, China.

27 November 2018: 1st Sino-Thailand joint workshop of "Historical Climate Change on the Maritime Silk Road", Chulalongkorn University, Bangkok, Thailand.

15 March 2019: The 20th National Graduate Research Conference, Khon Kaen, Thailand.

26-27 November 2019: The 7th China-Thailand Joint Seminar on climate Change, Krabi, Thailand.

1-5 December 2019: International Workshop on Monitoring the Ecosystem by Remote Sensing on the background of Global Change, Nanning, Guangxi, China

24–30 December 2019: The 6th Asian Dendrochronology Conference
"A window to the world of Asian Dendrochronology", Lucknow, Uttar Pradesh, India

China

16-18 May 2017: Intra-annual variations of soil CO_2 and drip water chemistry of cave Shihua, Beijing China and their implication for the formation of annual laminae in stalagmite. The U.S. Geological Survey Karst Interest Group (KIG) Workshop, Texas, USA.

21-24 May 2017: Multi-Decadal to Centennial Scale summer monsoon variation during early Holocene: A laminated stalagmite record from Northern China. The 8th International Conference on "Climate Change – The Karst Record VIII", Texas, USA.

2-6 April 2018: The water chemical characteristics of Qinglongdong karst spring,Kunming China. The 15th Multidisciplinary Conference on Sinkholes and the Engineering and Environmental Impacts of Karst. West Virginia, USA.

11-12 May 2019: A synthetic study on $\delta^{18}O$ in laminate stalagmite and $\delta^{18}O$ in cellulose extracted from Teak tree: a case study from NW Thailand, The International Conference on Silk-road Disaster Risk Reduction and Sustainable Development (SiDRR Conference), Beijing, China.

28-29 June 2019: Solar influence on the variability of East Asia Summer monsoon during Early Holocene: Annually-laminated stalagmite records from Beijing Shihua cave, Northern China. Eurasian Environmental Dynamics and Humans: Interactions over Different Time Scales. Belgrade, Serbia.

28-29 Jun 2019: Multi-decadal variability of Eastern Asian Summer Monsoon during 2.8 ka cold event and its responding to solar activity and Greenland climate. Eurasian Environmental Dynamics and Humans: Interactions over Different Time Scales. Belgrade, Serbia.

18 Oct 2019: Asian summer monsoon variability during the Holocene: A synthetic study on stalagmite and tree ring isotope from Fujian China and Thailand. Serbia Academy,

11 Jan 2020: Asian summer monsoon variability during the Holocene: A synthetic study on stalagmite and tree ring isotope from China and Thailand. Academic Committee Conference of Key Laboratoy of Humid Subtropical Eco-geographical Processes of the Ministry of Education,China. Fuzhou, China.

APPENDIX F

Rainfall reconstruction in Thailand

APPENDIX F

Rainfall reconstruction in Thailand

1. Summer monsoon rainfall total from March to October during the period AD 1804–1999, as inferred from tree ring oxygen isotopes collected from the Umpang (UP) district, Tak province, in Thailand by Xu et al. (2018)

Year (AD)	Tree ring $\delta^{18}O$ (‰, VSMOW)	Recon_Total rainfall from Mar to Oct (mm)
1804	26.07	1057.21
1805	25.26	1058.01
1806	24.57	1058.69
1807	24.93	1058.34
1808	24.89	1058.38
1809	23.87	1059.38
1810	24.65	1058.61
1811	23.96	1059.30
1812	24.40	1058.87
1813	23.80	1059.46
1814	24.14	1059.12
1815	24.40	1058.86
1816	25.61	1057.66
1817	26.71	1056.57
1818	23.03	1060.22
1819	22.69	1060.56
1820	25.20	1058.07
1821	23.98	1059.28
1822	24.26	1059.00
1823	24.75	1058.51
1824	25.85	1057.43
1825	26.13	1057.15
1826	25.24	1058.03
1827	25.82	1057.46
1828	25.51	1057.76
1829	25.22	1058.05
1830	24.45	1058.81
1831	24.03	1059.22
1832	26.62	1056.67
1833	24.85	1058.41
1834	24.19	1059.07
1835	24.49	1058.77
1836	24.99	1058.28
1837	25.80	1057.47
1838	25.83	1057.45
1839	24.39	1058.88
1840	24.87	1058.40

Year (AD)	Tree ring $\delta^{18}O$ (‰, VSMOW)	Recon_Total rainfall from Mar to Oct (mm)
1841	24.87	1058.40
1842	25.47	1057.81
1843	26.19	1057.09
1844	24.95	1058.31
1845	25.63	1057.65
1846	25.46	1057.81
1847	24.97	1058.30
1848	26.34	1056.94
1849	25.04	1058.23
1850	25.82	1057.46
1851	24.79	1058.48
1852	25.45	1057.83
1853	24.71	1058.55
1854	24.03	1059.23
1855	25.64	1057.63
1856	23.93	1059.32
1857	25.06	1058.20
1858	25.70	1057.58
1859	24.84	1058.43
1860	24.54	1058.72
1861	24.14	1059.11
1862	24.46	1058.80
1863	24.72	1058.55
1864	25.78	1057.49
1865	24.54	1058.72
1866	25.24	1058.03
1867	25.73	1057.54
1868	24.77	1058.49
1869	24.45	1058.81
1870	24.69	1058.57
1871	24.30	1058.96
1872	24.56	1058.71
1873	25.51	1057.77
1874	24.11	1059.15
1875	24.27	1058.99
1876	24.19	1059.07
1877	26.14	1057.14
1878	23.03	1060.22
1879	23.31	1059.94
1880	25.00	1058.27
1881	24.48	1058.78
1882	23.94	1059.32
1883	25.16	1058.11
1884	25.51	1057.77
1885	25.82	1057.46

Year (AD)	Tree ring $\delta^{18}O$ (‰, VSMOW)	Recon_Total rainfall from Mar to Oct (mm)
1886	25.22	1058.05
1887	24.58	1058.68
1888	25.64	1057.63
1889	24.43	1058.83
1890	25.29	1057.98
1891	25.29	1057.98
1892	24.93	1058.34
1893	24.72	1058.55
1894	24.90	1058.37
1895	26.02	1057.26
1896	25.43	1057.84
1897	24.02	1059.24
1898	24.21	1059.05
1899	25.88	1057.39
1900	24.67	1058.59
1901	24.06	1059.20
1902	25.47	1057.80
1903	23.66	1059.60
1904	24.95	1058.32
1905	25.19	1058.08
1906	25.89	1057.39
1907	25.10	1058.17
1908	24.00	1059.26
1909	25.18	1058.09
1910	24.35	1058.91
1911	25.34	1057.93
1912	25.70	1057.57
1913	25.78	1057.50
1914	26.43	1056.85
1915	24.50	1058.76
1916	24.66	1058.61
1917	23.89	1059.36
1918	26.57	1056.72
1919	25.81	1057.46
1920	25.34	1057.93
1921	25.30	1057.97
1922	24.86	1058.41
1923	25.19	1058.08
1924	25.22	1058.05
1925	25.97	1057.31
1926	24.13	1059.12
1927	25.39	1057.88
1928	25.37	1057.91
1929	25.53	1057.74
1930	25.64	1057.63

Year (AD)	Tree ring $\delta^{18}O$ (‰, VSMOW)	Recon_Total rainfall from Mar to Oct (mm)
1931	24.36	1058.90
1932	24.71	1058.55
1933	24.49	1058.78
1934	24.97	1058.30
1935	24.53	1058.73
1936	25.83	1057.45
1937	25.17	1058.10
1938	24.65	1058.62
1939	25.39	1057.89
1940	25.08	1058.18
1941	24.93	1058.33
1942	24.50	1058.76
1943	25.64	1057.64
1944	24.15	1059.11
1945	25.32	1057.95
1946	25.35	1057.92
1947	24.84	1058.43
1948	25.42	1057.85
1949	23.73	1059.52
1950	24.24	1059.02
1951	24.40	1058.87
1952	25.24	1058.03
1953	24.40	1058.86
1954	24.01	1059.24
1955	24.43	1058.83
1956	24.46	1058.80
1957	24.47	1058.79
1958	24.17	1059.08
1959	24.31	1058.95
1960	25.39	1057.88
1961	24.60	1058.67
1962	23.54	1059.71
1963	23.67	1059.58
1964	23.77	1059.48
1965	25.57	1057.70
1966	25.46	1057.81
1967	25.34	1057.93
1968	25.79	1057.49
1969	24.91	1058.36
1970	24.39	1058.87
1971	25.19	1058.08
1972	24.76	1058.50
1973	25.09	1058.18
1974	24.12	1059.14
1975	23.23	1060.01

Year (AD)	Tree ring $\delta^{18}O$ (‰, VSMOW)	Recon_Total rainfall from Mar to Oct (mm)
1976	24.87	1058.39
1977	26.11	1057.17
1978	24.10	1059.16
1979	26.61	1056.67
1980	25.03	1058.23
1981	24.92	1058.35
1982	25.81	1057.47
1983	25.00	1058.26
1984	25.73	1057.55
1985	25.19	1058.08
1986	26.87	1056.41
1987	25.81	1057.46
1988	24.32	1058.94
1989	25.64	1057.63
1990	25.24	1058.03
1991	25.45	1057.83
1992	26.48	1056.81
1993	26.32	1056.96
1994	25.60	1057.68
1995	24.15	1059.11
1996	24.41	1058.85
1997	26.23	1057.05
1998	25.55	1057.72
1999	24.68	1058.58

2. Monthly average rainfall from March to October during the period AD 1678–2015, as inferred from tree ring oxygen isotopes collected from Mae Hong Son province in Northwestern Thailand by Pumijumnong et al. (2020)

Year (AD)	Recon_Monthly average rainfall from Mar to Oct (mm)
1616	230.89
1617	243.53
1618	249.02
1619	276.48
1620	304.67
1621	330.80
1622	243.09
1623	250.84
1624	287.81
1625	263.71
1626	280.88
1627	245.32
1628	240.26
1629	273.93
1630	267.07
1631	262.15
1632	270.82
1633	267.95
1634	258.24
1635	244.23
1636	241.88
1637	259.46
1638	248.44
1639	246.55
1640	251.52
1641	258.95
1642	257.11
1643	240.72
1644	221.83
1645	265.02
1646	238.27
1647	241.21
1648	275.37
1649	226.13
1650	273.73
1651	271.55
1652	251.09
1653	268.31
1654	242.19
1655	246.94

Year (AD)	Recon_Monthly average rainfall from Mar to Oct (mm)
1656	239.46
1657	259.33
1658	258.91
1659	240.14
1660	233.85
1661	262.32
1662	259.40
1663	236.92
1664	247.66
1665	261.41
1666	236.94
1667	262.83
1668	245.91
1669	238.47
1670	254.12
1671	267.97
1672	253.91
1673	241.55
1674	255.89
1675	257.23
1676	257.51
1677	253.60
1678	277.81
1679	263.60
1680	250.40
1681	233.49
1682	266.50
1683	295.23
1684	281.39
1685	262.08
1686	254.51
1687	267.48
1688	245.69
1689	257.31
1690	259.51
1691	252.90
1692	268.19
1693	262.19
1694	254.64
1695	252.19
1696	252.34
1697	271.11
1698	264.08
1699	266.63

Year (AD)	Recon_Monthly average rainfall from Mar to Oct (mm)
1700	254.62
1701	248.09
1702	273.77
1703	257.27
1704	265.46
1705	237.92
1706	263.16
1707	274.48
1708	257.26
1709	256.10
1710	266.70
1711	300.29
1712	255.51
1713	253.34
1714	273.51
1715	253.82
1716	246.53
1717	233.36
1718	243.63
1719	267.73
1720	266.15
1721	256.63
1722	246.43
1723	261.49
1724	250.95
1725	245.77
1726	240.84
1727	240.72
1728	253.38
1729	276.02
1730	256.85
1731	243.14
1732	252.92
1733	242.35
1734	251.91
1735	262.49
1736	245.38
1737	237.61
1738	260.12
1739	244.63
1740	247.17
1741	264.85
1742	239.15
1743	252.63

Year (AD)	Recon_Monthly average rainfall from Mar to Oct (mm)
1744	265.61
1745	241.99
1746	240.39
1747	259.96
1748	242.57
1749	254.60
1750	228.74
1751	259.07
1752	265.26
1753	271.59
1754	262.12
1755	246.28
1756	278.71
1757	255.15
1758	228.98
1759	241.31
1760	264.66
1761	250.01
1762	248.53
1763	252.63
1764	265.03
1765	249.66
1766	262.85
1767	262.90
1768	231.81
1769	247.47
1770	254.21
1771	255.24
1772	250.67
1773	254.27
1774	258.82
1775	237.61
1776	265.97
1777	261.26
1778	249.60
1779	237.23
1780	256.06
1781	255.52
1782	231.70
1783	241.55
1784	236.90
1785	261.15
1786	253.71
1787	241.03

Year (AD)	Recon_Monthly average rainfall from Mar to Oct (mm)
1788	259.57
1789	265.65
1790	234.97
1791	228.06
1792	237.73
1793	242.97
1794	228.24
1795	243.31
1796	256.13
1797	266.66
1798	247.72
1799	245.31
1800	242.87
1801	256.83
1802	256.13
1803	239.06
1804	245.82
1805	262.84
1806	266.02
1807	254.29
1808	261.27
1809	257.88
1810	253.88
1811	236.68
1812	245.44
1813	261.91
1814	254.57
1815	260.08
1816	249.24
1817	245.72
1818	300.08
1819	298.16
1820	263.30
1821	240.34
1822	281.84
1823	253.72
1824	241.86
1825	241.25
1826	255.44
1827	249.05
1828	264.82
1829	264.50
1830	273.66
1831	286.47

Year (AD)	Recon_Monthly average rainfall from Mar to Oct (mm)
1832	239.79
1833	225.64
1834	270.55
1835	256.24
1836	261.68
1837	236.64
1838	243.72
1839	257.69
1840	233.52
1841	274.93
1842	253.30
1843	261.23
1844	256.48
1845	244.01
1846	259.80
1847	264.35
1848	255.41
1849	255.36
1850	262.08
1851	274.16
1852	256.57
1853	259.93
1854	272.11
1855	259.86
1856	283.83
1857	258.35
1858	230.47
1859	273.84
1860	252.64
1861	262.77
1862	269.36
1863	263.74
1864	253.20
1865	265.20
1866	269.80
1867	266.21
1868	269.75
1869	256.65
1870	277.83
1871	274.37
1872	272.62
1873	240.61
1874	281.48
1875	268.77

Year (AD)	Recon_Monthly average rainfall from Mar to Oct (mm)
1876	243.69
1877	245.20
1878	278.17
1879	299.09
1880	248.41
1881	260.53
1882	264.07
1883	257.70
1884	249.60
1885	221.48
1886	264.81
1887	254.60
1888	240.02
1889	249.94
1890	249.63
1891	222.03
1892	261.88
1893	279.92
1894	263.44
1895	243.83
1896	234.11
1897	247.85
1898	229.23
1899	206.56
1900	257.14
1901	239.65
1902	226.30
1903	279.43
1904	235.74
1905	236.93
1906	250.89
1907	236.57
1908	239.14
1909	267.00
1910	249.19
1911	236.01
1912	250.81
1913	239.04
1914	229.92
1915	216.24
1916	277.44
1917	270.23
1918	224.14
1919	239.15

Year (AD)	Recon_Monthly average rainfall from Mar to Oct (mm)
1920	229.88
1921	262.68
1922	232.81
1923	224.24
1924	231.80
1925	251.41
1926	239.50
1927	238.60
1928	244.84
1929	233.65
1930	247.05
1931	237.32
1932	246.79
1933	273.58
1934	264.89
1935	258.24
1936	238.55
1937	250.31
1938	278.75
1939	242.68
1940	251.20
1941	225.85
1942	259.34
1943	236.77
1944	239.72
1945	247.66
1946	222.56
1947	263.13
1948	252.11
1949	254.51
1950	246.52
1951	259.31
1952	247.42
1953	247.04
1954	254.43
1955	242.12
1956	250.41
1957	251.54
1958	243.56
1959	268.12
1960	247.32
1961	258.15
1962	256.68
1963	265.19

Year (AD)	Recon_Monthly average rainfall from Mar to Oct (mm)
1964	265.99
1965	238.58
1966	251.47
1967	243.85
1968	235.74
1969	258.74
1970	280.16
1971	264.28
1972	223.14
1973	287.57
1974	248.83
1975	285.79
1976	241.70
1977	247.76
1978	259.85
1979	220.96
1980	256.69
1981	250.73
1982	231.75
1983	254.34
1984	235.27
1985	229.84
1986	212.34
1987	236.27
1988	254.83
1989	255.07
1990	240.34
1991	240.09
1992	255.23
1993	233.00
1994	242.10
1995	266.99
1996	259.38
1997	237.16
1998	233.12
1999	231.81
2000	236.22
2001	250.34
2002	245.88
2003	243.00
2004	222.33
2005	244.48
2006	248.25
2007	243.03

Year (AD)	Recon_Monthly average rainfall from Mar to Oct (mm)
2008	238.56
2009	227.34
2010	266.87
2011	244.30
2012	216.05
2013	236.75
2014	215.03
2015	190.82

APPENDIX G

Summary of activities and outputs according to project's objectives

APPENDIX G

Summary of activity and output according to project's objectives

Objectives	Activities	Expected outputs	Outputs	Remarks
1. To produce high-resolution composite records of Asian summer monsoon over the past few centuries based on stalagmites and tree rings collected from Northern, Northwestern, and Southern Thailand.	1.1 Preliminary work 1.2 Sample collections 1.3 Laboratory experiment including analysis of tree rings and stalagmites 1.4 Data analysis and interpretation, including proxy calibration and proxy verification 1.5 Integration of multiples proxies for the reconstruction 1.6 Comparisons with climate indices	1.1.1 High-resolution composite records of Asian summer monsoon over the past centuries.	1) A preliminary result of comparison between high-resolution tree ring and stalagmite proxies from Mae Hong Son province in Northwestern Thailand. 2) The longest continuous paleo-rainfall (amount) reconstruction in Thailand based on tree rings oxygen isotopes covering 338 and 195 years. 3) The new continuous paleo-rainfall (amount) reconstruction in Thailand based on annual rings widths covering 177and 195 years. 4) High-resolution tree ring records of monsoon rainfall at monthly to seasonal timescales (i.e. intra-annual).	- Muangsong et al. (2019) - Pumijumnong et al. (2020) and Xu et al. (2018), respectively - Rainfall reconstruction in amounts were presented in Appendix E - Buareal et al. (2020) and Pumijumnong et al. (2020) - Muangsong et al. (2020)

Objectives	Activities	Expected outputs	Outputs	Remarks
			5) Factors controls Asian monsoon climate, were shown, by comparing proxies with several indices for examples; ENSO, IOD, and PDO.	- For examples; Muangsong et al. (2020) and Pumijumnong et al. (2020).
2. To reconstruct and synthesize the large-scale and long-term dynamic changes of the Holocene Asian monsoon based on stalagmites from the two Asian monsoon regions (Yunnan and Fujian, China) and one transition region (Mae Hong Son, Thailand).	2.1 Preliminary work 2.2 Sample collections 2.3 Laboratory experiment including analysis of tree rings and stalagmites 2.4 Data analysis and interpretation, including proxy calibration and proxy verification 2.5 Integration of multiples proxies for the reconstruction 2.6 Comparisons with climate indices	2.1.1 Stalagmite records of long-term dynamic changes of the Holocene Asian monsoon	1) History of the Holocene climate evolution derived from stalagmites and teak log coffins from Thailand or China.	- Buajan et al. (2020). - Chapter III Results and discussion.
3. To investigate both short-term and long-term driving mechanisms of the Asian monsoon circulation and its teleconnection to global	3.1 Data analysis and interpretation, including proxy calibration and proxy verification 3.2 Integration of	3.1.1 Factors controls Asian monsoon climate over the Holocene 3.1.2 Improving of public understanding of climate change and paleoclimate	1) Factors controls climate during the Holocene epoch, for examples; ENSO, ITCZ, Solar insolation. 11) Publications (10	- Chapter III Results and discussion. - Publications as mentioned in Appendix A - Appendices A-E

Objectives	Activities	Expected outputs	Outputs	Remarks
climate change.	multiples proxies for the reconstruction 3.3 Comparisons with climate indices	science. 3.1.3 Knowledge exchange, innovation experience, and inspiration among researchers. - Publications (7 articles in Quartile 1-2 of the SCI) - Website - Books (2 books in total) - Conferences/meeting (3 conferences)	articles, including 5 articles in quartile 1 of the SCI, 4 articles in quartile 2 of the SCI and 1 article in Scopus and Tier 1 of the TCI. 2) Website (1 website) 3) Conferences (16 conferences) 4) Book No. 2: Introduction to paleoclimate research in Thailand 5) Brochure	
4. To carry out a systematic cave and climate monitoring program in Thailand for better understanding of climate signal derived from stalagmites and tree rings.	4.1 Climate and cave monitoring in Thailand	4.1.1 Microclimatological data 4.1.2 Improving of public understanding of climate change and paleoclimate science. - Publications (7 articles in Quartile 1-2 of the SCI)	1) A comprehensive and systematic monitoring of cave and climate in Thailand and China 2) Datasets of cave and climate monitoring in Thailand 1) Publications (10 articles, including 5 articles in quartile 1 of the SCI, 4 articles in quartile 2 of the SCI and 1 article in Scopus and	- Muangsong et al. (2020) - Appendices A-E

Objectives	Activities	Expected outputs	Outputs	Remarks
		- Website - Books (2 books in total) - Conferences/meeting (at least 3 conferences)	Tier 1 of the TCI. 2) Website (1 website) 3) Conferences (12 conferences) 4) Book No. 1: Cave monitoring handbook 5) Brochure	

APPENDIX H

Benefits of Thai-Chinese collaboration

1. Results were published in high-quality international journals as well as presented in both local and international conferences. This is the best opportunity to share and discuss the research results with experts all around the world.

2. High-resolution and short-term proxy-calibrations provided the solid background for climate transfer functions and climate models, which further used to reconstruct the past climate changes as well as to improve future climate forecasts.

3. High-resolution and long-term paleoclimate data were used to establish the paleoclimate network in Asia and could provide greater insight into the factors controlling the past climate change.

4. A better understanding of the dominant factors controlling stalagmites and tree rings properties provided the interpretative frameworks for the Holocene Asian monsoon reconstruction

5. A comprehensive and systematic monitoring of cave and climate were carried out in Thailand. This would make the basis for future researches.

6. Microclimatological data could give a wide range of benefits for local people such as agricultural planning, natural disasters protection.

7. The cave monitoring data would further bring many benefits for the whole of the caving community in helping to conserve, protect, and interpret the overall cave and karst systems.

8. The collaboration between universities in Thailand and China becomes wider and deeper.

9. Researchers from each country were trained in order to get more knowledge, and exchange experience, innovation, and inspiration.